HEAT AND MASS TRANSFER CHARACTERISTICS OF ADSORBENTS IN HEAT PUMP AND REFRIGERATOR

A Thesis Submitted to
the Graduate School of Engineering and Sciences of
İzmir Institute of Technology
in Partial Fulfillment of the Requirements for the Degree of

DOCTOR OF PHILOSOPHY

in Chemical Engineering

by
Şefika Çağla GÜNDOĞAN

January 2023
İZMİR

ACKNOWLEDGEMENT

ABSTRACT

HEAT AND MASS TRANSFER CHARACTERISTICS OF ADSORBENTS IN HEAT PUMP AND REFRIGERATOR

Due to increasing drought, pandemic and climate crisis in recent years, researchers have increased their studies on environmentally friendly energy use. Although there are technological developments in the production of energy from renewable energy sources, the storage of this produced energy is still a problem that awaits a solution. At this point, adsorption heat pumps with high primary energy efficiency come to the fore as a developing technology and attract the attention of researchers. However, low heat transfer properties in the adsorbent bed reduce the performance of adsorption heat pumps and limit their applications.

The aim of this thesis was to improve the performance of the adsorption heat pump by increasing the effective thermal conductivity within the adsorbent bed. Two methods have been employed to enhance the effective thermal conductivity. In the first method, which was unconsolidated adsorbent bed design, it was aimed to increase the thermal conductivity of the bed with metal additives with a continuous structure. In the second method, which is known as consolidated bed design, the effective thermal conductivity of zeolite 13X was tried to be enhance with a high conductive material, reduced graphene oxide.

In the experimental studies, it was observed that the thermal conductivity increased from 0.12 W/m.K to 0.28 W/m.K in unconsolidated bed design by means of fin-shaped metal additive. In consolidated adsorbent bed design, the effective thermal conductivity of the Graphene/Zeolite 13X (1 wt% Graphene) was determined as 0.1613 W/m.K. In theoretical studies, the effect of thermal conductivity in the temperature, pressure and adsorbate concentration was investigated. The indirect and direct effects of effective thermal conductivity on specific cooling/heating power (SCP/SHP) and coefficient of performance (COP) values were examined. Although the effect of thermal conductivity on COP was ignored in most of the studies in the literature, it was observed that COP increased from 0.01 to 0.10 when thermal conductivity increased from 0.12 W/m.K to 1 W/m.K.

ÖZET

ISI POMPASI VE SOĞUTUCU İÇİN ADSORBENTLERİN ISI VE KÜTLE TRANSFERİ ÖZELLİKLERİ

Son yıllarda artan kuraklık, pandemi ve iklim krizi gibi nedenlerle araştırmacılar çevre dostu enerji kullanımına yönelik çalışmalarını arttırmışlardır. Her ne kadar yenilenebilir enerji kaynaklarından enerji üretimine yönelik teknolojik gelişmeler yaşansa da bu üretilen enerjinin depolanması hala çözüm bekleyen bir sorun olarak karşımıza çıkmaktadır. Bu noktada, birincil enerji verimliliği yüksek olan adsorpsiyonlu ısı pompaları geliştirilebilir teknoloji olarak ön plana çıkmakta ve araştırmacıların ilgisini çekmektedir. Fakat, adsorban yatağı içerisindeki düşük ısı transferi özellikleri adsorpsiyonlu ısı pompalarının performansını düşürmekte ve uygulamalarını sınırlamaktadır.

Bu tezin amacı, adsorban yatağı içindeki efektif termal iletkenliği artırarak adsorpsiyonlu ısı pompasının performansını iyileştirmektir. Efektif termal iletkenliği artırmak için iki yöntem kullanılmıştır. Birinci yöntem olan konsolide olmayan adsorban yatağı tasarımında, sürekli bir yapıya sahip metal katkı maddeleri ile yatağın termal iletkenliğinin arttırılması hedeflenmiştir. Konsolide yatak tasarımı olarak bilinen ikinci yöntemde, zeolit 13X'in efektif termal iletkenliği, yüksek termal iletkenliğe sahip indirgenmiş grafen oksit ile artırılmaya çalışılmıştır.

Deneysel çalışmalarda, konsolide olmayan yatak tasarımında kanat şeklindeki metal katkı sayesinde termal iletkenliğin 0.12 W/m.K'den 0.28 W/m.K'ye yükseldiği gözlenmiştir. Konsolide adsorban yatağı tasarımında, grafen/Zeolite 13X'in (ağırlıkça %1 grafen) etkin termal iletkenliği 0.1613 W/m.K olarak belirlenmiştir. Teorik çalışmalarda ısıl iletkenliğin sıcaklık, basınç ve adsorbat konsantrasyonu üzerindeki etkisi araştırılmıştır. Etkin termal iletkenliğin spesifik soğutma/ısıtma gücü (SCP/SHP) ve performans katsayısı (COP) değerleri üzerindeki dolaylı ve doğrudan etkileri incelenmiştir. Literatürdeki çalışmaların çoğunda termal iletkenliğin COP üzerindeki etkisi göz ardı edilmiş olsa da, termal iletkenlik 0.12 W/m.K'den 1 W/m.K'ye yükseldiğinde COP'un 0.01'den 0.10'a yükseldiği gözlenmiştir.

TABLE OF CONTENTS

LIST OF FIGURES

LIST OF TABLES

NOMENCLATURE

b   Langmuir Constant

c   adsorptive concentration in fluid phase, kg kg^{-1}

COP   coefficient of performance

D   diffusivity, m^2 s^{-1}

D_c intracrystalline diffusivity, m^2 s^{-1}

D_p pore diffusivity, m^2 s^{-1}

D_{eff} intracrystalline diffusivity, m^2 s^{-1}

D_{kn} knudsen diffusivity, m^2 s^{-1}

D_m molecular diffusivity, m^2 s^{-1}

D_s surface diffusivity, m^2 s^{-1}

D_0 reference diffusivity, m^2 s^{-1}

E   activation energy, J mol^{-1}

E_m energy density, kJ kg^{-1}

G   Gibbs free energy, kJ kg^{-1}

H   enthalpy, kJ kg^{-1}

h_{fg} heat of vaporization, kJ/kg^{-1}

K   Henry's law constant

m   mass of dry adsorbent, kg

P   pressure, Pa

P^{sat} saturation pressure, Pa

q   adsorbed amount, kg kg^{-1}

q_m monolayer capacity, kg kg^{-1}

q_∞ amount of adsorbed at equilibrium, kg kg^{-1}

$\bar{q}$ average adsorbate concentration, kg kg^{-1}

q_{st} isosteric heat of adsorption, kJ kg^{-1}

Q_{ev} heat of evaporation, kJ kg^{-1}

Q_{ab} heat of isosteric heating process, kJ kg^{-1}

Q_{bc} heat of isobaric desorption process, kJ kg^{-1}

Q_{cd} heat of isosteric cooling process, kJ kg^{-1}

Q_{da} heat of isobaric adsorption process, kJ kg^{-1}

r   pore radius, m

R   particle radius, m

S   entropy, kJ K^{-1}

SCP   specific cooling power, W kg^{-1}

SHP   specific heating power, W kg^{-1}

T   temperature, °C or K

T^{sat} saturation temperature, K

x   mass fraction of adsorbed adsorbate per dry adsorbent, kg kg^{-1}

Greek letters

$\Delta_a h$ differential heat of adsorption, J mol^{-1}

$\Delta_a H$ integral heat of adsorption, J kg^{-1}

ΔH heat of adsorption, kJ kg^{-1}

ε_p porosity

λ fraction of the adsorbate added in the step

τ_{cycle} period of cycle

ρ density, kg m^{-3}

τ dimensionless time variable

Subscripts

ads   adsorption

cond   condensation

eff   effective

ev   evaporator or evaporation

eq   equilibrium

i   initial

reg   regeneration

sat   saturation

∞ infinite

CHAPTER 1

INTRODUCTION

Increasing drought, epidemics and forest fires draw attention to climate change and global warming. Sustainable climate and environmental studies have accelerated around the world, especially after the World Meteorological Organization stated that a global warming of 1.5°C would be reached by 2025. In our country, the "National Climate Action Plan 2023" was published and the Paris Climate Agreement was approved by the Turkish Grand National Assembly in October 2021. With all these developments, adsorption in energy recovery and storage systems have gained importance once again. Thermal driven heat pumps which can be operated by renewable and sustainable energy sources such as geothermal energy, solar energy and waste heat can be a good option in decreasing effect of global warming.

Adsorption heat pumps, which are a type of thermal driven heat pumps, have higher primary energy efficiency compared to traditional heat pumps, do not contain any hazardous materials, and can operate without noise and vibration. Adsorption heat pumps consist of an adsorbent bed, an evaporator, a condenser, and an expansion valve. The working fluid is circulated between the adsorbent bed, evaporator, and condenser according to the Carnot cycle.

Although adsorption heat pumps have several advantages over traditional heat pumps, they still require enhancements due to low COP and SCP/SHP. Meunier claimed that the adsorption heat pumps could be an alternative to traditional heat pumps when COP and SCP values were at least 1 and 300-1000 W/kg, respectively (Meunier 1993). Furthermore, Meunier stated that the optimum values of thermal conductivity, heat transfer coefficient of the adsorbent bed and permeability should be 1 W/m^2K, 200 W/m^2K and 10^{-12} m^2, respectively to satisfy the indicated COP and SCP values.

Low effective thermal conductivity within the adsorbent bed still limits the applications of adsorption heat pumps. Therefore, different methods were developed to achieve the optimum COP and SCP values in the previous studies. Among them, using advanced adsorption cycles, producing new adsorbate-adsorbent pairs and enhancement of heat and mass transfer by new adsorbent bed designs draw attention.

Due to the intermittent behaviour of single-bed adsorption systems, the COP of the adsorption heat pump decreased. As a consequence, advanced cycles such as heat recovery

cycles, mass recovery cycles, thermal wave cycles and multistage and cascading cycles, and hybrid systems have been improved to achieve continuous operation (Meunier, 2001; Wang, 2001; Sumathy et al., 2003; Demir et al., 2008; Goyal et al., 2016). In these advanced cycle systems, two or more adsorbent beds are included in the cycle. For instance, while the same adsorbent is used in heat recovery cycle, different adsorbents are used in the beds in cascading cycle.

Selection of the appropriate working pair is too crucial in the design of the adsorption heat pump. Although high adsorption capacity and heat of adsorption values can be achieved with the available adsorbent-adsorbate pairs such as silica gel-water, active carbon-methanol and zeolite-water, the low thermal conductivity of the adsorbents limits the application of the adsorption heat pumps. Thus, researchers focused their studies on enhancement of high thermal conductive adsorbent materials. In order to obtain an adsorbent of high thermal conductive, methods such as mixing a material of high thermal conductive with current adsorbent, coating adsorbent onto a metal fin or a tube are performed.

Unconsolidated adsorbent bed design is another method to increase the effective thermal conductivity within the bed. In this method, the pellet, granule, or fibre adsorbent is added inside the heat exchanger or metal additives are included without any binder.

The aim of this study to enhance effective thermal conductivity with the adsorbent bed, so the performance of the adsorption heat pump. In order to do that, selection of working pair is taken into consideration first. Due to the high affinity to each other and high heat of adsorption value, zeolite 13X-water pair was selected as the working pair. The adsorption equilibrium and kinetics data were evaluated by a volumetric adsorption system at different adsorption temperatures (35,45 and 60°C) and at regeneration temperature of 90°C. The details of the experimental study are given in Chapter 6.

The improvement of the effective thermal conductivity of the bed was studied with two different methods. In the first method, aluminum wire was inserted inside the bed with different geometrical configurations and zeolite beads were filled into the spaces. In this method, the effective thermal conductivity measurements were with a homemade system which is detailed in Chapter 6.

The other improvement method was chosen as consolidated adsorbent bed design. In this method, high thermal conductive graphene is used by mixing and pelletizing with binderless zeolite 13X. The experimental method used to pelletize the graphene/zeolite 13X was explained in Chapter 6.

In addition to the experimental studies, the adsorptive flow inside the adsorbent bed was also examined for zeolite 13X-water pair by theoretical analysis in MATLAB. The heat,

mass and momentum equations were solved simultaneously and temperature, adsorptive pressure and adsorbate concentration distributions inside the bed were determined. The one and two-dimensional analysis of the adsorbent bed with constant temperature source were performed. The effect of temperature and adsorbate loading dependence of effective diffusivity of the adsorbent-adsorbate pair and effective thermal conductivity of the bed were investigated. Furthermore, different designs were also analysed by numerical method. The details of the theoretical studies and solution procedure were represented in Chapter 4 and Chapter 6, respectively.

The principles of adsorption heat pumps are explained in Chapter 2. The advantages and drawbacks of the adsorption heat pumps are also given in this section. The performance improvement methods of adsorption heat pumps are summarized, and details of the previous studies performed in literature are represented.

The adsorption phenomena are introduced in Chapter 3. Models to define adsorption equilibrium are explained in detail. The heat of adsorption and experimental evaluation of adsorption equilibrium data are summarized. Furthermore, the adsorption kinetics are discussed in this chapter, too. The isothermal and non-isothermal adsorption kinetics is summarized.

In Chapter 4, the fluid flow in a porous bed is stated and the governing equations used to define temperature, adsorptive pressure and adsorbate concentration within the adsorbent bed are discussed.

The framework structure of Zeolite is introduced in Chapter 5. Furthermore, the significant effect of pre-adsorbed water on adsorption applications and the studies performed with zeolite-water pair are also summarized in this section.

The details of selection of working pair, adsorption equilibrium experiments, producing high thermal conductive graphene, characterization studies, improvement methods of effective thermal conductivity inside the adsorbent bed, numerical solution of governing equations are given in Chapter 6 which is titled as Materials and Methods.

In Chapter 7, the results are given and discussed. Experimental and numerical studies are evaluated in detail in this section.

The conclusion is given in Chapter 8. The summary of the performed studies and suggestions about these studies are given in this chapter.

CHAPTER 2

ADSORPTION HEAT PUMPS

Due to the increase in world population, the effect of global warming and climate crisis become sensible. Furthermore, the energy crisis affects all industrial applications in the whole world. As a result, energy recovery and storage systems gain importance once again. Adsorption heat pumps, a type of thermal driven heat pumps, is crucial in energy recovery and storage systems because of being environmentally friendly system.

In this chapter, the working principle of adsorption heat pumps, performance analysis and the improvements performed in the previous studies are introduced in detail.

2.1. Adsorption in Energy Recovery and Storage Systems

The limitations in the natural sources prompt the researchers to improve systems that store energy for later uses. Among them, thermal energy storage underlies the adsorption, which is a spontaneous exothermic process which occurs at the solid/fluid interface due to the molecular or atomic interactions, in energy recovery and storage systems. In adsorption heat pumps, thermal energy can be stored as latent or sensible heat in the adsorbent from sources such as peak electricity, solar energy or waste heat during the desorption process which is the reverse of the adsorption and an endothermic process.

Open and closed cycle systems can be designed by means of adsorption-desorption cycle which was improved by Close and Dunkle (Close and Dunkle 1977). While the dehumidification of the air is the basis of the open cycle systems, closed cycle systems are mainly used in heat pump and heat transformer applications in which heat is extracted from low temperature source to high temperature sink by using a third energy source.

Adsorption heat pump cycle can be examined as the combination of two cyclic devices: a heat engine and a heat pump. While the working fluid is vaporized in evaporator by taking heat from low-temperature source and releasing heat to the first intermediate-temperature sink in the heat pump cycle (adsorption process), heat is extracted from high-temperature source and release heat to second intermediate-

temperature sink during condensation in the heat engine cycle (desorption process). The work obtained from heat engine can be used in heat pump cycle. The main components, which are an adsorbent bed, a condenser, an evaporator, and an expansion valve, are represented in Figure 2.1.
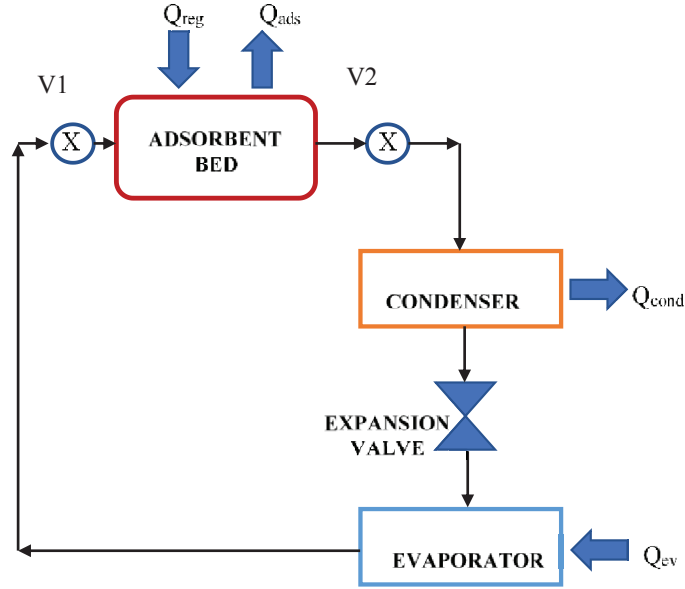
Figure 2.1.Components of Adsorption Heat Pump

The operation of adsorption heat pump can be represented by an isoster diagram as given in Figure 2.2. The cycle consists of isosteric heating (a-b), isobaric heating and desorption (b-c), isosteric cooling (c-d) and isobaric cooling and adsorption (d-a) processes. The amount of heat for each process are given in the set of equations, respectively (Equations 2.1-2.4).

Isosteric heating (a-b):

$$Q_{ab}=\int_{T_a}^{T_b} \left[m_s\left(Cp_s+x_2 Cp_v\right)+m_{bed}Cp_{bed}\right]dT \tag{2.1}$$

Isobaric heating and desorption (b-c):

$$Q_{bc}=\int_{T_b}^{T_c} \left[m_s\left(Cp_s+xCp_v\right)+m_{bed}Cp_{bed}\right]dT+\int_{b}^{c} m_s\,\Delta H_a dx \tag{2.2}$$

Isosteric cooling (c-d):

$$Q_{cd} = \int_{T_c}^{T_d} \left[m_s \left(Cp_s + x_1 Cp_v \right) + m_{bed} Cp_{bed} \right] dT \qquad (2.3)$$

Isosteric cooling and adsorption (d-a):

$$Q_{da} = \int_{T_d}^{T_a} \left[m_s \left(Cp_s + x Cp_v \right) + m_{bed} Cp_{bed} \right] dT + \int_{d}^{a} m_s \, \Delta H_a dx \qquad (2.4)$$
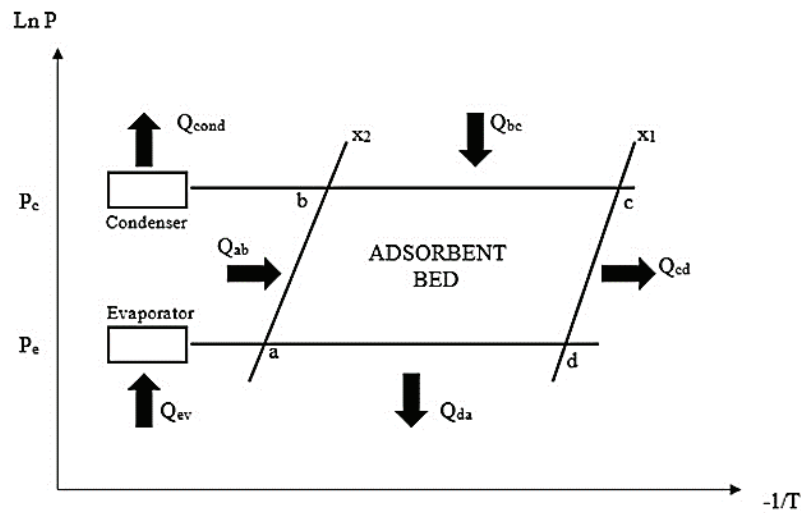
Figure 2.2. Thermodynamic cycle of adsorption heat pump

Furthermore, the heat of evaporation and condensation which are used for cooling and heating purposes respectively can be written as:

$$Q_{ev} = m_s \Delta x \Delta H_v + \int_{T_{cond}}^{T_{ev}} m_s \Delta x Cp_w dT \qquad (2.5)$$

$$Q_{cond} = m_s \Delta x \Delta H_v \qquad (2.6)$$

The performance analysis of adsorption heat pumps is based on two concepts: cooling of performance (COP) and specific cooling/heating power (SCP/SHP). COP can

be defined as the ratio of heat taken from the low-temperature source, in other words useful energy output, to the heat transferred from third energy source, energy input. For adsorption heat pumps, cooling and heating COPs can be written as:

$$COP_{cooling}=\frac{Q_{ev}}{Q_{ab}+Q_{bc}} \tag{2.7}$$

$$COP_{heating}=\frac{Q_{cond}+Q_{cd}+Q_{da}}{Q_{ab}+Q_{bc}} \tag{2.8}$$

Additionally, SCP and SHP can be described as the cooling and heating power per unit mass of adsorbent per cycle time of adsorption process, respectively, as follows.

$$SCP=\frac{Q_{ev}}{m\tau_{cycle}} \tag{2.9}$$

$$SHP=\frac{Q_{cond}+Q_{cd}+Q_{da}}{m\tau_{cycle}} \tag{2.10}$$

When compared to the traditional mechanical pumps, adsorption heat pumps are environmentally friendly, have higher primary energy efficiency, can be operated without noise and vibration, requires less maintenance and repairs, and can be worked with a low temperature source. For the simplest case where single adsorbent bed is included, adsorption heat pumps have advantages since they are zero-operational cost systems. Furthermore, the use of solar and geothermal energy sources in thermal driven heat pumps instead of electrical power which is mainly produced by the heat of fossil fuels is also a significant feature. As a result, the primary energy efficiency of adsorption heat pumps (130-180%) are higher than mechanical heat pumps (90-100%) (Ülkü et al 1987). Additionally, the exchange of adsorbent is not needed in adsorption heat pumps and the lifetime is longer since no corrosive materials are used. Nevertheless, adsorption heat pumps have lower COP than traditional heat pumps, so, the improvements are still required.

2.2. Improvements Performed in the Previous Studies

Although adsorption heat pumps have several advantages over traditional heat pumps, it still requires enhancements due to low COP, SCP and SHP. In order to be an alternative to the traditional heat pumps, COP and SCP of adsorption heat pumps should be 1 and 300-1000 W/kg, respectively. According to the study of Meunier, these COP and SCP values can be satisfied when the optimum values of thermal conductivity, heat transfer coefficient and permeability of the adsorbent bed are of 1 W/m.K, 200 W/m^2.K and 10^{-12} m^2, respectively (Meunier 1993).

In order to reach the requirements given above, several improvement methods were developed in the previous studies. Among them, three methods stepped forth (Demir et al. 2008; Gediz İliş 2012):

- Using advanced adsorption cycles which operate at low temperature sources and increase COP and provide continuous cooling and heating processes.

- Producing new adsorbate-adsorbent pairs or developing available pairs to increase COP and adsorption rate.

- Enhancement of heat and mass transfer by new adsorbent bed designs.

The intermittent behavior of single bed adsorption heat pumps leads to discontinuity of the operation and decrease in the COP value. Thus, advanced adsorption cycles such as heat recovery cycles, mass recovery cycles, thermal wave cycles and multistage and cascading cycles, and hybrid systems have been developed to achieve continuous operation (Meunier 2001; Wang 2001; Sumathy et al. 2003; Demir et al. 2008; Goyal et al., 2016).

In heat recovery cycle two or more adsorbent beds are utilized. Adsorbent bed is also used as heat recoverer in the system. The heat produced during the cooling of adsorbent bed is transferred to the second adsorbent bed to be heated which consists of sensible heat along with heat of adsorption. A schematic view of heat recovery cycle is illustrated in Figure 2.3. The process continuous until both adsorbent beds reach the same temperature. Then, while one adsorber is heated by external heat source, the other is cooled by external heat sink. This type of cycle can also be defined as uniform temperature cycle (Sumathy et al. 2003; Meunier 2001).
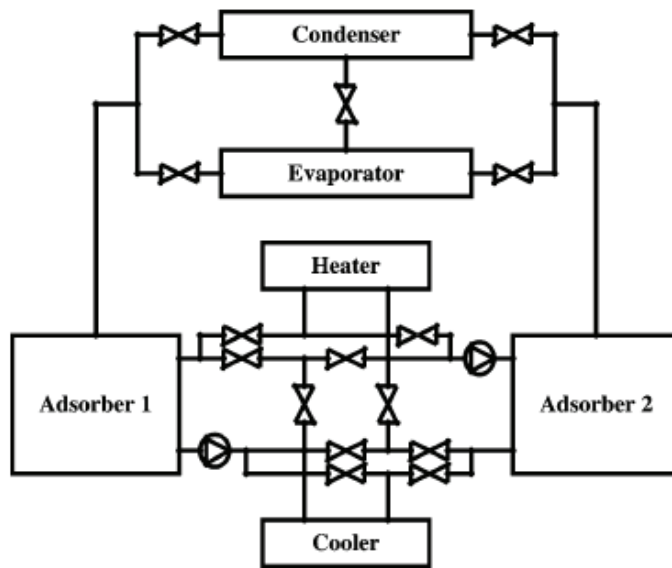
Figure 2.3. Schematic view of heat recovery cycle

(Source: Sumathy et al., 2003)

Cascading cycle, which is also defined as type of uniform temperature cycle (Meunier, 2001), is operated with different working pairs. For instance, in two stages cascading cycle while zeolite-water cycle can be used as high temperature source, activated carbon-methanol pair cycle can be used as low temperature source in heat recovery (Figure 2.4). In the performed studies (Table 2.2), the highest COP values are observed in the cascading cycle.
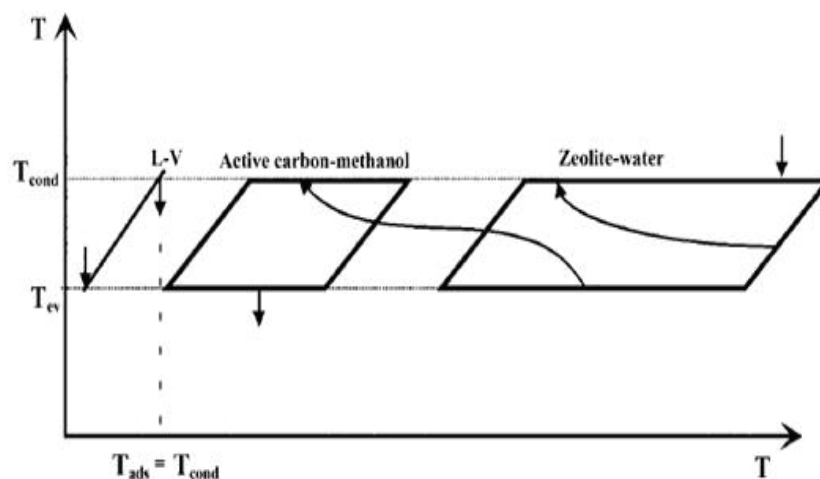
Figure 2.4. Working principle of a cascading cycle

(Source: Meunier 2001)

Mass recovery cycle is achieved by pressurization-depressurization of the adsorbent beds. The adsorbent bed which is at low pressure is pressurized to condensation pressure and the other which is at high pressure is depressurized down to the evaporator pressure. As seen in Figure 2.5, there is a single tube between two beds and vapor is transferring from high pressure bed to low pressure bed by opening valve A. Some researchers combined heat and mass recovery systems to enhance the COP further (see Table 2.2).
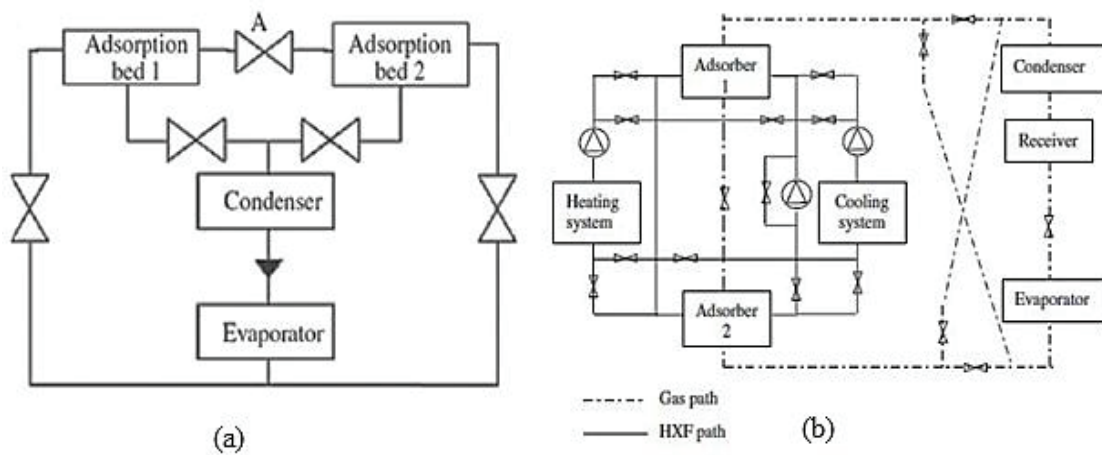
Figure 2.5. a) Mass recovery cycle b) Heat and mass recovery cycle

(Source: Goyal et al. 2016; Leong and Liu 2004)

On the other hand, in thermal wave cycles, it is desired to reduce heat requirement for desorption process by using exothermic heat produced during the adsorption process. The representative cycle is given in Figure 2.6. As seen, the cycle is conducted by circulating a heat transfer fluid between two adsorbent beds. By this way, the adsorption heat obtained in one adsorber can be transferred to the other adsorber to be used in desorption process.

In design of the adsorption heat pump, the selection of the working pair has crucial importance. In addition to the properties of adsorbate such as non-toxicity, availability, corrosiveness and minimum cost, the pair should satisfy the properties that also influence the energy density such as affinity to each other, high adsorption capacity, high thermal conductivity of adsorbent, high mass diffusivity and no loss in performance with repeated cycles. The common adsorbent-adsorbate pairs used in the studies of energy recovery systems are active carbon-methanol, silica gel-water, zeolite-water, and active carbon-ammonia.
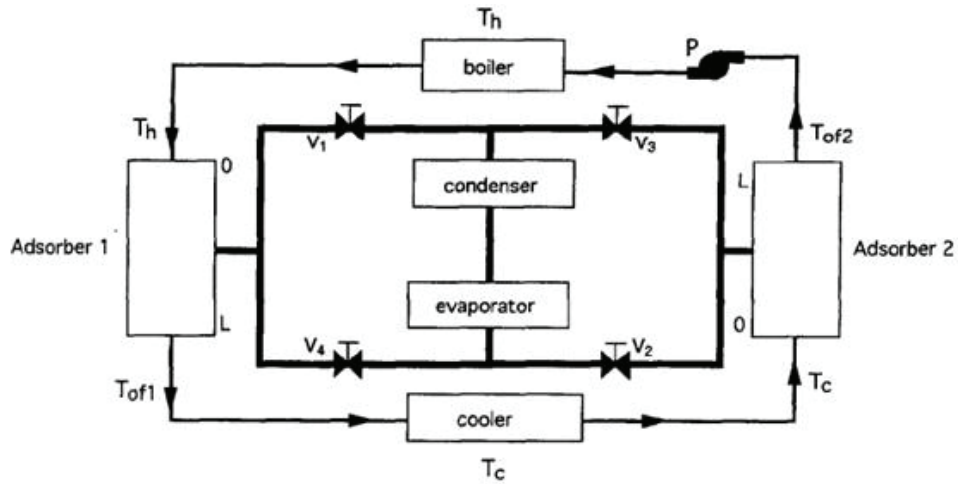
Figure 2.6. Schematic view of thermal wave cycle

(Source: Ben Amar et al., 1996)

In 2005, Anyanwu and Ogueke performed a study with different working pairs (Anyanwu and Ogueke, 2005). As a conclusion, they mentioned that while zeolite-water pair is the best for air-conditioning applications, activated carbon-ammonia was suggested for ice-making, deep freezing, and food preservation applications. Furthermore, maximum cooling COP values were found as 0.3, 0.19 and 0.16 for zeolite-water, activated carbon-ammonia and activated carbon-methanol pairs, respectively.

Unfortunately, low thermal conductivity of these adsorbents limited the applications of adsorption heat pumps. For instance, Demir et al. performed a numerical study in order to investigate the effect of heat and mass transfer in adsorbent bed during an adsorption heat pump cycle. They stated that thermal resistance controlled the mass and heat transfer through the bed (Demir et al. 2011). As a consequence, several researchers started to improve adsorbent bed design to enhance heat and mass transfer properties, thus decrease cycle time. Types of adsorbent beds that design to improve heat and mass transfer were unconsolidated adsorbent beds, coated adsorbent beds and consolidated adsorbent beds (Table 2.3).

The consolidated adsorber design was one of the improvement methods for heat and mass transfer (Eun et al. 2000; Aristov et al. 2002; Wang et al. 2004; Wang et al. 2006; Oliveira et al. 2007; Lu et al. 2007; Li et al. 2010; Jiang et al. 2014; Palomba et al. 2015; Kim et al. 2017). As a result of low adsorption rate of current pairs, advanced adsorbents were produced by researchers in order to increase heat and mass transfer properties of the pairs. Wang et al. described the synthesizing steps for consolidated

adsorbent as: a) adding calcium chloride powders to slurry of expanded graphite and water b) compression molding of well-mixed mixture c) removing of water to obtain consolidated composite adsorbent (Wang et al. 2006). Eun et al. used composite blocks that was obtained by mixing silica gel powders with graphite powders in their study. They reported that while the silica gel packed bed had a thermal conductivity of 0.17 W/mK,

Table 2.1.Comparison of Advanced Cycles

Researcher	Purpose	Advanced Cycle	Working Pair	Operation Temperature (°C)	COP	SCP/SHP (W/kg)	Remarks
Douss et al. (1988)	Cooling/ Heating	Heat recovery (uniform temperature) cycle	NaX-water	60-200	0.673/ 1.56	-	For intermittent cycle $COP_{cooling}$ was 0.524 and $COP_{heating}$ was 1.38.
Douss and Meunier (1989)	Cooling/ Heating	Cascading adsorption cycle	Zeolite-water	105-200	1.06/ 1.78	37/ 62	-
			Active carbon-methanol	30-100			
Miles and Shelton (1996)	Cooling/ Heating	Thermal wave cycle	Active carbon-ammonia	35-232	0.76/ 1.59	-	-
Ben Amar et al. (1996)	Cooling	Thermal wave cycle	NaX-water AX21-ammonia	40-220	1.07 0.99	~150 ~200	-
Wang et al. (2000)	Ice Making	Hybrid system	Activated carbon-methanol	20-81	0.144	-	10 kg ice /day was achieved.
Wang (2001)	Refrigeration	Heat and mass recovery cycle	Active carbon-methanol	30-100	~0.6	-	-
Critoph (2001)	Refrigeration	Multiple bed Regenerative Cycle	Active carbon-ammonia	30-200	0.6	142	Cycle time was 864 seconds.

Table 2.1. (cont.)

Researcher	Purpose	Advanced Cycle	Working Pair	Operation Temperature (°C)	COP	SCP/SHP (W/kg)	Remarks
Zhang and Wang (2002)	Refrigeration	Hybrid system	Active carbon-methanol	25-160	0.34* 0.18	17.6	-
Chahbani et al. (2004)	Refrigeration	Thermal wave cycle	Carbon-ammonia	40-257	0.86	181	When D_s/r_p^2 decreased from 1 to 10^{-3}, COP reduced to 0.48 and SCP decreased to 108 W/kg.
Akahira et al. (2004)	Refrigeration	Mass recovery cycle	Silica gel-water	30-70	0.46	-	Without heating/cooling process, 5.8 kW cooling capacity was achieved.
Leong and Liu (2004)	Refrigeration	Heat and Mass recovery	Silica gel-water	45-200	0.65	27.6	-
Wang et al. (2005a)	Chilling	Heat recovery cycle	Silica gel-water	29.4-85	0.46	-	-
Wang et al. (2005b)	Chilling	Mass recovery cycle	Silica gel-water	31-85	0.65	126	For the evaporation temperature of 20°C, 12.6 kW cooling capacity was achieved.
Oliveira et al. (2006)	Ice making	Mass recovery cycle	Active carbon-ammonia	30-115	0.10	-	Although maximum COP was obtained at regeneration temperature of 115°C, maximum ice production was obtained at regeneration temperature of 85°C.

(cont. on next page)

Table 2.1. (cont.)

Researcher	Purpose	Advanced Cycle	Working Pair	Operation Temperature (°C)	COP	SCP/SHP (W/kg)	Remarks
Liu and Leong (2006)	Refrigeration	Cascading adsorption cycle	Zeolite-water	100-200	1.35	42.7	-
			Silica gel-water	30-90			
Khan et al. (2007)	Chilling	Mass recovery cycle	Silica gel-water	30-90	~0.7	110	-
Li and Wu (2009)	Chilling	Hybrid system	Silica gel-water	30-85	0.44	-	Gas engine generator with 16 kW generating capacity and two bed chillers with cooling capacity of 10 kW was consisted.
Deshmukh et al. (2015)	Refrigeration	Multiple bed adsorption cycle	Silica gel-water	30-95	0.62	15.63	Cooling capacity achieved with three adsorber system was 0.8 kW for 24h and could generate an average refrigerant of 29 kg/day with a cycle time of 6 h.
Chekirou et al. (2016)	Refrigeration	Heat recovery cycle	AC 35-methanol	30-125	0.682	-	COP value without heat recovery was given as 0.483.

the thermal conductivity of these blocks was 10-20 W/m.K depending on the graphite bulk density in the block (Eun et al. 2000). However, Ilis indicated that although the adsorption rate was increased, the enhanced adsorbent may not be suitable for adsorption heat pump for given conditions and showed that while one condition is satisfied by the developed adsorbent, other properties may be failed. For instance, in that study, MIL101(Cr)@G05 had the best SCP for the volume of the bed, it had the worst COP when compared to FAM Z01, FAM Z02 and NH2-MIL 125 (Ti) (Ilis 2017).

Another improvement method was coating of adsorbent on a metal fin or a tube. The coating could be performed by two methods. The first one was crystallization of adsorbent directly on the metal support (Tatlıer and Şenatalar 1999; Bauer et al. 2009; Schnabel et al. 2010; Atakan et al. 2013; Bonaccorsi et al. 2013; Tatlıer et al. 2014). In this technique, the heat transfer at the interface of the metal and adsorbent layer was improved significantly due to the nearly perfect contact and mass transfer resistance was reduced due to the thin layer of adsorbent. Unfortunately, the method was expensive and has limitations due to the physical and chemical interactions between metal and adsorbent (Bonaccorsi et al. 2013).

The second method of coating was binder-based coating (Restuccia et al. 2002; Dawoud et al. 2007; Freni et al. 2013; Dawoud 2013; Freni et al. 2015). In this method, firstly, the metal support plunged into an aqueous solution including adsorbent powder and an inorganic or organic binder. Then, thermal treatment was performed to stabilize the adsorbent. As in direct coating method, while heat and mass transfer are enhanced, it had some drawbacks such as poor mechanical strength, generation of volatile compounds from organic binders and blockage of the pores of adsorbent by the binder (Freni et al. 2015). Dawoud investigated two types adsorber: extruded finned-tube heat exchanger and finned-plate exchanger with different thickness of zeolite layer. In that study, it was concluded that while thickness of zeolite layer increased the COP value, it lowered the the rate of adsorption which was compatible with the study of Restuccia et al. (Restuccia et al. 2002; Dawoud 2013).

On the other hand, in the design of unconsolidated adsorber, the pellet, granule or fibre adsorbent added inside the heat exchanger or metal additives are included without any binder (Gui et al. 2002; Demir et al. 2010; Ilis et al. 2011; Umair et al. 2016; Radu et al. 2017). In the study of Demir et al., they used stainless steel, copper, aluminium and

brass (40% zinc, 60% copper) as metal additives and investigate the effect these metals on the thermal conductivity and diffusivity of adsorbent bed. The adsorbent was chosen as silica gel and adsorbate was water vapor. They used two different size of additives by assuming that the shape of additives did not have significant effect on the mass diffusivity, and they concluded that addition of 15wt% aluminium pieces with sizes between 1.0 and 2.8 mm increases the effective thermal diffusivity and conductivity of silica gel bed by 157% and 242%, respectively (Demir et al. 2010). Furthermore, in the numerical study of Ilis et al., it was observed that if the ratio of the mass diffusivity of adsorbate in the particle to the thermal diffusivity throughout the adsorbent bed is low, the use of fins in the adsorbent bed would not increase the heat transfer rate significantly (Ilis et al. 2011).

In addition to these adsorbent bed designs, Demir constructed a microwave regenerated adsorbent bed. In that performed study, he used zeolite 4A-water pair and worked in the temperature range of 40-110°C. The obtained COP value was 0.81 for a cycle time of 35 min. However, due to the long period of isosteric cooling and adsorption processes, the maximum SCP value was 3.6 W/kg (Demir 2013a). In another study, Demir used silica gel instead of zeolite and obtained COP and SCP values of 1.13 and 7.24 W/kg, respectively (Demir 2013b).

While the studies on the enhancement of adsorption heat pumps were conducted, manufacturing of adsorption heat pumps under the name of adsorption chiller was continued at the countries such as USA, Japan, China, and Germany. The COP values of adsorption chillers produced in Germany were in the range of 0.5-0.6 and cooling capacity is 7.5 kW. In addition, the adsorption chiller which was manufactured by the HIJC company in USA had a cooling capacity of 150.15 kW with a COP value of 0.7. In the production of these adsorption chillers, silica gel-water and active carbon-methanol pairs were generally used.

Table 2.2. Improvements performed in literature for Adsorption Heat Pumps

Researcher	Adsorber Type	Purpose	Working Pair	Operation Temperature (°C)	λ_{eff} (W/mK)	D_{eff} (m²/s)	COP	SCP/ SHP (W/kg)
Poyelle et al. (1999)	Consolidated	Cooling	Graphite/zeolite composite-water	40-240	5-10	9×10^{-11}	0.41	97
Tatlier et al. (1999)	Direct coating	Heating Cooling	Zeolite 4A-water	20-150	-	-	-	-
Eun et al. (2000)	Consolidated	Heating Cooling	Graphite/silica gel composite-water	-	10-20	-	-	-
Gui et al. (2002)	Unconsolidated	Air conditioning	Active carbon-methanol	8-120	-	-	1.40	409
Aristov et al. (2002)	Consolidated	Air conditioning	SWSs-water	55-150 40-150	-	-	1.65* 0.8	-
Restuccia et al. (2002)	Binder-based coating	Air conditioning	Zeolite	50-200	0.80	-	-	1557
Wang et al. (2003)	Consolidated	Refrigeration	Active carbon-methanol	30-120	0.27-0.34	-	0.104	13.1
Liu and Leong (2005)	Unconsolidated	Cooling	Zeolite 13X-water	40-200	0.20	-	0.43	50
Hamamato et al. (2006)	Consolidated	Refrigeration	FX 400 methanol / KF 1000-methanol	30-85	-	-	~0.6 ~0.75	-
San (2006)	Unconsolidated	Cooling	Active carbon-methanol	30-90		$1.4\text{-}5.6 \times 10^{-10}$	~0.5	~388
Wang et al. (2006a)	Unconsolidated	Air conditioning	Zeolite 13X-water	40-450	-	-	~0.22	~200

(cont. on next page)

Table 2.2. (cont.)

Researcher	Adsorber Type	Purpose	Working Pair	Operation Temperature (°C)	λ_{eff} (W/mK)	D_{eff} (m²/s)	COP	SCP/ SHP (W/kg)
Wang et al. (2006b)	Consolidated	Ice making	Graphite/CaCl$_2$-water	30-150	6.5-9.8	-	0.41	640
Lu et al. (2007)	Consolidated	Ice making	CaCl$_2$/activated carbon-ammonia	30-126	-	-	0.3	495
Aristov et al. (2008)	Consolidated	Heating Cooling	SWS 1L-water	30-100	-	-	-	750-1900
Bauer et al. (2009)	Direct coating	Refrigerating	Zeolite/aluminium-water	30-85	-	-	~0.6	~560
Li et al. (2010)	Consolidated	Refrigerating	Graphite/CaCl$_2$-NH$_3$	-	-	-	0.27	422
Demir et al. (2010)	Unconsolidated	Heating Cooling	Silica gel-water	-	0.363 0.324 0.327	-	-	-
Chan et al. (2012)	Consolidated	Cooling	Zeolite 13X/CaCl$_2$-water	40-75			0.76	18.4
			Zeolite 13X-water	40-200	-	-	0.42	13.7
Dawoud (2013)	Binder-based coating	Heating	Zeolite-water	35-90	-	-	1.24	-
Demir (2013)	-	Cooling	Zeolite 4A-water	40-110	-	-	0.81	3.6
Tatler et al. (2014)	Direct coating	Cooling	NaA-water	40-95	-	-	-	-
Tso et al. (2015)	Consolidated	Cooling	Zeolite 13X/CaCl$_2$-water	30-90	-	-	0.16	106

(cont. on next page)

Table 2.2. (cont.)

Researcher	Adsorber Type	Purpose	Working Pair	Operation Temperature (°C)	λ_{eff} (W/mK)	D_{eff} (m²/s)	COP	SCP/ SHP (W/kg)
Graf et al. (2016)	Unconsolidated	Chilling	Silica gel 123-water	35-90	-	-	0.51	268
Trisupakitti et al. (2016)	Consolidated	Cooling	Metal impregnated zeolit 4A-water	30-225	-	-	0.56	-

CHAPTER 3

ADSORPTION PHENOMENA

In this chapter, the details of the adsorption are explained. The adsorption equilibrium models are summarized. Furthermore, the kinetic models used to evaluate mass transfer rate through an adsorbent are also involved in this part.

3.1. Adsorption

Adsorption phenomena can be defined as the atomic and molecular interactions that occurs at solid-fluid interface. According to the interactions between the solid and the fluid, two types of adsorptions, physisorption and chemisorption, may take place (Table 3.1).

Table 3.1. Differences between physical and chemical adsorption processes

(Source: Ruthven 1984)

PHYSISORPTION	CHEMISORPTION
Nonspecific interactions	Specific interactions
Low heat of adsorption (5-50 kJ/mol)	High heat of adsorption (40-800 kJ/mol)
Reversible	Irreversible
Monolayer or multilayer	Only monolayer
Occurs with polarization of adsorptive molecules	Electrons transfer due to bond formation between adsorptive and adsorbent surface

3.1.1. Adsorption Equilibria

Adsorption equilibrium can be described as the amount of adsorbate adsorbed by unit mass of adsorbent at specific temperature and pressure at equilibrium. Surface characteristics of the adsorbent, working temperature and pressure, thermophysical properties of the adsorbent and adsorbate concentration can affect the amount of adsorbate adsorbed on the adsorbent at equilibrium (Gediz-İliş 2012; Gundogan-Sayılgan 2013).

In order to define the relationship between the amount of adsorbate adsorbed on the adsorbent at equilibrium, several models have been reported with different assumption (Table 3.2). For instance, Langmuir relationship fulfil the requirement of Henry's law and saturation limits. However, the heat of adsorption is considered as independent of adsorbate loading and isosteric heat of adsorption is directly equal to the heat of adsorption value in this relationship. This assumption restricts the use of the model since isosteric heat of adsorption generally depends on the adsorbate loading in real systems.

Sips (Langmuir-Freundlich) relationship which is an empirical model does not have proper Henry's law limit. On the other hand, it has corrected saturation limit and the isosteric heat of adsorption is assumed to be dependent on adsorbate loading. Similar with Sips relationship, the adsorbate loading dependence of isosteric heat of adsorption is also taken into consideration in Toth's relationship. Furthermore, it also has proper Henry's law and saturation limits.

Ülkü used clinoptilolite-water pair for energy storage and heat pump applications and define the equilibrium relationship with experimental correlations (Ülkü 1986). Furthermore, the decrease of isosteric heat of adsorption with increasing adsorbate loading was also mentioned in the study.

On the other hand, silica gel-water (type A and type RD) pair and was used in the study of Chua et al (Chua et al. 2002). In that study, they used Toth's relationship to define the adsorption equilibria. The monolayer capacities of silica gel type A-water and silica gel type RD-water pairs were determined as 0.4 and 0.45 kg_w/kg_s, respectively. In 2018, Gabrus et al. studied dewatering aliphatic alcohols in temperature swing adsorption process (Gabrus et al. 2018). In that study, they used zeolite 3A and 4A and investigate the adsorption equilibrium behavior of these zeolites with water vapor. They observed that while adsorption of water vapor can be illustrated with statistical thermodynamic adsorption equilibrium model, Toth's model was better for zeolite 4A-water pair.

In the study of Cakıcıoglu-Ozkan and Ulku, adsorption of water vapor on acid-treated clinoptilolite was investigated. They obtained Type I isotherm and stated that Dubinin-Radushkevich relationship defined the equilibrium data better than Langmuir relationship for acid-treated zeolite-water pair (Cakıcıoglu-Ozkan and Ulku 2005). Saha et al. also used Dubinin-Radushkevich relationship to define adsorption equilibrium for active carbon fibre-ethanol pair (Saha et al. 2007).

Gundogan-Sayılgan et al. investigated adsorption of water vapor on zeolite 13X by a homemade volumetric system (Gundogan-Sayılgan et al. 2016). In that study, Type

I isotherm was obtained, and the experimental data was well fitted to Langmuir Relationship. The effect of adsorption and desorption temperature on the adsorption isotherm was also examined in that study.

On the other hand, instead of traditional adsorption equilibrium models and relationships, there are alternative models used in literature to illustrate the adsorption equilibria of zeolites (Table 3.2) such as Hill's, Aranovich-Donohue, Frenkel-Halsey-Hill and statistical thermodynamic adsorption models (Hill 1960; Wang and LeVan 2009; Liano-Restrepo and Mosquera 2009; Kim et al. 2016).

Table 3.2. Adsorption Equilibrium Models in Given in the Literature

MODEL	ASSUMPTIONS	EQUATION	REFERENCES	REMARKS
Henry's Law	-All adsorbate molecules are isolated from their neighbors at low pressure of adsorptive	$q = KP$	Yucel and Ruthven 1980; Ruthven 1984; Suzuki 1990; Valsaraj and Thibodeaux 1999)	
Langmuir Relationship	-The surface is homogenous -Heat of adsorption is independent of surface coverage -Monolayer coverage is observed -Adsorption rate is equal to desorption rate	$q = q_s \dfrac{bP}{1+bP}$ $b(T) = b_\infty \exp\left(\dfrac{Q}{RT}\right)$	Hall et al. 1966; Parfitt 1978; Gregg and Sing 1982; Ruthven 1984; Do et al. 1992; Kim et al. 2003; Hamamoto et al. 2006; Cansever-Erdogan and Ülkü 2011	*This model has proper Henry's law limit. *Isosteric heat of adsorption equals the heat of adsorption and independent of adsorbate loading
Dubinin-Radushkevich Relationship (semi-empirical)	-It is based on Polyani potential theory	$q = q_0 \exp\left[-\gamma \left(T\ln\dfrac{P^{sat}}{P}\right)^2\right]$	Gregg and Sing 1982; Ülkü and Mobedi 1989; Lavanchy et al. 1996; Jaroniec 1997; Teng et al. 1996; Sumathy et al. 2003; Cakicioglu-Ozkan and Ulku 2005	*Generally applicable for adsorption on microporous adsorbents
Dubinin-Astakhov Relationship	-Same with D-R relationship except the "n"	$q = q_0 \exp\left[-D \left(T\ln\dfrac{P^{sat}}{P}\right)^n\right]$	Wang et al. 1999; Sumathy et al. 2003; Dieng and Wang 2001; Clausse et al. 2009;	*Surface heterogeneity is high (n>2)

(Cont. on next page)

24

Table 3.2 (Cont.)

MODEL	ASSUMPTIONS	EQUATION	REFERENCES	REMARKS
Modified Dubinin-Astakhov Relationship	-Same with D-R relationship	$q=q_0\exp\left[-K\left(\frac{T_z}{T^{sat}}-1\right)^n\right]$	TamainotTelto and Wang et al. 2009	*Surface heterogeneity is high (n>2)
Experimental Correlations	-The difference in the heat capacity of the adsorbate in the adsorbed and vapor phase is neglected	$\ln P=a(q)+\dfrac{b(q)}{T}$ $a(q)=a_0+a_1q_1+a_2q^2+a_3q^3$ $b(q)=b_0+b_1q_1+b_2q^2+b_3q^3$	Ülkü 1986; Ülkü et al. 1986a; Mobedi 1987; Cacciola and Restuccia 1995; San and Lin 2008	
Three-term Langmuir Relationship	-There are two or three sites for adsorption with energy of adsorption constant at each site	$q=\dfrac{q_{s1}b_1P}{1+b_1P}+\dfrac{q_{s2}b_2P}{1+b_2P}+\dfrac{q_{s3}b_3P}{1+b_3P}$	Sun et al. 1995; Ben Amar et al. 1996; Liu and Leong 2005; Clausse et al. 2009	
Heterogeneous Langmuir Relationship	-The adsorbent surface acts as a patchwork of numerous, discrete homogeneous adsorption sites	$q=\displaystyle\sum_{n=1}^{m}\dfrac{q_{s,n}b_nP}{1+b_nP}$	Ladshaw et al. 2015	
Volmer Relationship	-Adsorbed molecules are mobile on adsorbent surface -There is no interaction between adsorbed molecules	$bP=\dfrac{\theta}{1-\theta}\exp\left(\dfrac{\theta}{1-\theta}\right)$	Ruthven 1984; Do 1998	

(Cont. on next page)

Table 3.2 (Cont.)

MODEL	ASSUMPTIONS	EQUATION	REFERENCES	REMARKS
Freundlich Relationship (empirical)	- Surface is heterogeneous with a non-uniform distribution of adsorption energy -Sites having the same adsorption energy are gathered into one patch -There is no interaction between patches -On each patch, one adsorbate molecule can be adsorbed onto only one adsorption site	$q=KP^{1/n}$	Gray and Do 1992; Cho and Kim 1992; Do 1998; Afonso and Silveria 2005; Liu and Leong 2006; Gerente et al. 2007; Leppäjärvi et al. 2012	*n is related with the heterogeneity and greater than unity. *This model does not have a proper Henry law behavior at low pressure, and it does not a finite limit when pressure is sufficiently high
Sips (Langmuir-Freundlich) Relationship (empirical)		$q=q_s\dfrac{(bP)^{1/n}}{1+(bP)^{1/n}}$ $b(T)=b_\infty\exp\left(\dfrac{Q}{RT}\right)$ $Q=(-\Delta H)_{\theta=1/2}$	Do 1998; Gaeini et al. 2016	*Unlike Freundlich isotherm, it has finite limit when pressure is sufficiently high. Same with Freundlich, it does not have a correct Henry law limit. *Isosteric heat takes a value infinity at zero loading and minus infinity at saturation.

(Cont. on next page)

26

Table 3.2 (Cont.)

MODEL	ASSUMPTIONS	EQUATION	REFERENCES	REMARKS
Toth's Relationship (empirical)		$$q = q_s \frac{bP}{\left[1+(bP)^t\right]^{1/t}}$$	Do 1998; Chua et al. 2003; Kim et al. 2002; Wang et al. 2009; Leppäjärvi et al. 2012	*It has proper Henry's law limits when pressure approaches either zero or infinity. *t characterizes heterogeneity of the system and smaller than unity. *Isosteric heat takes a value infinity at zero loading and minus infinity at saturation.
Hill-de Boer Relationship	-Adsorbed molecules are mobile on adsorbent surface -There is a lateral interaction among adsorbed molecules	$$bP = \frac{\theta}{1-\theta} \exp\left(\frac{\theta}{1-\theta}\right)\exp(-c\theta)$$ $$c = \frac{2a}{RT\sigma_0} = \frac{zw}{RT}$$	Do 1998	
Fowler-Guggenheim Relationship	-There is a lateral interaction among adsorbed molecules	$$bP = \frac{\theta}{1-\theta}\exp(-c\theta)$$	Do, 1998	
Unilan Relationship	-Surface of adsorbent is patch wise -Each patch is ideal -Energy distribution is uniform	$$q = \frac{q_s}{2s}\ln\left(\frac{1+\bar{b}e^{s}P}{1+\bar{b}e^{-s}P}\right)$$	Do, 1998	

Table 3.2 (Cont.)

MODEL	ASSUMPTIONS	EQUATION	REFERENCES	REMARKS
Jovanovich Relationship		$q=q_s\left(1-e^{-bP}\right)$ $$b(T)=b_\infty\exp\left(\frac{Q}{RT}\right)$$	Do, 1998; Saadi et al. 2015	-Applicable to mobile and localized adsorption
Fritz-Schlunder Relationship		$q=q_s\dfrac{AP^\alpha}{C+BP^\beta}$	Fritz and Schlunder 1974; Subramanyam and Ashutosh 2012	
Radke-Prausnitz Relationship	-Adsorbed molecules are ideal solution	$q=q_s\dfrac{bP}{1+bP^{1-\beta}}$	Radke and Prausnitz 1972; Largitte and Pasquier 2016	*β<1
Redlich-Peterson Relationship		$q=\dfrac{AP}{1+BP^n}$	Kumar and Sivanesan 2006; Tolazzi et al. 2018	
S-type Isotherm	-s numbers of adsorbate molecules are adsorbed on each adsorbent site	$q=q_s\dfrac{K(P/P_s)^m}{1+(K-1)(P/P_s)^m}$	Sun and Chakraborty, 2014; Teo et al., 2017	
Modified Langmuir Relationship	-Different zones are identified by the functional adsorbent surface according to binding energy of surface atoms -The binding energy of each surface atom is independent of surrounding atoms	$q=q_s\dfrac{\beta\left(\frac{P}{P_s}\right)\exp\left\{\frac{\phi_m}{RT}\left\{1-\left(\frac{P}{P_s}\right)^n\right\}+z\right\}}{1+\left(\frac{P}{P_s}\right)\exp\left\{\frac{\phi_m}{RT}\left\{1-\left(\frac{P}{P_s}\right)^n\right\}+z\right\}}$	Chakraborty and Sun 2014	

(Cont. on next page)

Table 3.2 (Cont.)

MODEL	ASSUMPTIONS	EQUATION	REFERENCES	REMARKS
Hill's model	-Adsorbent is a macroscopic system of m statistical subsystems that are equivalent, noticeable, and statistical independent	$q = q_s \dfrac{1}{m}\left[\dfrac{\sum_{n=0}^{m} n q_n \lambda_a^n}{\sum_{n=0}^{m} q_n \lambda_a^n}\right]$	Hill 1986; Llano-Restrepo and Mosquera 2009	
Generalized Statistical Thermodynamic Relationship	-Adsorbent is a macroscopic system of m statistical subsystems that are equivalent, noticeable, and statistical independent -Adsorptive behaves as ideal gas	$q = q_s \dfrac{1}{m}\left[\dfrac{\sum_{n=1}^{m} n K_n P^n}{1+\sum_{n=1}^{m} K_n P^n}\right]$	Llano-Restrepo and Mosquera 2009; Ladshaw et al. 2015	
Universal Adsorption Isotherm Relationship	-An agglomeration of numerous homogenous patches with same energy level are related with the heterogeneous surfaces of adsorbent	$\theta = \displaystyle\sum_{i=1}^{n} \alpha_i \left\{ \dfrac{\left(\dfrac{P}{P_s}\exp\left(\dfrac{\varepsilon_{oi}}{RT}\right)\right)^{\frac{RT}{mi}}}{1+\left(\dfrac{P}{P_s}\exp\left(\dfrac{\varepsilon_{oi}}{RT}\right)\right)^{\frac{RT}{mi}}} \right\}_i$	Ng et al. 2017; Burhan et al. 2018	
Fractional Polynomial Equation (Empirical)		$q = \dfrac{a_0+a_1 A+a_2 A^2+a_3 A^3}{1+a_4 A+a_5 A^2+a_6 A^3}$ $A = R_{ads} T \ln\left(\dfrac{P_{sat}}{P}\right)$	Semprini et al. 2017	
Langmuir-Jovanovic Relationship		$q = \dfrac{rP}{1+P}\left(1-e^{-bpz}\right)$	Shahbeig et al. 2013	

3.1.1.1. Heat of Adsorption

The spontaneous behavior of adsorption process and energy loss of the adsorption molecules during the adsorption process causes the enthalpy of the adsorption process to be negative, generally. The heat released from the system is named as heat of adsorption.

The heat of adsorption value depends on the surface coverage, temperature, and pressure. According to the value of the heat of adsorption, the interactions between solid-fluid phases and the desorption conditions can be estimated.

The heat of adsorption can be defined in three ways: the differential heat of adsorption, the integral heat of adsorption and the isosteric heat of adsorption. In an isolated system, the heat released during the adsorption process is known as differential heat of adsorption. Differential heat of adsorption value can be evaluated by measuring the amount of heat released upon a small amount of adsorbate is adsorbed at constant temperature (Eq 3.1) and can be measured by using Calvet calorimeter (Ostrovskii 2002; Ülkü et al. 2006; Garcia-Cuello et al. 2009).

$$\Delta_a\dot{h} = -\left(\frac{\partial Q}{\partial n_a}\right)_T + V\left(\frac{\partial P}{\partial n_a}\right)_T \tag{3.1}$$

where Q is heat released during the adsorption process, n_a is the adsorbate loading, P is the adsorptive pressure and V is the volume of the gas phase.

In the simplest case, the integral heat of adsorption can be defined as the total heat evolved from initial state to final state of adsorption. By taking integral of Eq 3.1, the integral heat of adsorption can be calculated as follows:

$$\Delta_a H = \int_0^{n_a} \Delta_a\dot{h} \, dn_a \tag{3.2}$$

On the other hand, when the adsorption reaches an equilibrium state, the chemical potential, which can be defined in terms of the Gibbs free energy, of the adsorbed and adsorptive phases are equal. By applying ideal gas equation of state, the thermodynamic relationship takes the form given in Equation 3.3 since the volume of the adsorptive phase is greater than the adsorbed phase.

$$\left(\frac{dlnP}{dT}\right)_{n_a} = -\frac{\Delta_a\dot{s}}{RT} = -\frac{\Delta_a\dot{h}}{RT^2} \tag{3.3}$$

When Equation 3.3 is rearranged, Clausius-Clapeyron equation is obtained (Eq 3.4) and q_{st} is known as isosteric heat of adsorption. Although isosteric heat of adsorption is considered as independent of adsorbate loading in Langmuir relationship, it decreases with increasing adsorbate loading in many systems due to the heterogeneity of the surface and interactions between molecules.

$$\left(\frac{dlnP}{d(-1/T)}\right)_{n_a} = -\frac{\Delta_a\dot{h}}{R} = \frac{q_{st}}{R} \tag{3.4}$$

3.1.2. Adsorption Kinetics

The transfer of an adsorbate molecule from the bulk phase to the adsorption sites occurs in five steps (Figure 3.1). When the bulk fluid phase is uniform, which means that there is no concentration gradient through the adsorptive, bulk diffusion cannot be considered as the rate limiting. Then, the adsorption kinetics may be controlled by one or more of the following resistances: diffusional resistance in external fluid film on the particle surface, diffusional resistance in the meso and macropores, a possible barrier to mass transfer at the external surface of the microparticle (skin resistance), and diffusional resistance in the micropores within the microparticles.

As a result of heat released during the adsorption process and heat transfer rate, temperature gradient may occur both through the adsorbent particle, and between adsorbent particle and the surrounding fluid during the adsorption processes. In general, heat transfer by conduction within the particle is assumed to be greater than heat transfer by convection at the external surface of the particle. This assumption is mainly based on the definition of a dimensionless Biot number (Eq 3.5).
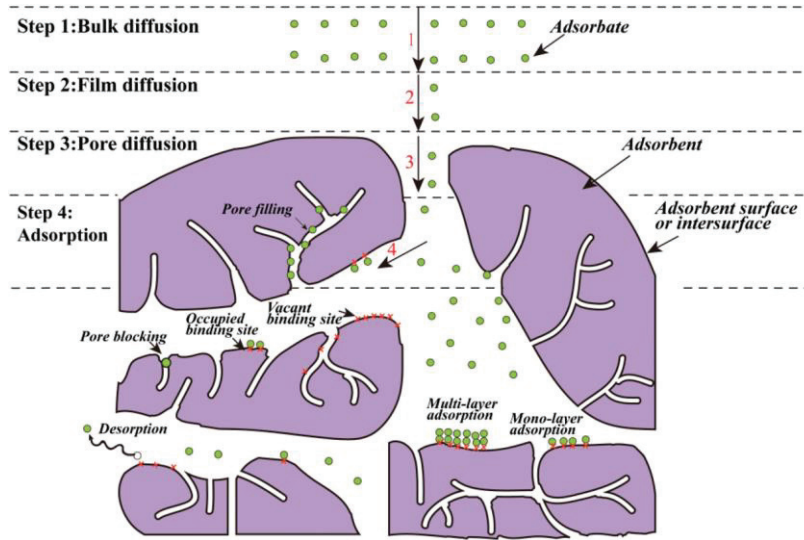
Figure 3.1.Diffusional resistances involved in adsorption kinetics

$$Bi_h = \frac{hr_p}{3k_a} = \frac{Nu}{6} \frac{k_v}{k_a} \qquad (3.5)$$

where h is heat transfer coefficient, k_a is thermal conductivity of adsorbent, k_v is thermal conductivity of vapour, r_p is the adsorbent particle radius and Nu is the Nusselt number.

$$Nu = 2.0 + 1.1Pr^{1/3}Re^{0.6} \qquad (3.6)$$

where Pr is the Prandtl number and Re is the Reynolds number. As seen in equation 3.6, Nusselt number is always greater than 2 and $k_v/k_a \sim 10^{-2}$-10^{-3} for gaseous systems, so it is clear that at any acceptable Reynolds number $Bi_h \ll 1$ illustrating that the temperature within the particle is uniform and external resistance is the rate-controlling mechanism (Ruthven, 1984; Ülkü and Mobedi, 1989).

However, the relative importance of internal and external resistances for mass transfer is opposite. In general, the concentration gradient within the particle is greater than the concentration gradient at the external surface of the particle. The definition of Biot number for mass transfer can be given as:

$$Bi_m = \frac{k_f r_p}{3\varepsilon_p D_p} = \frac{Sh}{6} \frac{D_m}{\varepsilon_p D_p} \qquad (3.7)$$

where k_f is the external mass transfer coefficient, r_p is the particle radius, ε_p is the total porosity of the adsorbent particle, D_p is the pore diffusivity and D_m is the molecular diffusivity in gas phase.

$$Sh=2.0+0.6Sc^{1/3}Re^{1/2} \tag{3.8}$$

where Sc is the Schmidt number. Since Sh≥2 (Eq 3.8) and $D_p \leq D_m/\tau$, then for practical purposes Eq 3.7 becomes $Bi_m > \tau/3\varepsilon$. For the limiting case, Bi_m number would be approximately equal to 3 indicating that there exists concentration gradient within the particle and intraparticle diffusion resistance is rate-controlling step (Ruthven 1984; Ülkü and Mobedi 1989).

Furthermore, when heat and mass transfers are simultaneously occurred, another dimensionless number (Eq 3.9), Lewis number which is the ratio of thermal diffusivity, α, to mass diffusivity, D, is defined.

$$Le=\frac{Sc}{Pr}=\frac{\alpha}{D} \tag{3.9}$$

In order to design an adsorption system, mass transfer controlling mechanism of through the adsorbent should be well evaluated. Karger and Ruthven classified adsorption kinetics in batch systems depending on different parameters such as heat transfer rate, linearity of adsorption equilibrium relationship, controlling mass transfer resistance and boundary conditions at the particle surface (Karger and Ruthven 1992).

In most of the studies, the adsorption process is assumed to be isothermal. However, heat released during the adsorption process, and it cannot be drawn away from the adsorbent as fast as it is generated in conventional systems. As a result, temperature of the adsorbent increases at the beginning of adsorption, reaches a maximum level and then reduces to the initial temperature value when the equilibrium has been achieved. This situation generally occurs due to the temperature dependence of equilibrium adsorbate concentration and diffusivity (Sircar and Kumar 1984; Ruthven 1984). Ruthven stated that although the temperature dependency of diffusivity would be ignored by decreasing the step size of the concentration step over which the uptake curve was determined, the temperature dependency of adsorbed amount was independent of step size (Ruthven 1984).

In order to describe the isothermal and non-isothermal sorption, several models have been derived (Table 3.3). While Fickian diffusion model is generally used in describing the mass transfer in adsorbent particle, linear driving force model is also used due to the simplicity and giving approximate solution. The general assumptions used in describing mass transfer through the particle are:

- The shape of the particle is spherical.
- The initial concentration of adsorbate in the solid is zero.
- The initial concentration of adsorptive is constant.

Table 3.3. Adsorption Kinetics Models (Ruthven 1984)

Assumptions	Model	Boundary Conditions
-Isothermal adsorption -Linear System (q*=KC) - External fluid film or surface resistance control	$$\frac{d\bar{q}}{dt}=\frac{3k_f}{KR_p}\left(q^*-\bar{q}_\infty\right)$$ $$\frac{\bar{q}}{q_\infty}=1-\exp\left[-\frac{3k_f t}{KR_p}\right]$$	t<0, C=q=0 t>0, C=C$_\infty$=q$_\infty$/K
-Isothermal adsorption -For all equilibrium relationships -Micropore diffusion control -Step change followed by constant adsorptive concentration	$$\frac{\partial q}{\partial t}=D_c\left(\frac{\partial^2 q}{\partial r^2}+\frac{2}{r}\frac{\partial q}{\partial r}\right)$$ $$\frac{m_t}{m_\infty}=\frac{\bar{q}-q_0}{q_\infty-q_0}=1-\frac{6}{\pi^2}\sum_{n=1}^\infty\frac{1}{n^2}\exp\left(-\frac{n^2\pi^2 D_c t}{r_c^2}\right)$$	t<0, C=C$_0$, q=q$_0$ t≥0, C=C$_\infty$, q(r$_c$, t)=q$_\infty$ $\left(\frac{\partial q}{\partial r}\right)_{r_c=0}=0$ for all t
-Isothermal adsorption -For all equilibrium relationships -Micropore diffusion control -Step change followed by time varying concentration	$$\frac{\partial q}{\partial t}=D_c\left(\frac{\partial^2 q}{\partial r^2}+\frac{2}{r}\frac{\partial q}{\partial r}\right)$$ $$\frac{m_t}{m_\infty}=1-6\sum_{n=1}^\infty\frac{\exp(-D_c p_n^2 t/r_c^2)}{9\lambda/(1-\lambda)+(1+\lambda)q_n^2}$$	t<0, C=C$_0$, q=q$_0$ t≥0, C=C$'_0$, q(r$_c$,t)=q*(t) $-V_f\frac{dC}{dt}=\frac{3V_s}{r_c}D\frac{\partial q}{\partial r}\Big|_{r_c}$
-Isothermal adsorption -Linear system (q*=KC) -Macropore diffusion control -Step change followed by constant concentration	$$(1-\epsilon_p)\frac{\partial q}{\partial t}+\epsilon_p\frac{\partial c}{\partial t}=\epsilon_p D_p\left(\frac{\partial^2 c}{\partial R^2}+\frac{2}{R}\frac{\partial c}{\partial R}\right)$$ $$\frac{m_t}{m_\infty}=\frac{\bar{q}-q_0}{q_\infty-q_0}=1-\frac{6}{\pi^2}\sum_{n=1}^\infty\frac{1}{n^2}\exp\left(-\frac{n^2\pi^2 D_{eff}t}{R_p^2}\right)$$ $$D_{eff}=\frac{\epsilon_p D_p}{\epsilon_p+(1-\epsilon_p)K}$$	c(R,0)=c$_0$, q(R,0)=q$_0$ c(R$_p$,t)=c$_\infty$ q(R$_p$,t)=q$_\infty$ $\left(\frac{\partial c}{\partial t}\right)_{R=0}=\left(\frac{\partial q}{\partial t}\right)_{R=0}=0$
-Isothermal adsorption -Non-linear system (Langmuir) -Micropore diffusion control	$$\frac{q^*}{q_s}=\frac{bP}{1+bP}$$ $$D_c=\frac{D_0}{1-q/q_s}$$ $$\frac{\partial q}{\partial t}=\frac{D_0}{r^2}\frac{\partial}{\partial r}\left(\frac{r^2}{1-q/q_s}\frac{\partial q}{\partial r}\right)$$	q(r,0)=0 (saturation) q(r,0)=q$_0$ (regeneration) q(r$_c$, t)=q* $\frac{\partial q}{\partial r}\Big|_{r_c=0}=0$ for all t

(cont. on next page)

Table 3.3. (cont)

Assumptions	Model	Boundary Conditions
-Isothermal adsorption -Non-linear system (Langmuir) -Macropore diffusion control	$$\frac{dq^*}{dc}=\frac{bq_s}{(1+bc)^2}=bq_s\left(1-q/q_s\right)^2$$ $$\frac{\partial q}{\partial t}=\frac{\epsilon_p D_p}{(1-\epsilon_p)bq_s}\frac{1}{R^2}\frac{\partial}{\partial R}\left(\frac{R^2}{\left(1-q/q_s\right)^2}\frac{\partial q}{\partial R}\right)$$	$t=0:\ \bar{q}(R,0)=0$ $$\bar{q}(R_p,t)=\frac{q_s bc}{1+bc}$$ $$\left.\frac{\partial\bar{q}}{\partial R}\right|_{R=0}=0$$
LDF model* -Isothermal adsorption -Linear system -Macropore diffusion control	$$\frac{d\bar{q}}{dt}=\frac{15D}{r^2}(q-\bar{q})$$ $$\frac{\bar{q}}{q_\infty}=1-\exp\left[-\frac{15Dt}{r^2}\right]$$	
-Non-isothermal adsorption -Linear system -Micropore diffusion control	$$\frac{\partial q}{\partial t}=\frac{1}{r^2}\frac{\partial}{\partial r}\left(r^2 D_c\frac{\partial q}{\partial r}\right)$$ $$(-\Delta H)\frac{d\bar{q}}{dt}=C_s\frac{dT}{dt}+ha(T-T_0)$$ $$\frac{q'-q'_0}{q_0-q'_0}=\left(\frac{\partial q^*}{\partial T}\right)_P\left(\frac{T-T_0}{q_0-q'_0}\right)$$ $$\frac{m_t}{m_\infty}=1-\sum_{n=1}^{\infty}\frac{9\left[\frac{(p_n\cot p_n-1)}{p_n^2}\right]^2\exp\left(-\frac{p_n^2 D_c t}{r_c^2}\right)}{\frac{1}{\beta}+\frac{3}{2}\left[\frac{p_n\cot p_n(p_n\cot p_n-1)}{p_n^2}+1\right]}$$	$q(r,0)=0$ $$\frac{\partial q}{\partial r}(0,t)=0$$
LDF model** -Non-isothermal adsorption -External mass transfer resistance control -External heat transfer resistance	$$\frac{dq}{dt}=k\left(q^*-q\right)$$ $$c_p\frac{dT}{dt}=\Delta H\frac{dq}{dt}-ha(T-T_0)$$ $$(q_\infty-q^*)=\left(\frac{\partial q^*}{\partial T}\right)_{\substack{q=q_\infty\\T=T_0}}(T_0-T)$$ $$\frac{m_t}{m_\infty}=1+\frac{\beta\alpha^2}{1-\beta\alpha^2}\left(\exp(rt)-\frac{\exp[-k(1-\alpha\beta)t]}{\beta\alpha^2}\right)$$	$t=0\rightarrow q=q_0\ ;\ T=T_0$ $t=\infty\rightarrow q=q_\infty\ ;\ T=T_0$ $t=0\rightarrow q_0=q_0^*(P_0,T_0)$ $t=\infty\rightarrow q_\infty=q_\infty^*(P_\infty,T_0)$ $t=t\rightarrow q^*=q^*(P_\infty,T)$

*Glueckauf 1955

**Sircar 1983

CHAPTER 4

HEAT AND MASS TRANSPORT IN ADSORBENT BED

In an adsorbent bed, the heat, mass, and momentum transfer occur simultaneously. As a result, temperature, pressure, and adsorbate concentration gradients exist. In order to define the cyclic conditions and analyse the performance of adsorption heat pump, transport equations should be solved simultaneously numerically with appropriate boundary conditions and assumptions. In this chapter, the details of fluid flow in a porous media and the governing equations used to represent transport in the adsorbent bed are introduced.

4.1. Porosity and Fluid Flow in a Porous Media

Porous media can basically be defined as the media that includes voids. This media may be a solid with pores such as adsorbents or a bed filled with solids such as packed bed columns and adsorbent beds (Figure 4.1). Different from other adsorbents, the crystalline structure of zeolites is uniform, so the micropores are located in the crystal channels.
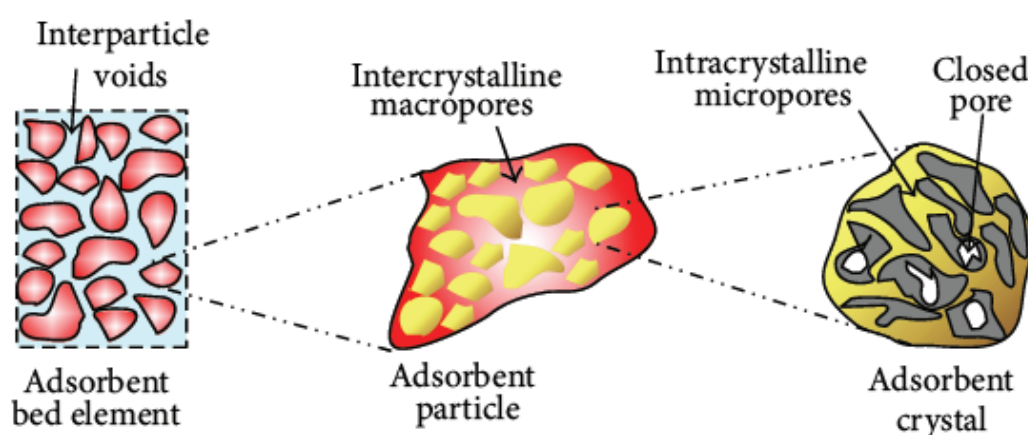
Figure 4.1.Schematic view of porous media

(Source: Hassan 2013)

The ratio of void volume to the total bed volume in a porous media gives the bed voidage. For an isotropic adsorbent bed, the voidage can be defined as:

$$\varepsilon = \frac{V_{void}}{V_{total}} = 1 - \frac{\rho_b}{\rho_p} \tag{4.1}$$

where ε is the bed voidage, ρ_b is the bulk density of the adsorbent particle and ρ_p is the particle density of the adsorbent.

In a porous media, the resistance to the fluid flow occurs depending on the voidage of the bed. The decrease in the value of bed voidage will increase the cross-sectional area that is occupied with the particles and leads to decrease in the velocity of the fluid (Eq 4.2).

$$u = \frac{Q}{A} \tag{4.2}$$

where u is the superficial velocity of the fluid, Q is the volumetric flowrate of the fluid and A is the cross-sectional area of the bed. Furthermore, the resistance to fluid flow causes the pressure drop within the fluid. According to the flow regimes, the relationship between the pressure drops and the superficial velocity of the fluid has been illustrated by the researchers.

When the fluid flow regime is laminar, the relationship between the superficial velocity and the pressure drop is generally explained by Darcy's law (Eq 4.3). In this equation, while the fluid velocity is directly proportional to the pressure drop and the permeability at a specified distance in the bed, it is inversely proportional to the fluid velocity. According to the Darcy's law, the flow will only exist if there is a pressure drop in the fluid and the flow will occur from the high pressure to the low pressure which leads to a negative sign in the equation.

$$u = -\frac{K}{\mu} \nabla P \tag{4.3}$$

where K is the apparent permeability of the bed, μ is the viscosity of the fluid. At low pressures, the effect of collision of molecules cannot be neglected for the fluid flow

in a porous bed. Therefore, an apparent permeability is defined including both collision of molecules and inherent permeability as follows (Marletta et al. 2002).

$$K_{app}=K_{inh}+\frac{\varepsilon\mu}{P}D_{bed} \qquad (4.4)$$

where K_{inh} is the inherent permeability, and D_{bed} is the diffusion coefficient of adsorptive through the bed. For laminar flow regime and $\varepsilon < 0.5$, Blake-Kozeny equation can be used (Eq 4.5) in order to define the inherent permeability in the porous medium. In this model, the porous medium is considered as bundled of capillary tubes (Bird et al. 1961).

$$K_{inh}=\frac{r_p^2\varepsilon^3}{37.5(1-\varepsilon)^2} \qquad (4.5)$$

where r_p is the particle radius.

On the other hand, the diffusion of molecules through the bed can be explained by both Knudsen, molecular or surface diffusion mechanisms. However, surface diffusion can be neglected in large macroporous bed. Then, the diffusion of the fluid through the adsorbent bed can be given as (Ruthven 1984, Suzuki 1990):

$$\frac{1}{D_{bed}}=\tau\left(\frac{1}{D_m}+\frac{1}{D_{Kn}}\right) \qquad (4.6)$$

where D_m is the molecular diffusion coefficient (m^2/s) obtained from Chapman-Enskog equation for moderate pressures (Eq 4.7) and D_{Kn} is the Knudsen diffusion coefficient (m^2/s) (Eq 4.8). τ is the tortuosity which is a geometric factor independent of temperature or the nature of the fluid. Although tortuosity is generally found in the range of 2-6 in the experimental studies, it can be assumed as 3 for the straight, random oriented cylindrical pores (Ruthven 1984).

$$D_m=1.8583\text{x}10^{-7}\frac{\sqrt{T^3/M}}{P\sigma^2\Omega} \qquad (4.7)$$

$$D_{Kn}=97r_p\sqrt{\frac{T}{M}} \tag{4.8}$$

where T is temperature of bed, M is the molecular weight of the water vapor, P is the pressure of the water vapor (atm), σ is the collision diameter of the water vapor and Ω is the collision integral of the water vapor.

When the flow regime is turbulent, Darcy's law cannot be used. In such cases, Ergun's equation is used to explain the relationship between the pressure drop and the superficial velocity of the fluid. In Ergun's equation (Eq 4.9), in addition to the viscous effects, inertial effects are also taken into the consideration (Bird et al. 1961).

$$\Delta P=\frac{150\mu u}{d_p^2}\frac{(1\text{-}\varepsilon)^2}{\varepsilon^2}+1.75\frac{\rho u^2}{d_p}\frac{(1\text{-}\varepsilon)}{\varepsilon^3} \tag{4.9}$$

where ρ is the density of the fluid and d_p is the diameter of the solid.

4.2. Governing Equations for Heat and Mass Transfer in an Adsorbent Bed

In an adsorbent bed, the adsorptive flows between the particles (inter-particle voidage) and within the particles (intra-particle pores) with different transfer mechanisms. In the modelling of an adsorption process in the bed, the effect of adsorptive flow on the temperature, pressure, adsorbate concentration profiles inside the bed can be determined by solving heat and mass transfer equations. Therefore, the following governing equations of the momentum, heat and mass transfer in an adsorbent bed are solved simultaneously with appropriate assumptions and boundary conditions to define the temperature, pressure, and concentration profiles in the bed (see Appendix A).

1) Continuity equation in the adsorbent bed for a cylindrical adsorbent bed (neglecting dispersion effect):

$$\varepsilon\frac{\partial\rho_v}{\partial t}+\frac{1}{r}\frac{\partial}{\partial r}\left(r\rho_v u_r\right)+\frac{\partial}{\partial\phi}\left(\rho_v u_\phi\right)+\frac{\partial}{\partial z}\left(\rho_v u_z\right)+\rho_s\frac{\partial\overline{w}}{\partial t}=0 \tag{4.10}$$

where ρ_v and ρ_s are the density of the adsorptive and bulk density of adsorbent, respectively, $\overline{w}$ is the average adsorbate concentration inside the bed.

2) The relationship between the velocity of the adsorptive and the pressure drop within the bed which are given in the section 4.1.

3) Energy balance equation for the cylindrical adsorbent bed:

$$k_{eff}\left[\frac{1}{r}\frac{\partial}{\partial r}\left(r\frac{\partial T}{\partial r}\right)+\frac{\partial^2 T}{\partial z^2}+\frac{\partial^2 T}{\partial \phi^2}\right]-\frac{1}{r}\frac{\partial}{\partial r}\left(rC_{pv}\rho_v u_r T\right) \tag{4.11}$$

$$-\frac{\partial}{\partial \phi}\left(C_{pv}\rho_v u_\phi T\right)-\frac{\partial}{\partial z}\left(C_{pv}\rho_v u_z T\right)+\rho_s\Delta H_{ads}\frac{\partial \overline{w}}{\partial t}=\left[\varepsilon C_{pv}\rho_v+C_{ps}\rho_s+C_{pl}\rho_s\overline{w}\right]\frac{\partial T}{\partial t}$$

$$k_{eff}=k_z^{(1-\varepsilon)}\times k_v^\varepsilon \tag{4.12}$$

where k_{eff} is the effective thermal conductivity within the bed, k_z is the thermal conductivity of the adsorbent, k_v is the thermal conductivity of the adsorptive, C_{pv}, C_{ps} and C_{pl} are the specific heat capacity of adsorptive, adsorbent and adsorbate, respectively where the adsorbed phase is considered as liquid. When $Bi_h \ll 1$, the temperature gradient within the particle is neglected. Thus, only heat transfer equation inside the bed is taken into consideration. Furthermore, the heat losses in the cycle are neglected and not included in Eq 4.11.

4) Equation to define mass transfer within the adsorbent particle which were given in Section 3.1.2.

In the adsorbent bed, the interparticle mass transfer occurs as a result of the concentration gradient (or pressure gradient) in the bed. When the interparticle mass transfer resistance in the bed is neglected, the pressure within the bed will be uniform and there will be no pressure drop in the bed. Therefore, the mass transfer within the adsorbent particle (intraparticle mass transfer) and heat transfer through the adsorbent bed will be enough to determine the concentration and temperature profiles of the adsorbent bed.

In order to solve the governing equations, some additional information is required for the adsorptive and adsorbate concentrations. For instance, a relationship between the density, pressure and temperature of the adsorptive is necessary to determine the velocity profile of the adsorptive. In most of the studies, the adsorptive is considered as an ideal gas which is logical for low pressure operations. Furthermore, a relationship between

equilibrium adsorbate concentration, temperature and pressure is also desired to solve mass transfer equation within the adsorbent particle (Section 3.1.1).

There are several studies performed to simulate the temperature, pressure and adsorbate concentration for the adsorption heat pumps and adsorption columns with different boundary conditions and assumptions. In these studies, the adsorbent particles was considered as identical in size, so the bed voidage was assumed uniform. The thermophysical properties of the adsorbate, adsorptive and adsorbent such as specific heat capacity and viscosity of the adsorptive were also assumed constant.

The pressure through the bed was considered as uniform and the velocity of the fluid was assumed constant in most of the studies for the simplification of the modelling (Ruthven and Rojo 1990, Park and Knaebel 1992, Sun et al. 1997, Yun et al. 2000, Delage et al. 2000, Restuccia et al. 2002, Chahbani et al. 2004, Ilis et al. 2010, Ilis et al. 2011, Deshmukh et al. 2015, Gaeini et al. 2016, Radu et al. 2017). However, in real systems, there would be a pressure drop through the bed which leads a velocity distribution of the fluid along the bed. In order to define the velocity profile of the fluid, different models have been used in the performed studies. Some of the researchers used only inherent permeability with Darcy's law to explain the velocity profile of the adsorptive (Zhong et al. 1992, Ben Amar et al. 2009, Wu et al. 2009, Chan et al. 2012, Duquesne et al. 2014, Narayanan et al. 2014, Solmuş et al. 2015, Golparvar et al. 2018, Mohammed et al. 2018). On the other hand, as mentioned before, due to the effect of collisions of molecules, the apparent permeability was used instead of inherent permeability in some of the studies (Leong and Liu 2004, Liu and Leong 2005, Demir et al. 2008, Demir et al. 2009, Demir et al. 2011, Niazmand et al. 2012, Demir 2013, Gediz Ilis et al. 2015). Ergun's equation which involves turbulent and laminar flow regime was also used in the performed studies (Bart et al. 1996, Marletta et al. 2002, Maggio et al. 2006, Xue et al. 2015, Xiao et al. 2016).
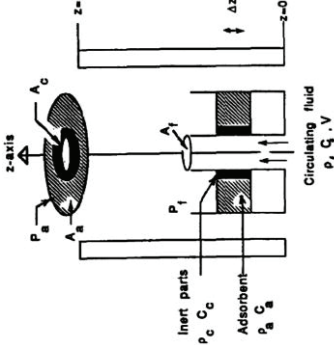
It was seen that the axial dispersion was also contributed to the mass transfer for the fluid especially in the column studies (Zhong, et al. 1992, Bart et al. 1996, Yun et al. 2000, Kim et al. 2004, Gaeini et al. 2016, Xiao et al. 2016). Axial dispersion occurs due to the contribution of the molecular diffusion and turbulent mixing. Since the contribution of molecular diffusion is more significant in the laminar flow regime for the gas phase (Suzuki 1990), it is logical to neglect axial dispersion for adsorption heat pump applications.

In adsorbent bed design, one of the most important thermophysical parameters of the working pair is the heat of adsorption. In the study of Gündoğan-Sayılgan et al. which was performed with zeolite 13X-water pair, it was observed that the heat of adsorption was decreasing with increasing adsorbate concentration in the adsorbent (Gündoğan-Sayılgan et al. 2016). Therefore, it is significant to define the relationship between the heat of adsorption and adsorbate concentration. In the previous studies, the relationship was defined by some of the researchers (Ülkü 1986, Park and Knaebel 1992, Bart et al. 1996, Delage et al. 2000, Kim et al. 2004, Dawoud et al. 2007, Chan et al. 2012, Narayanan et al. 2014, Gaeini et al. 2016, Pinheiro et al. 2016). For instance, Ülkü was obtained heat of adsorption values from the slope of the isosters by applying Clausius-Clapeyron equation for different adsorbate concentrations. Then, a third order polynomial equation was obtained to explain the relationship between the heat of adsorption and adsorbate concentration for the clinoptilolite-water pair (Ülkü 1986).

On the other hand, the mass transfer through the adsorbent particle was generally defined by linear driving force model or Fickian diffusion model and the effective diffusivity was considered as temperature dependent. So, the researchers used Eyring equation to define the effective diffusivity in their study. However, in the study of Gündoğan-Sayılgan et al. 2016, it was seen that the effect of adsorbate loading has a significant effect on the effective diffusivity rather than temperature (Gündoğan-Sayılgan et al. 2016). Pinheiro et al. also stated adsorbate loading dependency on effective diffusivity. They applied constant effective diffusivity, temperature dependent effective diffusivity and both temperature and adsorbate loading dependent effective diffusivity in their study. As a conclusion, they claimed that the use of an average constant effective diffusivity value with linear driving force model is sufficient to predict the heating performance of adsorption heat pump rather than dependence of effective diffusivity on temperature and adsorbate loading (Pinheiro et al. 2016).
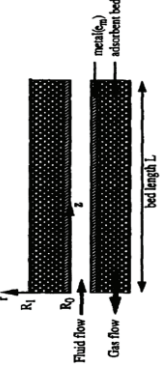
Several parameters were evaluated in literature. In Table 4.1, the studies were summarized. For instance, Liu and Leong and Yaici et al. gave limits for velocity of heat transfer fluid (Liu and Leong 2005; Yaici et al. 2019). They concluded that up to a limit, the velocity of HTF significantly affect the performance of adsorption heat pump, but after that limit, it would have no significant effect.

Table 4.1.Parametric Studies Performed in Literature

ASSUMPTIONS	I.C. / B.C.	GOVERNING EQUATIONS	PARAMETRIC STUDIES
-The uptake and cross-stream temperature gradients are neglected -Heat conduction in axial direction is neglected -The liquid velocity is uniform and constant -Density, specific heat, heat and mass transfer coefficients are constant -Pressure through the adsorbent bed is uniform	**Working Pair** Zeolite-water **I.C.** $T(z,0)=T_f(z,0)=T_c$ $w(z,0)=w_{eq}(z,0)=w_{eq}(T_c,T_{ev})$ **B.C.** $T_f(0,t)=T_h$ $T_f(l,t)=T_c$ $T_s=F(T,w_{eq})=\begin{cases}T_{co} & \text{during des}\\ T_{ev} & \text{during ads}\end{cases}$	**Mass Transfer Equation for the Adsorbent Bed** No mass transfer resistance. **Velocity Profile of Adsorptive** Constant. **Heat Transfer Equation for the Adsorbent** $\rho_a A_a C_a \left[1+\left(\dfrac{C_s}{C_a}\right)w + \dfrac{\rho_c A_c C_c}{\rho_a A_a C_a}\right]\dfrac{\partial T}{\partial t} -$ $\rho_a A_a q_{st}\dfrac{\partial w}{\partial t}=P_f h(T_f-T)$ **Heat Transfer Equation for the Fluid** $\rho_f A_f C_f \left[\dfrac{\partial T_f}{\partial t}+V\dfrac{\partial T_f}{\partial z}\right]=P_f h(T-T_f)$ **Equilibrium Relationship** Not given. **Mass Transfer Equation for Adsorbent Particle** $\rho_a A_a \dfrac{\partial w}{\partial t}=h_m\left(w_{eq}-w\right)$	**Parameters:** -Condenser Temperature -Evaporator Temperature -Desorption Temperature **Conclusions:** - A 5°C decrease in temperature difference of condenser and evaporator led a 15-20% improvement in COP value. -Decreasing maximum bed temperature by 5°C increased COP 5%.
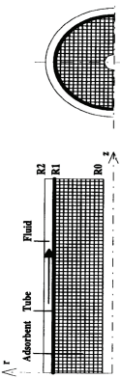
1991, Hajji and Worek

(cont. on next page)

Table 4.1. (Cont.)

	ASSUMPTIONS	I.C. / B.C.	GOVERNING EQUATIONS	PARAMETRIC STUDIES
Ben Amar et al., 1996	-The size of adsorbent particles is uniform and bed porosity is constant -Adsorbent, adsorptive and adsorbate are in equilibrium -Adsorptive behaves as ideal gas -The flow of adsorptive is defined by Darcy's law -The properties of thermal fluid and tube are constant -The thermal energy induced by gas compression is neglected -The system was considered as one-dimensional system -No heat losses in adsorption cycle	**Working Pair** NaX-water **I.C.** $T_s(r,z)=T_f(z)=T_m(z)=T_0$ $P(r,z)=P_0$ **B.C.** $-\lambda_s\vec{\nabla}T_s.\vec{n}=h(T_s-T_e)$ $-\vec{\nabla}P.\vec{n}=k_f(P-P_e)$ During heating: $\quad T_f\big|_{z=0}=T_h$ During cooling: $\quad T_f\big|_{z=0}=T_c$ $\dfrac{\partial T_f}{\partial z}\Big|_{z=L}=\dfrac{\partial T_m}{\partial z}\Big|_{z=0}=0$ $\dfrac{\partial T_m}{\partial z}\Big|_{z=L}=\dfrac{\partial T_m}{\partial z}\Big|_{z=0}=0$	**Mass Transfer Equation for the Adsorbent Bed** $$\varepsilon_t\frac{\partial\rho_g}{\partial t}+\vec{\nabla}\left(\rho_g\vec{u}\right)+\rho_b\frac{\partial q}{\partial t}=0$$ **Velocity Profile of Adsorptive (Darcy's law)** $$\vec{u}=-\frac{K}{\mu}\vec{\nabla}P \; ; \; K=\frac{\varepsilon_b^3\times d_p^2}{150\times(1-\varepsilon_b)^2}$$ **Heat Transfer Equation for the Bed** $$\rho C_p\frac{\partial T_s}{\partial t}+\rho_g C_{pg}\vec{u}.\vec{\nabla}T_s=\vec{\nabla}.(\lambda_s\vec{\nabla}T_s)+\rho_b|\Delta H|\frac{\partial q}{\partial t}$$ $$\rho C_p=\varepsilon_t\rho_g C_{pg}+\rho_b(C_{ps}+qC_{pa})$$ **Heat Transfer Equation for the Fluid** $$\frac{\partial T_f}{\partial t}+v_f\frac{\partial T_f}{\partial z}-D_f\frac{\partial^2 T_f}{\partial z^2}+\frac{h_f S_f}{V_f\rho_f C_{pf}}(T_f-T_m)=0$$ **Heat Transfer Equation for the Tube** $$\frac{\partial T_m}{\partial t}-\frac{\lambda_m}{\rho_m Cp_m}\frac{\partial^2 T_m}{\partial z^2}=\frac{h_f S_f}{V_m\rho_m C_{pm}}(T_f-T_m)+\frac{h_s S_s}{V_m\rho_m C_{pm}}(T_s-T_m)$$ **Equilibrium Relationship (Three-term Langmuir Relationship)** $$q=\frac{q_{s1}b_1 P}{1+b_1 P}+\frac{q_{s2}b_2 P}{1+b_2 P}+\frac{q_{s3}b_3 P}{1+b_3 P}$$ **Mass Transfer Equation for Adsorbent Particle** Not required.	**Parameters:** -Adsorber radius -Cycle time -Heating temperature -Heat transfer parameters -Permeability **Conclusions:** -The radius of the bed should be optimized -At shorter cycle times, COP decreased as a result of low amount of adsorbate cycled. At longer cycle times it decreased due to low heat regeneration efficiency. It was necessary to use consolidated adsorbents that have large thermal conductivities -In the case of axial gas flow, mass transfer resistances were important, even for large permeability values.
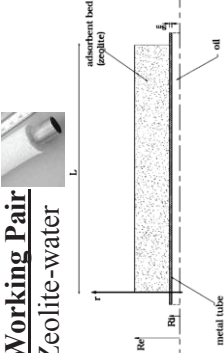
(cont. on next page)

Table 4.1. (Cont.)

	ASSUMPTIONS	I.C. / B.C.	GOVERNING EQUATIONS	PARAMETRIC STUDIES
1997, Sun et al.	-Mass transfer inside the bed is too fast, therefore pressure throughout the bed is uniform -Adsorbent and adsorbate are in thermal equilibrium -Heat transfer in axial direction is neglected in adsorbent bed and the tube -Axial conduction inside the tube is too slow compared to thermal wave propagation of the fluid -Model parameters such as velocity, density, heat transfer coefficient and heat of adsorption are constant -Adsorption equilibrium is nonlinear -Adsorbate is considered as liquid phase	**Working pair** Zeolite NaX-ammonia **I.C.** $T_f(z) = T_m(z) = T_s(r,z) = T_0$ $P = P_0$ **B.C.** During heating: $T_f|_{z=0} = T_H$; $\left.\dfrac{\partial T_f}{\partial z}\right|_{z=L} = 0$ During cooling: $\left.\dfrac{\partial T_f}{\partial z}\right|_{z=0} = 0$; $T_f\Big|_{z=L} = T_L$ Internal heating/cooling: $-\lambda_s \left.\dfrac{\partial T_s}{\partial r}\right|_{r=R_0} = h_s(T_m - T_s|_{r=R_0})$ $\left.\dfrac{\partial T_s}{\partial r}\right|_{r=R_i} = 0$ External heating/cooling: $\left.\dfrac{\partial T_s}{\partial r}\right|_{r=R_0} = 0$ $-\lambda_s \left.\dfrac{\partial T_s}{\partial r}\right|_{r=R_i} = h_s(T_s|_{r=R_i} - T_m)$	**Mass Transfer Equation for the Adsorbent Bed** No mass transfer resistance. **Velocity Profile of Adsorptive** Uniform. **Heat Transfer Equation for the Bed** $C_s \dfrac{\partial T_s}{\partial t} - |\Delta H| \dfrac{\partial q}{\partial t} = \dfrac{\lambda_s}{r} \dfrac{\partial}{\partial r}\left(r \dfrac{\partial T_s}{\partial r}\right)$ $C_s = \rho_s c_s + q c_a$ **Heat Transfer Equation for the Fluid** $\dfrac{\partial T_f}{\partial t} + v \dfrac{\partial T_f}{\partial z} - D_f \dfrac{\partial^2 T_f}{\partial z^2} + \dfrac{h_f S_f}{V_f \rho_f C_{pf}}(T_f - T_m) = 0$ $D_f = \dfrac{\lambda_f}{\rho_f c_f} + \dfrac{4R^2 v^2 \rho_f c_f}{192 \lambda_f}$ **Heat Transfer Equation for the Tube** $V_m \rho_m C_{pm} \dfrac{\partial T_m}{\partial t} + h_f S_f(T_m - T_f) + h_s S_s(T_m - T_s|_{f-s}) = 0$ **Equilibrium Relationship (Dubinin-Radushkevich)** $q = 221.2 \exp\left[-1.916 \times 10^{-7}\left(T \ln \dfrac{P_s}{P}\right)^2\right]$ **Mass Transfer Equation for Adsorbent Particle** No mass transfer resistance.	**Parameters:** -Effective thermal conductivity -Cycle time -Global unit surface conductance **Conclusions:** -Both COP and PCP was increased with thermal conductivity, as expected -Cycle time should have been optimized for both COP and PCP values.
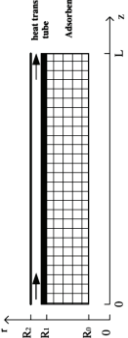
Table 4.1. (Cont.)

ASSUMPTIONS	I.C. / B.C.	GOVERNING EQUATIONS	PARAMETRIC STUDIES
-Pressure and temperature distribution inside the bed is non-uniform -Axial dispersion is neglected -The temperature of heating/cooling fluid is considered to be constant.	**Working Pair** Zeolite-water **I.C.** $T_m\|_{t=0}=T_s\|_{t=0}=T_0$ $p\|_{t=0}=p_0$ **B.C.** During heating: $T_f=T_{oil,h}$ During cooling: $T_f=T_{oil,c}$; $\dfrac{\partial T_s}{\partial r}\Big\|_{r=R_e}=0$ $-\lambda_{eq}\dfrac{\partial T_s}{\partial r}\Big\|_{r=R_i}=h_w(T_m-T_s)$ Adsorption/desorption phase: $p\|_{r=R_e}=p_{ev/con}$ Isosteric heating/cooling phase: $\dfrac{\partial p}{\partial r}\Big\|_{r=R_e}=0$	**Mass Transfer Equation for the Adsorbent Bed** $$\varepsilon_t\frac{\partial\rho_v}{\partial t}+\frac{1}{r}\frac{\partial(r\rho_v v_0)}{\partial r}+(1-\varepsilon_t)\frac{\partial w}{\partial t}=0$$ **Velocity Profile of Adsorptive (Darcy's law)** $$v_0=-\frac{K}{\mu_v}\frac{\partial p}{\partial r}$$ **Heat Transfer Equation for the Bed** $$(1-\varepsilon_t)\frac{\partial}{\partial t}[\rho(1+w)C_{peq}T_s]+\frac{1}{r}\frac{\partial}{\partial r}(r\rho_v C_{pv}T_s v_0)+\varepsilon_t\frac{\partial(\rho_v C_{pv}T_s)}{\partial t}$$ $$=\lambda_{eq}\frac{\partial}{r\,\partial r}\left(r\frac{\partial T_s}{\partial r}\right)+(1-\varepsilon_t)\rho|\Delta H|\frac{\partial w}{\partial t}$$ **Heat Transfer Equation for the Tube** $$\frac{\partial T_m}{\partial t}+\frac{h_{fm}A_{fm}(T_m-T_f)}{\rho_m C_{pm}V_m}+\frac{h_w A_w(T_m-T_{s|m})}{\rho_m C_{pm}V_m}=0$$ **Equilibrium Relationship** Not given. **Mass Transfer Equation for Adsorbent Particle** Not required.	**Parameters:** -Wall heat transfer coefficient -Equivalent thermal conductivity -Permeability -Coating thickness of the bed **Conclusions:** -Thickness of the bed decreased the power of the pump -The power of the pump increased with increasing of other parameters, especially with permeability.

2002, Restuccia et al.

(cont. on next page)

Table 4.1. (cont.)

ASSUMPTIONS	I.C. / B.C.	GOVERNING EQUATIONS	PARAMETRIC STUDIES

-The pressure inside the adsorbent bed is uniform
-Adsorbent and adsorptive are thermodynamically in equilibrium
-Adsorptive behaves as ideal gas
-Heat losses are negligible
-The size of adsorbent particles are uniform and bed porosity is constant
	Working pair
	Carbon-Ammonia
	
	I.C.
	$P=P_{ev}$
	B.C.
	$\left.\dfrac{\partial T_s}{\partial r}\right|_{r=R_0}=0$
	$-\lambda_s\left.\dfrac{\partial T_s}{\partial r}\right|_{r=R_1}=h_s(T_s-T_m)$
	During heating:
	$T_f|_{z=0}=T_H$; $\left.\dfrac{\partial T_f}{\partial r}\right|_{z=L}=0$
	During cooling:
	$T_f|_{z=L}=T_{co}$; $\left.\dfrac{\partial T_f}{\partial r}\right|_{z=0}=0$
	$\dfrac{\partial}{\partial t}\left(\int_0^L\int_{R_0}^{R_1}(\varepsilon_t c+q)rdrdz\right)=0$
	Where
	$c=\dfrac{P}{RT}$; $\varepsilon_t=\varepsilon+(1-\varepsilon)\varepsilon_p$
		Mass Transfer Equation for the Adsorbent Bed
		No mass transfer resistance.
		Velocity Profile of Adsorptive
		Not required.
		Heat Transfer Equation for the Bed
		$(\rho_s C_{ps}+\overline{q}C_{pa})\dfrac{\partial T_s}{\partial t}-\Delta H\dfrac{\partial \overline{q}}{\partial t}=\dfrac{\lambda_s}{r}\dfrac{\partial}{\partial r}\left(r\dfrac{\partial T_s}{\partial r}\right)$
		Heat Transfer Equation for the Fluid
		$\dfrac{\partial T_f}{\partial t}+v\dfrac{\partial T_f}{\partial z}-D_f\dfrac{\partial^2 T_f}{\partial z^2}+\dfrac{h_f S_f}{V_f\rho_f C_{pf}}(T_f-T_m)=0$
		Heat Transfer Equation for the Tube
		$\rho_m Cp_m\dfrac{\partial T_m}{\partial t}+h_f S_f(T_m-T_f)+h_s S_s(T_m-T_s)=0$
		Equilibrium Relationship (Modified Dubinin Astakhov)
		$q^*=q_0\exp\left(-k\left(\dfrac{T}{T_{sat}}-1\right)^n\right)$
		Mass Transfer Equation for Adsorbent Particle
		$\dfrac{\partial \overline{q}}{\partial t}=\dfrac{\partial q^*}{\partial t}$; $\dfrac{\partial \overline{q}}{\partial t}=\dfrac{15D_s}{r_p^2}(q^*-\overline{q})$; $\overline{q}=\dfrac{3}{r_p^3}\int_0^{r_p}x^2 qdx$
			Parameters:
			-Intraparticle mass transfer limitations on
			  -COP and SCP
			  -Coefficient of heat regeneration
			  -Refrigerant flow rate
			  -Process times
			-Cycle time
			-Thermal conductivity
			Conclusions:
			-As the intraparticle mass transfer resistance decreased, both COP and SCP were increased
			-Cycle time should have been optimized
			-Intraparticle mass limitations reduced the flowrate of the refrigerant and increased the process times
			-Increase in thermal conductivity increased both COP and SCP

2004, Chahbani et al.

(cont. on next page)

47
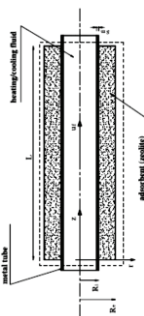
Table 4.1. (Cont.)

ASSUMPTIONS	I.C. / B.C.	GOVERNING EQUATIONS	PARAMETRIC STUDIES
-Adsorbed phase is considered as liquid -Adsorptive behaves as ideal gas -The size of adsorbent particles is uniform and bed porosity is constant -The properties of thermal fluid, tube and adsorptive are constant -No heat losses in adsorption cycle -Thermal resistance between tube and bed is neglected	**Working Pair:** 13X-water **I.C.** $T_f(z,r)=T_m(z,r)=T_s(z,r)=T_a$ $P=P_e$ **B.C.** During the heating process: $T_f\|_{z=0}=T_{h,in}$ During the cooling process: $T_f\|_{z=0}=T_{c,in}$ $\dfrac{\partial T_f}{\partial z}\Big|_{z=L}=0$ $\dfrac{\partial T_m}{\partial z}\Big|_{z=L}=\dfrac{\partial T_m}{\partial z}\Big|_{z=0}=0$ $\dfrac{\partial T_s}{\partial z}\Big|_{z=L}=\dfrac{\partial T_s}{\partial z}\Big|_{z=0}=\dfrac{\partial T_s}{\partial r}\Big|_{r=R}=0$ $\dfrac{\partial P}{\partial z}\Big|_{z=L}=\dfrac{\partial P}{\partial z}\Big|_{z=0}=\dfrac{\partial P}{\partial r}\Big|_{r=R}=0$ When connected to the evaporator: $P\|_{z=0}=P\|_{z=L}=P\|_{r=R}=P_e$ When connected to the condenser: $P\|_{z=0}=P\|_{z=L}=P\|_{r=R}=P_c$	**Mass Transfer Equation for the Adsorbent Bed** $$\varepsilon\frac{\partial \rho_g}{\partial t}+\nabla\left(\rho_g u\right)+\rho_s\frac{\partial \bar{q}}{\partial t}=0$$ **Velocity Profile of Adsorptive (Darcy's law)** $$u=-\frac{K_{app}}{\mu}\nabla P\ ;\ K_{app}=\frac{\varepsilon_a\mu}{\tau P}D_g\ ;\ K=\frac{\varepsilon_a^3\times d^2}{150\times(1-\varepsilon_a)^2}$$ $$\frac{1}{D_g}=\frac{1}{D_m}+\frac{1}{D_k}\ ;\ D_m=0.02628\frac{\sqrt{T^3/M}}{P\sigma^2\Omega}\ ;\ D_k=97r_p\left(\frac{T}{M}\right)^{1/2}$$ **Heat Transfer Equation for the Bed** $$\left(\varepsilon\rho_g C_{pg}+\rho_s(C_{ps}+qC_{pa})\right)\frac{\partial T_s}{\partial t}+\frac{\partial\left(\rho_g C_{pg}uT_s\right)}{\partial z}$$ $$+\frac{1}{r}\frac{\partial}{\partial r}\left(rp_g C_{pg}vT_s\right)=\frac{\partial}{\partial z}\left(\lambda_{eq}\frac{\partial T_s}{\partial z}\right)+\frac{1}{r}\frac{\partial}{\partial r}\left(r\lambda_{eq}\frac{\partial T_s}{\partial r}\right)+\rho_s\Delta H\frac{\partial q}{\partial t}$$ **Heat Transfer Equation for the Fluid** $$\frac{\partial\left(\rho_f C_{pf}T_f\right)}{\partial t}+\frac{\partial\left(\rho_f C_{pf}u_fT_f\right)}{\partial z}=\frac{\partial}{\partial z}\left(\lambda_f\frac{\partial T_f}{\partial z}\right)+\frac{1}{r}\frac{\partial}{\partial r}\left(r\lambda_f\frac{\partial T_f}{\partial r}\right)$$ **Heat Transfer Equation for the Tube** $$\frac{\partial\left(\rho_m C_{pm}T_m\right)}{\partial t}=\frac{\partial}{\partial z}\left(\lambda_m\frac{\partial T_m}{\partial z}\right)+\frac{1}{r}\frac{\partial}{\partial r}\left(r\lambda_m\frac{\partial T_m}{\partial r}\right)$$ **Equilibrium Relationship (Three-term Langmuir Relationship)** $$q_{eq}=\frac{q_{s1}b_1P}{1+b_1P}+\frac{q_{s2}b_2P}{1+b_2P}+\frac{q_{s3}b_3P}{1+b_3P}$$ **Mass Transfer Equation for Adsorbent Particle (LDF)** $$\frac{\partial\bar{q}}{\partial t}=\frac{15D_e}{r_p^2}\left(q_{eq}-\bar{q}\right)\ ;\ D_e=D_0exp(-E_D/RT)$$	**Parameters:** -Condenser temperature -Evaporator temperature -Adsorption temperature -Desorption temperature -Heat transfer fluid temperature -Velocity of heat exchange fluid **Conclusions:** -While COP increased with decreasing condenser temperature, it increased with increasing evaporator temperature -COP increased and tended to a constant value with an increase in desorption temperature -SCP increased with increasing heat transfer fluid temperature -While COP increased very little, cycle time decreased significantly with increasing HTF velocity.

2005, Liu and Leong
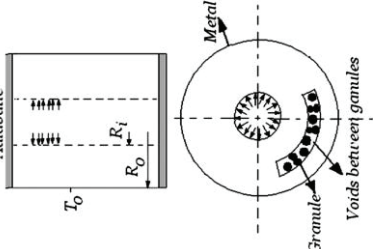
(cont. on next page)

Table 4.1. (Cont.)

	ASSUMPTIONS	I.C. / B.C.	GOVERNING EQUATIONS	PARAMETRIC STUDIES
2006, Maggio et al.	-Two adsorbent bed have identical thermophysical, structural and geometrical properties -Heat losses are neglected -The evaporator and condenser are ideal -The size of adsorbent particles is uniform and bed porosity is constant -Adsorbate, adsorptive and adsorbent are in thermal equilibrium -There is no temperature gradient in radial direction for heat transfer fluid and metal tube -Adsorptive behaves as ideal gas -The properties of metal tube and adsorptive are constant -The properties of heat transfer fluid and adsorbent are temperature dependent	**Working pair** Zeolite 4A-water **I.C.** Adsorber-1 $T_{f,1}\|_{t=0}=T_{m,1}\|_{t=0}=T_{s,1}\|_{t=0}=T_{min}$ $p_1\|_{t=0}=p_{ev}$ Adsorber-2 $T_{f,2}\|_{t=0}=T_{m,2}\|_{t=0}=T_{s,2}\|_{t=0}=T_{max}$ $p_2\|_{t=0}=p_{con}$ **B.C.** $T_f\|_{z=0}=\begin{cases}T_{in,b} & \text{for the heating ph} \\ T_{in,u} & \text{for the cooling ph}\end{cases}$ $\frac{\partial T_f}{\partial z}\|_{z=L}=0; \quad \frac{\partial T_m}{\partial z}\|_{z=0}=\frac{\partial T_m}{\partial z}\|_{z=L}=0$ $\frac{\partial T_f}{\partial z}\|_{z=L}=\frac{\partial T_f}{\partial r}\|_{r=R_e}=0$ $\frac{\partial T_f}{\partial z}\|_{z=0}=0$ $-\lambda_{eq}\frac{\partial T_s}{\partial r}\|_{r=R_i}=-h_{ms}(T_m-T_s)$ $p\|_{z=L}=p\|_{r=R_e}=p_{ev/con}$ For bed connected to evaporator/condenser: $\frac{\partial p}{\partial z}\|_{z=0}=\frac{\partial p}{\partial z}\|_{z=L}=\frac{\partial p}{\partial r}\|_{r=R_e}=0$	**Mass Transfer Equation for the Adsorbent Bed** $$\varepsilon_t\frac{\partial \rho_g}{\partial t}+\frac{1}{r}\frac{\partial(rv_{or}\rho_g)}{\partial r}+\frac{\partial(v_{oz}\rho_g)}{\partial z}+(1-\varepsilon_t)\rho_s\frac{\partial w}{\partial t}=0$$ **Velocity Profile of Adsorptive (Ergun's equation)** $$\vec{v}_0+\frac{\rho_g}{\mu_g}K_E\vec{v}_0\|\vec{v}_0\|=-\frac{K_a}{\mu_g}\text{grad}(p)$$ $$K_E=\frac{1.75D_p}{150(1-\varepsilon)} \quad ; \quad K_a=K_d+\frac{D_g\mu_g}{p} \quad ; \quad K_d=\frac{\varepsilon^3 D_p^{\ 2}}{150(1-\varepsilon)^2}$$ $$D_g=\left(\frac{1}{D^*}+\frac{1}{D_k}\right)^{-1}\frac{\varepsilon}{\eta_T}; D^*=0.02628\frac{\sqrt{T^3/M}}{P\sigma^2\Omega};D_k=48.5d_{pore}\sqrt{\frac{T}{}}$$ **Heat Transfer Equation for the Bed** $$\varepsilon_t\frac{\partial\left(\rho_g C_{pg}T_s\right)}{\partial t}+(1-\varepsilon_t)\rho_s\frac{\partial}{\partial t}\left[(1+w)C_{pbed}T_s\right]$$ $$+\frac{1}{r}\frac{\partial}{\partial r}\left[r\left(\rho_g C_{pg}T_s+p\right)v_{or}\right]+\frac{\partial}{\partial z}\left[\left(\rho_g C_{pg}T_s+p\right)v_{oz}\right]$$ $$=-\lambda_{eq}\left[\frac{1}{r}\frac{\partial}{\partial r}\left(r\frac{\partial T_s}{\partial r}\right)+\frac{\partial^2 T_s}{\partial z^2}\right]+(1-\varepsilon_t)\rho_s\|\Delta H\|\frac{\partial w}{\partial t}$$ **Heat Transfer Equation for the Fluid** $$\frac{\partial T_f}{\partial t}+u_f\frac{\partial T_f}{\partial z}-a_f\frac{\partial^2 T_f}{\partial z^2}+\frac{h_{fm}A_{fm}}{V_f\rho_f C_{pf}}(T_f-T_m)=0$$ **Heat Transfer Equation for the Tube** $$\frac{\partial T_m}{\partial t}-a_m\frac{\partial^2 T_m}{\partial z^2}=\frac{h_{fm}A_{fm}}{V_m\rho_m C_{pm}}(T_f-T_m)+\frac{h_{ms}A_{ms}}{V_m\rho_m C_{pm}}(T_{slm}-T_m)$$ **Equilibrium Relationship** $$\ln p=A(w)+\frac{B(w)}{T}$$	**Parameters:** -Permeability -Minimum temperature gradient -Metal/adsorbent heat transfer coefficient -Adsorbent bed thickness **Conclusions:** -Permeability should be greater than 5×10^{-12} m^2 -Metal/adsorbent heat transfer coefficient was efficient in determining limitations in the bed. When $h_{ms}<100$ W/m^2.K, heat transfer limitations became crucial and at higher values mass transfer limitations became significant (for $K_d<.10^{-12}$ m^2) -Bed thickness of 2-3 mm was recommended to reach high performance

(cont. on next page)

Table 4.1. (Cont.)

ASSUMPTIONS	I.C. / B.C.	GOVERNING EQUATIONS	PARAMETRIC STUDIES
-The size of adsorbent particles is uniform and bed porosity is constant -Adsorptive and adsorbent are thermodynamically in equilibrium -Adsorptive behaves as ideal gas -Thermal resistance within the adsorbent is neglected -Adsorbent and adsorptive are in thermal equilibrium -Thermal properties od adsorbent and adsorptive are constant -Heat transfer rate at R=R$_i$ is neglected	**Working pair** Silica gel-water $T=T_{init}$ **I.C.** **B.C.** At R=R$_i$ $\frac{\partial T}{\partial R}=0$; $\rho_w = f(P,T)$;P=P$_{ev}$ W=f(P,T) ; U=f(ρ_w,K$_{app}$) At R=R$_0$ $T=T_{sur}$; ρ_w= f(P,T) ; $\frac{\partial P}{\partial R}=0$ $\frac{\partial U}{\partial R}=0$ W=f(P,T)	**Mass Transfer Equation for the Adsorbent Bed** $\frac{\partial \rho_w}{\partial t}+\left(\frac{1}{\varepsilon}\right)\frac{\partial W}{\partial t}\rho_s+\frac{1}{\varepsilon R}\frac{\partial}{\partial R}(R\rho_w u)=0$ **Velocity Profile of Adsorptive (Darcy's law)** $u=-K_{app}\frac{R}{M\mu}\frac{\partial(\rho_w T_w)}{\partial r}$ $K_{app}=K+\frac{\varepsilon\mu}{\tau P}D_{bed}$; $K=\frac{\varepsilon^3 r_p^2}{37.5(1-\varepsilon)^2}$; $D_m=0.02628\frac{\sqrt{T^3/M}}{P\sigma^2\Omega}$; $\frac{1}{D_{bed}}=\frac{1}{D_m}+\frac{1}{D_k}$ $D_k=97r_p\left(\frac{T}{M}\right)^{1/2}$ **Heat Transfer Equation for the Bed** $\left((\rho C_p)_{eff}+\rho_s C_{pw}W\right)\frac{\partial T}{\partial t}=\lambda_{eq}\frac{1}{R}\frac{\partial}{\partial R}\left(R\frac{\partial T}{\partial R}\right)-$ $\frac{1}{R}\frac{\partial}{\partial R}(R\rho_w C_{pw}uT)+\rho_s\Delta H_{st}\frac{\partial W}{\partial t}$ $(\rho C_p)_{eff}=\varepsilon(\rho C_p)_w+(\rho C_p)_s$ **Equilibrium Relationship (Freundlich relationship)** $W_\infty=W_0\left(\frac{P_{sat}}{P}\right)^{1/n}$ **Mass Transfer Equation for Adsorbent Particle (LDF)** $\frac{\partial W}{\partial t}=\frac{15D_{eff}}{r_p^2}(W_\infty-W)$; $D_{eff}=D_0\exp(-E_D/RT)$	**Parameters:** -Voidage of the bed **Conclusions:** - The increase of bed voidage decreased the thermal conductivity of the bed, heat transfer rate in the bed and the period of the adsorption process.
2009, Demir et al.			
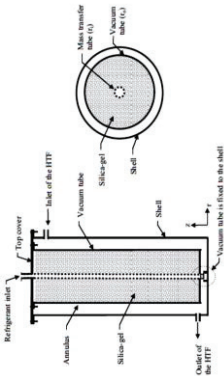
Table 4.1. (Cont.)

ASSUMPTIONS	I.C. / B.C.	GOVERNING EQUATIONS	PARAMETRIC STUDIES
-The size of adsorbent particles are uniform and bed porosity is constant -Heat losses are neglected -Adsorbate is considered as liquid -Adsorptive behaves as ideal gas -Thermophysical properties except density of adsorbent are constant -The condenser and evaporator are ideal with constant temperature during isobaric process -The flow of heat transfer fluid is fully developed turbulent flow	**Working pair** Silica gel-water I.C. $T_b = T_f = T_{tube} = T_{fin} = T_0$ $P_b = P_f = P_{tube} = P_{fin} = P_0$	(see below)	(see below)

GOVERNING EQUATIONS

Mass Transfer Equation for the Adsorbent Bed

$$\int \frac{\partial \rho_g}{\partial t}\varepsilon_t \, dA + Ap\int \left(\rho_g \vec{u_g}\right) dA + \int \rho_b \frac{\partial w}{\partial t} \, dA = 0$$

Velocity Profile of Adsorptive (Darcy's law)

$$u = -\frac{K_{app}}{\mu}\vec{\nabla}P \;;\; K_{app} = K_d + \frac{\varepsilon_p \mu}{\tau P}D_{eq} \;;\; K_d = \frac{\varepsilon_b^3 d_p^2}{150(1-\varepsilon_b)^2}$$

$$D_m = 0.02628\frac{\sqrt{T^3/M}}{P\sigma^2\Omega} \;;\; D_k = 48.5 d_p\left(\frac{T}{M}\right)^{1/2}$$

$$\frac{1}{D_{bed}} = \frac{1}{D_m} + \frac{1}{D_k}$$

Heat Transfer Equation for the Bed

$$\int \rho C_p \frac{\partial T_b}{\partial t}\,dV + \int \left(\rho_g C_{pg}\vec{u_g}T_b\right)dA$$
$$= \int (\lambda\vec{\nabla}T_b)\,dA + \int \rho_b \Delta H \frac{\partial w}{\partial t}\,dV$$

Heat Transfer Equation for the Fluid

$$\int (\rho C_p)_f \frac{\partial T_f}{\partial t}\,dV + \int (\rho_f C_{pf}\vec{u_f}\vec{T_f})\,dA = h_f A(T_f - T_{if})$$

Heat Transfer Equation for the Tube

$$\int (\rho C_p)_{tube}\frac{\partial T_{tube}}{\partial t}\,dp = \int (\lambda_{tube}\vec{\nabla}T_{tube})\,dA + \gamma Q_{tube\text{-}fin}$$

Heat Transfer Equation for the Fin

$$\int (\rho C_p)_{fin}\frac{\partial T_{fin}}{\partial t}\,dV = \int (\lambda_{fin}\vec{\nabla}T_{fin})\,dA + \gamma Q_{fin\text{-}b}$$

Equilibrium Relationship (Toth's relationship)

$$w^* = \frac{1.6\times10^{-12}C_{w^*}}{\left[1+\left(2\times10^{-12}C_{w^*}\right)^{1.1}\right]^{1/1.1}} \;;\; C_{w^*} = P\exp\left(\frac{\Delta H}{RT_b}\right)$$

Mass Transfer Equation for Adsorbent Particle

$$\frac{\partial w}{\partial t} = \frac{15 D_{eff}}{R_p^2}(w^* - w) \;;\; D_{eff} = D_0 \exp(-E_a/RT_b)$$

PARAMETRIC STUDIES

Parameters:

Modelling considerations:
- Effect of fins
- Variable thermal conductivity of the bed
- Contact resistance

Bed heat exchanger configurations:
- Effect of fin geometry on the bed averaged values
- Effect of fin height and spacing on the bed performance
- Fin geometry for a given operating condition

Conclusions:
- Relatively large SCP could be obtained by annular fins with a spacing of 3 mm
- For the case of COP, annular fins were not sufficient
- Taking thermal conductivity as constant caused an error in COP value
- Neglecting thermal contact resistance led an error in SCP value.
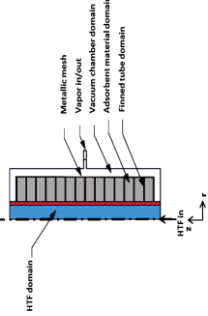
2012, Niazmand et al.

(cont. on next page)

Table 4.1. (Cont.)

ASSUMPTIONS	I.C. / B.C.	GOVERNING EQUATIONS	PARAMETRIC STUDIES
- The size of adsorbent particles is uniform and bed porosity is constant -Adsorptive behaves as ideal gas -Radiative heat transfer, viscous dissipation and the work done by pressure changes are neglected -Surface porosity is considered to be equal to the total porosity -Physical properties such as thermal conductivity, specific heat capacities and viscosity are independent of temperature -Thermal resistance of vacuum tube is neglected	**Working pair** Silica gel-water **I.C.** $T_g(0,r,z)=T_s(0,r,z)=T_i$ $P(0,r,z)=P_i$; $X(0,r,z)=X_i$ **B.C.** $\dfrac{\partial T_g}{\partial r}(t,r_i,z)=\dfrac{\partial T_s}{\partial r}(t,r_i,z)=0$ $P(t,r_i,z)=P_{ev}$ $-k_{ge}\dfrac{\partial T_g}{\partial r}(t,r_0,z)=h(T_g-T_c)$ $-k_{se}\dfrac{\partial T_s}{\partial r}(t,r_0,z)=h(T_s-T_c)$ $\dfrac{\partial P}{\partial r}(t,r_0,z)=0$ $\dfrac{\partial T_g}{\partial z}(t,r,L)=\dfrac{\partial T_s}{\partial r}(t,r,L)=0$ $P(t,r,L)=P_{ev}$ $-k_{ge}\dfrac{\partial T_g}{\partial z}(t,r,0)=h(T_g-T_c)$ $-k_{se}\dfrac{\partial T_s}{\partial z}(t,r,0)=h(T_s-T_c)$ $\dfrac{\partial P}{\partial z}(t,r,0)=0$	**Mass Transfer Equation for the Adsorbent Bed** $$(1-\varepsilon_t)\rho_s\frac{\partial X}{\partial t}+\frac{\partial(\rho_g v_z)}{\partial z}+\frac{1}{r}\frac{\partial(r\rho_g v_r)}{\partial r}+\varepsilon_t\frac{\partial\rho_g}{\partial t}=0$$ $$\varepsilon_t=\varepsilon_b+(1-\varepsilon_t)\varepsilon_p$$ **Velocity Profile of Adsorptive (Darcy's law)** $$v=-\frac{K}{\mu_g}\nabla P \; ; \; K=\frac{\varepsilon_b^3 d_p^2}{150(1-\varepsilon_b)^2}$$ **Heat Transfer Equation for the Adsorptive** $$C_{pg}\rho_g\left[\varepsilon_g\frac{\partial T_g}{\partial t}+v_r\frac{\partial T_g}{\partial r}+v_z\frac{\partial T_g}{\partial z}\right]+(1-\varepsilon_t)\rho_s\frac{\partial X}{\partial t}C_{pg}(T_s-T_g)$$ $$=\frac{1}{r}\frac{\partial}{\partial r}\left(rk_{ge}\frac{\partial T_g}{\partial r}\right)+\frac{\partial}{\partial z}\left(k_{ge}\frac{\partial T_g}{\partial z}\right)+a_v h_{gs}(T_s-T_g)$$ **Heat Transfer Equation for the Adsorbent** $$\rho_s(1-\varepsilon_t)[C_{ps}+XC_{pw}]\frac{\partial T_s}{\partial t}-(1-\varepsilon_t)\rho_s\frac{\partial X}{\partial t}Q_{ad}$$ $$=\frac{1}{r}\frac{\partial}{\partial r}\left(rk_{se}\frac{\partial T_s}{\partial r}\right)+\frac{\partial}{\partial z}\left(k_{se}\frac{\partial T_s}{\partial z}\right)-a_v h_{gs}(T_s-T_g)$$ $$a_v=6\frac{(1-\varepsilon_t)}{d_p}$$ **Equilibrium Relationship (Dubinin-Astakhov relationship)** $$X_\infty=0.346\exp\left[-5.6\left(\frac{T_s}{T_{sat}}-1\right)^{1.6}\right]$$ **Mass Transfer Equation for Adsorbent Particle (LDF)** $$\frac{\partial X}{\partial t}=\frac{60D_0\exp(-E_a/RT_s)}{d_p^2}(X_\infty-X)$$	**Parameters:** -Evaporator pressure -Driven heat source temperature -Cooling source temperature -Condenser pressure -Heat transfer coefficient **Conclusions:** -COP and SCP were increased with increasing evaporator pressure and driven heat source, and with decreasing condenser pressure and cooling source temperature -Time consumed during adsorption process decreased with increasing heat transfer coefficient up to value of 50 W/m2K. From this point it did not have significant effect due to low thermal conductivity -The thermal conductivity of the bed should have been at least 0.01 m to decrease cycle time
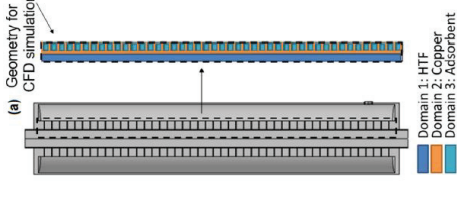
2015, Solmuş et al.

(cont. on next page)

Table 4.1. (Cont.)

	ASSUMPTIONS	I.C. / B.C.	GOVERNING EQUATIONS	PARAMETRIC STUDIES
2019, Elsheniti et al.	-Adsorbate, adsorptive and adsorbent are in thermal equilibrium -The volume occupied by adsorbate is neglected -Adsorptive behaves as ideal gas -Adsorbate is considered as liquid -The heat conduction throughout the bed is characterized by equivalent thermal conductivity -The size of adsorbent particles is uniform and bed porosity is constant -Viscous dissipation, effect of radiation and work done by pressure are neglected -Heat of adsorption is constant throughout the bed	**Working pair** Type RD silica gel-water [figure: Metallic mesh, Vapor in/out, Vacuum chamber domain, Adsorbent material domain, Finned tube domain, HTF domain, HTF out, HTF in] I.C. $T_s = T_f = T_m = T_0$ $P = P_0$ B.C. During heating: $T_{f|z=0} = T_{hot,in}$ $u_f = u_{ave,in,heat}$ During cooling: $T_{f|z=0} = T_{cool,in}$ $u_f = u_{ave,in,cool}$ $\dfrac{\partial T_f}{\partial r}\Big|_{r=0} = \dfrac{\partial T_f}{\partial z}\Big|_{z=L} = 0$ During desorption: $\dfrac{\partial T_v}{\partial r}\Big|_{r=r_{valve}} = 0$ $P = P_{con}$ During adsorption: $T_v = T_{eva}$ $P = P_{eva}$	**Mass Transfer Equation for the Adsorbent Bed** $$\varepsilon_T\frac{\partial \rho_v}{\partial \tau} + \nabla\cdot(\rho_v\vec{u}) + (1-\varepsilon_T)\rho_b\frac{\partial x}{\partial t} = 0$$ **Velocity Profile of Adsorptive** $$\frac{\rho_v}{\varepsilon_T}\left[\frac{\partial u}{\partial t} + \frac{1}{\varepsilon_T}u.\nabla(u)\right] = \nabla\left[-pI + \frac{\mu}{\varepsilon_T}(\nabla u + (\nabla u)^T) - \frac{2}{3}\frac{\mu}{\varepsilon_T}(\nabla.u)I\right] - \left[\frac{\mu}{k_p} + \frac{Q_m}{\varepsilon_T^2}\right]u$$ **Heat Transfer Equation for the Adsorbent Bed** $$\frac{\partial(\rho C_p T_s)}{\partial t} + \nabla(\rho_v C_{pv}uT_s) - \nabla(k_e\nabla T_s) - (1-\varepsilon_T)\rho_s\Delta H_s\frac{\partial w}{\partial t} = 0$$ **Heat Transfer Equation for the Fluid** $$\rho_f C_{pf}\frac{\partial T_f}{\partial t} + \nabla(\rho_f C_{pf}u_f T_f) - \nabla((k_f + k_T)\nabla T_f) = 0$$ **Heat Transfer Equation for the Fins** $$\rho_m C_{pm}\frac{\partial T_m}{\partial t} - \nabla(k_m\nabla T_m) = 0$$ **Heat Transfer Equation for the Vacuum Chamber** $$\frac{\partial(\rho_v C_{pv}T_v)}{\partial t} + \nabla(\rho_v C_{pv}uT_v) - \nabla(k_v\nabla T_v) = 0$$ **Equilibrium Relationship (Toth's relationship)** $$w_{eq} = \frac{K_0\exp\left(\frac{\Delta H_s}{RT}\right)P}{\left\{1 + \left[\frac{K_0}{X_m}\exp\left(\frac{\Delta H_s}{RT}\right)P\right]^{t_1}\right\}^{\frac{1}{t_1}}}$$ **Mass Transfer Equation for Adsorbent Particle (LDF)** $$\frac{\partial x}{\partial t} = \frac{15 D_s}{R_p^2}(w_{eq} - w) \; ; \; D_s = D_{s0}\exp(-E_a/RT)$$	**Parameters:** -Fixed evaporator and condenser pressures -Cycle time -Flow regime of HTF -Ratio of desorption and adsorption time periods -Fin height -Fin number - Length of the heat transfer fluid **Conclusions:** -Flow regime of HTF was desired to be turbulent to decrease cycle time -Time ratio of desorption and adsorption was affected both SCP and COP. The ratio was recommended as in the range of 0.7-0.9.

(cont. on next page)

Table 4.1. (Cont.)
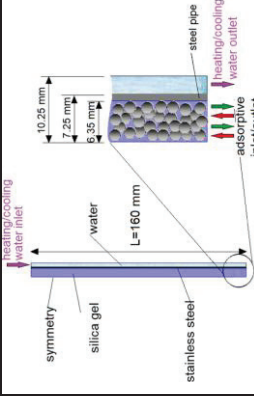
	ASSUMPTIONS	I.C. / B.C.	GOVERNING EQUATIONS	PARAMETRIC STUDIES
2019, Yaïci et al.	-The finned tube adsorption bed operates under unsteady-state, non-equilibrium conditions -The surface porosity is considered to be equal to the total porosity -The volume fraction of the gas phase is assumed to be equal to the total porosity -The working fluid is water at high velocity is assumed to be Newtonian, incompressible flow inside the tubes, the viscous dissipation and viscous work are neglected -The work done by pressure changes, the radiative heat transfer and the viscous dissipation are neglected -The wall thickness of the vacuum tube is assumed to be very thin and hence, its thermal resistance was neglected	 **(a)** Geometry for CFD simulation Domain 1: HTF Domain 2: Copper Domain 3: Adsorbent **Working Pair** Silica gel-water **I.C. and B.C.** Not given.	**Mass Transfer Equation for the Adsorbent Bed** $$\varepsilon\frac{\partial \rho_v}{\partial \tau}+\Delta(\rho_v u)-D_m\Delta^2\rho_v+(1-\varepsilon)\rho_s\frac{\partial x}{\partial t}=0$$ **Velocity Profile of Adsorptive** $$\rho\frac{\partial u}{\partial t}+\rho(u.\nabla)u=\nabla.[-\rho I+\mu(\nabla u+(\nabla u)^2)]$$ $$\rho\nabla.(u)=0$$ **Heat Transfer Equation for the Adsorbent Bed** $$(1-\varepsilon)\rho_s C_{ps}\frac{\partial T_s}{\partial t}-\varepsilon\rho_v C_{pv}\frac{\partial T_s}{\partial t}+(1-\varepsilon)\rho_s X C_{pl}\frac{\partial T_s}{\partial t}$$ $$-(1-\varepsilon)\rho_s\Delta H\frac{\partial X}{\partial t}-k_s\Delta^2 T_s+\rho_v C_{pv}u\Delta T_s=0$$ $$\Delta H=2950-1400X$$ **Heat Transfer Equation for the Fluid** $$\rho_f C_{pf}\frac{\partial T_f}{\partial t}+\rho_f C_{pf}v_f\Delta T-k_f\Delta^2 T_f=0$$ **Heat Transfer Equation for the Metal** $$\rho_t C_{pt}\frac{\partial T_t}{\partial t}-k_t\Delta^2 T_t=0$$ **Equilibrium Relationship (Freundlich relationship)** $$X_{eq}=a\left(\frac{P}{P_{sat}}\right)^b$$ **Mass Transfer Equation for Adsorbent Particle (LDF)** $$\frac{\partial X}{\partial t}=\frac{15D_m}{R_p^2}(X_{eq}-X)\ ;\ D_m=D_{s0}\exp(-E_a/RT_s)$$	**Parameters** -Velocity of HTF -Adsorbent Bed Thickness -Tube Thickness -Adsorbent Particle Diameter **Conclusions** - Bed thickness is a crucial geometric parameter within the design phase because as it increases, both the water amount that is absorbed and cycle time increase simultaneously. - When selecting for the adsorbent material, a smaller particle diameter is desirable for minimising the cycle time. A lower, 2 mm threshold was identified - Over the operation's duration, the fluid velocity is to be operated at a higher velocity for minimizing the cycle time as well. For this, an upper threshold of 0.005 m/s was identified.

Table 4.1. (Cont.)

	ASSUMPTIONS	I.C. / B.C.	GOVERNING EQUATIONS	PARAMETRIC STUDIES
2021, Ilis et al.	-The water vapor is assumed as an ideal gas and flows in laminar. -The thermal conductivities of the adsorbate and adsorbent particles are taken as constant values. -The heat transfer inside the adsorbent particles is ignored. -The silica gels are assumed to have a uniform size and spherical shape, and the bed porosity is constant -The thermal properties of the adsorbent, adsorptive, adsorbate, and the heat of adsorption are assumed constant.	 **I.C.** $T = T_d$ $v_x = v_y = 0$ $P = 3500\ Pa$ **B.C.** At Bottom Side for Adsorptive $\frac{\partial T}{\partial y} = 0$; $\rho_v = f(P,T)$; $P = 3500\ Pa$ $W = f(P,T)$; $v_x = f(\rho_v)$; $v_y = f(\rho_v)$	**Mass Transfer Equation for the Adsorbent Bed** $(\varepsilon - 1)\rho_a \dfrac{\partial W}{\partial t} = \varepsilon\dfrac{\partial \rho_v}{\partial t} + \dfrac{\partial}{\partial x}(\rho_v v_x) + \dfrac{\partial}{\partial y}(\rho_v v_y)$ **Velocity Profile of Adsorptive (Darcy's law)** $v_x = -\dfrac{K_{app}}{\mu}\dfrac{\partial P}{\partial x}$; $v_y = -\dfrac{K_{app}}{\mu}\dfrac{\partial P}{\partial y}$ $K_{app} = K + \dfrac{\varepsilon\mu}{\tau P}D_{bed}$; $K = \dfrac{\varepsilon^3 R_p^2}{37.5(1-\varepsilon)^2}$; $r_p = \dfrac{2R_p}{3}\dfrac{\varepsilon}{(1-\varepsilon)}$ $\dfrac{1}{D_{bed}} = \dfrac{1}{D_m} + \dfrac{1}{D_k}$; $D_m = 0.02628\dfrac{\sqrt{T^3/M}}{P\sigma^2\Omega}$; $D_k = 97 r_p\left(\dfrac{T}{M}\right)^{1/2}$ **Heat Transfer Equation for the Bed** $(\rho C_p)_{eff}\dfrac{\partial T}{\partial t} + \dfrac{\partial(\rho_v C_{pv}v_x T)}{\partial x} + \dfrac{\partial(\rho_v C_{pv}v_y T)}{\partial y}$ $= \dfrac{\partial}{\partial x}\left(\lambda_{eq}\dfrac{\partial T}{\partial x}\right) + \dfrac{\partial}{\partial y}\left(\lambda_{eq}\dfrac{\partial T}{\partial y}\right) + (1-\varepsilon)\rho_a \Delta H \dfrac{\partial W}{\partial t}$ **Equilibrium Relationship (Toth's relationship)** $W_\infty = \dfrac{K_0\exp\left(\frac{\Delta H_{st}}{RT}\right)P}{\left\{1 + \left[\frac{K_0}{W_m}\exp\left(\frac{\Delta H_{st}}{RT}\right)P\right]^b\right\}^{1/b}}$ **Mass Transfer Equation for Adsorbent Particle (LDF)** $\dfrac{\partial W}{\partial t} = \dfrac{15D_{eff}}{R_p^2}(W_\infty - W)$; $D_{eff} = D_0\exp(-E_a/RT_b)$	**Parameters** Heating Fluid Temperature **Conclusions** -The desorption rate increases by increasing heating water temperature

CHAPTER 5

ZEOLITE

Zeolites, which are found in natural form or can easily be synthesized, are used in several industrial applications such as drying processes, water treatment and softening, agriculture and animal husbandry, mining and metallurgy, construction, and energy recovery and storage systems as an adsorbent, ion exchanger or catalysis.

In this chapter, the structural information about zeolites, the effect of pre-adsorbed water on zeolitic applications and the use of zeolite as adsorbent in energy recovery and storage systems are discussed.

5.1. Framework Structure of Zeolites

Zeolites, porous crystalline aluminosilicates, have a tetrahedron framework in which aluminum or silicon atoms are occupied at the center, and oxygen atoms are located at the corners (Figure 5.1). A polyanionic three-dimensional network arises as a result of sharing of oxygen atoms between two tetrahedra. Thus, additional positive charges must be located in the structure to balance the electrical charge and to obtain a stable crystal structure. This additional charge is maintained by cations such as Na, Ca, K, Mg, Ti which are replaceable and easily removable from the structure.
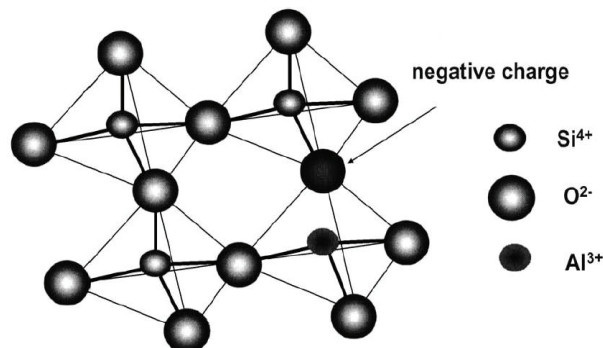
Figure 5.1.(SiO_4) and (AlO_4) tetrahedron

(Source: Querol et al. 2002)

Framework structure of zeolites affects most of the properties of zeolites such as stability, cation exchange properties, adsorption of gases and vapors, catalytic properties, electrical conductivity, the behavior of zeolitic water (Breck 1974).

Zeolites can be classified into seven groups according to the secondary building units which present the subunit of the structure with a specific array of AlO4 and SiO4 tetrahedra. For instance, while double 4-ring tetrahedra (D4R) is found in the structure of zeolite A, zeolite X consists of double 6-ring tetrahedra (D6R) (Figure 5.2). The framework structures of both zeolites consist of β-cages which was characteristic structure of sodalite. The cations are mainly located in site I and site II and oxygen molecules are appeared in each cubic face of zeolite A. On the other hand, the cations in zeolite X are located within the hexagonal prism unit (site I), single 6-rings (site II) and main cavities (site III). On the other hand, group 7 which includes clinoptilolite has a more complex structure.
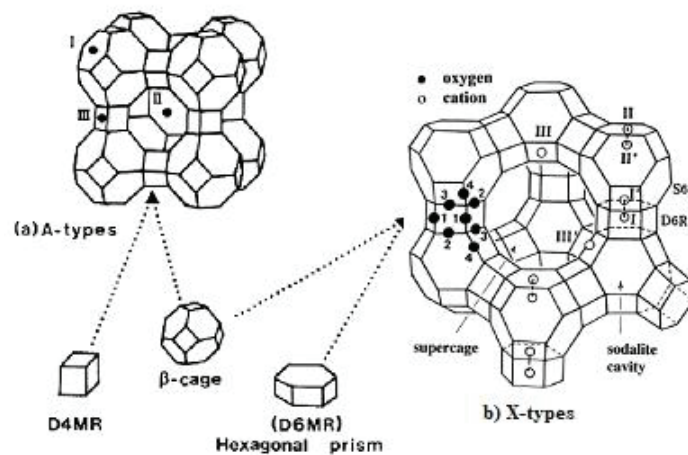
Figure 5.2.Secondary Building Units in Zeolite Structure

The crystal lattice of zeolites is literally uniform, and it separates zeolites from other adsorbents. Si/Al ratio, the location, size, and number of cations which are the adsorption sites of zeolites, and the dehydration conditions are the properties that affect the adsorption ability of zeolites. The Si/Al ratio affects inversely the adsorption ability of zeolites. On the other hand, thermal stability increases as Si/Al ratio increases because of the less energy requirement to break Al-O bonds instead of Si-O bonds (Tsitsishvili et al. 1992; Narin et al., 2011).

The presence of cations in the structure of zeolites prevents the homogeneous distribution of the electrostatic field at the ionic surface of the zeolites and adsorption

center is formed in the structure of zeolites for polar molecules. Especially, zeolites with Si/Al ratio lower than 10 have a higher affinity for polar molecules. Furthermore, when polar adsorbates adsorbed by the adsorbents with ionic structure, the electrostatic interactions become too high which leads high heat of adsorption values.

In zeolites, the dehydration can occur without structural defects and the water molecules are removed at different temperatures according to the energy of cation-water bond distance and the exchangeable cation sites (Van Reenwijk 1974; Knowlton et al. 1981; Bish 1993). In addition, the desorbed water, namely zeolitic water, can be adsorbed again when the zeolite is cooled. The extraction of zeolitic water causes structural changes in zeolite framework since it accomplishes the coordination of the cations in the cavities and minimizes the electrostatic attraction forces between the oxygen molecules (Tsitsishvili et al. 1992; Ozkan 1996).

In recent years, the effect of cation size and location on water adsorption capacity of zeolites gain attention by several researchers (Dzhigit et al. 1971; Ozkan 1996; Moise et al. 2001; Janchen et al. 2004; Fan et al. 2014). In zeolite crystals, the total void space must remain the same, therefore the water adsorbed by zeolites will increase as the ionic radius of the cation decreases. In the study of Moise et al., they compare the water adsorption capacities of several exchanged X and Y zeolites given in literature and observe that while the adsorption capacity of zeolite X is mainly depended on cation radius, cation location becomes also effective in adsorption capacity of zeolite Y (Moise et al., 2001).

5.2. Effect of Pre-Adsorbed Water and Regeneration Conditions on Zeolite Applications

Although zeolites have high affinity to various gases and vapor, water has a special value for applications in which zeolites are used as adsorbent, catalyst or ion exchanger. The pre-adsorbed water in the framework structure of the zeolites affects the properties such as adsorption capacity, heat of adsorption value and mass transfer rate and the strength and heterogeneity of electric field (Malka-Edery et al. 2001; Szanyi et al. 2004; Brandani and Ruthven 2004; Fan et al. 2014; Purdue and Qiao 2018). As a consequence, the thermal behavior of zeolites as a function of the type, amount, and position of cations within the structure, the coordination of cations with water molecules,

Si/Al ratio, dehydration temperature, water vapor pressure and heating rate should be well evaluated (Bish 1993; Bish and Wang 2010). Furthermore, the cation locations may change during reversible and continuous dehydration process without topographic changes in the framework structure of zeolites (Breck 1974; Tsitsishvili et al. 1992; Bish 1995; Narin et al. 2011). As a result, the adsorption ability of zeolites is affected inversely.

Under vacuum conditions, the complete regeneration of zeolites, which is dependent on the degree of vacuum and evacuation period, is generally accomplished at temperatures above 350°C (Breck 1974). However, due to the poor hydrothermal stability of aluminum-rich zeolites and the possibility of destruction of crystallinity even at low temperatures in the presence of water, the regeneration should be relatively slow at a moderate temperature under a good vacuum (Ruthven 1984). In the study of Yucel and Ruthven, which was performed with zeolite 4A and 5A, it was indicated that the temperature should be increased 2-3°C/min during regeneration under vacuum (Yucel and Ruthven, 1980). Furthermore, the adsorption capacity and mass diffusivity were also affected by regeneration conditions especially at the initial period of the adsorption (Ruthven 2012; Sayılgan et al. 2016).

5.3. Zeolite-Water Pair in Adsorption Studies

Due to the high affinity to each other and high heat of adsorption values, zeolite-water pair has special importance in adsorption studies. Some of the studies performed by this pair in the previous studies are summarized Table 5.1. Although there are several studies on adsorption equilibria zeolite-water pair, the kinetic studies are still not enough. In most of these studies, the adsorption equilibrium relationship has been obtained for regeneration temperature above 200°C.

On the other hand, San and Lin performed a study to compare the effect of different working pairs such as zeolite 13X-water, silica gel-water and active carbon-methanol on the performance of adsorption heat pump (San and Lin 2008). In their study, the regeneration temperature was in the range of 80-120°C and they used experimental correlation to define adsorption equilibrium relationship of zeolite 13X-water pair. Maximum adsorption capacity of this pair was introduced as 0.23 wt/wt. For this operation conditions, the COP and SCP values for zeolite 13X-water pair was lower than other pairs.

In 2009, Wang and LeVan compared adsorption of CO_2 and H_2O on zeolite 13X and 5A for different adsorption temperatures (Wang and LeVan 2009). The samples were regenerated at 175°C under vacuum condition and it was seen that Toth's relationship was well fitted to the experimental data at all temperatures.

In the study of Gaeini et al., the effect of kinetic parameters on thermal performance of sorption heat storage reactor was investigated by using zeolite 13X-water pair (Gaeini et al. 2016). Langmuir and Sips relationships were taken into consideration to define adsorption equilibrium of the pair. They found that Sips relationship was better fit to experimental data for this pair.

Tatlıer and Erdem-Şenatalar designed a consolidated adsorbent bed in which zeolite 4A was coated on the bed (Tatlıer and Erdem-Şenatalar 1999). In their study, they searched the effect of thermal and mass diffusivities of zeolite 4A-water pair on adsorption heat pump performance. In that study, they found the effective diffusivity of the pair in the range of $4x10^{-11}$-$1x10^{-9}$ m^2/s by means of solid diffusion model and mentioned that the mass diffusivity of the pair was the limiting parameter to specify the coating thickness on metal support of adsorbent bed.

The diffusion mechanism of clinoptilolite-water pair was examined by Çakıcıoğlu-Ozkan and Ulku and they stated that while the intraparticle diffusional resistance was rate controlling mechanism at initial periods of the adsorption process, external heat transfer resistance became significant above the Henry's law region (Çakıcıoğlu-Ozkan and Ulku 2008).

In the study of Sayılgan-Gündoğan et al. 2016, a volumetric system was used to define adsorption equilibrium and kinetics of zeolite 13X-water pair for different adsorption and regeneration temperatures (Sayılgan-Gündoğan et al. 2016). In that study, they observed that although temperature had a significant effect of adsorption capacity, the effective diffusivity was dependent on adsorbate loading rather than temperature. They measured the effective diffusivity of this pair in the range of $4x10^{-9}$-$6x10^{-8}$ m^2/s and the effective diffusivity decreased with increasing adsorption adsorbate loading in the long time period.

From the beginning of the studies on adsorption technology in energy recovery and storage systems, zeolite-water pair gains attention of the researchers especially for the heating systems. The performed studies are given in Table 2.1, Table 2.2, and Table 4.1.

For instance, Douss designed an adsorption heat pump with two adsorber and NaX-water pair was used in the experimental study (Douss 1988). The heating coefficient of performance was determined as 1.56 for two adsorber case. In 1996, BenAmar et al. performed a numerical study with temperature wave regenerative heat pump (BenAmar et al. 1996). In their study, they used zeolite NaX-water and activated carbon AX21-ammonia in the adsorbent beds. It was concluded that COP greater than 1 and SCP near 200 W/kg could be obtained for that advanced heat pump cycle.

On the other hand, Poyelle et al. preferred to use composite adsorbent in which thermal conductivity of zeolite was enhanced by natural expanded graphite (Poyelle et al. 1999). The effective thermal conductivity of zeolite was increased from 0.1 W/m.K to the range of 5-10 W/m.K. However, the permeability was decreased due to the consolidation of the adsorbent. As a result, while the COP value decreased due to the mass transfer resistance, SCP value increased due to the decrease in cycle time with the enhance of thermal conductivity.

In 2009, Bauer et al. produced zeolite/aluminum composite adsorbent for adsorption refrigeration (Bauer et al. 2009). In their study, they coated zeolite (SAPO-34) onto the aluminum substrate and determine COP and SCP values. They claimed that the composite material had a promising potential to enhance the performance value of the adsorption refrigerators.

Table 5.1.Previous Studies on Adsorption of Water on Zeolites

(Source: Sayılgan-Gündoğan and Ülkü 2018)

Year	Researcher	Zeolite	Operating Temperature (°C)	Adsorption Equilibrium Relationship	Max. Adsorption Capacity (wt/wt)	Diffusion Coefficient (m²/s)
1961a-1961b	Barrer and Fender	Chabazite Gmelinite Heulandite	30-80	Langmuir	0.28 0.27 0.19	4.8×10^{-10} 1.5×10^{-10} 1.6×10^{-10}
1969	Dzhigit et al.	LiNaX NaX KNaX RbNaX Cunaxa	23-400	-	0.36 0.31 0.28 0.22 0.19	
1986	Ülkü	Clinoptilolite rich zeolitic tuff	25-250	Experimental correlation	0.14	-
1986a	Ülkü et. al	Clinoptilolite	20-220	-Dubinin-Radushckevich -Experimental correlation	0.08-0.115 0.04-0.115	-
1986b	Ülkü et al.	Clinoptilolite	20-200	-	0.12	-
1987	Karger and Pfeifer	NaX	20	-	-	4×10^{-10}- 2 $\times 10^{-9}$
1992	Ülkü et al.	Clinoptilolite	25-200	-	-	5×10^{-10}
1995	Cacciola and Restuccia	13X 4A	5-55	Experimental correlation	-	-
1995	Sun et al.	13X	20-200	Three-term Langmuir	-	-
1997	Hunger et al.	NaA NaX NaY Na,K-erionite Na-mordenite NaZSM-5	-	-	0.26 0.30 0.29 0.16 0.13 0.08	-
1999	Tatlıer and Erden-Şenatalar	4A	20-150	-	-	4×10^{-11} - 1 $\times 10^{-12}$
2001	Ryu et al.	13X	25-340	Langmuir-Freundlich model	0.30	1×10^{-11} - 1 $\times 10^{-10}$
2001	Moise et al.	BaX BaY	25-400	Dubinin-Radushkevich	0.28 0.28	-
2003	Cakicioglu-Ozkan and Ulku	Ba-rich clinoptilolite	25-400	Dubinin-Astakhov	0.13	-
2003	Lu et al.	13X	10-250	Dubinin-Astakhov	0.26	-
2004	Kwapinski and Tsotsas	4A	25-350	Experimental correlation	0.24	2.8×10^{-10}-1 $\times 10^{-9}$
2004	Janchen et al.	NaX MgNaX LiX CaNaA	20-350	-	0.192 0.212 0.244 0.162	-
2005	Liu and Leong	13X	45-200	Three-term Langmuir	-	-
2006	Ülkü et al.	Zeolitic Tuff 4A	20-300	Langmuir	-	-
2007	Caputo et al.	Zeolitic tuff	20-250	Dubinin-Astakhov	0.022-0.117	-

(cont. on next page)

Table 5.1 (cont.)

Year	Researcher	Zeolite	Operating Temperature (°C)	Adsorption Equilibrium Relationship	Max. Adsorption Capacity (wt/wt)	Diffusion Coefficient (m²/s)
2008	San and Lin	13X	30-120	Experimental correlation	0.236	-
2008	Çakıcıoğlu-Ozkan and Ülkü	Clinoptilolite rich zeolitic tuff	18-400	-	0.15	1.2×10^{-8}-3.154×10^{-6}
2009	Simo et al.	3A	100-270	Langmuir	0.07-0.16	-
2009	Wang and LeVan	5A 13X	25-175	Toth's	0.13-0.24 0.15-0.26	-
2009	Llano-Restrepo and Mosquera	3A	0-100	Generalized statistical thermodynamic model	0.03-0.23	-
2010	Ivanova et al.	Clinoptilolite	20-200	-	0.016	2.5×10^{-12}-4.4×10^{-12}
2010	Cortes et al.	13X	50-450	Dubinin-Radushkevich	0.20-0.25	-
2014	Mette et al.	13X	20-350	Dubinin-Astakhov	0.02-0.32	-
2016	Sayılgan et al.	13X	35-200	Langmuir	0.19-0.23	4×10^{-9}-6×10^{-8}

CHAPTER 6

MATERIALS AND METHODS

High consumption of the fossil fuel-based electricity increases the effect of global warming in recent years. This increase not only effect the weather conditions, but it also brings diseases, scarcity, and drought. Therefore, eco-friendly solutions must be carried out immediately. Although producing electricity from renewable energy sources has been increasing in recent years, the storage of the produced energy still turns out to be the biggest problem. The current energy storage systems are not sufficient to be environmentally friendly and researchers try to enhance alternative systems. At this point, adsorption heat pumps which use renewable energy sources and waste heat as heat source gains attention of the researchers. However, they still require enhancement due to the low heat transfer in the adsorbent bed.

In the scope of this thesis, the theoretical analysis of the adsorbent bed with different design and parameters have been conducted. Zeolite 13X-water pair has been chosen as the working pair and adsorption equilibrium and kinetic data have been determined from the experimental data performed at regeneration temperature of 90°C. The enhancement of the effective thermal conductivity within the bed has been investigated with metal additives and manufacturing high thermal conductive zeolite-graphene pellet. Furthermore, synthesizing of graphene from graphite is also summarized in this section. The details of the study have been introduced in the following sections.

6.1. Selection of the Working Pair

Water is a non-toxic, non-flammable, low-cost adsorbate with high latent heat of evaporation. Furthermore, due to high electronegativity and oppositely charged oxygen and hydrogen atoms, water is a polar molecule with dipole moment. As mentioned before, zeolites with Si/Al ratio smaller than 10 have great affinity to polar molecules and high heat of adsorption values can be obtained from the adsorption of water by these zeolites. High affinity to each other and high heat of adsorption value of zeolite-water make these pair suitable especially for energy recovery and storage systems.

Additionally, when compared to other adsorbents, the uniform crystal structure gives advantages to zeolites in adsorption processes. In many adsorbents, the molecular structure of the adsorbents is destroyed as water is adsorbed and desorbed. However, due to the uniform crystal structure of zeolites, water can easily move in the channels without any destruction in the structure of zeolite.

Zeolites, which are found in natural form or can easily be synthesized, are used in several industrial applications such as drying processes, water treatment and softening, agriculture and animal husbandry, mining and metallurgy, construction, and energy recovery and storage systems as an adsorbent, ion exchanger or catalysis (Gündoğan-Sayılgan et al. 2016). As mentioned before, the pre-adsorbed water affects the zeolite applications quietly. However, the studies on adsorption of water on zeolites are limited and the discussion of heat and mass transfer properties of this pair is not sufficient. So, in the thesis zeolite 13X which has high affinity to water vapor and high heat of adsorption value has been chosen as adsorbent and water has been chosen as the adsorbate.

Furthermore, in literature, there are several studies on adsorption heat pumps working with silica gel-water, active carbon-methanol pairs. However, the studies on the zeolite-water pair are limited especially. Therefore, in this study, the application of zeolite-water pair in the adsorption heat pump design has been discussed.

6.2. Characterization of Zeolites

Prior to applications, affinity to water vapor, framework structure, thermal behavior of zeolites should be characterized to detect the suitability of the properties for the processes. Thermal and structural properties of zeolites such as 4A from Sigma Aldrich Co., 13X from Alfa Aeser (4-8 mesh), 5A from Alfa Aeser Co. (3-5 mm) and Clinoptilolite-rich natural zeolitic material from Gördes-Turkey can be determined by different methods such as thermal gravimetric analysis (TGA), scanning electron microscopy (SEM) and infrared spectroscopy (IR). The experimental conditions for the characterization of zeolite samples used in the study are summarized in Table 6.1.

Table 6.1. Characterization methods

Methods	Apparatus	Conditions
TGA	Shimadzu TGA-51	Heating rate: 5°C/min N_2 flow: 40 mL/min Temperature:25-1000°C **(Dehydrated in saturated KCl solution prior to analysis)**
SEM-EDX	SEM, FEI QUANTA 250 FEG	-
FTIR	Shimadzu FTIR-8201 model	KBr pellet technique

6.3. Adsorption Equilibrium

In this study, a volumetric system has been used to determine the adsorption equilibrium and diffusivity of pairs. The schematic view of the set-up is illustrated in Figure 6.1. The details of the system have been given in the master thesis (Gündoğan-Sayılgan 2013).
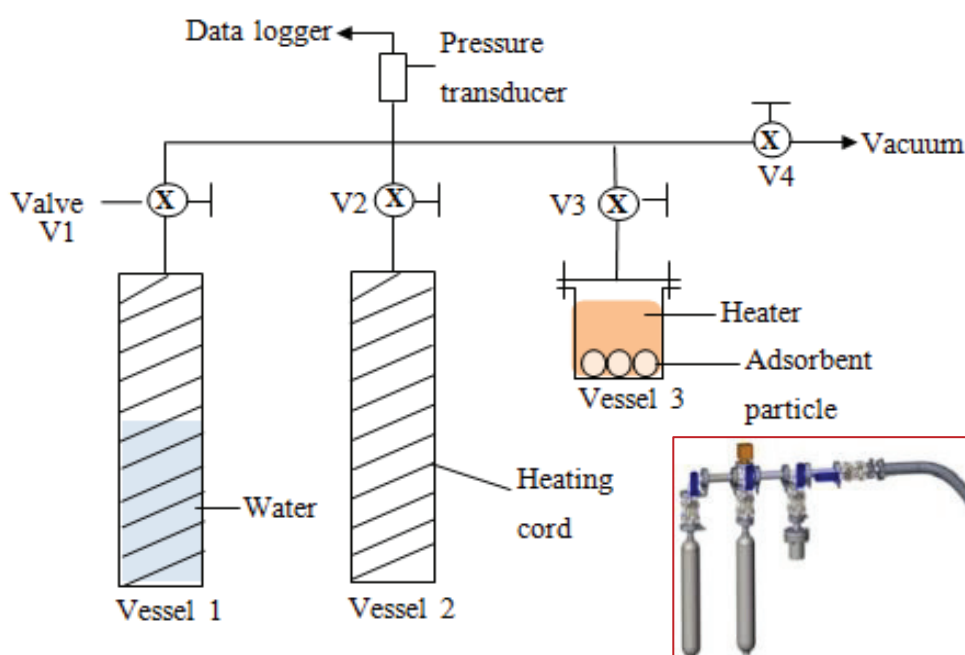
Figure 6.1. Schematic view of experimental setup

Since adsorption experiments are conducted under vacuum conditions and zeolite can adsorb water vapor even at low adsorptive pressure, the leakage tests have been performed similar with the master thesis study of Gündoğan-Sayılgan. It has been seen that there is no leakage in the system for 60 hours.

After the leakage test has been accomplished, the adsorption experiments are performed by the following experimental procedure:

1) All four valves are closed,

2) Temperature and pressure loggings are on,

3) Temperature controllers connected to vessel 2 and vessel 3 are set to the desired regeneration temperature (90°C) and the temperature controller connected to the pipes is set to the 60°C.

4) Vacuum pump is turned on,

5) V2, V3 and V4 are opened,

6) Evacuation is continued for a week at selected regeneration temperature,

7) After a week, the temperature controllers are set to the desired adsorption temperature while evacuation continued,

8) When the temperature of the system reaches to the adsorption temperature and come to equilibrium, V3 and V4 are closed,

9) Vacuum pump is closed,

10) V1 is opened until the saturation water vapor pressure is reached, then it is closed,

11) When the adsorptive pressure reaches equilibrium in entire system, V3 is opened until equilibrium pressure is reached, and then it is closed.

The adsorption experiments performed at different adsorption temperatures of 35, 45 and 60°C. Adsorptive pressure versus time data was recorded during the experiments. The adsorption capacity, heat of adsorption, uptake rate and effective diffusion coefficient were calculated from these data by using ideal gas law.

After determination of adsorption isotherm and effective diffusion coefficient, the proper equilibrium and kinetic model should be selected. In order to determine the appropriate equilibrium model for zeolite 13X-water regenerated at 90°C, Langmuir, Sips and Toth's models applied by curve fitting method in excel.

6.3.1. Non-isothermal Adsorption Analysis

Heat is released during the adsorption process, and it cannot be drawn away from the adsorbent as fast as it is generated in conventional systems. As a result, temperature of the bed increases significantly at the beginning of the adsorption and then decreases

slowly to the initial value. Although this increment is generally neglected in the previous studies, it should be considered in the design of an adsorbent bed.

In determining the non-isothermal adsorption kinetics, both the models based on Fickian diffusion (Ruthven 1984), and linear driving force (LDF) approximation (Sircar 1983) are used, and the set of equations are solved numerically. The assumptions and boundary conditions of the models are given in Table 3.3. The nodal equations of mass and energy transfer equations for non-isothermal LDF model have been obtained by applying Euler's method (Eq 6.1-6.5). Both the Langmuir and Sips relationships were used to define adsorption equilibrium where q* represents the amount adsorbed at the solid surface at equilibrium. It is assumed that the bed and the sample reached thermal equilibrium instantaneously. Therefore, the specific heat capacity in heat transfer equation is the average specific capacity including both the sample and the bed. The parameter "a" in the model is the external surface area of the adsorbent bed in the test apparatus with the units of m^2/kg (Eq 6.3). The external heat transfer coefficient, h, has been obtained from Nusselt equation.

$$\frac{q(i)^{k+1}-q(i)^k}{\Delta t}=\frac{15D_{eff}}{r_p^2}\left(q^*-q(i)^k\right) \qquad \text{(Eq 6.1)}$$

$$q(i)^{k+1}=\frac{15D_{eff}}{r_p^2}*q^*+\left(1-\frac{15D_{eff}}{r_p^2}\right)q(i)^k \qquad \text{(Eq 6.2)}$$

$$C_p\frac{T(i)^{k+1}-T(i)^k}{\Delta t}=q_{st}\frac{q(i)^{k+1}-q(i)^k}{\Delta t}-ha\left(T(i)^k-T_0\right) \qquad \text{(Eq 6.3)}$$

$$T(i)^{k+1}=\frac{q_{st}*farkq(i)+CT(i)^k+D}{B} \qquad \text{(Eq 6.4)}$$

$$farkq(i)=\frac{q(i)^{k+1}-q(i)^k}{\Delta t} \ ; \ B=\frac{C_p}{\Delta t} \ ; \ C=\frac{C_p}{\Delta t}-ha \ ; \ D=h_a T_0 \qquad \text{(Eq 6.5)}$$

In non-isothermal solid diffusion model, implicit finite difference model has been used in to solve the mass transfer through the adsorbent particle and the Euler's method has been used to solve the heat transfer equation. The average adsorbate concentration

was used in heat transfer equation. The equilibrium relationship was defined by Langmuir relationship and the specific heat capacity in the heat transfer equation is the average specific capacity including both the sample and the pan. On the other hand, the parameter "a" in the solid diffusion model is the external surface area per unit volume of the adsorbent sample.

$$\frac{q(i)^{k+1}-q(i)^k}{\Delta t}=D_{eff}\left[\frac{q(i+1)^{k+1}-2q(i)^{k+1}+q(i-1)^{k+1}}{\Delta r^2}+\frac{2}{r(i)}\frac{q(i+1)^{k+1}-q(i-1)^{k+1}}{2\Delta r}\right] \qquad (6.6)$$

$$q(i)^{k+1}=\frac{Bq(i+1)^{k+1}+Cq(i)^k+Dq(i-1)^{k+1}}{A} \qquad (6.7)$$

$$A=\frac{1}{\Delta t}+\frac{2D_{eff}}{\Delta r^2} \ ; \ B=\frac{D_{eff}}{\Delta r^2}+\frac{D_{eff}}{r(i)\Delta r} \ ; \ C=\frac{1}{\Delta t} \ ; \ D=\frac{D_{eff}}{\Delta r^2}-\frac{D_{eff}}{r(i)\Delta r} \qquad (6.8)$$

$$C_p\frac{T(i)^{k+1}-T(i)^k}{\Delta t}=q_{st}\frac{\bar{q}(i)^{k+1}-\bar{q}(i)^k}{\Delta t}-ha\left(T(i)^k-T_0\right) \qquad (6.9)$$

$$T(i)^{k+1}=\frac{q_{st}*fark\bar{q}(i)+CT(i)^k+D}{B} \qquad (6.10)$$

$$fark\bar{q}(i)=\frac{\bar{q}(i)^{k+1}-\bar{q}(i)^k}{\Delta t}; \ B=\frac{C_p}{\Delta t} \ ; \ C=\frac{C_p}{\Delta t}-ha \ ; \ D=h_aT_0 \qquad (6.11)$$

6.4. Thermal conductivity measurements

Thermal conductivity measurements of zeolite beads have been performed by KEM QTM-500 device which works according to the standardized hot wire method and by a homemade measurement apparatus which is given at Figure 6.2.

In hot wire method which is a transient method used to measure thermal conductivity (Figure 6.2a), it is assumed that the hot wire diameter is infinitely small, and heat losses due to convection and radiation are neglected. An electric current with a constant power is applied to the wire on the probe and the temperature rise exponentially.

From the slope of the linear line of temperature versus time, which is in logarithmic scale, the thermal conductivity of the sample is determined (Eq 6.12).

$$k_{eff} = \frac{q}{4\pi(T_2 - T_1)} \ln\frac{t_2}{t_1} \qquad (6.12)$$

Figure 6.2. Measurement device for thermal conductivity a) Hot wire method b) Heat Source method

This method can be used for the measurement of several species in the form of liquid, granular or powder with a thermal conductivity less than 15 W/m.K (Griesinger et al. 1999; Wang et al. 2006; Franco 2007). In the study of Franco, it was mentioned that the required sample thickness was related with the thermal diffusivity of the sample and the optimum conditions for thermal conductivity measurement with hot wire method was given (Table 6.2) (Franco 2007).

Table 6.2. Minimum dimensions required for the sample in hot wire method

(Source: Franco 2007)

λ (W/mK)	Length (mm)	Width (mm)	Thickness (mm)
0.02	50	20	10
0.05	35	15	6
0.1	30	12	5
0.2	40	15	6
0.5	50	36	9
1.0	70	35	12
2.0	80	50	18
5.0	120	80	30

Besides standardized methods, alternative methods are also used in literature. One of the most popular methods is heat source method (Huetter et al. 2004; Demir et al. 2008; Guo et al. 2013). In this method, a long cylindrical vessel which is filled with the sample is suddenly plunged into the water bath and the temperature change is monitored against time (Figure 6.3). By applying transient heat conduction equation, the thermal conductivity of a sample with a known specific heat capacity is calculated (Eq 6.13).

$$\rho_b C_p \frac{\partial T}{\partial t} = k_{eff} \left(\frac{\partial^2 T}{\partial r^2} + \frac{1}{r} \frac{\partial T}{\partial r} \right) \qquad (6.13)$$
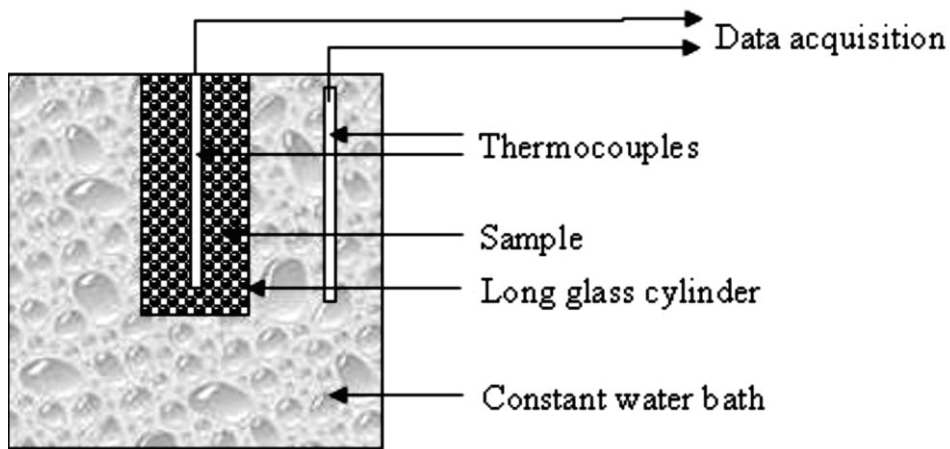
Figure 6.3. Schematic view of test apparatus

(Source: Demir et al. 2008)

In this study, heat source method was applied with a homemade system (Figure 6.2b) which included of a hot water bath (1), a data logger (2), a cold-water bath (3), a computer to record the temperature data against time (4) and a sample holder (5). During the experiments, two different sample holders were used. The first one was a long cylinder (SH-1) with dimensions of 45 mm inner diameter, 50 mm outer diameter and 150 mm length. However, since it was hard to locate the metal additives due to small diameter, a larger sample holder with dimensions of 85 mm inner diameter, 90 mm outer diameter and 125 mm length was used (SH-2). Insulation was placed at the top and the bottom of the sample holder to prevent end effects.

The experiments with the homemade system are performed with the following steps:

1) The hot water bath is heated to the temperature of 40°C.

2) When the temperature of the bed reached equilibrium, the sample holder is placed into the water bath.

3) Meanwhile, the increase in temperature at the center of the of the sample holder is measured with a grounded K-type thermocouple (later two additional thermocouples are located at the sides of the sample holder) (Figure 6.4).

4) When the temperature at the center of the sample holder reaches equilibrium, it is taken from hot water bath and placed into the cold-water bath which is at 5°C.

5) The change in temperature with time (30 seconds interval) is recorded by data logger and computer program.

Figure 6.4. Sample holder (SH-2) with three K-type thermocouples

After obtaining experimental data, the transient heat conduction equation given in Eq 6.11 was solved numerically by using MATLAB program with appropriate boundary conditions (Eq 6.14- 6.15).

$$\left.\frac{\partial T}{\partial r}\right|_{r=0}=0 \tag{6.14}$$

$$-k_{eff}\left.\frac{\partial T}{\partial r}\right|_{r=R}=h_w\left(T|_{r=R}-T_\infty\right) \tag{6.15}$$

In the numerical study, both SH-1 and SH-2 have been considered as long cylinder. The end effects, the conductive heat transfer through the wall of the sample holder and contact resistance between the sample holder and metal additives have been neglected. Furthermore, since only the temperature in radial direction is recorded, the change of temperature in axial direction has not been taken into consideration. Then, the numerical and experimental data has been fitted by using curve fitting method and effective thermal diffusivity of the sample is obtained. Finally, by multiplying effective thermal diffusivity with effective thermal capacitance, the effective thermal conductivity is obtained (Eq 6.16).

$$\left(\rho C_p\right)_{eff} = x\left(\rho C_p\right)_m + (1-x)\left(\rho C_p\right)_s \tag{6.16}$$

where x is the mass fraction of the metal additives. In order to increase the effective thermal conductivity, metal additives with different geometries have been used (Figure 6.5).

Figure 6.5. Metal additives with different geometries

When the equilibrium temperature is reached, the temperature at each side of the sample holder should be equal to the temperature of the water bath which is maintained at 5°C. Therefore, in the numerical solution of the thermal diffusivity, the convergence criterion is determined as:

$$\max|T_{center} - T_\infty| < 10^{-3} \tag{6.17}$$

6.5. Heat and Mass Transfer in the Adsorbent Bed

As mentioned in Chapter 4, the heat, mass, and momentum transfer equations should be solved simultaneously to determine the temperature, pressure, and adsorbate concentration distribution within the adsorbent bed. In this thesis, three different bed designs were evaluated. Within the scope of the thesis, the effect of parameters such as the thermal conductivity of the adsorbent, the effective diffusivity through the adsorbent particle, the cold fluid velocity and temperature and the hot fluid temperature on the performance of the bed were investigated. The details of the study are given in the following sections.

6.5.1. Adsorbent Bed-1

In the first design, the considered annular bed is given in Figure 6.6 (Demir et al. 2009). The inner radius (R_i) of the bed is taken as 0.06 m and the outer radius (R_o) is taken as 0.16 m with a length of 0.35 m. The bed voidage was taken as 0.36. Furthermore, the top and bottom of the bed was considered as adiabatic.
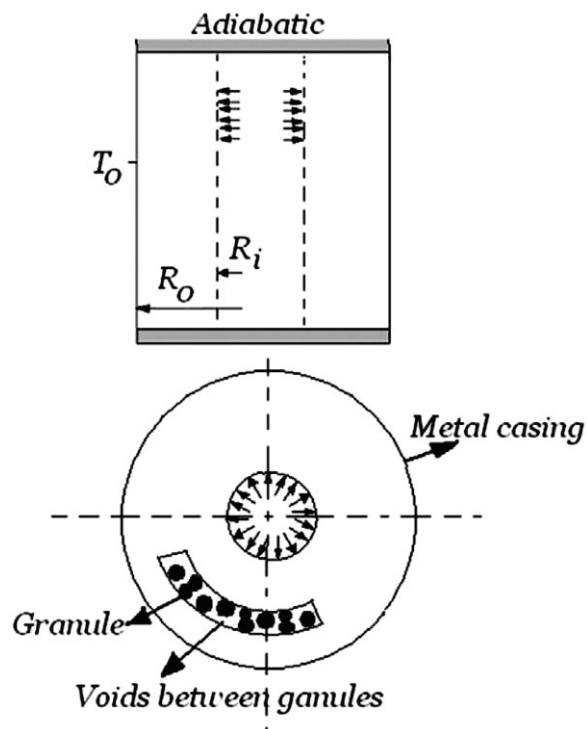

Figure 6.6. Considered annular Adsorbent Bed-1

6.5.1.1. One-Dimensional Analysis of the Adsorbent Bed-1 (Case I)

The heat, mass and momentum transfer equations were solved simultaneously for the adsorbent bed-1 (Figure 6.6). In that design, it was assumed that the flow of the adsorptive was laminar flow in radial direction and the bed was adiabatic. Thus, the continuity and heat transfer equations became:

$$\varepsilon \frac{\partial \rho_v}{\partial t} + \frac{1}{r}\frac{\partial}{\partial r}\left(r\rho_v u_r\right) + \rho_s \frac{\partial \overline{w}}{\partial t} = 0 \tag{6.18}$$

$$k_{eff}\left[\frac{1}{r}\frac{\partial}{\partial r}\left(r\frac{\partial T}{\partial r}\right)\right] - \frac{1}{r}\frac{\partial}{\partial r}\left(rC_{pv}\rho_v u_r T\right) + \rho_s \Delta H_{ads}\frac{\partial \overline{w}}{\partial t} \tag{6.19}$$
$$= \left[\varepsilon C_{pv}\rho_v + C_{ps}\rho_s + C_{pl}\rho_s\overline{w}\right]\frac{\partial T}{\partial t}$$

Since the flow regime was laminar, Darcy's law with apparent permeability was used to define the pressure drop and velocity profile of the adsorptive (Eq 4.1-4.8). Furthermore, while the adsorptive was assumed as ideal gas, the adsorbed phase was considered as liquid. The thermophysical properties of adsorptive, adsorbate and adsorbent except adsorptive density and heat of adsorption were taken as constant.

One of the parameters examined during the numerical study was the effect of effective thermal conductivity of adsorbent on the performance of adsorption heat pump. In order to evaluate that, the effective thermal conductivity has been taken as 0.12 W/mK and 1 W/mK which is the value given by Meunier (Meunier 1993).

As mentioned in Chapter 4, equilibrium relationship is also required to solve the governing equations. According to the results of experimental study, Sips relationship (Eq 6.21) has been used to define adsorption equilibrium where the isosteric heat depends on the adsorbate loading.

$$q = q_s \frac{(bP)^{1/n}}{1 + (bP)^{1/n}} \tag{6.20}$$

Since the constants b and n are temperature dependent parameters, they are defined as a function of temperature as (Do 1998):

$$b = b_\infty \exp\left[\frac{Q}{RT}\right] \qquad (6.21)$$

$$\frac{1}{n} = \frac{1}{n_0} + \alpha\left(1 - \frac{T_0}{T}\right) \qquad (6.22)$$

$$q_{st} = Q - (\alpha RT_0)n\ln(bP) \qquad (6.23)$$

where b_∞ is the pre-exponential factor of the affinity constant. n is the surface heterogeneity, Q is the heat of adsorption, n_0 is the parameter at reference temperature of T_0, q_{st} is the isosteric heat of adsorption, and α is a constant parameter.

The change of amount of adsorbate in the adsorbent can be determined with different kinetic models with appropriate assumptions and boundary conditions which have been given in Section 3.1.2. In this study, due to the simplicity and giving approximate solution, linear driving force (LDF) model has been used to determine the change in adsorbed amount of adsorbate with time (Eq 6.24). The effect of temperature and adsorbate loading dependence of effective diffusivity value on the performance of adsorption heat pump is another parameter evaluated in this study.

$$\frac{d\bar{q}}{dt} = \frac{15D_{eff}}{r_p{}^2}(q - \bar{q}) \qquad (6.24)$$

where $\bar{q}$ is the average adsorbate concentration at the adsorbent surface, D_{eff} is the effective diffusivity within the adsorbent particle and r_p is the particle radius. The effect of adsorbate loading, and temperature on effective diffusivity has been also evaluated in Case I.

6.5.1.2. Two-dimensional Analysis of the Adsorbent Bed-1 (Case II)

Two-dimensional analysis of the Adsorbent Bed-1 (Figure 6.6) was also performed to decide the effect of adsorptive flow in axial direction within the bed. Therefore, two-dimensional forms of the heat and mass transfer equations were taken into consideration (Eq 6.25- 6.26).

$$\varepsilon\frac{\partial\rho_v}{\partial t}+\frac{1}{r}\frac{\partial}{\partial r}\left(r\rho_v u_r\right)+\frac{\partial}{\partial z}\left(\rho_v u_z\right)+\rho_s\frac{\partial\overline{w}}{\partial t}=0 \tag{6.25}$$

$$k_{eff}\left[\frac{1}{r}\frac{\partial}{\partial r}\left(r\frac{\partial T}{\partial r}\right)+\frac{\partial^2 T}{\partial z^2}\right]-\frac{1}{r}\frac{\partial}{\partial r}\left(rC_{pv}\rho_v u_r T\right)-\frac{\partial}{\partial z}\left(C_{pv}\rho_v u_z T\right)$$
$$+\rho_s\Delta H_{ads}\frac{\partial\overline{w}}{\partial t}=\left[\varepsilon C_{pv}\rho_v+C_{ps}\rho_s+C_{pl}\rho_s\overline{w}\right]\frac{\partial T}{\partial t} \tag{6.26}$$

Similar with the Case I, the adsorption equilibrium has been represented by Sips relationship (Eq 6.20-6.23). The adsorption rate was represented by LDF model with an average effective diffusivity value (Eq 6.24). The velocity profile of the adsorptive and pressure drop in the bed was defined by the Darcy's law (Eq 4.3).

6.5.2. Validation of the Theoretical Model for Adsorbent Bed-1

The validation of theoretical model with experimental data was achieved by taking experimental data from the study of Mobedi (Mobedi 1987). In that study, Zeolite 13X-water pair was used. The experimental design constructed by Mobedi is presented in Figure 6.7.

1. Zeolit
2. Kollektör
3. Evaporatör
4. Flanş
5. Konsender
6. Konser kabı
7. Termoeleman haznesi
8. O'ring halkası
9. Isıtıcı
10. İzolasyon
11. Su seviyesi gözetleme camı
12. Termoeleman haznesi
13. Vakummetre
14. Diyaframlı vana
15. Su seviye cetveli
16. Su banyosu
17. Vakum bağlantı rekoru
18. Elek borusu
19. O'ring halkası
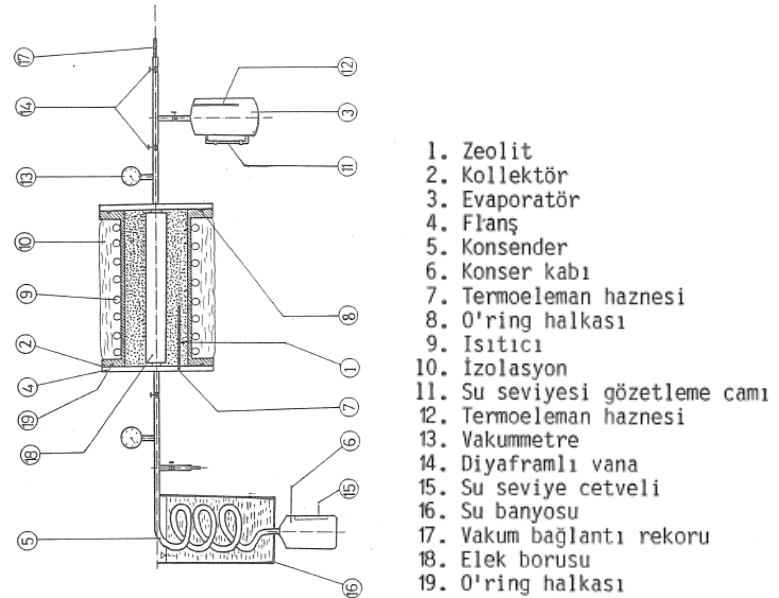
Figure 6.7. Experimental design of Mobedi

(Source Mobedi 1987)

The one-dimensional governing equations obtained for Adsorbent Bed-1 were used in the validation. The adsorption equilibrium was defined by Sips Relationship and the parameters for equilibrium relationship was obtained from the experimental data. The evaporator pressure was taken as 2 kPa. The outer radius of the bed was 110 mm.

6.5.3. Adsorbent Bed-2 (Case III)

In the second design, the top and bottom of the bed was non-adiabatic, and the heating was done by a constant temperature source at the outer region of the bed (Figure 6.8). The governing equations were the same with two-dimensional analysis of the adsorbent bed-1 (Eq 6.25-6.26), except the boundary conditions.
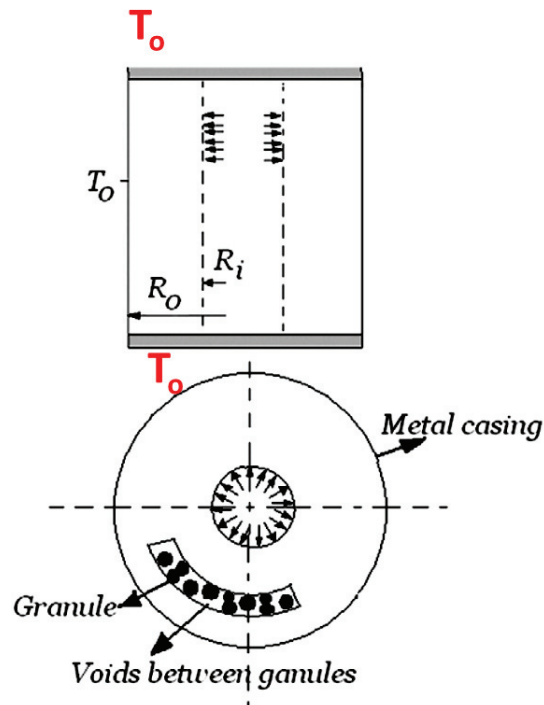
Figure 6.8. The considered annular Adsorbent Bed-2 (Case III)

6.5.4. Adsorbent Bed-3 (Case IV)

In the third adsorbent bed design, the adsorbent bed was supposed to be heated with a heat transfer fluid flowing at the outside of the annular adsorbent bed rather than constant temperature source (Figure 6.9). In the design, the axial dispersion of the adsorptive was also taken into consideration. The top and bottom of bed was considered as adiabatic as in the Adsorbent Bed-1.
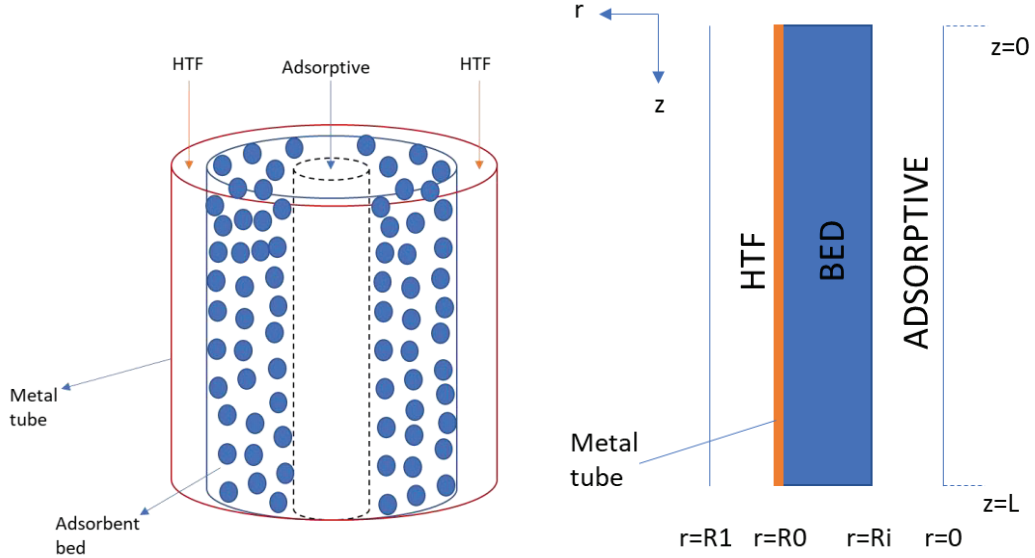
Figure 6.9. The considered annular Adsorbent Bed-3 (Case IV)

According to the assumptions given above, two-dimensional analysis of the heat and mass transfer equations are performed for the Adsorbent Bed-3 which were the same with Case II (Eq 6.25-6.26).

In addition to the adsorbent bed, heat transfer equations for the heat transfer fluid and the metal tube were also taken into consideration for this case. The thermal gradients in radial direction were neglected for both heat transfer fluid and the metal tube. Thermal properties of metal tube and heat transfer fluid were assumed to be constant. The thermal resistance between the metal tube and the adsorbent bed was neglected.

Energy balance for the heat transfer fluid:

$$\frac{\partial T_f}{\partial t}+u_f\frac{\partial T_f}{\partial z}-D_f\frac{\partial^2 T_f}{\partial z^2}+\frac{h_fA_f}{\rho_fC_{pf}V_f}(T_f-T_m)=0 \tag{6.27}$$

Energy balance for the metal tube:

$$\rho_mC_{pm}V_m\frac{\partial T_m}{\partial t}-k_m\frac{\partial^2 T_m}{\partial z^2}+h_fA_f(T_m-T_f)+h_sA_s(T_m-T)=0 \tag{6.28}$$

where u_f is the velocity of the HTF, D_f is the thermal dispersion coefficient, V, ρ, Cp are the volume, density and specific heat capacity for both HTF and metal tube, A_f

and h_f are the surface area and heat transfer coefficient at the HTF-metal tube interface, and A_s and h_s are the surface area and heat transfer coefficient at the adsorbent bed-metal tube interface, respectively.

Similar with the Adsorbent Bed-1 and Adsorbent Bed-2, the adsorption equilibrium was represented by Sips relationship (Eq 6.20-6.23). The adsorption rate was represented by LDF model with an average effective diffusivity value (Eq 6.24). The velocity profile of the adsorptive and pressure drop in the bed was defined by the Darcy's law (Eq 4.3).

In this design, parametric studies were also performed. The effect of velocity of heat transfer fluid (0.1, 1, 10 m/s), hot fluid temperature (464 K, 484 K and 504 K) and cold fluid temperature (298 K, 288 K and 278 K) were investigated for Adsorbent Bed-3.

6.5.5. Numerical Solution of the Governing Equations

The governing equations used in the design of adsorption heat pumps are nonlinear parabolic differential equations which defines how an unknown varies in both space and time. In order to solve these type of equations, different numerical methods such as finite element, finite difference and finite volume have been represented. In this study, finite difference method which is applicable in boundary value problems was employed. In this method, the domain is discretised in both space (Figure 6.10) and time and the differential equation is turned into a linear algebraic equation for each node.
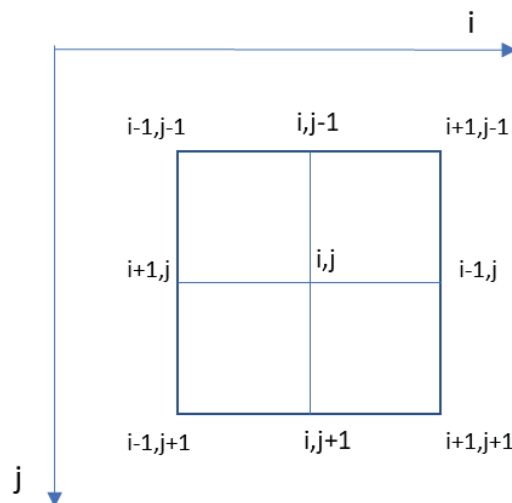
Figure 6.10. Grids used for the finite difference solution of parabolic partial differential equations

In linearization of the differential equations central difference is generally used for the space derivatives.

$$\frac{\partial^2 y}{\partial x^2} = \frac{y_{i+1,j} - 2y_{i,j} + y_{i-1,j}}{(\Delta x)^2} \tag{6.29}$$

$$\frac{\partial y}{\partial x} = \frac{y_{i+1,j} - y_{i-1,j}}{2\Delta x} \tag{6.30}$$

On the other hand, two methods called implicit and explicit can be used for the time dependent differential equations. While each node at future time is obtained by using the present values of at the node and its neighbours in explicit method (Eq 6.31), the approximation is performed at an advanced time level in implicit method (Eq 6.32). A forward finite difference is generally used to approximate the time derivative. In this study, implicit method is used to solve the governing equations due to the stability of the method.

$$\frac{y_{i,j}^{k+1} - y_{i,j}^{k}}{\Delta t} = \frac{y_{i+1,j}^{k} - 2y_{i,j}^{k} + y_{i-1,j}^{k}}{(\Delta x)^2} \tag{6.31}$$

$$\frac{y_{i,j}^{k+1} - y_{i,j}^{k}}{\Delta t} = \frac{y_{i+1,j}^{k+1} - 2y_{i,j}^{k+1} + y_{i-1,j}^{k+1}}{(\Delta x)^2} \tag{6.32}$$

6.5.5.1. Discretization of Governing Equations of Adsorbent Bed-1 for Case I

As mentioned in Section 6.5.1, the considered annular bed is cylindrical and only gradients in the radial direction are taken into the consideration for Case I. By applying finite difference method, the continuity and heat transfer equations become:

$$T(i)^{k+1} = \frac{AT(i+1)^{k+1} + BT(i)^k + CT(i-1)^{k+1} + D\rho_b \Delta H_{ads}}{E} \tag{6.33}$$

$$A=\frac{k_{eff}}{2r(i)\Delta r}+\frac{k_{eff}}{(\Delta r)^2}-\frac{\rho_w(i+1)^{k+1}C_{pw}u(i+1)^{k+1}}{2\Delta r} \; ; \; B=\frac{\left(\rho C_{peff}\right)^k}{\Delta t}; \tag{6.34}$$

$$C=-\frac{k_{eff}}{2r(i)\Delta r}+\frac{k_{eff}}{(\Delta r)^2}+\frac{\rho_w(i-1)^{k+1}C_{pw}u(i-1)^{k+1}}{2\Delta r} \; ; D=\frac{\overline{w}(i)^{k+1}-\overline{w}(i)^k}{\Delta t} \tag{6.34}$$

$$E=\frac{\left(\rho C_{peff}\right)^{k+1}}{\Delta t}+\frac{\rho_w(i)^{k+1}C_{pw}u(i)^{k+1}}{r(i)}+\frac{2k_{eff}}{(\Delta r)^2} \tag{6.34}$$

The change in adsorbate concentration in the adsorbent with time has been defined with the LDF model. Since it is a first order ordinary differential equation, Euler's method is used.

$$\frac{\overline{w}(i)^{k+1}-\overline{w}(i)^k}{\Delta t}=\frac{15D_{eff}}{r_p^2}\left(\overline{w}_\infty(i)^{k+1}-\overline{w}(i)^k\right) \tag{6.35}$$

Furthermore, the velocity profile of the adsorptive which is obtained by Darcy's law is calculated by means of central finite difference approximation.

$$u(i)^{k+1}=-\frac{K_{app}}{\mu}\left[\frac{P(i+1)^{k+1}-P(i-1)^{k+1}}{2\Delta r}\right] \tag{6.36}$$

The initial and boundary conditions are given in Table 6.3. The given initial conditions for the isobaric cooling process are start-up values. After the first cycle completes, the initial conditions of isobaric cooling process are taken from the final values of isosteric cooling process. The temperature at point c (Figure 2.2) is taken as 473 K and the condenser pressure is taken as 8.5 kPa.

6.5.5.2. Discretization of Governing Equations of Adsorbent Bed-1 for Case II and Adsorbent Bed-2 (Case III)

In the second case, axial dispersion has also been taken into consideration. Therefore, the governing equations for mass and heat transfer equations for the bed are analysed for two-dimensional flow and given below, respectively.

Mass transfer of adsorptive in the adsorbent bed:

$$\rho_w(i,j)^{k+1}= \tag{6.37}$$

$$\frac{A\rho_w(i+1,j)^{k+1}+B\rho_w(i,j)^k+C\rho_w(i-1,j)^{k+1}-D\rho_b+F\rho_w(i,j+1)^{k+1}+G\rho_w(i,j-1)^{k+1}}{E}$$

$$A=-\frac{u_r(i+1,j)^{k+1}}{2\Delta r}\;;\;B=\frac{\varepsilon}{\Delta t}\;;\;C=\frac{u_r(i-1,j)^{k+1}}{2\Delta r}\;;\;D=\frac{\overline{w}(i,j)^{k+1}-\overline{w}(i,j)^k}{\Delta t} \tag{6.38}$$

$$E=\frac{\varepsilon}{\Delta t}+\frac{u_r(i,j)^{k+1}}{r(i)}\;;\;F=-\frac{u_z(i,j+1)^{k+1}}{2\Delta z}\;;G=\frac{u_z(i,j-1)^{k+1}}{2\Delta z} \tag{6.38}$$

Heat transfer in the adsorbent bed:

$$T(i)^{k+1}= \tag{6.39}$$

$$\frac{AT(i+1,j)^{k+1}+BT(i,j)^k+CT(i-1,j)^{k+1}+D\rho_b\Delta H_{ads}+ET(i,j+1)^{k+1}+FT(i,j-1)^{k+1}}{G}$$

$$A=\frac{k_{eff}}{2r(i)\Delta r}+\frac{k_{eff}}{(\Delta r)^2}-\frac{\rho_w(i+1,j)^{k+1}C_{pw}u_r(i+1,j)^{k+1}}{2\Delta r}\;;\;B=\frac{\left(\rho C_{peff}\right)^k}{\Delta t}\;; \tag{6.40}$$

$$C=-\frac{k_{eff}}{2r(i)\Delta r}+\frac{k_{eff}}{(\Delta r)^2}+\frac{\rho_w(i-1,j)^{k+1}C_{pw}u_r(i-1,j)^{k+1}}{2\Delta r}\;;D=\frac{\overline{w}(i,j)^{k+1}-\overline{w}(i,j)^k}{\Delta t} \tag{6.40}$$

$$E=\frac{k_{eff}}{(\Delta z)^2}-\frac{\rho_w(i,j+1)^{k+1}C_{pw}u_z(i,j+1)^{k+1}}{2\Delta z} \tag{6.40}$$

$$F=\frac{k_{eff}}{(\Delta z)^2}+\frac{\rho_w(i,j-1)^{k+1}C_{pw}u_z(i,j-1)^{k+1}}{2\Delta z} \tag{6.40}$$

$$G=\frac{\left(\rho C_{peff}\right)^{k+1}}{\Delta t}+\frac{\rho_w(i,j)^{k+1}C_{pw}u_r(i,j)^{k+1}}{r(i)}+\frac{2k_{eff}}{(\Delta r)^2}+\frac{2k_{eff}}{(\Delta z)^2} \tag{6.40}$$

Velocity distribution of the adsorptive within the adsorbent bed was defined by Darcy's law with two-dimensional approach.

$$u_r(i,j)^{k+1}=-\frac{K_{app}}{\mu}\left[\frac{P(i+1,j)^{k+1}-P(i-1,j)^{k+1}}{2\Delta r}\right]$$

(6.41)

$$u_z(i,j)^{k+1}=-\frac{K_{app}}{\mu}\left[\frac{P(i,j+1)^{k+1}-P(i,j-1)^{k+1}}{2\Delta z}\right]$$

(6.42)

7.5.4.3. Discretization of Governing Equations of Adsorbent Bed-3 (Case IV)

In the Case IV, the mass and heat transfer equations take the similar form with Case II and Case III. On the other hand, heat transfer equations for metal tube and HTF were discretized according to the one-dimensional approach, respectively.

$$T_m(i,j)^{k+1}=\frac{A+B\left(T_m(i,j+1)^{k+1}+T_m(i,j-1)^{k+1}\right)+CT_m(i,j)^k}{G}$$

(6.43)

$$A=h_fA_fT_f(i,j)^{k+1}+h_sA_sT(i,j)|_{r=R_0}{}^{k+1}$$

(6.44)

$$B=\frac{k_m}{(\Delta z)^2}\;;\;C=\frac{\rho_mC_{pm}V_m}{\Delta t}\;;\;D=\frac{\rho_mC_{pm}V_m}{\Delta t}+\frac{2k_m}{(\Delta z)^2}+h_fA_f+h_sA_s$$

(6.45)

$$T_f(i,j)^{k+1}=\frac{AT_f(i,j+1)^{k+1}+BT_f(i,j-1)^{k+1}+CT_f(i,j)^k+D}{E}$$

(6.46)

$$A=-\frac{u_f}{2\Delta z}+\frac{D_f}{(\Delta z)^2}\;;\;B=\frac{u_f}{2\Delta z}+\frac{D_f}{(\Delta z)^2}$$

(6.47)

$$C=\frac{1}{\Delta t}\;;\;D=\frac{h_fA_f}{\rho_fC_{pf}V_f}T_m(i,j)^{k+1}\;;\;E=\frac{1}{\Delta t}+\frac{2D_f}{(\Delta z)^2}\frac{h_fA_f}{\rho_fC_{pf}V_f}$$

(6.47)

6.5.5.3. Algorithm of the Solution Procedure

The solution procedure of the governing equations for all designs are similar with the study of Gediz Ilis et al. (2013). In details, the adsorption equilibrium, which was defined by Sips equilibrium relationship, adsorption rate equation (LDF model), heat transfer equation and continuity equation are solved simultaneously in order to obtain the temperature and adsorptive density gradients in the adsorbent bed. By using the new values of the adsorptive density and temperature, pressure distribution is calculated by using ideal gas law and velocity profile was calculated from Darcy's law. After obtaining solution for a time step, the next time step is started until the convergence criteria for inner iterations are satisfied (Eq 6.48).

$$\left|\frac{\varphi^{k+1}-\varphi^k}{\Delta t}\right|<10^{-5} \tag{6.48}$$

where φ illustrates values of the temperature or adsorptive density. On the other hand, the convergence criterion for the outer iteration is $\overline{w} \leq 0.18$ for the isobaric cooling process and $\overline{w} \geq 0.08$ for the isobaric heating process. The average values of the adsorbate concentration, temperature, adsorptive pressure, and adsorptive density in axial directions are calculated by arithmetic mean. For the radial direction, the average values are obtained from:

$$\overline{\varphi}(t)=\frac{\int_{R_i}^{R_0} 2r\varphi(r,t)dr}{\left(R_0^2-R_i^2\right)} \tag{6.49}$$

The number of nodes inside the bed has been taken as 7 in the radial direction and 7 in the axial direction. However, it has been seen that the time interval is affected from the value of the porosity in the bed. Therefore, time interval has been taken in the range of 0.00005-0.000001. The initial and boundary conditions for Case I, Case II, Case III and Case IV are given in Table 6.3, Table 6.4, Table 6.5 and Table 6.6.

Table 6.3. The initial and boundary conditions of the AHP for Case I

Process	Dependent variable	Boundary conditions at R=R$_i$	Boundary conditions at R=R$_0$	Initial conditions (t=0)
Isobaric cooling	Temperature (K)	$\partial T/\partial R = 0$	T=300	T=300
	Pressure (kPa)	P=P$_{ev}$=2	$\partial P/\partial R = 0$	P=f(T,ρ)
	Adsorptive density (kg/m³)	ρ$_w$= f(T,P)	ρ$_w$= f(T,P)	ρ$_w$≈0
	Amount of adsorbate (kg$_w$/kg$_z$)	W= f(T,P)	W= f(T,P)	W≈0
	Adsorptive velocity (m/s)	u= f(ρ$_w$,K$_{app}$)	$\partial u/\partial R = 0$	u=0
Isosteric heating	Temperature (K)	$\partial T/\partial R = 0$	T=363	Last values of isobaric cooling process
	Pressure (kPa)	$\partial P/\partial R = 0$	$\partial P/\partial R = 0$	
	Adsorptive density (kg/m³)	ρ$_w$= f(T,P)	ρ$_w$= f(T,P)	
	Amount of adsorbate (kg$_w$/kg$_z$)	W= f(T,P)	W= f(T,P)	
	Adsorptive velocity (m/s)	∂u/∂R=0	∂u/∂R=0	
Isobaric heating	Temperature (K)	$\partial T/\partial R = 0$	T=473	Last values of isosteric heating process
	Pressure (kPa)	P=P$_{cond}$=8.5	$\partial P/\partial R = 0$	
	Adsorptive density (kg/m³)	ρ$_w$= f(T,P)	ρ$_w$= f(T,P)	
	Amount of adsorbate (kg$_w$/kg$_z$)	W= f(T,P)	W= f(T,P)	
	Adsorptive velocity (m/s)	u= f(ρ$_w$,K$_{app}$)	$\partial u/\partial R = 0$	
Isosteric cooling	Temperature (K)	$\partial T/\partial R = 0$	T=300	Last values of isobaric heating process
	Pressure (kPa)	$\partial P/\partial R = 0$	$\partial P/\partial R = 0$	
	Adsorptive density (kg/m³)	ρ$_w$= f(T,P)	ρ$_w$= f(T,P)	
	Amount of adsorbate (kg$_w$/kg$_z$)	W= f(T,P)	W= f(T,P)	
	Adsorptive velocity (m/s)	$\partial u/\partial R = 0$	$\partial u/\partial R = 0$	

Table 6.4. The initial and boundary conditions of the AHP for Case II

Process	Dependent variable	BCs at R=R$_i$	BCs at R=R$_0$	BCs at z=0	BCs at z=L	IC (t=0)
Isobaric cooling	Temperature (K)	$\partial T/\partial R$ =0	T=300	$\partial T/\partial R$ =0	$\partial T/\partial R$ =0	T=300
	Pressure (kPa)	P=P$_{ev}$=2	$\partial P/\partial R$ =0	$\partial P/\partial z$ =0	$\partial P/\partial z$ =0	P=f(T,ρ)
	Adsorptive density (kg/m^3)	ρ$_w$= f(T,P)	ρ$_w$= f(T,P)	ρ$_w$= f(T,P)	ρ$_w$= f(T,P)	ρ$_w$≈0
	Amount of adsorbate (kg$_w$/kg$_z$)	W= f(T,P)	W= f(T,P)	W= f(T,P)	W= f(T,P)	W≈0
	Adsorptive velocity (m/s)	u= f(ρ$_w$,K$_{app}$)	$\partial u/\partial R$ =0	$\partial v/\partial z$ =0	$\partial v/\partial z$ =0	u=0
Isosteric heating	Temperature (K)	$\partial T/\partial R$ =0	T=363	$\partial T/\partial R$ =0	$\partial T/\partial R$ =0	Last values of isobaric cooling process
	Pressure (kPa)	$\partial P/\partial R$ =0	$\partial P/\partial R$ =0	$\partial P/\partial z$ =0	$\partial P/\partial z$ =0	
	Adsorptive density (kg/m^3)	ρ$_w$= f(T,P)	ρ$_w$= f(T,P)	ρ$_w$= f(T,P)	ρ$_w$= f(T,P)	
	Amount of adsorbate (kg$_w$/kg$_z$)	W= f(T,P)	W= f(T,P)	W= f(T,P)	W= f(T,P)	
	Adsorptive velocity (m/s)	∂u/∂R=0	∂u/∂R=0	$\partial v/\partial z$ =0	$\partial v/\partial z$ =0	
Isobaric heating	Temperature (K)	$\partial T/\partial R$ =0	T=473	$\partial T/\partial R$ =0	$\partial T/\partial R$ =0	Last values of isosteric heating process
	Pressure (kPa)	P=P$_{cond}$=8.5	$\partial P/\partial R$ =0	$\partial P/\partial z$ =0	$\partial P/\partial z$ =0	
	Adsorptive density (kg/m^3)	ρ$_w$= f(T,P)	ρ$_w$= f(T,P)	ρ$_w$= f(T,P)	ρ$_w$= f(T,P)	
	Amount of adsorbate (kg$_w$/kg$_z$)	W= f(T,P)	W= f(T,P)	W= f(T,P)	W= f(T,P)	
	Adsorptive velocity (m/s)	u= f(ρ$_w$,K$_{app}$)	$\partial u/\partial R$ =0	$\partial v/\partial z$ =0	$\partial v/\partial z$ =0	
Isosteric cooling	Temperature (K)	$\partial T/\partial R$ =0	T=300	$\partial T/\partial R$ =0	$\partial T/\partial R$ =0	Last values of isobaric heating process
	Pressure (kPa)	$\partial P/\partial R$ =0	$\partial P/\partial R$ =0	$\partial P/\partial z$ =0	$\partial P/\partial z$ =0	
	Adsorptive density (kg/m^3)	ρ$_w$= f(T,P)	ρ$_w$= f(T,P)	ρ$_w$= f(T,P)	ρ$_w$= f(T,P)	
	Amount of adsorbate (kg$_w$/kg$_z$)	W= f(T,P)	W= f(T,P)	W= f(T,P)	W= f(T,P)	
	Adsorptive velocity (m/s)	$\partial u/\partial R$ =0	$\partial u/\partial R$ =0	$\partial v/\partial z$ =0	$\partial v/\partial z$ =0	

Table 6.5. The initial and boundary conditions of the AHP for Case III

Process	Dependent variable	BCs at R=R$_i$	BCs at R=R$_0$	BCs at z=0	BCs at z=L	IC (t=0)
Isobaric cooling	Temperature (K)	$\partial T/\partial R$ =0	T=300	T=300	T=300	T=300
	Pressure (kPa)	P=P$_{ev}$=2	$\partial P/\partial R$ =0	$\partial P/\partial z$ =0	$\partial P/\partial z$ =0	P=f(T,ρ)
	Adsorptive density (kg/m^3)	ρ_w= f(T,P)	ρ_w= f(T,P)	ρ_w= f(T,P)	ρ_w= f(T,P)	ρ_w≈0
	Amount of adsorbate (kg$_w$/kg$_z$)	W= f(T,P)	W= f(T,P)	W= f(T,P)	W= f(T,P)	W≈0
	Adsorptive velocity (m/s)	u= f(ρ_w,K$_{app}$)	$\partial u/\partial R$ =0	$\partial v/\partial z$ =0	$\partial v/\partial z$ =0	u=0
Isosteric heating	Temperature (K)	$\partial T/\partial R$ =0	T=363	T=363	T=363	Last values of isobaric cooling process
	Pressure (kPa)	$\partial P/\partial R$ =0	$\partial P/\partial R$ =0	$\partial P/\partial z$ =0	$\partial P/\partial z$ =0	
	Adsorptive density (kg/m^3)	ρ_w= f(T,P)	ρ_w= f(T,P)	ρ_w= f(T,P)	ρ_w= f(T,P)	
	Amount of adsorbate (kg$_w$/kg$_z$)	W= f(T,P)	W= f(T,P)	W= f(T,P)	W= f(T,P)	
	Adsorptive velocity (m/s)	$\partial u/\partial R$=0	$\partial u/\partial R$=0	$\partial v/\partial z$ =0	$\partial v/\partial z$ =0	
Isobaric heating	Temperature (K)	$\partial T/\partial R$ =0	T=473	T=473	T=473	Last values of isosteric heating process
	Pressure (kPa)	P=P$_{cond}$=8.5	$\partial P/\partial R$ =0	$\partial P/\partial z$ =0	$\partial P/\partial z$ =0	
	Adsorptive density (kg/m^3)	ρ_w= f(T,P)	ρ_w= f(T,P)	ρ_w= f(T,P)	ρ_w= f(T,P)	
	Amount of adsorbate (kg$_w$/kg$_z$)	W= f(T,P)	W= f(T,P)	W= f(T,P)	W= f(T,P)	
	Adsorptive velocity (m/s)	u= f(ρ_w,K$_{app}$)	$\partial u/\partial R$ =0	$\partial v/\partial z$ =0	$\partial v/\partial z$ =0	
Isosteric cooling	Temperature (K)	$\partial T/\partial R$ =0	T=300	T=300	T=300	Last values of isobaric heating process
	Pressure (kPa)	$\partial P/\partial R$ =0	$\partial P/\partial R$ =0	$\partial P/\partial z$ =0	$\partial P/\partial z$ =0	
	Adsorptive density (kg/m^3)	ρ_w= f(T,P)	ρ_w= f(T,P)	ρ_w= f(T,P)	ρ_w= f(T,P)	
	Amount of adsorbate (kg$_w$/kg$_z$)	W= f(T,P)	W= f(T,P)	W= f(T,P)	W= f(T,P)	
	Adsorptive velocity (m/s)	$\partial u/\partial R$ =0	$\partial u/\partial R$ =0	$\partial v/\partial z$ =0	$\partial v/\partial z$ =0	

Table 6.6. The initial and boundary conditions of the AHP for Case IV

Process	Dependent variable	BCs at R=R$_i$	BCs at R=R$_0$	BCs at z=0	BCs at z=L	ICs (t=0)
Isosteric Cooling	Temperature (K)	$\partial T / \partial R = 0$	$-k_{eff}\dfrac{\partial T}{\partial r} = h_s(T - T_m)$	$\partial T / \partial R = 0$	$\partial T / \partial R = 0$	T=300
	Pressure (kPa)	P=P$_{ev}$=2	$\partial P / \partial R = 0$	$\partial P / \partial R = 0$	$\partial P / \partial R = 0$	P=f(T,ρ)
	Adsorptive density (kg/m^3)	ρ$_w$= f(T,P)	ρ$_w$= f(T,P)	ρ$_w$= f(T,P)	ρ$_w$= f(T,P)	ρ$_w$≈0
	Amount of adsorbate (kg$_w$/kg$_z$)	W= f(T,P)	W= f(T,P)	W= f(T,P)	W= f(T,P)	W≈0
	Adsorptive velocity (m/s)	u=f(ρ$_w$,K$_{ap}$)	$\partial u / \partial R = 0$	v= 0	v= 0	u=0 v=0
Isobaric Heating	Temperature (K)	$\partial T / \partial R = 0$	$-k_{eff}\dfrac{\partial T}{\partial r} = h_s(T - T_m)$	$\partial T / \partial R = 0$	$\partial T / \partial R = 0$	Last values of isobaric cooling process
	Pressure (kPa)	$\partial P / \partial R = 0$	$\partial P / \partial R = 0$	$\partial P / \partial R = 0$	$\partial P / \partial R = 0$	
	Adsorptive density (kg/m^3)	ρ$_w$= f(T,P)	ρ$_w$= f(T,P)	ρ$_w$= f(T,P)	ρ$_w$= f(T,P)	
	Amount of adsorbate (kg$_w$/kg$_z$)	W= f(T,P)	W= f(T,P)	W= f(T,P)	W= f(T,P)	
	Adsorptive velocity (m/s)	u=f(ρ$_w$,K$_{ap}$)	u=0	v= 0	v= 0	
Isosteric Heating	Temperature (K)	$\partial T / \partial R = 0$	$-k_{eff}\dfrac{\partial T}{\partial r} = h_s(T - T_m)$	$\partial T / \partial R = 0$	$\partial T / \partial R = 0$	Last values of isosteric heating process
	Pressure (kPa)	P=P$_{cond}$=8.5	$\partial P / \partial R = 0$	$\partial P / \partial R = 0$	$\partial P / \partial R = 0$	
	Adsorptive density (kg/m^3)	ρ$_w$= f(T,P)	ρ$_w$= f(T,P)	ρ$_w$= f(T,P)	ρ$_w$= f(T,P)	
	Amount of adsorbate (kg$_w$/kg$_z$)	W= f(T,P)	W= f(T,P)	W= f(T,P)	W= f(T,P)	
	Adsorptive velocity (m/s)	u= f(ρ$_w$,K$_{app}$)	u=0	v= 0	v= 0	

Table 6.6. (Cont)

Process	Dependent variable	BCs at $R=R_i$	BCs at $R=R_0$	BCs at z=0	BCs at z=L	ICs (t=0)
Isobaric Cooling	Temperature (K)	$\partial T/\partial R = 0$	$-k_{eff}\dfrac{\partial T}{\partial r} = h_s(T - T_m)$	$\partial T/\partial R = 0$	$\partial T/\partial R = 0$	Last values of isobaric heating process
	Pressure (kPa)	$\partial P/\partial R = 0$	$\partial P/\partial R = 0$	$\partial P/\partial R = 0$	$\partial P/\partial R = 0$	
	Adsorptive density (kg/m^3)	$\rho_w = f(T,P)$	$\rho_w = f(T,P)$	$\rho_w = f(T,P)$	$\rho_w = f(T,P)$	
	Amount of adsorbate (kg$_w$/kg$_z$)	$W = f(T,P)$	$W = f(T,P)$	$W = f(T,P)$	$W = f(T,P)$	
	Adsorptive velocity (m/s)	$u = f(\rho_w, K_{app})$	$\partial u/\partial R = 0$	$u = f(\rho_w, K_{app})$	$u = f(\rho_w, K_{app})$	
Heat Transfer Fluid	Temperature (K)			$T_f = T_{h,in}$ $T_f = T_{c,in}$	$\partial T_f/\partial z = 0$	T=300
Metal Tube	Temperature (K)			$\partial T_m/\partial z = 0$	$\partial T_m/\partial z = 0$	T=300

6.6. Enhancement of Effective Thermal Conductivity of Zeolite by High Thermal Conductive Material (Consolidated Bed Design)

The low thermal conductivity of the available adsorbents is one of the biggest obstacles in enhancement of the adsorption heat pumps. Therefore, the researchers try to develop a high thermal conductive material which also maintains high adsorption capacity, high mass transfer properties and high heat of adsorption value. Although, zeolite 13X-water provides most of the expected properties, low thermal conductivity still requires enhancement. Therefore, some researchers pay attention to increase the heat transfer in the adsorbent bed by consolidated bed design method (see Chapter 2).

Due to its advance physical and chemical properties such as high Young modulus, high electrical and thermal conductivity, graphene is one of the most remarkable chemicals that gains attention of researchers.

In this thesis, the enhancement of the thermal conductivity in the bed is performed by consolidating zeolite 13X with a commercial graphene powder (Nanokar).

Furthermore, the manufacturing procedure of graphene from graphite powder is also introduced in this chapter. The effect of reaction time, amount of H_2O_2 and amount

of HCl and ethanol during synthesizing graphene oxide and the effect of reducing agent on removal of oxygen functional groups are investigated in this chapter, too.

6.6.1. Graphene

Graphene which has a hexagonal honeycomb lattice, is a single layer allotrope of carbon atom. It is the thinnest material that is known with a one carbon atom thick. This 2D layer structural chemical gains attention of the researchers in recent years due to its advance physical and chemical properties such as high young modulus, high electrical and thermal conductivity. For instance, for single layer graphene, Balandin et al. reported thermal conductivity as approximately 5000 W/m.K (Balandin et al. 2008). Due to the reported thermal conductivity values of graphene, it was used as high thermal conductive material within the consolidating adsorbent bed design.

6.6.1.1. Manufacturing Zeolite/Graphene Pellet

The enhancement of thermal conductivity of zeolite 13X is supposed to be performed by mixing crystal zeolite 13X with reduced graphene oxide. However, for practically use of the adsorbent, a macroporous adsorbent with suitable dimensions, mechanical strength and porosity should be produced (Ruthven 1984). Furthermore, it is undesirable to increase mass transfer resistance within the adsorbent particle and decrease of water vapor adsorption capacity.

In order to obtain pellets, extrusion or granulation can be used to form cylindrical or spherical pellets, respectively. In agglomeration of the crystals, clay binder such as kaolin, sepiolite, attapulgite can be used to increase the mechanical strength. Especially, metakaolin, which was obtained by calcination of kaolin at 500-600°C, is preferred in binderless zeolite applications. By this way, the adsorption capacity of the adsorbent is not decreased and the increase in mass transfer resistance can be eliminated.

In literature, the amount of the zeolite, binder and water is not given, properly. Thus, prior to manufacturing graphene/zeolite pellet, the amount of zeolite, binder and water is optimized. In these studies, kaolin is used as binder. However, it is seen that it is hard to agglomerate the zeolite and kaolin without an organic binder. Therefore, 1 g of methyl cellulose, which is added in the dry mixing step, is used in the manufacturing

process. The steps for producing zeolite pellet are also given in Figure 6.11. Extrusion is used in the process and cylindrical zeolites are obtained.
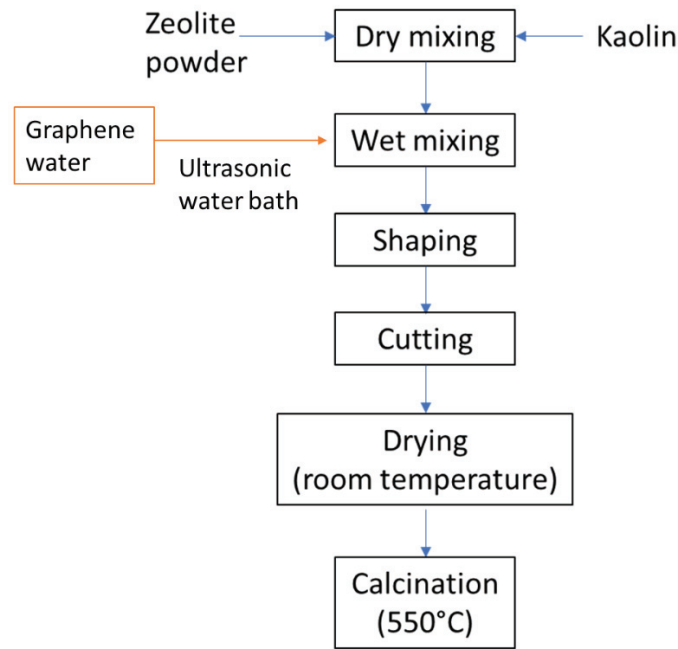

Figure 6.11. Manufacturing procedure of zeolite 13X pellet

After determining the optimum amount of zeolite and binder, first graphene was dispersed with deionized water in ultrasonic bath, then added into the zeolite-binder mixture. It was undesirable to decrease the adsorption capacity of the zeolite and to deteriorate its structural form. Therefore, 1 wt% of graphene was added into the mixture. In order to prevent the removal of the graphene from the pellet, the calcination process is performed in N_2 atmosphere.

The effective thermal conductivity of zeolite/graphene pellet was calculated by Eq 6.50 which is derived by Maxwell to define thermal conductivity of composite solids. In that equation, the material made of spheres of thermal conductivity k_1 enclosed in a continuous solid phase with thermal conductivity k_0. Although the volume fraction of enclosed sphere, ϕ, was considered as sufficiently small in Maxwell's equation it was still applicable for large volume fractions with neglecting the effect of nonuniform sphere distributions (Bird et al. 2001).

$$\frac{k_{eff}}{k_0} = 1 + \frac{3\phi}{\left(\dfrac{k_1 + 2k_0}{k_1 - k_0}\right) - \phi} \tag{6.50}$$

The characterization of the obtained pellets with commercial zeolite 13X achieved by means of TGA, FTIR, SEM analysis. The effective thermal conductivity measurements of synthesized Zeolite 13X and Zeolite 13X/Graphene pellet was performed with hot wire method.

6.6.1.2. Previous Studies Performed with Graphene and Zeolites

Graphene oxide and reduced graphene oxide can be used in different application fields such as membrane, lithium-ion battery, solar cell, supercapacitor, biomedical applications (Zhao et al. 2011; Boukhvalov et al. 2013; Han et al. 2013; Perrozzi et al. 2015; Yoo et al. 2017; Liu et al. 2017; Huang et al. 2017). For instance, Liu et al. performed a study with graphene oxide (HGO) which was prepared by Hummer's method and reduced graphene oxide (RGO) that was reduced by thermal reduction in air at 200°C (Liu et al. 2017). In that study, they investigated the water adsorption capacity of HGO and RGO papers for air dehumidification and compared their results with silica gel. According to the results, the water adsorption capacity of HGO was higher than silica gel and obtained Type IV adsorption isotherm which indicated the multilayer adsorption with capillary condensation. On the other hand, while the water adsorption capacity of RGO was small at low relative humidity values, it was increased at relative humidity of 90% which showed that the water-water interactions were dominated for RGO.

On the other hand, the studies with zeolite are mainly focused on the separation and biomedical applications (He et al. 2012; Zhang et al. 2013; Todd et al. 2013; Yu et al. 2013; Nagarjuna et al. 2015; Khatamian et al. 2015; Yang et al. 2015; Xu et al. 2016; Khatamian et al. 2017; Liu et al. 2017; Cheng et al. 2017). In the study of Yu et al., they functionalized graphene oxide nanosheets with acid treated clinoptilolite-rich zeolite for cationic dye removal (Yu et al. 2015). In that study, they observed that covalent ester bonds were occurred between carboxyl groups of graphene oxide and hydroxyl groups of acid-treated zeolite. The covalent ester linkage was also observed by Cheng et al. who used acid treated Beta zeolite and graphene oxide to investigate rhodamine B adsorption (Cheng et al. 2017). On the other hand, Yang et al. performed a study with composite disks which were obtained by compression molding of zeolite 13X and graphene oxide and few layers graphene powders under pressure range of 100-350 MPa (Yang et al. 2015). In the water adsorption studies, they observed that the adsorption capacity was

only decreased by 2% when 3% graphene oxide was added to composite disks. Furthermore, they observed that while graphene oxide did not have effect on thermal conductivity of zeolites, it was increased by 6-21% in the case of few layers graphene.

In 2021, Rocky et al. performed a study to enhance the thermal conductivity of a chabazite type zeolite with graphene which would be used in adsorption heat pumps later (Rocky et al. 2021). They used commercial graphene (H-grade and M-grade) in their studies (Table 6.7). In order to obtain a composite material, they mixed powders of graphene and zeolite in water to obtain a slurry. Then, they compressed the slurry and dried the sample at 150°C for 3 hours. In the experimental study, they observed that the effective thermal conductivity of zeolite was increased from 0.088 W/m.K to approximately 3 W/m.K when 50 wt% H-grade graphene was used.

Table 6. 7. Thermophysical properties of graphene

(Source: Rocky et al. 2021)

Property	H25-GNPs	M25-GNPs
Average particle diameter (μm)	25	25
Average thickness (nm)	15	6-8
Bulk density (g cm^{-3})	0.03-1	0.03-1
Thermal conductivity (parallel to surface) (W m^{-1} K^{-1})	3000	3000
Thermal conductivity (perpendicular to surface) (W m^{-1} K^{-1})	6	6
Surface area (m^2 g^{-1})	50-80	120-150

6.6.2. Preparation of High Conductive Graphene

Although graphene has extremely high thermal conductivity, difficulty in large scale synthesize of graphene and the high price of commercial graphene is limiting the applications. Therefore, the possibility of manufacturing graphene from graphite by chemical processes and reduction has increased the attraction of researchers. In the scope of the thesis, first the production of the graphite oxide is optimized, then reduction is performed with two different reducing agents.

6.6.2.1. Synthesizing Graphite Oxide (GO)

Although the scientists tried to manufacture graphene since 1859, the first manufacturing of graphene was succeeded in 2004 by Geim and Novoselov. In their study, they put an ordinary scotch tape on the graphite stone and obtain monolayer graphene which will later bring them Nobel Prize in 2010. On the other hand, the manufacturing of graphene oxide was earlier. In 1859, Brodie synthesized graphite oxide by adding potassium chlorate ($KClO_3$) to graphite flakes in fuming nitric acid (HNO_3). The Brodie's method was improved by Staudenmaier in 1898. Instead of using only HNO_3, Staudenmaier reduced the amount of HNO_3 by the ratio of two thirds and placed H_2SO_4 in the same ratio (Dreyer et al. 2010; Yu et al. 2016). The addition of H_2SO_4 increased the oxidation of graphite oxide. In 1958, Hummer and Offeman (Hummer's method) used potassium permanganate ($KMnO_4$) and $NaNO_3$ instead of HNO_3 and $KClO_3$ with H_2SO_4 in manufacturing process. Although Hummer's method survived, it still required improvements due the generation of toxic gases such as NO_2 and N_2O_4 and incomplete oxidation. Therefore, researchers improved the Hummer's method in different ways (Figure 6.12). In 2010, Marcano et al. improved the Hummer's method by increasing the $KMnO_4$ amount and used phosphoric acid (H_3PO_4) instead of $NaNO_3$ (Marcano et al. 2010). This method is also known as Tour's method. In this method, the oxidation degree was increased, large scale production was achieved, and toxic gas generation was eliminated. In all of these methods, the reaction is stopped by using hydrogen peroxide (H_2O_2). In the study of Kumar et al., they claimed that the concentration of H_2O_2 influenced surface and molecular structure of graphene oxide (Kumar et al. 2017). They used 50, 70 and 100 mL of 30% H_2O_2 solution in the study and observed that the exfoliation of graphene oxide increased with increasing H_2O_2 concentration. Furthermore, the increase in H_2O_2 concentration caused the epoxy groups to vanish from the structure of graphene oxide.

In Brodie's, Hummer's and Tour's methods, multilayer graphite oxide is synthesized. Therefore, in order to obtain single layer graphene oxide exfoliation is performed by means of ultrasonication (Figure 6.13). Botas et al. stated that the exfoliation time should be optimized. They emphasized that when exfoliation time was too long, the break-up of graphene oxide sheets was observed due to the effect of hydroxyl and epoxy groups on the strength of graphene oxide (Botas et al. 2013).
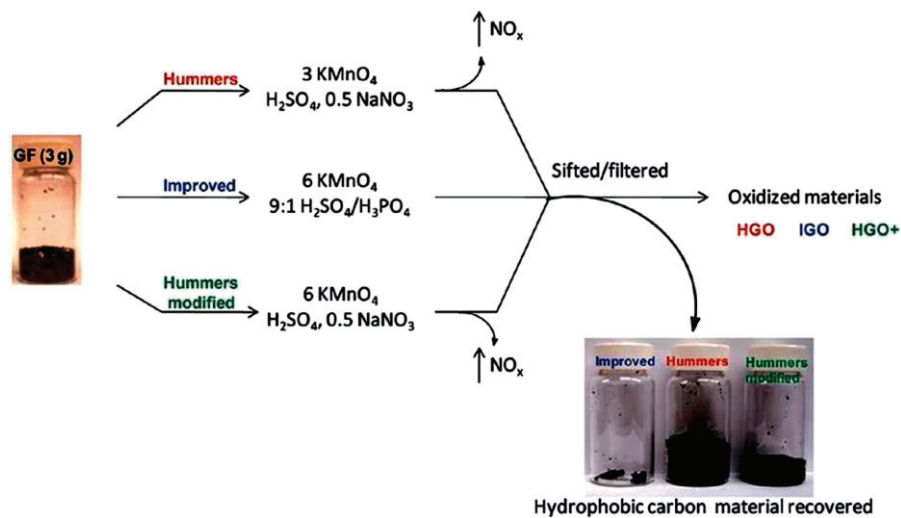
Figure 6.12. Methods to produce graphite oxide
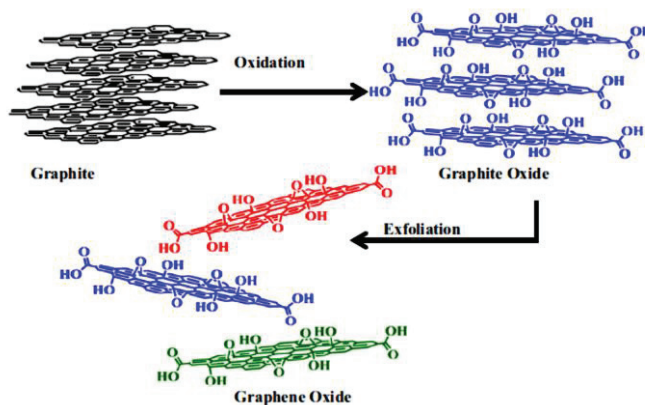
(Source: Marcano et al. 2010)

Figure 6.13. Manufacturing procedure of graphene oxide

(Source: Ammar et al. 2016)

In the structure of graphene oxide, oxygen functionalized groups such as carboxyl, epoxy and hydroxyl have been located (Figure 6.14). While the carboxyl groups are placed at the edges of the plane, the epoxy and hydroxyl groups are located at the basal plane. These functional groups give the hydrophilic property to the graphene oxide. On the other hand, they also reduce the conductive properties of the graphene oxide. Mu et al. emphasized that the thermal conductivity of graphene oxide was reduced by 50% when compared with pristine graphene at an oxygen content of 0.5% (Mu et al. 2014).
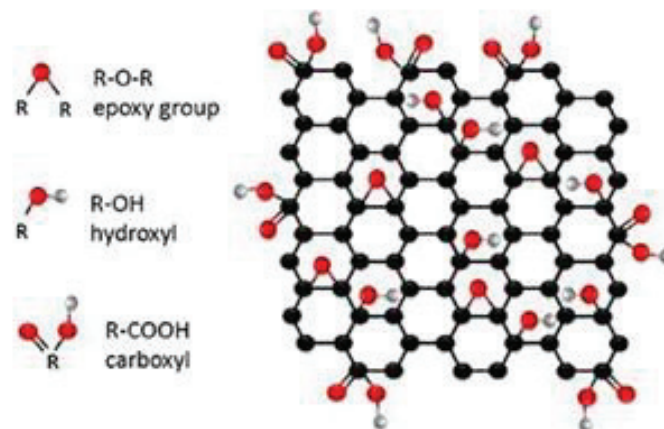
Figure 6.14. Chemical structure of graphene oxide

(Source: Chiu et al. 2014)

Botas et al. and Diker et al. studied the effect of raw particle size of graphite on the structure of graphene oxide (Botas et al. 2012; Diker et al. 2017). Both of them claimed that the size of raw graphite had a key role on the distribution and amount of oxygen functionalized groups which also affect the interlayer spacing of graphene oxide. They stated that as the particle size of raw graphite flakes decreased, while the amount of epoxy groups in the basal plane was increasing, the amount of carboxyl groups at the edges was decreasing. Diker et al. claimed that this may be related with the slower diffusion of $KMnO_4$ and lower amount of H_3PO_4 per unit area of graphene oxide (Diker et al. 2017). On the other hand, they stated that smaller raw graphite size increased the lateral size of graphene oxide which was the opposite of the statement of Dao and Jeong (Dao and Jeong 2015).

Due to the presence of oxygen functional groups in the structure of graphene oxide, they have excellent hydrophilic properties. In the study of Lian et al., they stated that the water vapor adsorption capacity of graphene oxide was 0.13 g/g and 0.58 g/g at relative pressures of 0.1 and 0.9, respectively (Lian et al. 2018). They also indicated that the isotherm type was combination of type I and type IV isotherms related to the d-spacing of graphene oxide layers which was increased with increasing relative pressure (Figure 6.15). Furthermore, they observed that at high relative pressures water-water interactions were dominated which confirms the capillary condensation between graphene oxide layers.
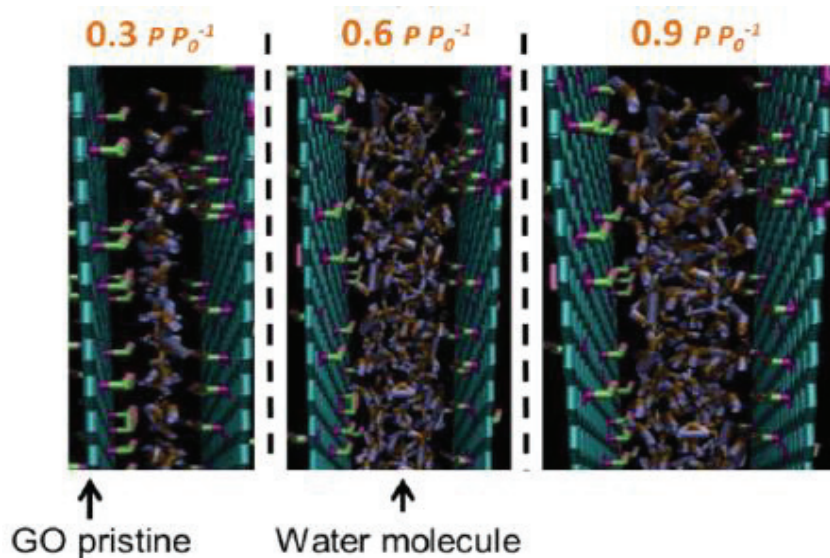
Figure 6.15. Water vapor adsorption on graphene oxide

(Source: Lian et al. 2018)

In the scope of this thesis, improved Hummer's method (Tour's method) has been used due to having high oxidation degree, opportunity for large scale production and generating no toxic gas. Graphite powder is oxidized in $KMnO_4$ and mixture of H_2SO_4/H_3PO_4 (9:1 volume ratio) in order to produce graphite oxide. As a detailed procedure (Marcano et al. 2010; Diker et al. 2017), H_2SO_4 and H_3PO_4 (180:20 mL) is mixed in a bottle and put in refrigerator which was at +4°C. Meanwhile, graphite powder (2.6 g) and $KMnO_4$ (14 g) is mixed in a beaker. Then, due to the highly exothermic reaction, the mixture of H_2SO_4/H_3PO_4 is added very slowly with a dropper during stirring continues in an ice bath. Then, the reaction is started at 50°C in a shaking water bath at 120 rpm. The reaction is stopped by adding H_2O_2 into ice water (300 mL) and pouring the GO mixture onto the H_2O_2 mixture. At that point, it is expected that the colour of the mixture turns from dark brown to golden. Finally, the mixture is washed and centrifuged by HCl (%30), ethanol and distilled water until the solution neutralized, then dried in vacuum drier.

However, there is an inconsistency in the performed studies for the method especially for the amount of H_2O_2, the reaction time and the amount of HCl and ethanol used in washing of graphite oxide. Therefore, the effect of these parameters is examined before the reduction is performed (Table 6.8).

Table 6.8. Parameters used in synthesizing graphite oxide

Sample Name	Reaction time (h)	H₂O₂ (mL)	HCl and ethanol (mL)
S1	16	2	200
S2	16	2	300
S3	16	20	300
S4	12	20	300

6.6.2.2. Reduction of Graphite Oxide to High Conductive RGO

Due to the functionalized groups in the structure of graphene oxide, it works as insulating material. In order to increase conductive properties of graphene oxide, reduction process is performed. In literature, different reduction techniques such as chemical, thermal, and electrochemical have been illustrated (Gao et al. 2010; Chen et al. 2010; Haubner et al. 2010; Pei and Cheng 2013; Dao and Jeong 2015; Alam et al. 2017). In thermal reduction, the graphene oxide is exposed to high temperature. On the other hand, in chemical reduction, there are several organic and inorganic reducing agents such as hydrazine hydrate, glucose, amino acids, etc. that can be used (Singh et al. 2016; Emiru and Ayele 2017). Besides, hydrazine hydrate is the most common reducing agent used in literature (Marcano et al. 2010; Park et al. 2011; Cao and Zhang 2015).

In 2014, Xu et al. claimed that the selective reduction of graphene oxide could be achieved by using ethanol, ethyl glycol and glycerol which were reduced epoxy groups and provided higher conductive property of graphene oxide (Xu et al. 2014). Similar reduction can be obtained for hydroxyl groups (Chua and Pumera, 2013). In hydrazine hydrate reduction, the epoxy and hydroxyl groups located at the basal plane can be removed. On the other hand, the hydroxyl groups at the edge of the aromatic plane were not removed and carboxyl groups are partially removed. Furthermore, the previous works showed that the chemical reduction would increase thermal conductivity and thermal stability of graphene oxide more than thermal reduction (Haubner et al. 2010; Park et al. 2011).

As in the synthesis of the graphene oxide, the size of raw graphite also affects the properties of reduced graphene oxide. Tran et al. studied the effect of raw particle size on electrochemical properties of reduced graphene oxide (Tran et al. 2014). Different from graphene oxide, the small particle size had a favorable effect on the reduced graphene

oxide. Tran et al. indicated that the electrochemical properties of graphene oxide reduced by hydrazine hydrate was increased with decreasing raw particle size.

Although, there are several reducing agents and reducing methods in literature. In this study, hydrazine hydrate which is commonly used in reduction of graphite oxide and ascorbic acid which is an environmentally friendly are used as reducing agent and chemical reduction is performed.

The reduction is started by exfoliation of 400 mg graphite oxide in 400 mL distilled water (1 mg/mL). The exfoliation is performed in two steps. First, the graphite oxide solution is stirred at high speed for 24 hours and then, it is sonicated in ultrasonic bath for 1 hour. Then, the reducing agent is added (4 mL hydrazine hydrate or 400 mg ascorbic acid) and the reduction is performed at 95°C for 3 hours. Finally, the solution is filtrated by vacuum filtration and washed with distilled water until the pH is neutralized.

Furthermore, it is seen that some of the researchers also use NH_3 during the reducing graphite oxide. In order to investigate the effect of NH_3 on reduction, NH_3 (30%) is added until pH of the solution is reached approximately to 9 before adding reducing agent.

CHAPTER 7

RESULTS AND DISCUSSIONS

In this section, the results of the experimental and theoretical studies will be discussed. The characterization results of the zeolites enlighten the water vapor affinity of zeolite 13X. Then, the adsorption experiments performed with zeolite 13X-water pair will be discussed and equilibrium and kinetic data will be evaluated. The effective thermal conductivity measurement of zeolite is also represented and the effect of the metal additives on the effective thermal conductivity in the bed will be investigated. By means of the obtained results, the theoretical analysis of the adsorption heat pump will be discussed in detail and the effect of different parameters on the performance of adsorption heat pump will be illustrated. Finally, the experimental study performed to obtain high thermal conductive zeolite/RGO pellet are summarized in the scope of the thesis.

7.1. Characterization of Zeolites

Particle and surface morphologies, crystal size and structures and elemental compositions are determined with scanning electron microscopy (SEM). The crystal structures of zeolites can be observed in Figure 7.1. While zeolite 4A and 5A crystals have cubic, zeolite 13X crystals have spherical morphology.
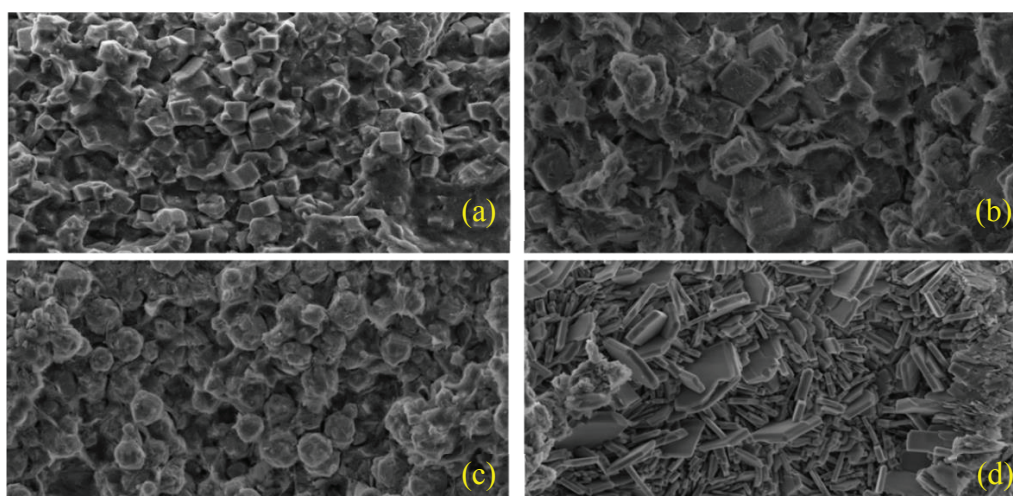

Figure 7.1. Representative SEM images of zeolites at 10000X magnification a) 4A b) 5A c) 13X d) Clinoptilolite

The elemental compositions (atomic %) obtained from EDX are represented in Table 7.1. The atomic Si/Al ratio, which affects the affinity of zeolites to water vapor, is in the range of 1.30-1.40 for zeolite 13X and type A, and 4.85 for Clinoptilolite, respectively which is consistent with the literature (Breck 1974).

Table 7. 1. Elemental compositions of zeolites

Element	4A (Atomic %)	5A (Atomic %)	13X (Atomic %)	Clinoptilolite (Atomic %)
O	73.32	71.36	71.70	75.83
Na	4.84	2.62	8.26	0.31
Mg	1.39	1.10	0.95	0.44
Al	7.69	8.30	8.15	3.72
Si	10.14	11.56	10.94	18.03
K	2.36	-	-	0.81
Ca	0.25	5.06	-	0.85

The weight losses of zeolites 4A, 5A, 13X and Clinoptilolite-rich zeolitic material, which were hydrated in saturated KCl solution medium prior to analysis, are illustrated in Figure 7.2 which is obtained from thermogravimetric analysis. In thermogravimetric analysis, it is observed that maximum weight loss is achieved for zeolite 13X. Different inflections points can clearly be detected from the graph. For example, the externally and loosely bounded water inflection points for zeolite 13X are at approximately 100°C and 180°C, respectively. Above ≈180 °C, slow dehydration of tightly bound water takes place for zeolite 13X. Additionally, there is an interruption in the curve of zeolite 13X at 600°C which indicates the deteriorations in the framework structure and is consistent with the results given in literature (Breck 1974; Tsitsishvili et al. 1992).
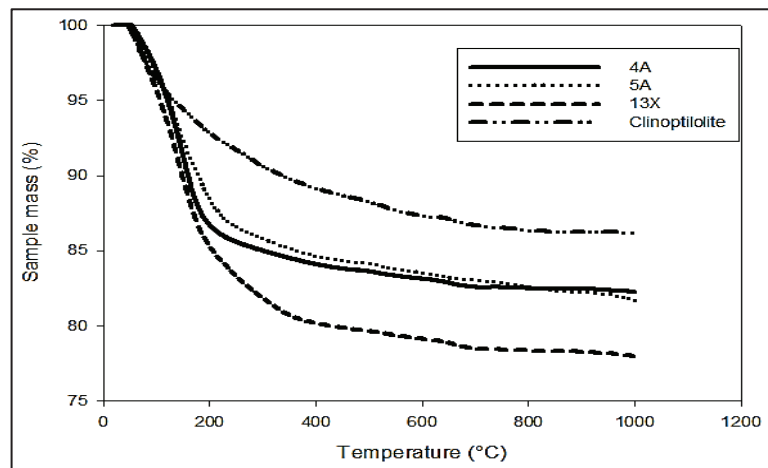

Figure 7.2. TGA curves of different zeolites

The structural characterization of zeolites is provided by infrared spectroscopy (IR) by KBr pellet technique. The experimental data is normalized according to the maximum peak value to compare properly. The normalized data have been represented in Figure 7.3. The characteristic spectra of zeolites are summarized in Table 7.2. The position of internal tetrahedra asymmetric stretching band depends on the Si/Al ratio and can be considered as indicative for the aluminium content in the framework. The peak that can be observed at approximately 1645 cm^{-1} is the characteristics of bending vibration of water molecule. On the other hand, three different bands may be examined indicating the hydroxyl groups in the structure of zeolites (Breck 1974). The peak at 3740 cm^{-1} can be observed in all dehydrated zeolites illustrating OH groups on the surface. The protons bonded to the framework can be recognized at the 3650 cm^{-1} (high frequency OH) and 3540 cm^{-1} (low frequency OH) and refers to cation hydrolysis.
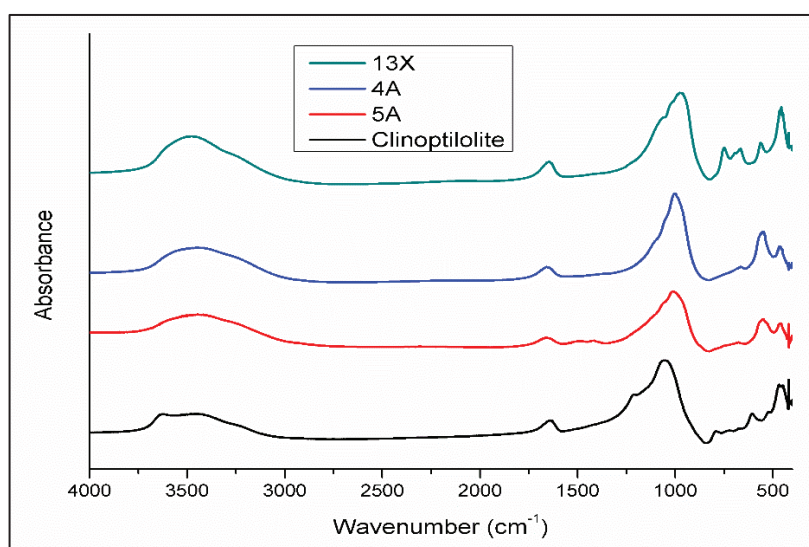

Figure 7.3. FTIR spectra of zeolites

Table 7.2. Characteristic IR-bands of zeolites

(Source: Breck, 1974)

	Asymmetric stretching due to internal vibrations	1250-950 cm^{-1}
Internal Tetrahedra	symmetric stretching	720-650 cm^{-1}
	T-O bending	500-420 cm^{-1}
	Double ring	650-500 cm^{-1}
	Pore opening	300-420 cm^{-1}
External linkages	symmetric stretching	750-820 cm^{-1}
	asymmetric stretching	1150-1050 cm^{-1}

7.2. Adsorption Equilibrium and Kinetics

The adsorption experiments have been performed at 35, 45 and 60°C. During the adsorption process, pressure and temperature data have been collected against time as mentioned in Chapter 6. The representative graph of pressure and temperature change for the adsorption temperature of 35°C is given in Figure 7.4.
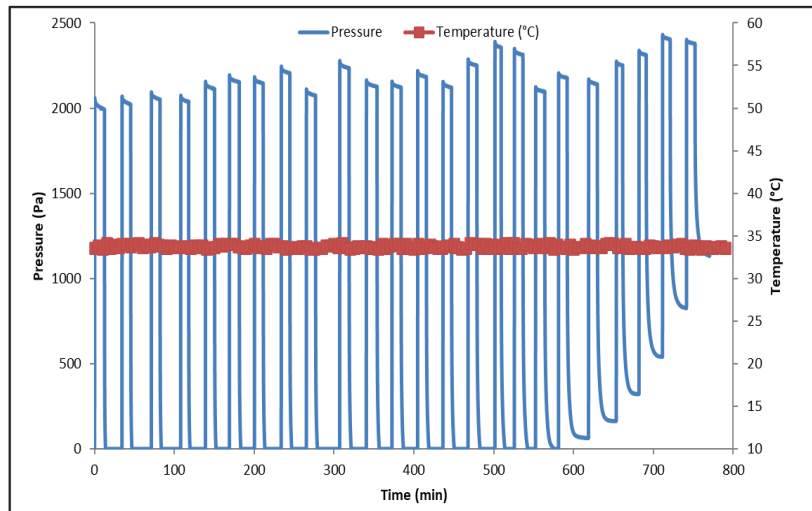

Figure 7.4. Pressure and temperature changes of zeolite 13X-water pair (T_{ads}=35°C)

It is known that under vacuum conditions, water vapour behaves as an ideal gas. Therefore, the amount of adsorbed is calculated by applying ideal gas law. The isotherms obtained at three temperatures are represented in Figure 7.5.
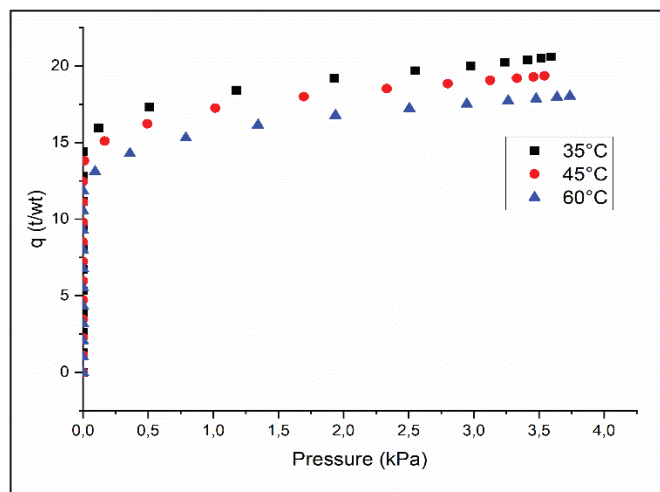

Figure 7.5. Adsorption isotherms of zeolite 13X-water pair at different adsorption temperatures (T_{reg}=90°C)

In the design of the adsorption heat pump, the equilibrium relationship of the working pair should also be defined. The availability of experimental data with Langmuir, Sips (Langmuir-Freundlich), Toth's and Freundlich relationships are examined. The obtained parameters from the relationships are given in Table 7.3. In determination of deviation of model from experimental data sum of square root (SSR) method is used (Eq 7.1-7.2). According to the SSR values, the experimental data is better fit to the Sips and Toth's relationships.

$$SR = \left(q_{model} - q_{experimental}\right)^2 \qquad (7.1)$$

$$SSR = \sum SR \qquad (7.2)$$

Table 7.3. Parameters of equilibrium relationships for zeolite 13X-water pair

Model	Parameter	Value	SSR
Langmuir	q_m(wt/wt)	0.181	0.191
	b_∞ (kPa^{-1})	7.94×10^{-10}	
	Q(kJ/kg)	3802	
Sips	q_m(wt/wt)	0.552	0.184
	b_∞ (kPa^{-1})	4.28×10^{-11}	
	Q(kJ/kg)	2430	
Toth's	q_m(wt/wt)	0.238	0.185
	b_∞ (kPa^{-1})	3.49×10^{-11}	
	Q(kJ/kg)	5473	
Freundlich	K	0.173	0.188
	n	13.40	

The comparison of the isotherm models with the experimental data at 35°C is represented in Figure 7.6. It is seen that Sips relationship is better fitted to the experimental data especially at high pressure.

The isosteric heat of adsorption has also been determined by means of equilibrium relationship models. The average isosteric is determined as 5280 kJ/kg for Sips relationship and 3800 kJ/kg and 5470 kJ/kg for Langmuir and Toth's relationships, respectively. In literature, the isosteric heat of adsorption for Zeolite 13X-water pair is given as 4400 kJ/kg (Mobedi and Ülkü 1987). It is observed that while the isosteric heat of adsorption is independent of surface loading and equal to the heat of adsorption value for Langmuir and Toth's relationship, it decreases with increasing surface loading for

Sips relationship (Figure 7.7). Furthermore, as indicated by Do, the heat of adsorption value is equal to the isosteric heat of adsorption when the surface loading was equal to 0.5 for Sips equation (Do 1998). In determination of isosteric heat of adsorption value, the equation (Eq 7.3) given by Do is used for different temperatures (Do 1998).

$$q_{st} = Q - (\alpha R T_0) n^2 ln \left(\frac{q}{q_s - q} \right) \tag{7.3}$$

where Q represents the heat of adsorption, α is a constant parameter, T_0 is the reference temperature, n is the heterogeneity parameter and q_s is the monolayer capacity.
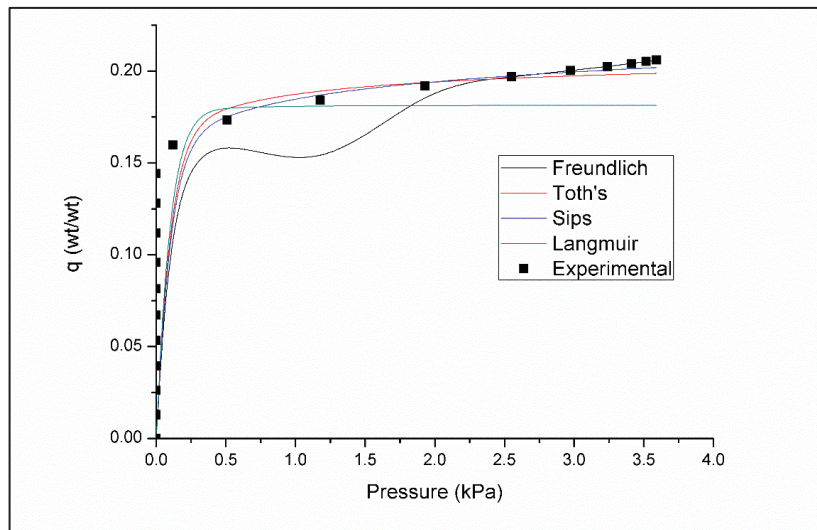

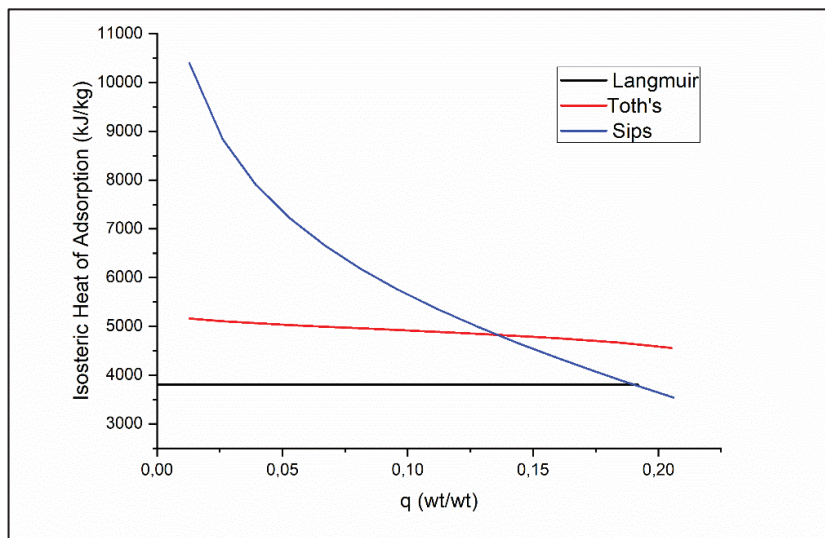Figure 7.6. Adsorption isotherms with different models

Figure 7.7. The change of isosteric heat of adsorption with adsorbate loading

The adsorption kinetics were also determined from the experimental data. The adsorption experiments were performed as successive runs as seen in Figure 7.4. For each pulses the uptake curves were obtained (Figure 7.8). As the amount of water vapour adsorbed increased, the time required to reach equilibrium increased. Thus, the effective diffusivity of the water vapor through Zeolite 13X was expected to decrease as the amount of adsorbed increased.
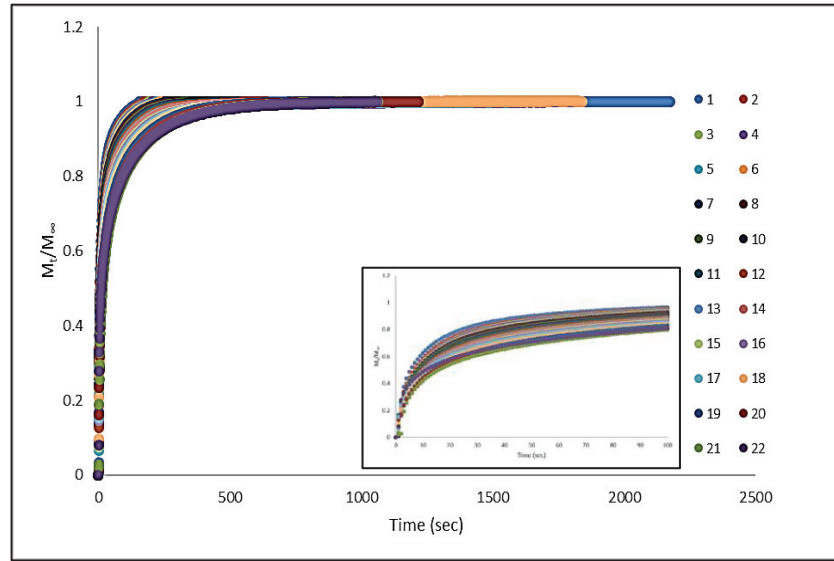

Figure 7.8. Representative uptake curves for zeolite 13X-water pair (T_{ads}=35°C)

In order to obtain effective diffusivity for each successive run, long term solution of Crank's model (Eq 7.3), which is obtained from Fick's second law of diffusion for spherical particles, has been used.

$$\frac{m_t}{m_\infty} = \frac{\overline{q}\text{-}q_0}{q_\infty\text{-}q_0} = 1 - \frac{6}{\pi^2} \sum_{n=1}^{\infty} \frac{1}{n^2} \exp\left(-\frac{n^2\pi^2 D_{eff} t}{R_p^2}\right) \qquad (7.3)$$

where D_{eff} is the effective diffusivity coefficient, $\overline{q}(t)$ is the average adsorbate concentration through the particle, $q(R,t)$ is the adsorbed phase concentration, R_p is the particle radius and n is the number of terms taken in the model.

A linear plot of ln(1-M_t/M_∞) versus time is plotted. From the slope of the linear line, the effective diffusivity of zeolite 13X-water pair is calculated for each successive run. The representative graphs are given in Figure 7.9 on which the range of amount of adsorbed are indicated as title.
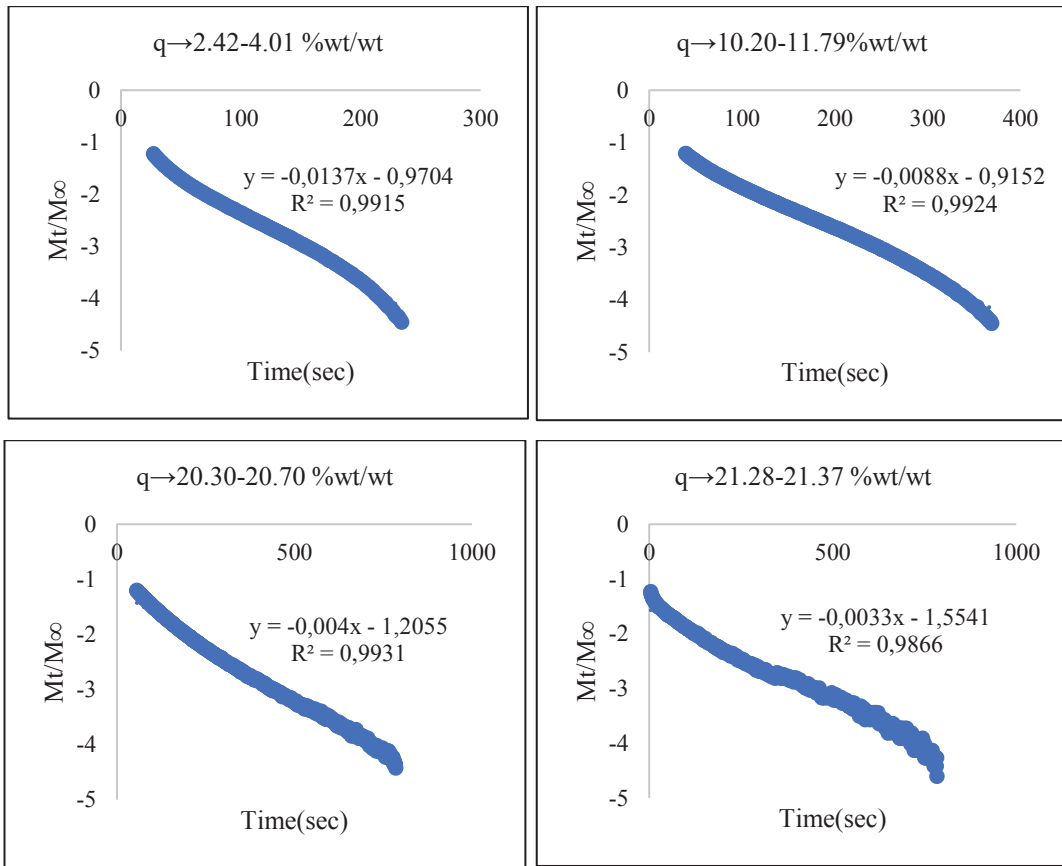
Figure 7.9. Representative graphs of long-term solution of Crank's model (T_{ads}=35°C)

As seen in Figure 7.10, the effective diffusivity is nearly constant while the amount of water vapour adsorbed increases and the effect of adsorption temperature is not significant. Thus, constant diffusivity assumption is appropriate for zeolite 13X-water pair.
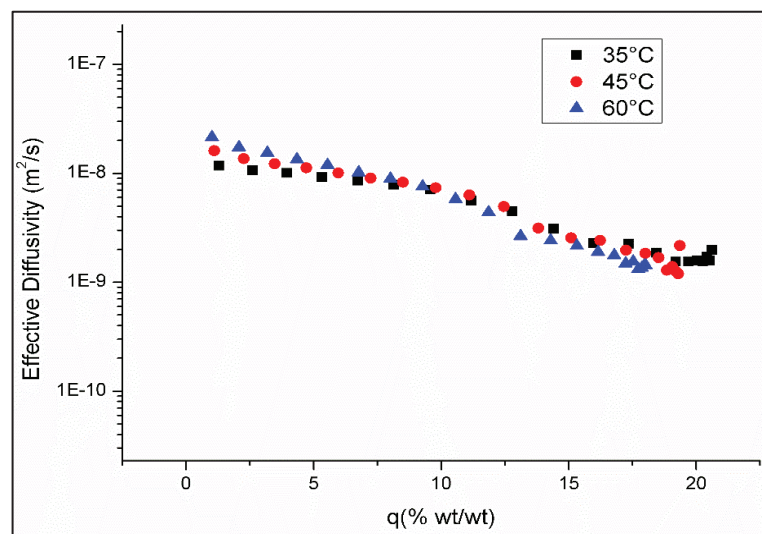

Figure 7.10. Effect of adsorption temperature on the effective diffusivity

The effective diffusivity was calculated from the Crank's model (n=4) and LDF model (Table 3.3). It can be said that Crank's model better defines the uptake of zeolite 13X-water pair almost all successive runs (Figure 7.11). However, the long-term solution of Crank's model is poor in defining the initial times of the uptake curve.
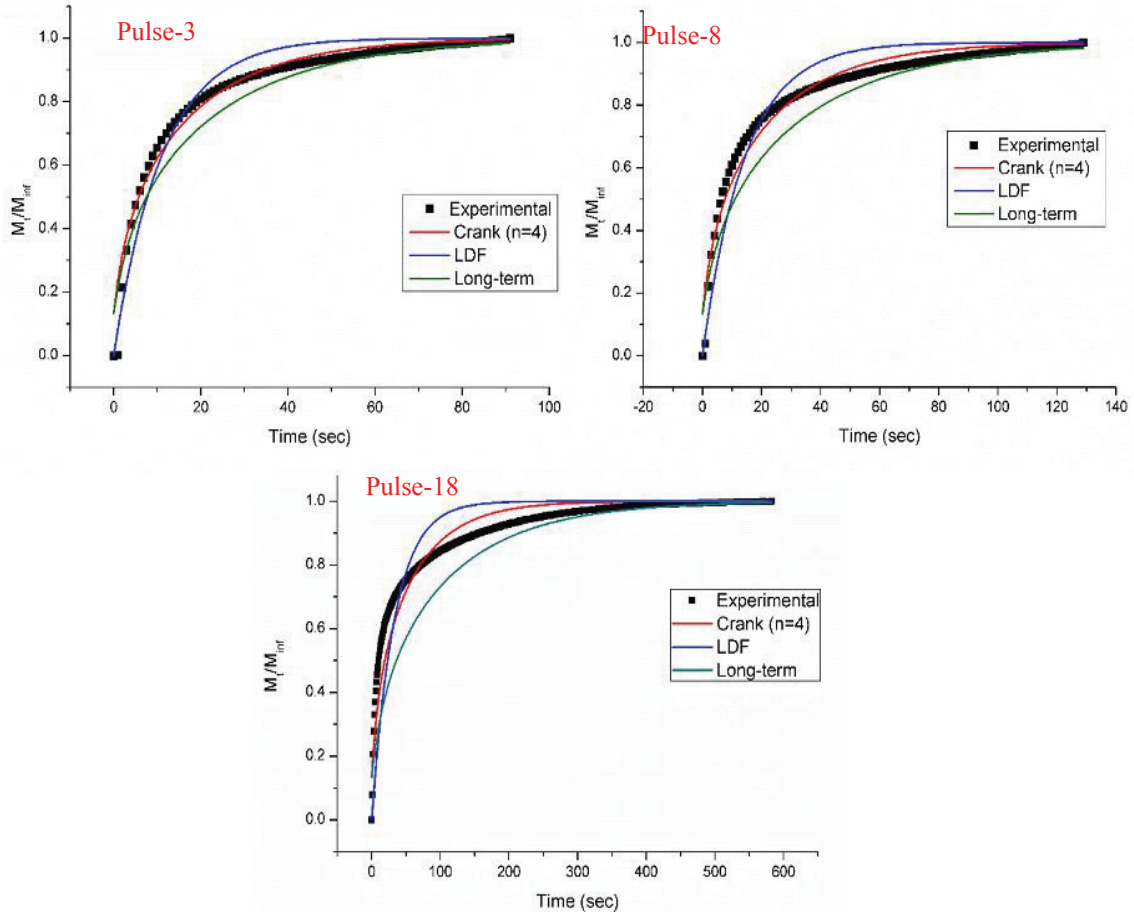

Figure 7.11. Comparison of kinetic models (T_{ads}=35°C)

Average effective diffusivity was calculated as 1.01×10^{-8} m^2/s and 1.18×10^{-8} m^2/s by using Crank's and LDF models, respectively. Although LDF model was not ideal to represent the uptake of the zeolite 13X-water pair, the effective diffusivity coefficient obtained from the LDF model was too close to the Crank's model which was related with LDF model's giving approximate solution (Figure 7.12). Thus, using LDF model in defining the mass transfer within the adsorbent particle was sufficient in design of the adsorption heat pump.
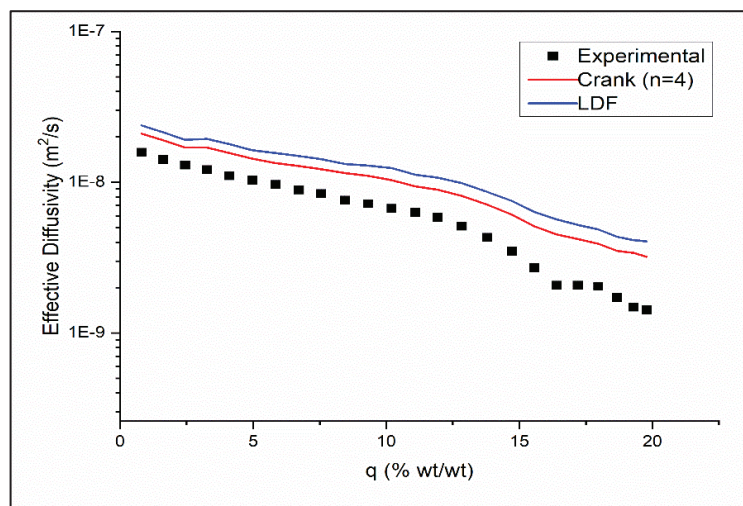
Figure 7.12. Effective diffusivity coefficients obtained from different kinetic models

7.2.1. Non-isothermal Adsorption Analysis

Due to the heat released during the adsorption, an instant temperature rise may be observed. Therefore, the assumption of isothermal system can cause error in the adsorption kinetics analysis. In order to determine the effect of temperature rise, the kinetics of the adsorption is examined according to assumption of non-isothermal sorption.

In order to investigate the temperature change in the adsorbent bed during the adsorption of water vapor on zeolite 13X, the solid diffusion model given by Ruthven and LDF model defined by Sircar were used. The details of the models and the method were given in Chapter 3 and Chapter 6.

The results of the numerical analysis are shown in Figure 7.13. It can be seen that the solid diffusion model is more compatible to the experimental data than LDF model. However, in both models, the temperature increment is too low. This situation arises from the weight ratio of the adsorbent sample and the bed. Due to the weight difference between adsorbent bed and the sample, the heat released during the adsorption process does not have a significant effect on the bed temperature. Furthermore, the LDF model is also analysed with Sips equilibrium relationship (Figure 7.13c). The adsorption rate is the same with Langmuir relationship. On the other hand, the temperature increment at the beginning of the adsorption is a bit higher than Langmuir relationship which may be related with the amount of adsorbate loading dependency of the isosteric heat of adsorption for Sips relationship.
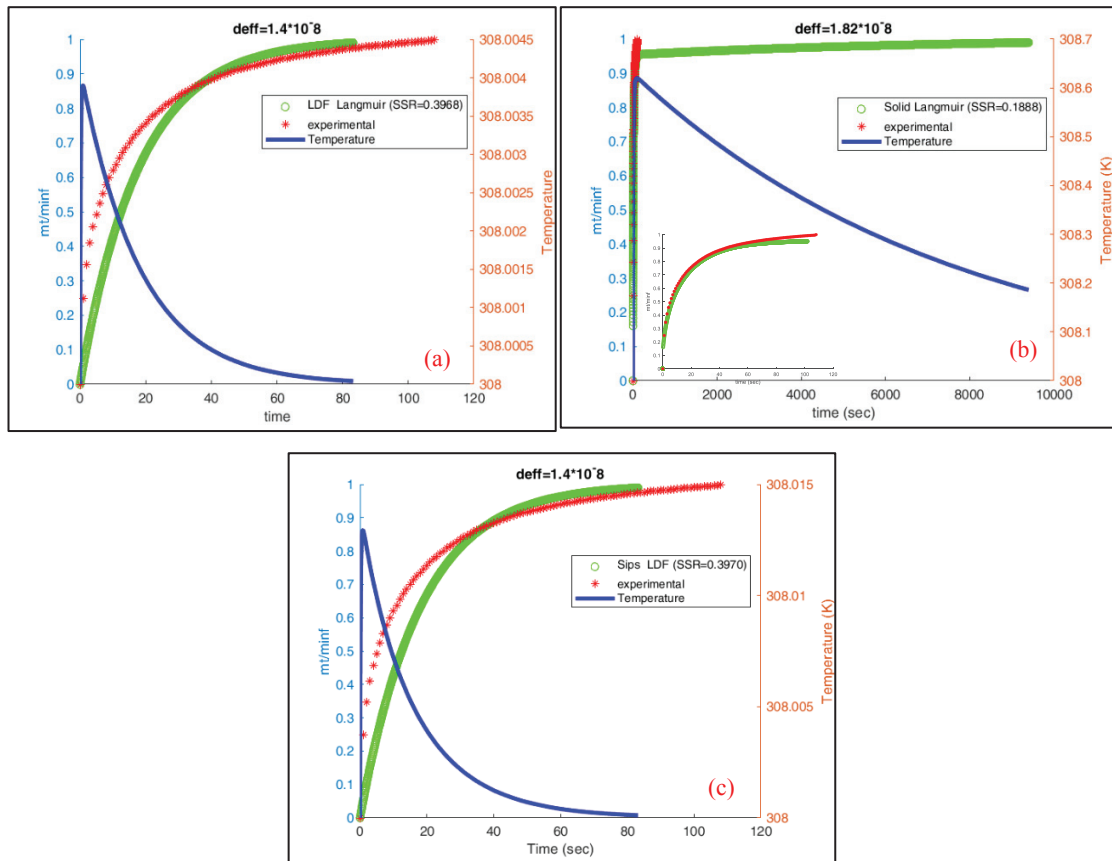
Figure 7.13. The non-isothermal uptake curves and the temperature change in the adsorbent bed during the adsorption a) LDF model with Langmuir relationship b) Solid diffusion model with Langmuir relationship c) LDF model with Sips relationship

7.3. Thermal Conductivity Measurement Results

Thermal conductivity measurements have been performed with different methods as mentioned in Chapter 6. The first one is hot wire method. By this method, the effective thermal conductivity of zeolite 13X, 3A and 4A beads have been measured at a current of 0.250 A and temperature of 33°C. The thermal conductivity results obtained from hot wire measurement apparatus are given in Table 7.4.

Table 7.4.Effective thermal conductivity of zeolites

Sample	Thermal Conductivity (W/m.K)
13X	0.124
3A	0.151
4A	0.132

In design of adsorption heat pumps, the mail drawback is the low heat transfer properties of the adsorbent bed. In order to increase the effective thermal conductivity of the adsorbent bed, metal additives have been utilized. In the previous studies, disconnected wire has been used by the researchers (Demir et al. 2008). Although there is an increase in effective thermal conductivity, the effect of the wire is not distributed at all sides of the bed due to discontinuous structure of the wire. In this study, aluminium wire with 1 mm and 2 mm thickness are used in different geometries.

As mentioned in Chapter 6, two different sample holders have been used. The thermal conductivity of the zeolite 13X is measured as 0.1152 W/m.K for SH-1 (Figure 7.14a). In order to fix the metal additives inside the sample holder, a stainless-steel cage has been used. However, it is seen that the effective thermal conductivity is decreased to 0.0996 W/m.K (Figure 7.14b) which may related with the thermal resistance at the boundary where cage is located. Then, meshes are built within the cage and it is observed that meshes with 1 mm thickness do not increase the effective thermal conductivity significantly (Figure 7.14c). On the other hand, when a helix shape wire is used (Figure 7.14d), the effective thermal conductivity increases to 0.1243 W/m.K.
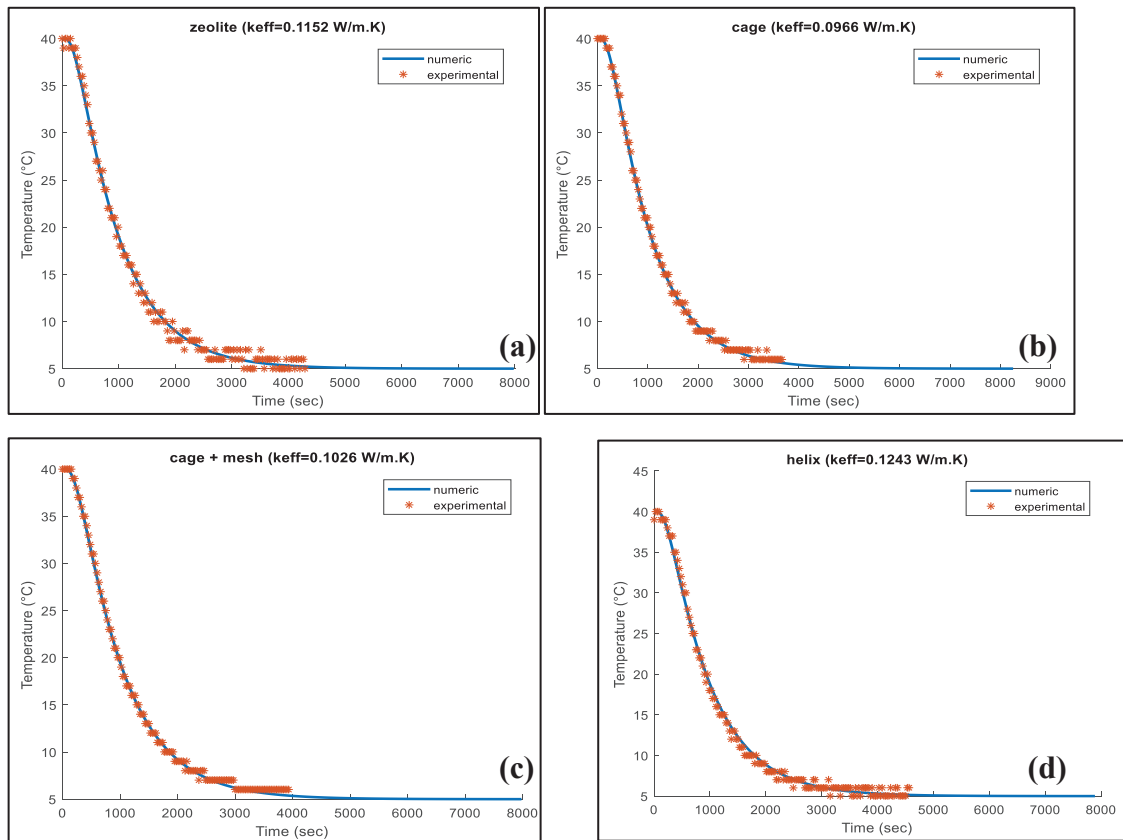

Figure 7.14. Effective thermal conductivities measured with SH-1

In the experiments performed with SH-2, first aluminium wire with 1 mm thickness is used with different geometries (Figure 7.15). It is seen that the effective thermal conductivity is increased to 0.1589 W/m.K when concentric wire with a mass of 10.5 g is used (Figure 7.15d).
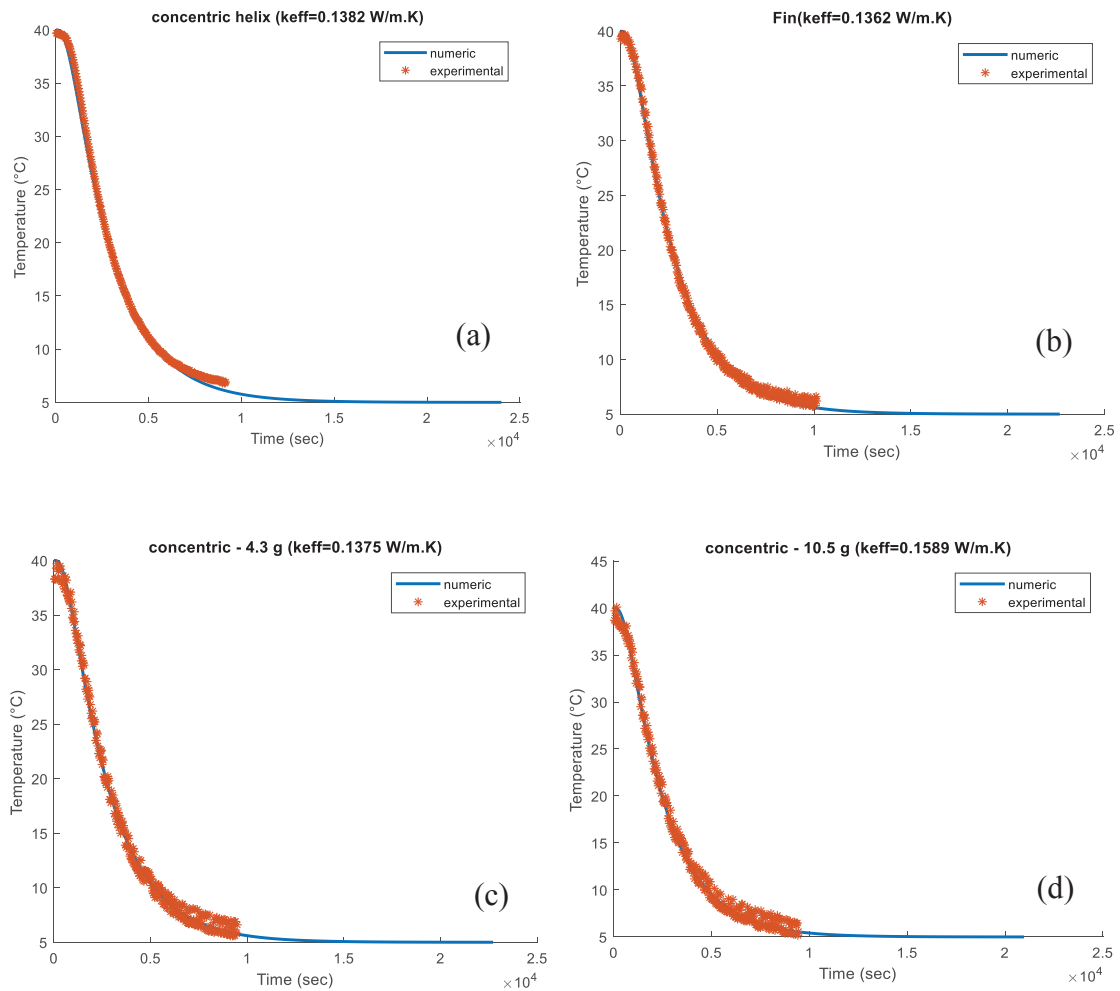

Figure 7.15. Thermal conductivity measurements in SH-2 (thickness of wire was 1 mm)

Although there was an increase in effective thermal conductivity value, it was still not sufficient and further enhancement was still required. Thus, the wire with 2 mm thickness was started to use.

The concentric and fin shaped wires were tasted for 2 mm wire. It was seen that the thickness of wire did not have significantly affect the effective thermal conductivity for concentric shape wire (Figure 7.16a). On the other hand, it was seen that when the thickness of wire increased in finned shape arrangement, the effective thermal conductivity increased from 0.1362 W/mK (Figure 7.15b) to 0.1638 W/mK (Figure

7.16b). Then, the diameter, number of fins and sides were increased and it was seen that the effective thermal conductivity was risen to 0.2830 W/m.K which means approximately %140 enhancement of thermal conductivity inside the bed when extensive fin shape wire with 6 fins and 8 sides was used (Figure 7.16e). However, it was still requires improvements since the optimum value of effective thermal conductivity has been given as 1 W/m.K by Meunier (Meunier 1993).
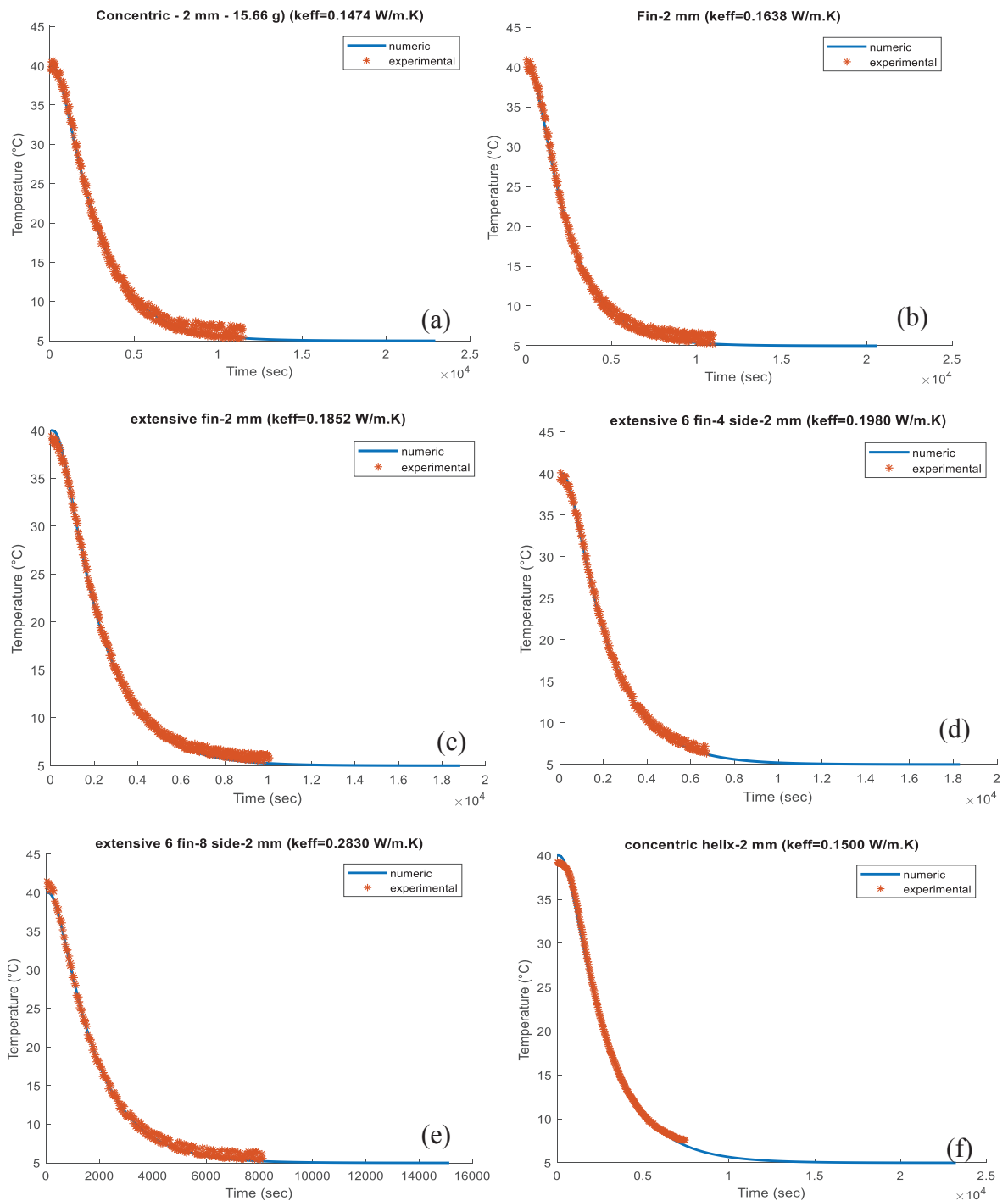

Figure 7.16. Thermal conductivity measurements in SH-2 (thickness of wire was 2 mm)

7.4. Adsorbent Bed-1

7.4.1. One-Dimensional Analysis of the Adsorbent Bed-1 (Case I)

The mass, heat and momentum transfer equations have been solved numerically to determine the temperature, pressure, and adsorbate concentration distribution inside the adsorbent bed. Meanwhile, the effect different parameters on the performance of the adsorption pump have also investigated.

As a first step, the temperature, pressure, and adsorbate concentration distribution inside the adsorbent bed are analysed with Sips Relationship in which isosteric heat of adsorption is dependent of adsorbate loading. The parameters given in Table 7.3 have been used to define the adsorption equilibrium and adsorption isotherms and isoster are shown in Figure 7.17. The maximum temperature of the adsorbent bed has been taken as 200°C and the condenser pressure is 8.5 kPa. The effective thermal conductivity of adsorbent sample has been taken as 0.12 W/m.K.
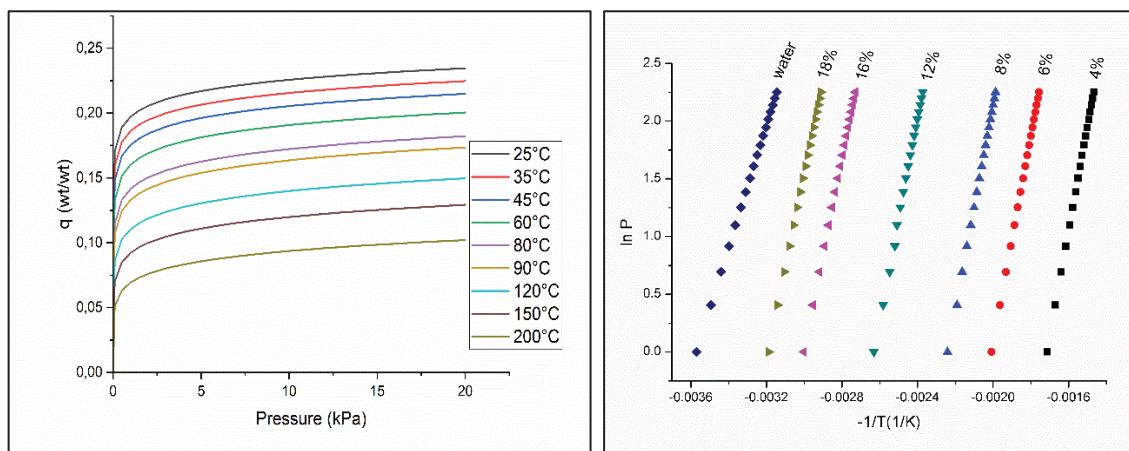
Figure 7.17. Isotherm and Isoster Obtained by Sips Relationship for Zeolite 13X-water pair

The start-up and 2nd cycles of Case I are illustrated in Figure 7.18. It is known that at the beginning of the adsorption process, the temperature of the adsorbent bed increases due to the heat released and then the temperature turns to the initial adsorption temperature. The effect of heat of adsorption can be observed in the start-up cycle, too. The adsorbent bed temperature suddenly increases approximately to 450 K as a result of the heat released, then the temperature of the adsorbent bed started to decrease during

isobaric cooling process. It is obvious that the adsorption and desorption processes are isobaric, and they stay constant throughout the adsorption and desorption processes at 2 kPa and 8.5 kPa, respectively. The isosteric heating and cooling cycles almost fits the ideal cycle. The deviations in isosteric processes may be related with the sudden temperature changes. The adsorbate concentration increases from 0.08 kg_w/kg_z to 0.18 kg_w/kg_z during the isobaric adsorption process.
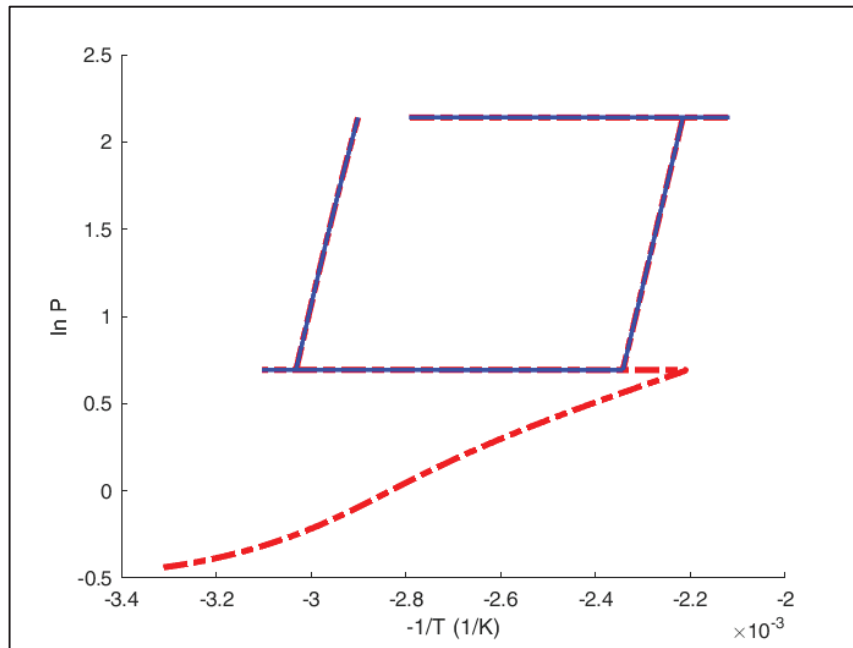

Figure 7.18. Ln P vs -1/T diagram of simulated a) start up cycle b) 2nd cycle of Case I with Zeolite 13X-water Pair

In more details, the distributions in radial direction of the bed are examined according to the data obtained in 2nd cycle of case I for each process. For the isobaric adsorption process, it is seen that while the outer surface of the bed was 300 K, the inner surface of the bed is approximately 338 K Figure 7.19a. This temperature difference occurs due to the low thermal conductivity of the adsorbent and the heat released at the beginning of the adsorption process. In Figure 7.19b, the changes in adsorptive pressure during isobaric adsorption process is illustrated. The adsorptive pressure almost remains constant at evaporator pressure. The changes in adsorbate concentration are given in Figure 7.19c. The adsorbate concentration at the outer surface is higher than the inner regions due to the low temperature at the outer surface of the adsorbent bed. This situation also indicates the effect of thermal resistance on heat and mass transfer in the adsorbent

bed. The adsorptive density also increases due to the low temperature at the outer surface of the adsorbent bed (Figure 7.19d).
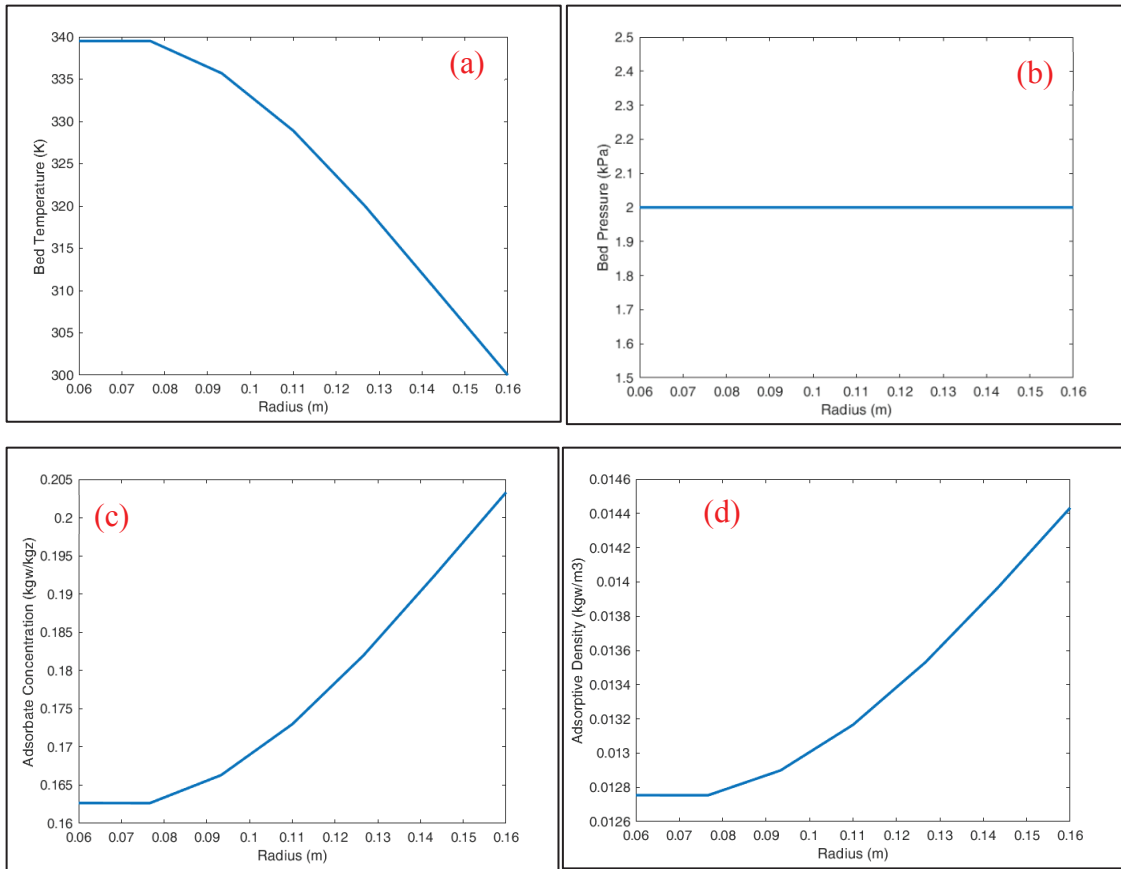

Figure 7.19. Distributions in the adsorbent bed during isobaric cooling (adsorption) process of Case I for zeolite 13X-water pair

During the isosteric heating process, the inner region temperature of the bed is 350 K and a sharp temperature gradient occurs close to the outer region due to the low thermal conductivity within the bed (Figure 7.20a). The bed temperature increases to 363 K at the outer region of adsorbent bed. On the other hand, the adsorptive pressure during isosteric process is uniform throughout the bed due to the constant adsorbate concentration (Figure 7.20b and Figure 7.20c). The effect of bed temperature on adsorptive density can be observed in Figure 7.20d. As the temperature of the bed increases, the adsorptive density decreases.

The distributions during isobaric desorption process are given in Figure 7.21. A small temperature gradient occurs during the process which indicates that the equilibrium is nearly approached. The temperature gradient also causes gradients for adsorbate concentration and adsorptive density. On the other hand, the bed pressure is constant at 8.5 kPa which is the condenser pressure during the isobaric heating process.
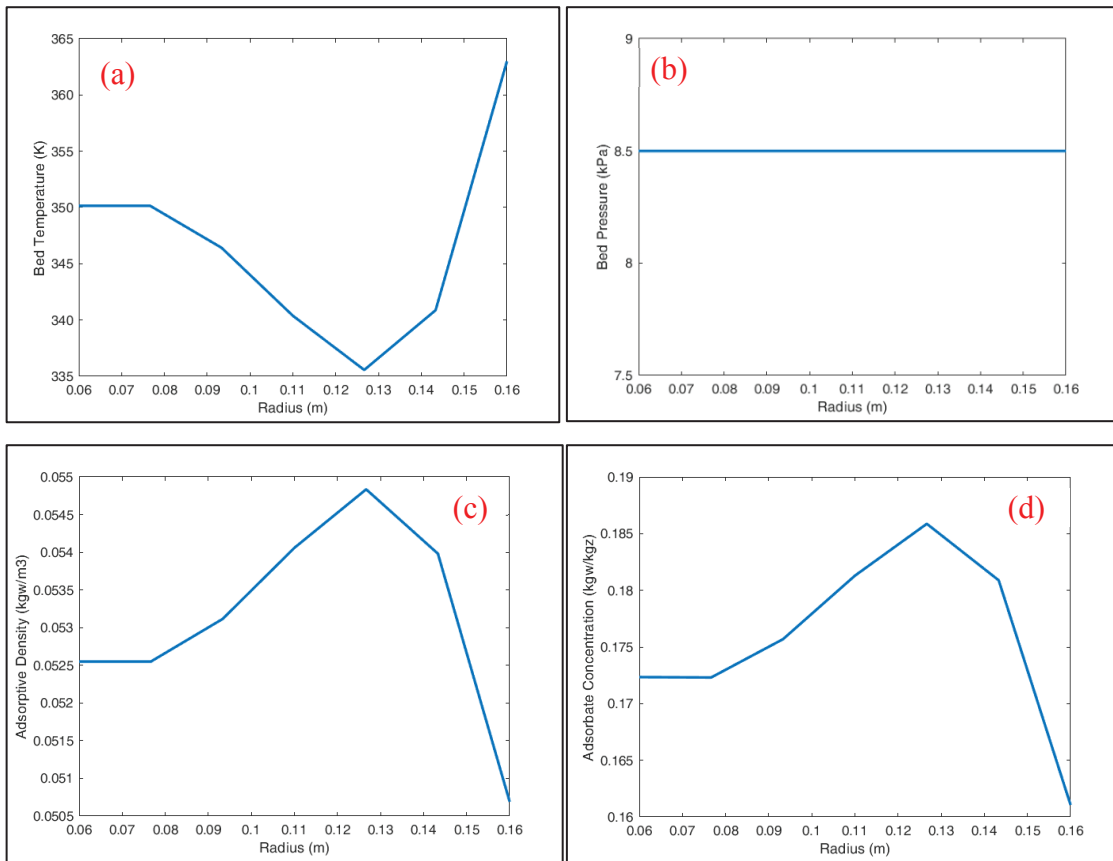
Figure 7.20. Distributions in the adsorbent bed during isosteric heating process of Case I for zeolite 13X-water pair

In isosteric cooling process (Figure 7.22), a temperature gradient occurs within the adsorbent bed as expected. The bed pressure is reduced to evaporator pressure at the end of this process. The effect of temperature on both adsorbate concentration and adsorptive density can be seen during the isosteric heating process, too.
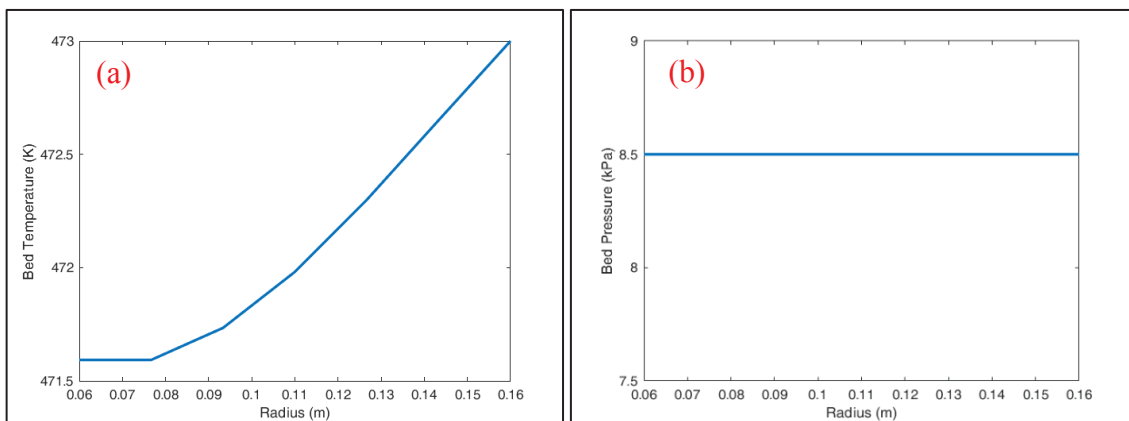
Figure 7.21. Distributions in the adsorbent bed during isobaric heating (desorption) process of Case I for zeolite 13X-water pair
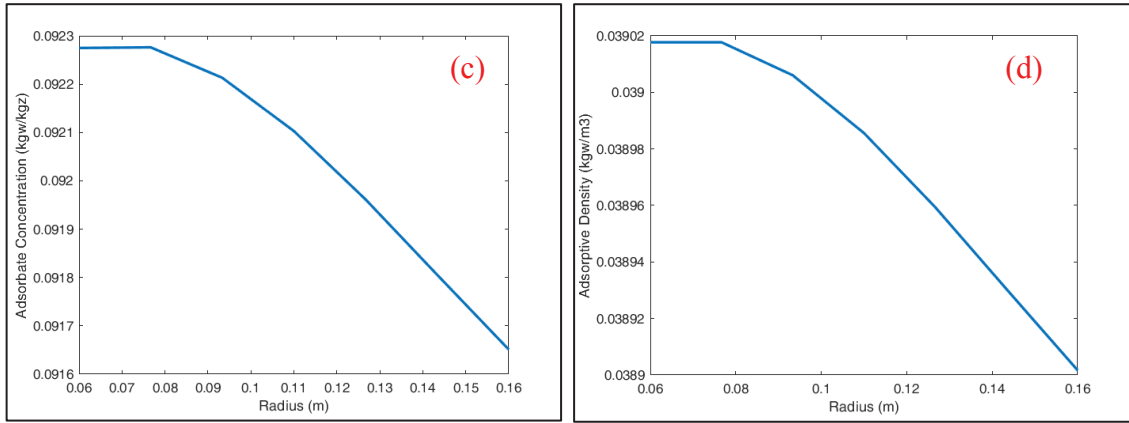
Figure 7.21. (cont)
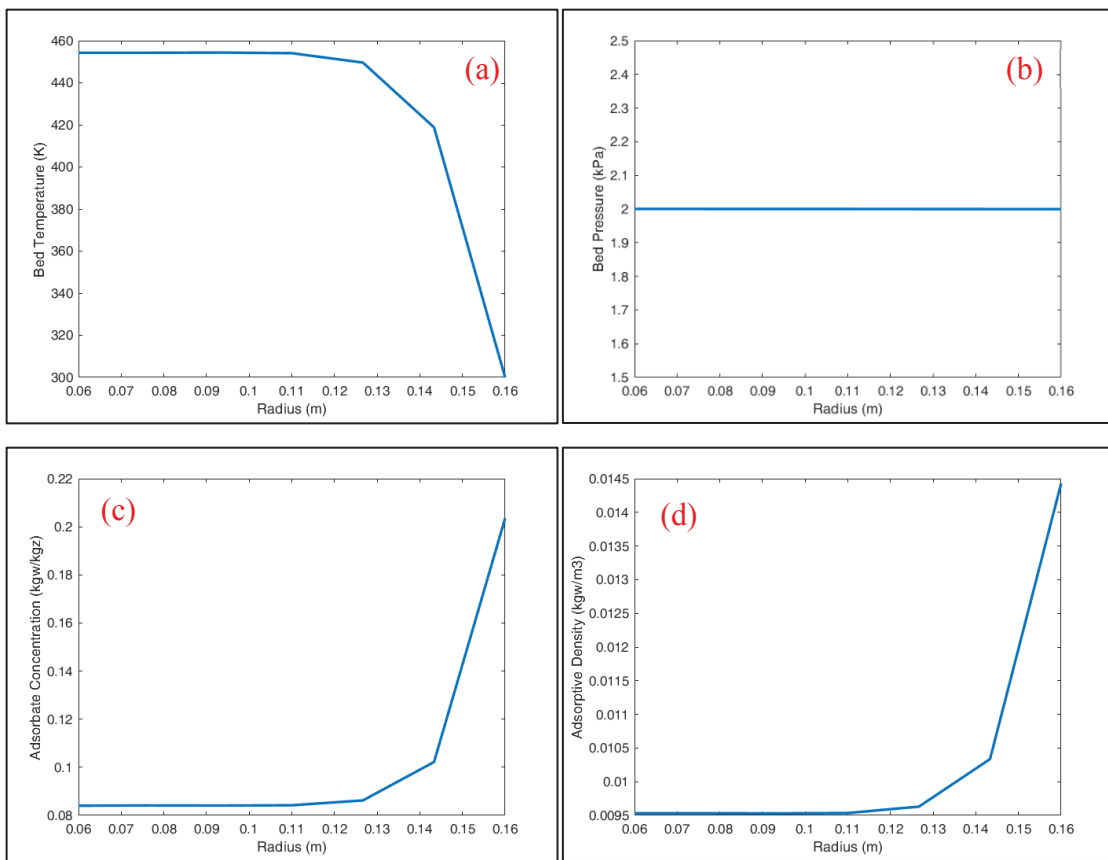
Figure 7.22. Distributions in the bed during isosteric cooling process of Case I for zeolite
13X-water pair

The average temperature change in the adsorbent bed during all process is represented in Figure 7.23. While the blue line shows the change in average adsorbent temperature, the black dashes signify the outer boundary of the adsorbent bed. It can be observed that the isosteric heating and isosteric cooling processes occurs too fast compared to the isobaric heating and cooling processes. This is related with the low

thermal conductivity of the adsorbent. At the beginning of the isobaric cooling process, the sudden increase in average temperature appears due to the heat released as mentioned before and the temperature reaches 426 K. Then, the temperature of the bed decreases slowly to 322 K after 31 hours. The temperature increases to 345 K during the isosteric heating process. The increase in average temperature continues during the isobaric heating process and it reaches 472 K at the end of the process.
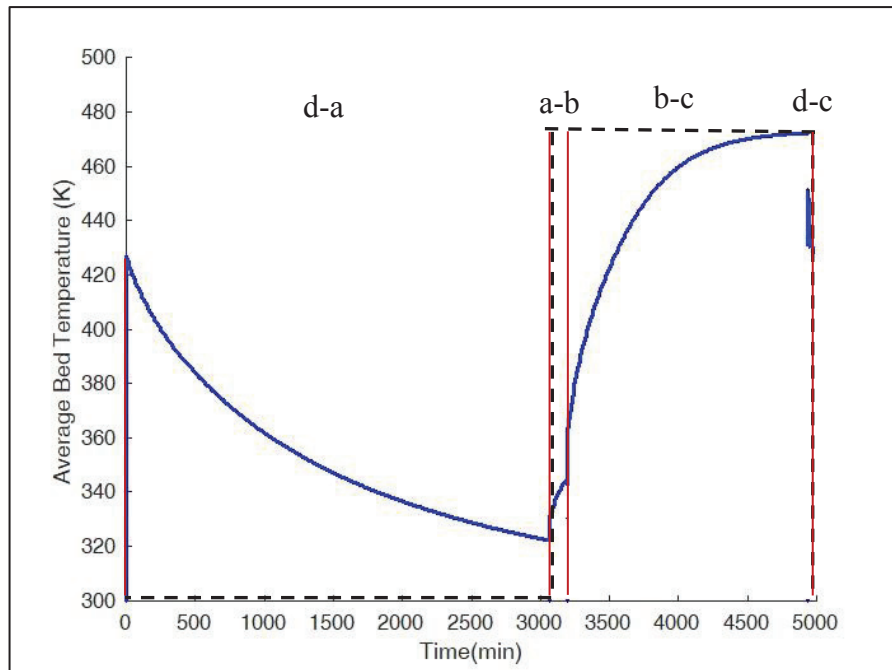
Figure 7.23. Change in average bed temperature during the complete cycle of Case I for zeolite 13X-water pair

The variations in average bed pressure during the complete cycle has been illustrated in Figure 7.24. The average pressure of the bed remains constant at 2 kPa and 8.5 kPa during the isobaric heating and isobaric cooling processes, respectively, as expected. The pressure of the bed increases during the isosteric heating process.

When we look at the variations in average adsorbate concentration during the complete cycle (Figure 7.25), the adsorbate concentration increases up to 0.18 kg_w/kg_z during the isobaric cooling process and remains constant during the isosteric heating process. While the temperature of the adsorbent bed increases during the isobaric heating process, the adsorbed water is desorbed from the adsorbent and the adsorbate concentration reduces to 0.08 kg_w/kg_z. The long period of the isobaric heating and cooling processes arises from the thermal resistances in the adsorbent bed.
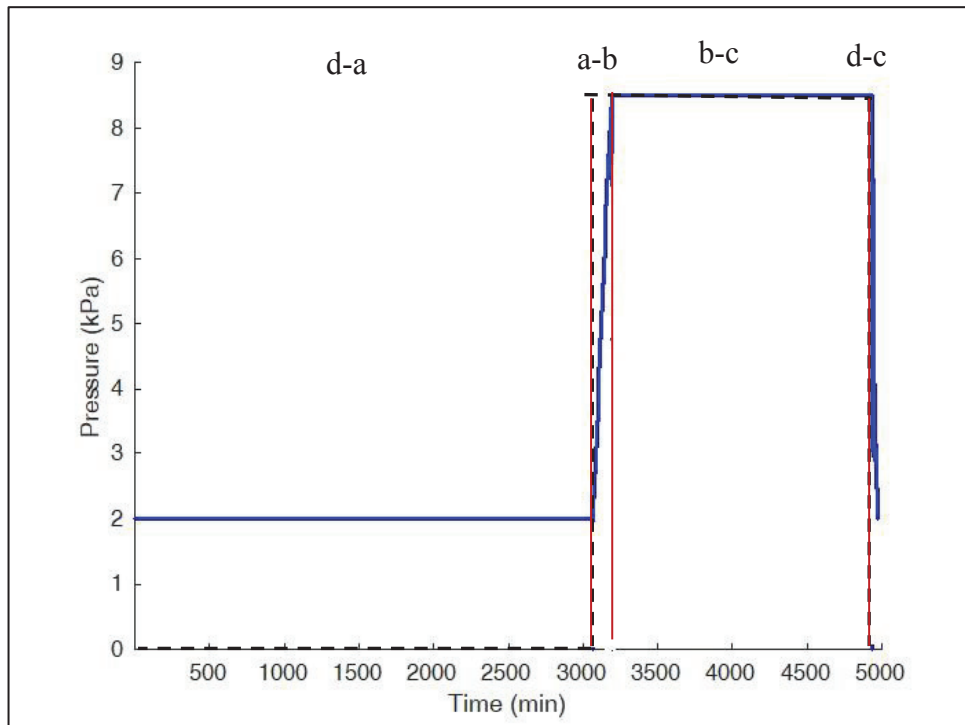
Figure 7.24. Change in average adsorptive pressure during the complete cycle of Case I
for zeolite 13X-water pair
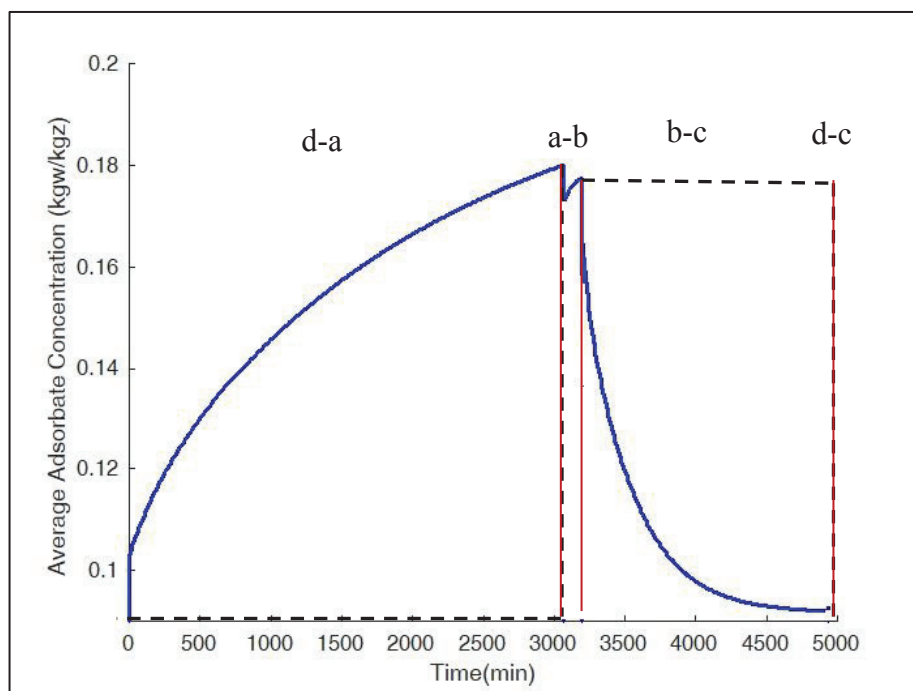
Figure 7.25. Change in average adsorbate concentration during the cycle of Case I for
zeolite 13X-water pair

7.4.1.1. Effect of Effective Thermal Conductivity on the Performance of the Adsorption Heat Pump for Adsorbent Bed-1

The effect of effective thermal conductivity on the change in average bed temperature in the adsorbent bed and the performance of adsorption heat pump was investigated as a first parameter for Case I. The effective thermal conductivity was increased from 6.48×10^{-2} W/mK to 2.51×10^{-1} W/mK with the assumption that the thermal conductivity of zeolite 13X increased from 0.12 W/mK (Case A) to 1 W/mK (Case B).

By solving the governing equations simultaneously, the average temperature change inside the bed with time is determined. The result of the numerical solution is illustrated in Figure 7.26. While the temperature of is not changed for the processes, the cycle time is reduced from 86 hours to 44 hours which directly affects the specific cooling and heating power of the adsorption heat pump.
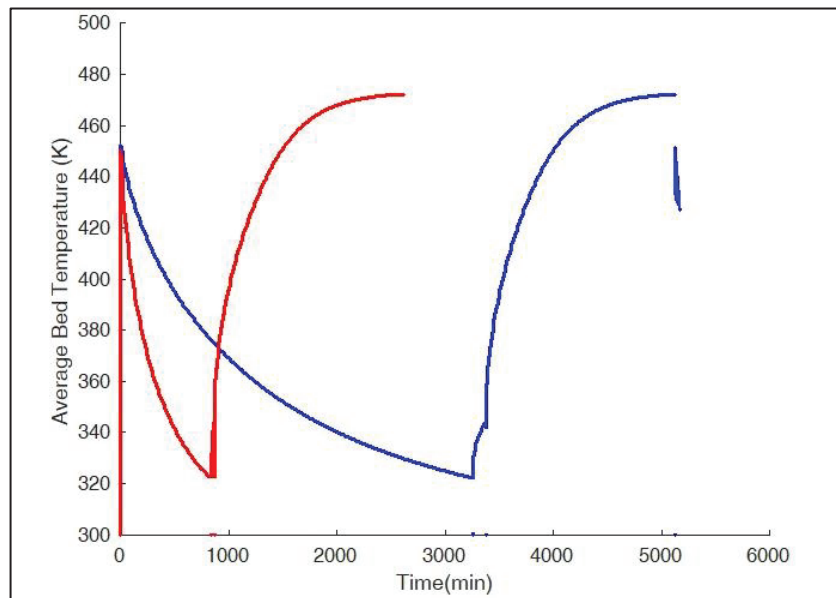
Figure 7.26. Effect of thermal conductivity on temperature of adsorbent bed for zeolite 13X-water pair (Blue: Case A; Red: Case B)

In most of the studies, the effect of thermal conductivity is ignored since it does not have a direct effect on the COP value of the adsorption heat pump. However, the amount of heat released and taken in a unit time is changed during each process. Thus, the COP is also increased when the effective thermal conductivity increases (Table 7.5). The value enhanced 90% when the effective thermal conductivity increased to 1 W/mK.

The price of electricity for an industrial facility is 3.44 TL/kWh in Turkey. When the COP of the adsorption heat pump increases the amount of utilized heat will increase which leads an economical benefit to the consumer. Thus, the enhancement of 90% in COP corresponds 3.096 TL/kWh saving for the same electrical consumption.

Table 7.5. Effect of effective thermal conductivity on the performance of AHP

	Case A	Case B
Qab (W)	6	640
Qbc (W)	1746	126
Qcd (W)	-21	-3427
Qda (W)	-61	-238
Qev (W)	20	79
Qcond (W)	-540	-39
COPc	0,01	0,10
COPh	0,36	4,83
SCP	0,76	1,50
SHP	3,47	6,84
Cycle Time (h)	86	44

7.4.1.2. Effect of Adsorbate Loading and Temperature Dependence of Effective Diffusivity on Performance of Adsorption Heat Pump for Adsorbent Bed-1

In the analysis of mass transfer of adsorptive through the adsorbent, linear driving force (LDF) model is used to due to the simplicity and giving approximate solution. On the other hand, the effective diffusivity is analysed for two cases. In the first case, an average value of effective diffusivity is used. Adsorption equilibrium is defined by Langmuir Relationship.

In the second case, both adsorbate loading and temperature dependent effective diffusivity equation is used. The equation obtained from experimental data by curve fitting method is represented in Figure 7.27. The model is applicable for the adsorbate loading range of 0.05-0.20 wt/wt.
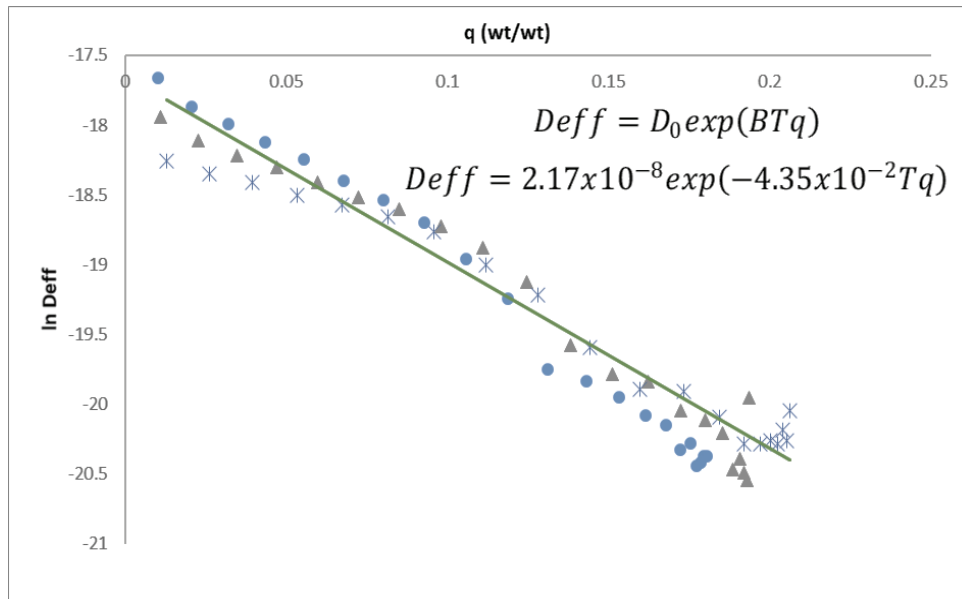
Figure 7.27. Adsorbate loading and temperature dependence of effective diffusivity for zeolite 13X-water pair

During determination of adsorption kinetics of zeolite 13X-water pair from experimental data, it was claimed that the effective diffusivity coefficient could be considered as independent of adsorbate loading and temperature (Figure 7.12). When the adsorbate loading, and temperature dependency of the effective diffusivity was examined by numerical analysis, it was seen that taking an average effective diffusivity value was applicable for the design of the adsorbent bed (Figure 7.28).
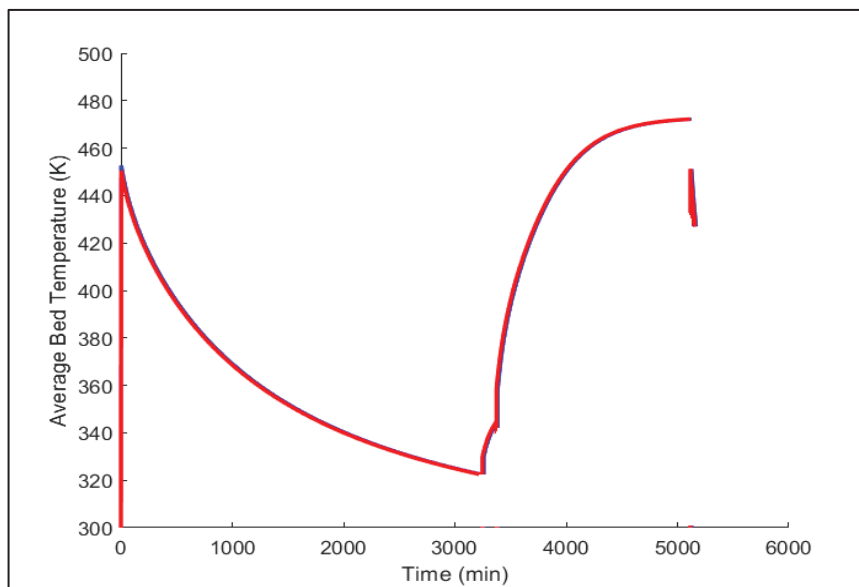
Figure 7.28. Effect of temperature and adsorbate loading dependency of effective diffusivity on performance of AHP for zeolite 13X-water pair

7.4.1.3. Effect of Bed Thickness on Performance of Adsorption Heat Pump for Adsorbent Bed-1

The transient heat conduction is also a function of radius of the bed and there is an inverse proportion with the heat transfer rate and thickness of the bed. Therefore, the poor heat transfer within the bed can also be eliminated by reducing the thickness of the adsorbent bed.

In order to determine the effect of bed thickness on the performance of the adsorption heat pump, the governing equations for isobaric cooling process were solved simultaneously for the bed thickness of 110 mm and 60 mm.

In Figure 7.29, the change in average bed temperature with time is presented. As expected, when thickness of the bed is reduced from 110 mm to 60 mm, the duration of the isobaric cooling process decreases from approximately 870 min to 350 min. Furthermore, the temperature difference between inner and outer regions reduces when the thickness decreases.
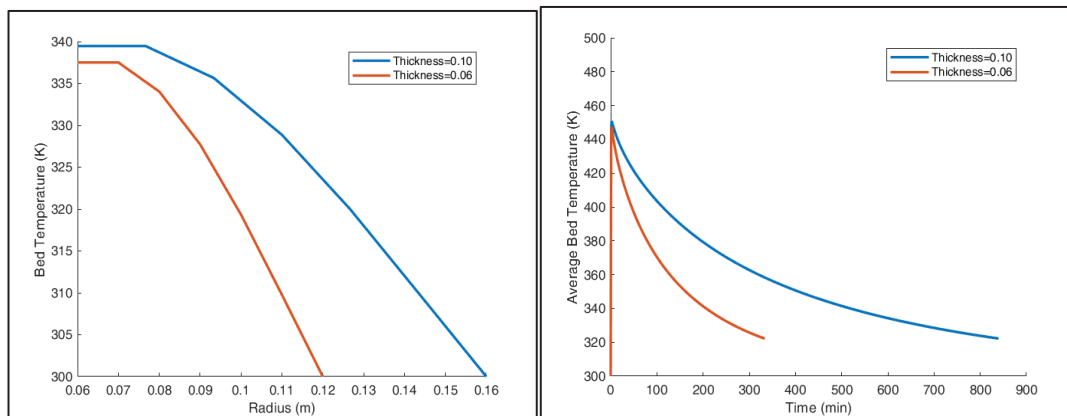
Figure 7.29. Effect of bed thickness on performance of AHP for zeolite 13X-water pair

7.4.2. Validation of Theoretical Model with Experimental Data

In order to validate the theoretical model for Adsorbent Bed-1, the experimental data taken from the study of Mobedi have been used (Mobedi 1987). In that study, Mobedi performed experiments with zeolite 13X-water pair. Prior to theoretical analysis, Sips Relationship parameters are derived from the experimental data (Figure 7.30).
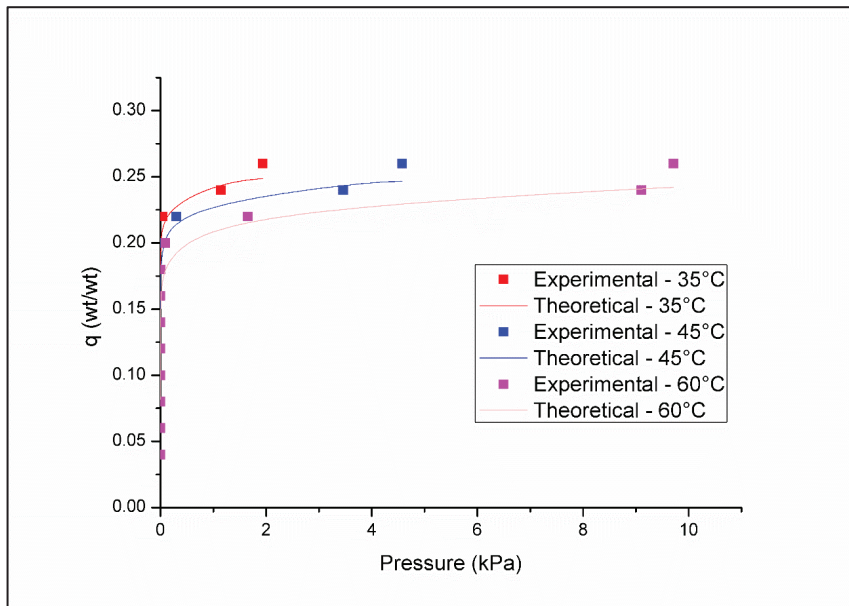
Figure 7.30. Sips Relationship for the Experimental Study of Mobedi

After determination of the equilibrium parameters, theoretical analysis has been performed. The result of the validation of theoretical model for isobaric cooling is illustrated in Figure 7.31. It can be observed that the experimental data is not fitted to the theoretical model. This situation may arise from the low accuracy of the pressure transducer and other technological equipment during those years. Therefore, the experimental study should be performed with new devices.
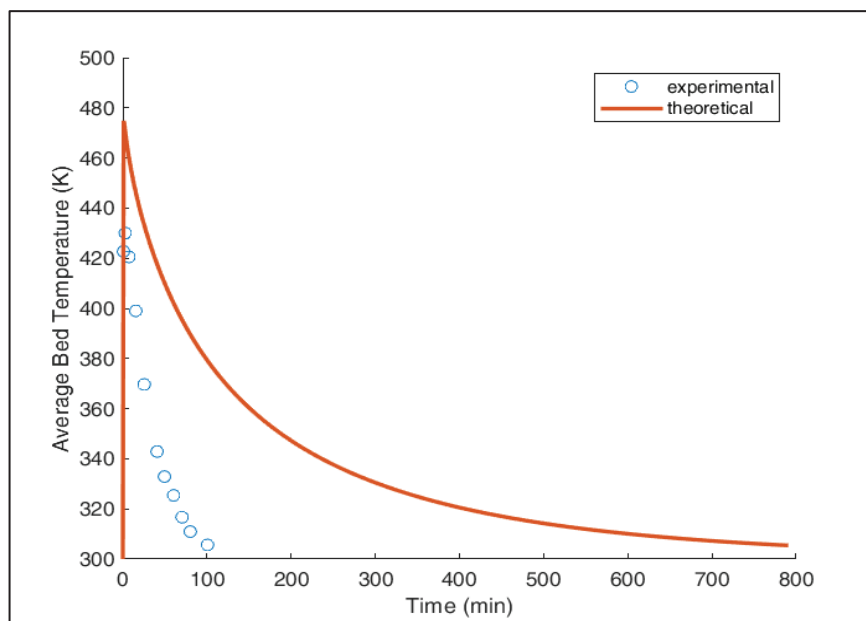
Figure 7.31. Comparison of Theoretical and Experimental Data

7.4.3. Two-Dimensional Analysis of the Adsorbent Bed-1 (Case II)

In order to determine the effect of the axial flow of the adsorptive within the adsorbent bed, two-dimensional analysis was performed with the Adsorbent Bed-1.

The change in average temperature of the bed with time is presented in Figure 7.30. It is obvious that the axial flow of adsorptive does not have significant effect on temperature distribution within the adsorbent bed and one-dimensional analysis is quite enough in designing adsorption heat pump.
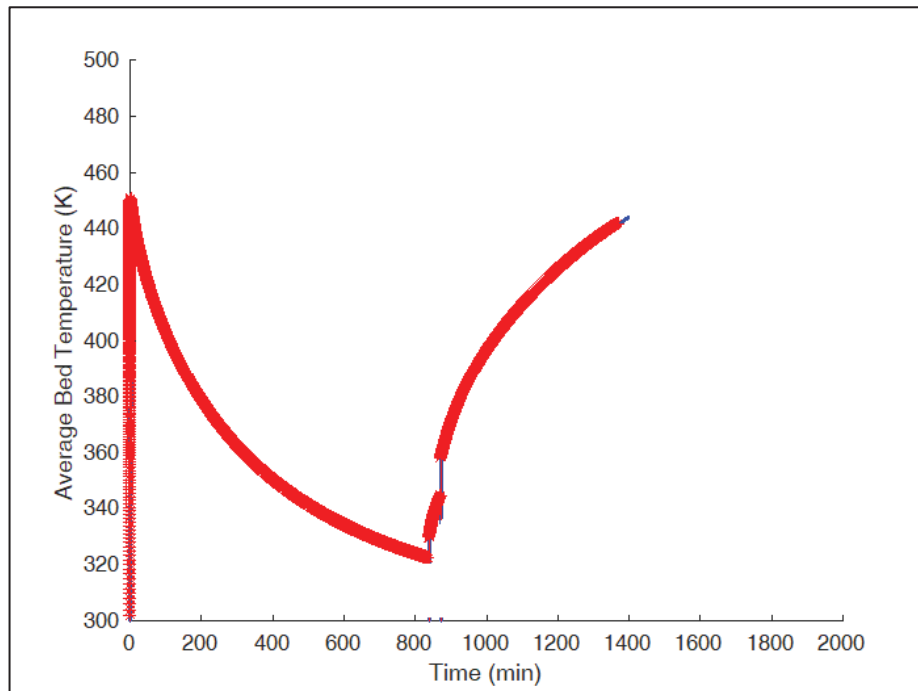
Figure 7.32. Effect of axial flow of adsorptive on temperature change in adsorbent bed

7.5. Adsorbent Bed-2 (Case III)

In order to enhance the performance of the adsorption heat pump, different designs of the bed were also studied. In Adsorbent Bed-2, the heating of the bed was provided from top and bottom in addition to the outer radius of the adsorbent bed.

The representative temperature and pressure distribution within the adsorbent bed during isobaric cooling process is presented in Figure 7.33. While the pressure is approximately uniform through the bed, there is a temperature gradient within the bed which is related with the low heat transfer conditions within the bed.
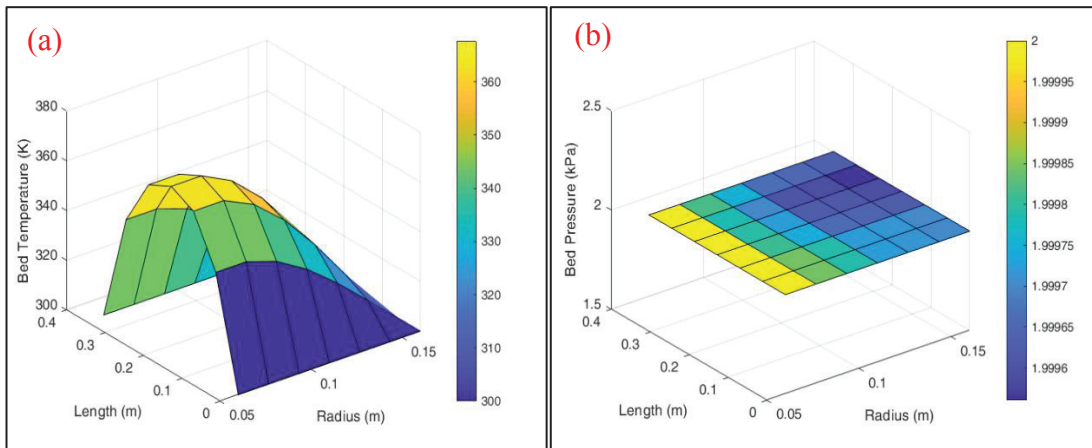
Figure 7.33. Distribution of a) Bed Temperature b) Adsorptive Pressure through the adsorbent bed during isobaric cooling process for zeolite 13X-water pair

Full cycles of Adsorbent Bed-1 (Case I) and Adsorbent Bed-2 (Case III) are compared, too (Figure 7.34). In the graphs, the blue and red lines indicate Adsorbent Bed-1 and Adsorbent Bed-1, respectively. Two-dimensional heating of the bed decreases cycle duration of the processes significantly. It is determined that the cycle time is reduced from 86 hours to 17 hours when two-dimensional heating is performed. Furthermore, the average temperature of the bed decreased for Case III which indicated that the heat transfer within the bed was enhanced for this design.
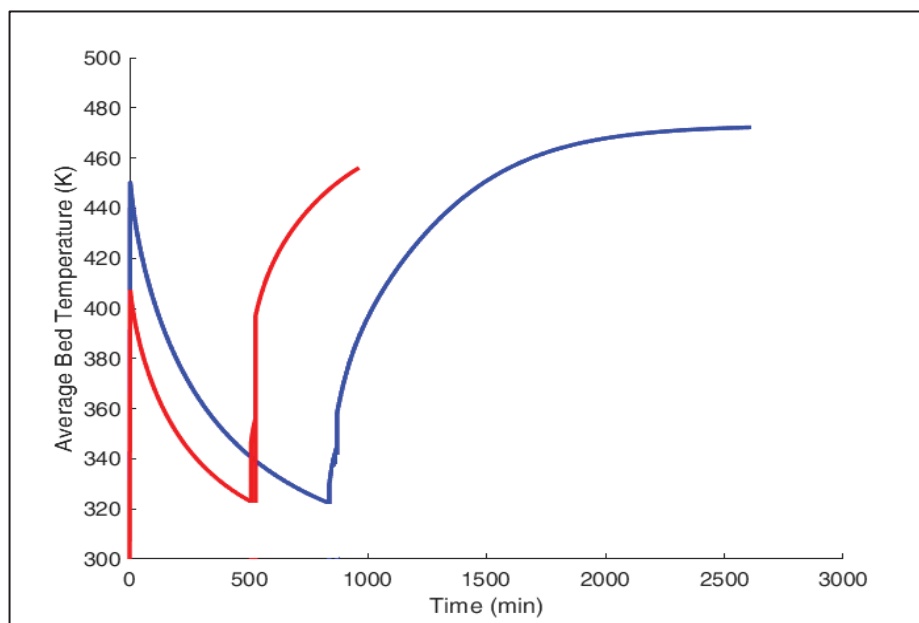
Figure 7.34. Comparison of cycles for Case I (blue) and Case III (red) for zeolite 13X-water pair

The performance analysis was also performed for Case III (Table 7.6). The amount of heat gained and released from the system were changed due to the change in average temperature of the bed and periods of the processes. Thus, the COP and SCP/SHP of the adsorption heat pump increased.

Table 7.6. Two-Dimensional Analysis of the Adsorbent Bed for Zeolite 13X-water

	Adsorbent Bed-1	Adsorbent Bed-2
Qab (W)	6	1127
Qbc (W)	1746	504
Qcd (W)	-21	-1239
Qda (W)	-61	-392
Qev (W)	20	131
Qcond (W)	-540	-156
COPc	0,01	0,08
COPh	0,36	1,10
SCP	0,76	3,94
SHP	3,47	18,04
Cycle Time (h)	86	17

7.6. Adsorbent Bed-3 (Case IV)

Since most of the adsorption heat pump designs are constructed with heat transfer fluid, the effect of heat transfer fluid parameters such as hot and cold fluid temperature and velocity of the heat transfer fluid are investigated in the following part. The results have been illustrated for isobaric cooling process.

7.6.1. Effect of Velocity of Heat Transfer Fluid on Average Bed Temperature

The effect of heat transfer fluid velocity on the average bed temperature is represented in Figure 7.35. It is seen that velocity of heat transfer fluid does not have any significant effect on temperature distribution of adsorbent bed. That is compatible with the study of Liu and Leong which is presented in Table 4.1. In that study, it was mentioned that when the fluid velocity was smaller than 0.1 m/s, the cycle time would increase very quickly with an increase in fluid velocity, however, for velocity larger than 0.5 m/s, the

cycle time did not change with velocity leading to very little change in SCP (Liu and Leong 2005).
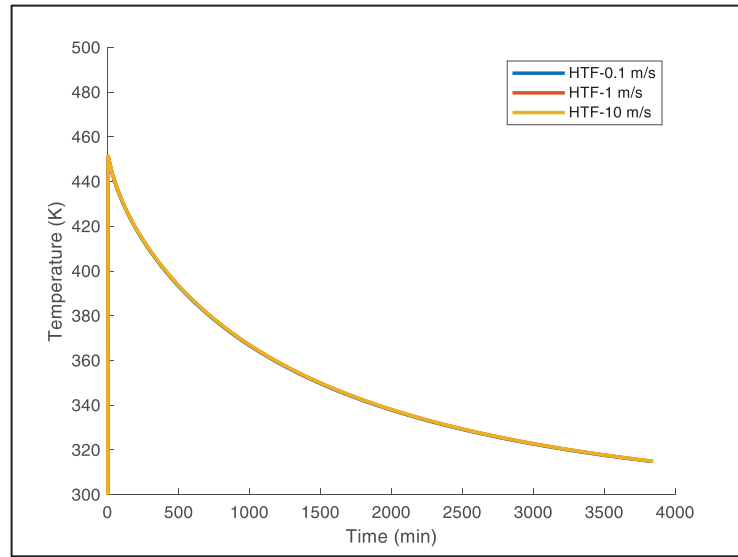
Figure 7.35. Effect of velocity of heat transfer fluid on temperature distribution in the bed

7.6.2. Effect of Cold Fluid Temperature on Average Bed Temperature

In Figure 7.36, it can be seen that the time consumed during adsorption process decreases as decreasing temperature of heat transfer fluid. This leads a direct increase in SCP of the adsorbent bed. Furthermore, heat released during the adsorption process per unit time will also increase by decreasing cold fluid temperature, so the COP will also increase as the cold fluid temperature decreases.
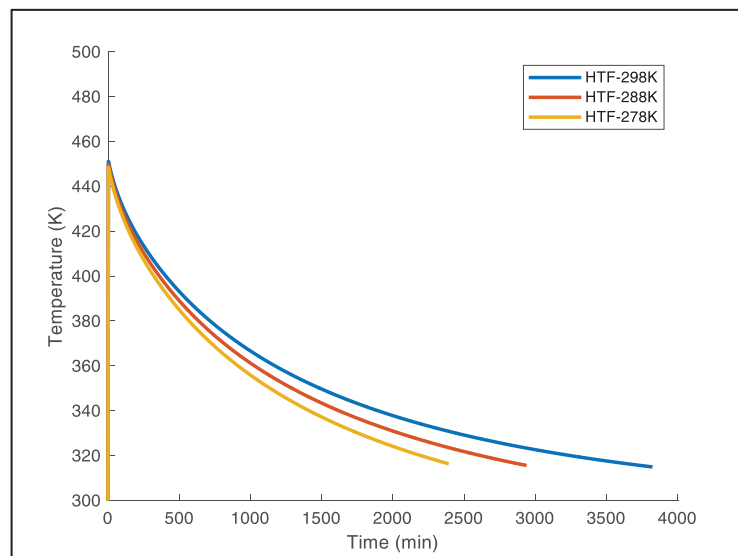
Figure 7.36. Effect of cold fluid temperature on temperature distribution of adsorbent bed

7.6.3. Effect of Hot Fluid Temperature on Average Bed Temperature

In Figure 7.37, it can be seen that the time consumed during adsorption process decreases as increasing temperature of heat transfer fluid. This leads a decrement in SCP of the adsorbent bed. Furthermore, heat released during the adsorption process per unit time will also increase by increasing hot fluid temperature, so the COP will also increase as the hot fluid temperature increases.
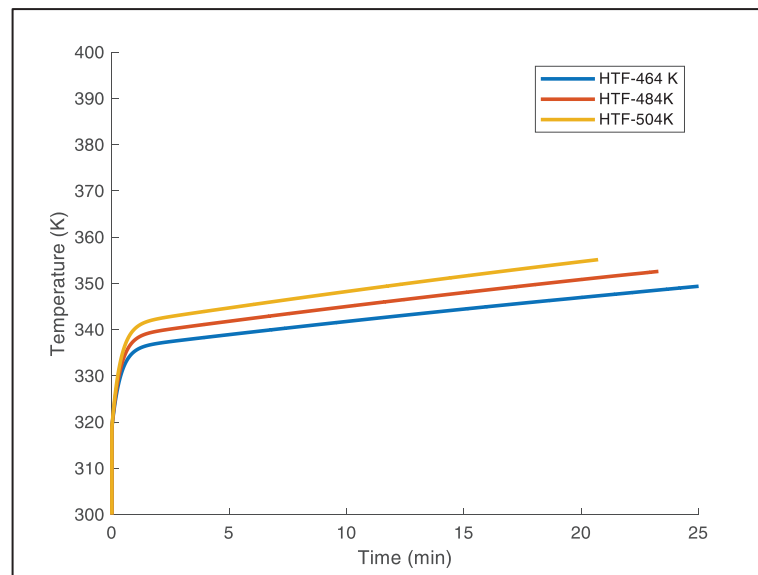
Figure 7.37. Effect of hot fluid temperature on temperature distribution of adsorbent bed

7.7. Enhancement of Effective Thermal Conductivity of Zeolite

7.7.1. Zeolite/Graphene Pellet

As mentioned in Chapter 6, the optimization of kaolin and water amount was performed prior to mix graphene with zeolite 13X. The analysis was performed with the amount of kaolin of 15 wt% and 20 wt%. Then, 30-40 wt% of deionized water was used to obtain a paste. The calcination was performed at 550°C for 2 hours.

The obtained pellets are compared with the commercial cylindrical 13X (Sigma Aldrich Co.) by means of thermal gravimetric analysis (Figure 7.38). It is seen that there is no significant difference on the amount of water loss for three zeolites. Additionally, the zeolites are put into water to observe physical strength. It is observed that the strength of zeolite with kaolin of 20 wt% is better than kaolin of 18 wt%.
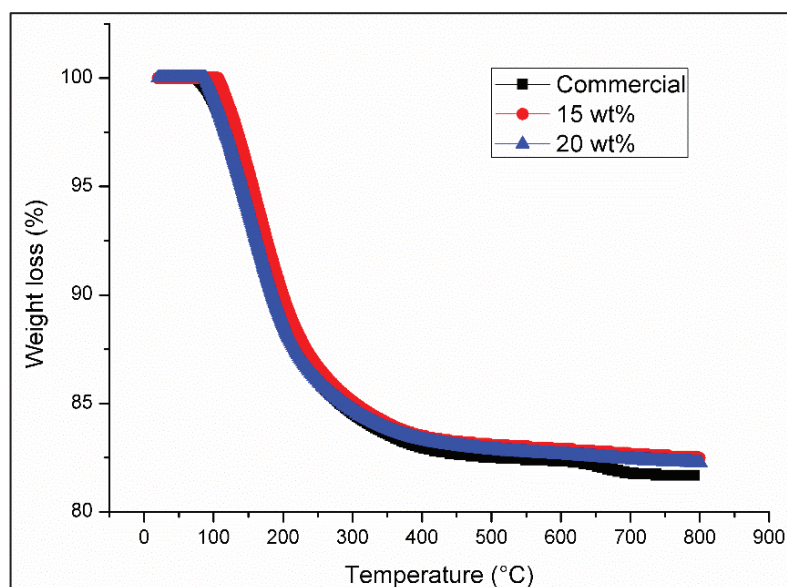
Figure 7.38. The effect of kaolin content on thermogravimetric behaviour of Zeolite 13X

Due to the difference in physical strength of the zeolites, 20 wt% of kaolin is used in the latter studies. The manufacturing procedure is similar but this time commercial graphene (1 wt% graphene/zeolite 13X) is exfoliated in water than added during. The calcination is performed at N_2 atmosphere.

In the normalized FTIR results (Figure 7.39), the spectrum of zeolite 13X/graphene pellet is similar with the commercial zeolite 13X, and any spectrum of the graphene is observed in the analysis. This may be related with the low amount of the graphene in the zeolite pellet.
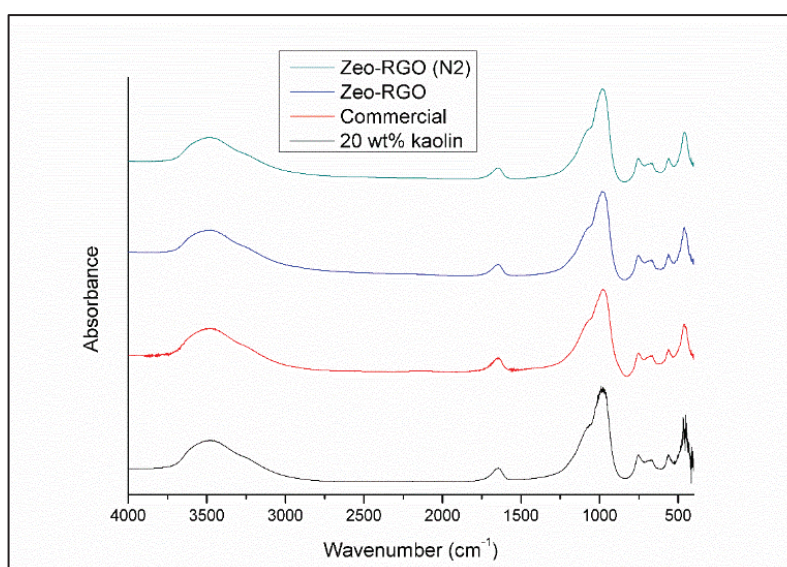
Figure 7.39. FTIR spectrum of zeolite 13X pellet

In Figure 7.40, SEM images have been represented. The analysis is performed with 5000 magnifications. The graphene layers between crystals of the zeolite can obviously be seen in Figure 7.40c. which means that the pelletization and calcination of zeolite/graphene is achieved successfully.
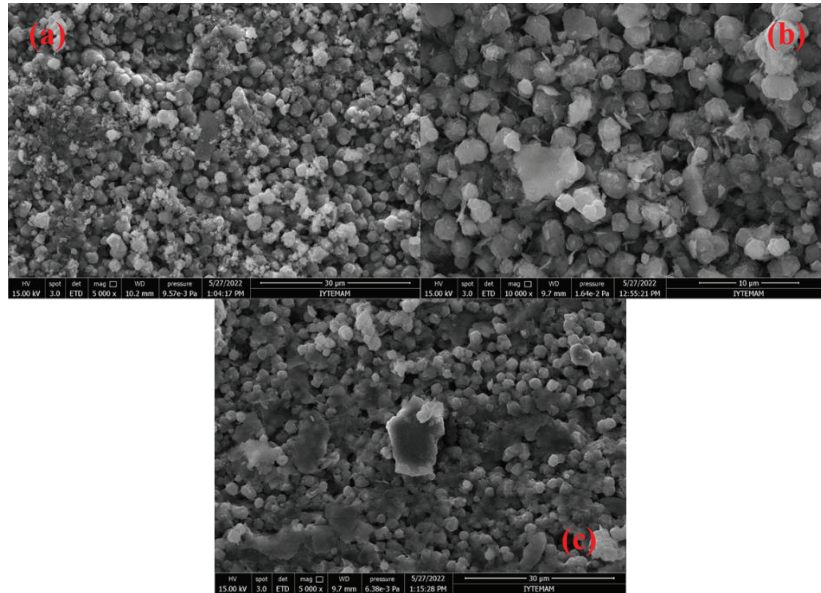
Figure 7.40. SEM images a) Commercial Zeolite 13X b) Zeolite 13X with 20%wt. kaolin c) Zeolite 13X /graphene pellet

The measurement of thermal conductivity of the produced pellet was achieved by hot wire method. The results of the measurement are presented in Table 7.7. The effective thermal conductivity of zeolite 13X is determined as 0.12 W/m.K which is compatible with the results obtained by homemade system. Furthermore, the effective thermal conductivity of zeolite 13X is increased approximately 30% when graphene is added.

Table 7.7. Effective thermal conductivity measurement with hot-wire method

Sample	Measurement-1	Measurement-2	Measurement-3
Zeolite 13X	0.1226 W/m.K	0.1223 W/m.K	0.1240 W/m.K
Zeolite 13X	Average: 0.1230 W/m.K		
Zeolite 13X-RGO	0.1621 W/m.K	0.1586 W/m.K	0.1632 W/m.K
Zeolite 13X-RGO	Average: 0.1613 W/m.K		

According to the study of Rocky et al., the thermal conductivity of graphene was given as 3000 W/m.K and the bulk density of graphene was in the range of graphene was

in the range of 0.3-1 g/cm^3. According to Maxwell equation given in Equation 6.49, the effective thermal conductivity of the zeolite/graphene was supposed to be in the range of 15-51 W/mK when 1 wt% graphene was used.

On the other hand, the thermal conductivity of graphene was calculated from experimental result as 2.5-8 W/mK when graphene density was in the range of 0.3-1 g/cm^3. In order to obtain a material with a thermal conductivity of 1 W/mK, at least 20 wt% of graphene should be used.

From an economic point of view, commercial graphene (Nanokar, 800 m^2/g) has a price of 26,019 TL/kg. In an adsorption heat pump, approximately 50 kg adsorbent is used. This means that 20 kg of graphene should be used to achieve a thermal conductivity of 1W/mK. In Table 7.5, it is seen that the COP increases from 0.01 to 0.1 when thermal conductivity increased to 1 W/mK. For an industry that consumes 100 kWh/day electricity for cooling purpose, the yearly energy saving will be 125,560 TL according to the current electricity price for those COP changes. In adsorption heat pumps, one of the main advantages is no requirement for maintenance and long cycle life. Therefore, although the initial investment cost is high, considering the electricity prices, it is seen that the cost of graphene is covered in a short period of 3 years. Furthermore, the adsorption heat pumps utilize the solar energy and waste heat rather than mechanical energy, so they have a high primary energy efficiency which makes the adsorption heat pumps environmentally friendly. Additionally, the increment in electricity price makes solar energy attractive. For instance, the payback of a facility with 55 kW installed capacity is approximately 7 years according to the current legislations in Turkey.

7.7.2. Synthesizing Graphite Oxide

Although there are several studies to manufacture graphite oxide, there is still inconsistencies in the procedure which affect the functional properties of the graphite oxide. In synthesizing GO, Tour's method has been utilized and different parameters were examined are examined in the scope of the thesis.

The first parameter investigated during the study is the amount of HCl, and ethanol used during the washing procedure. It is seen that unoxidized C=C cannot be drawn away from the solution effectively when 200 mL ethanol and 200 mL HCl is used during the washing process (Figure 7.41). So, 300 mL HCl and 300 mL ethanol is decided to be used in the later synthesizes.
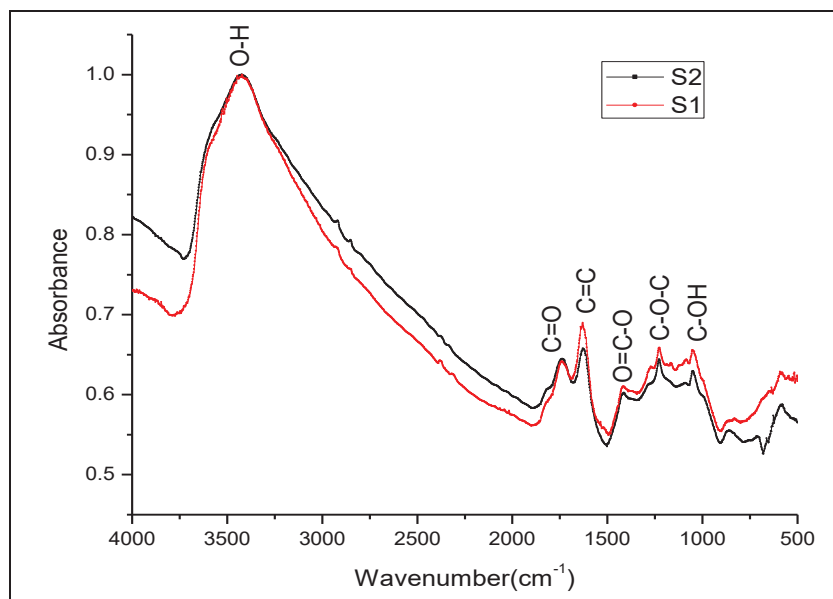
Figure 7.41. Effect of amount of HCl and ethanol on synthesized GO

The second parameter is the amount of H_2O_2 used during stopping the reaction. In the literature, the amount of H_2O_2 is not consistent. Some of the researchers have used 2 mL H_2O_2 and the others have used 50 mL H_2O_2 for the same procedure and same amount of graphite. On the other hand, Kumar et al. claims that the increase in the amount of will increase the exfoliation of the graphene oxide. Therefore, the procedure is performed with 2 mL (S2) and 20 mL (S3) H_2O_2 with the same amount of graphite. The FTIR results are given in Figure 7.42. It is seen that the oxidization of graphite achieves better when 20 mL H_2O_2 is used. Furthermore, the stability of the S3 sample is longer than the S2 sample.
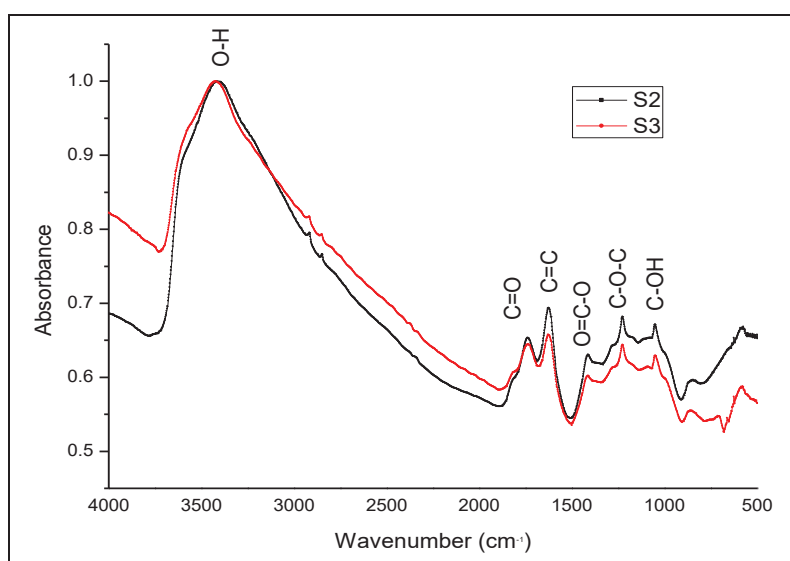
Figure 7.42. Effect of amount of H_2O_2 on synthesized GO

The last parameter is the reaction time which affects the stability of the graphene oxide. The reaction time is chosen as 16 hours (S3) and 12 hours (S4). It is observed that the amount of carboxylic acid groups and epoxy groups increase for the sample S4 (Figure 7.43). Furthermore, the stability increases when the reaction time decreases to 12 hours.
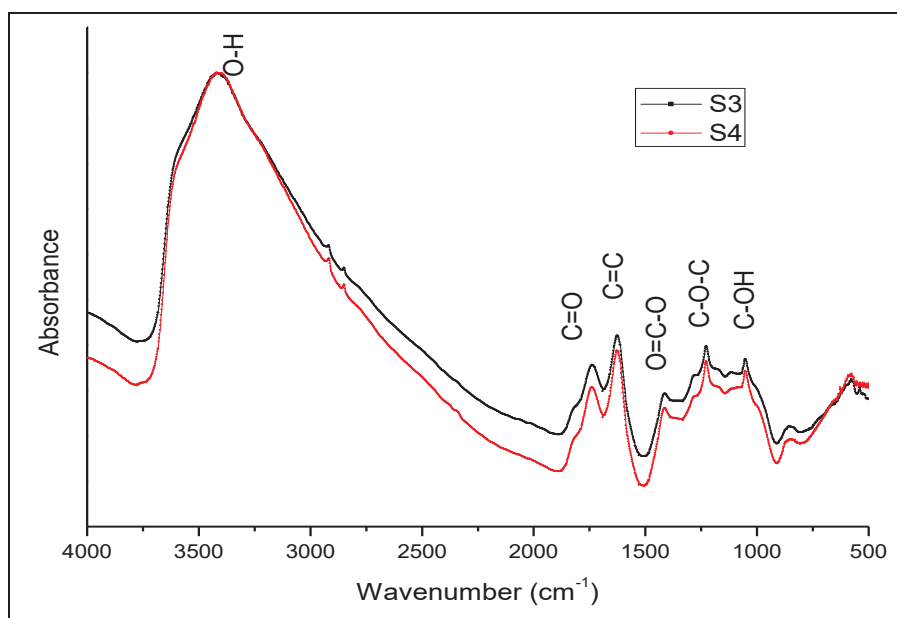
Figure 7.43. Effect of reaction time on synthesized GO

7.7.3. Reduction of Graphite Oxide to Graphene

According to the FTIR results and the stability of the solution, sample S4 has been utilized in the reduction studies. The reduction is performed with both hydrazine hydrate and ascorbic acid. The details of the procedure have been given in Chapter 6. Furthermore, effect of NH_3 in reduction process has also been investigated.

The normalized FTIR results of RGO samples are given in Figure 7.44. It is seen that the removal of oxygen functional groups and alkene groups from the graphene oxide is better achieved when hydrazine hydrate is used with additional NH_3. It is known that the functional groups in the structure of the RGO reduces the thermal conductivity. Therefore, RGO obtained by reducing GO with hydrazine hydrate by additional NH_3 is used to enhance the thermal conductivity of the zeolite. On the other hand, due to being eco-friendly, ascorbic acid can be alternative to hydrazine hydrate in reduction of graphene oxide.
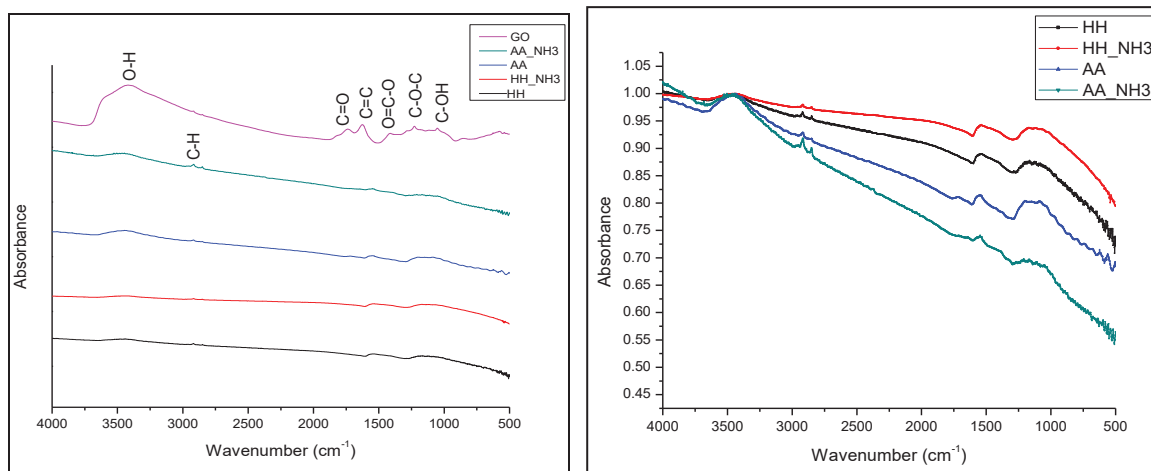
Figure 7.44. FTIR results of reduced graphene oxide

From the experimental data, the optimum conditions to obtain graphene has been determined. However, still the thermal conductivity measurements should be performed. Furthermore, eco-friendly chemicals should be taken into consideration during synthesizing both graphene oxide and reduced graphene oxide.

CHAPTER 8

CONCLUSIONS

In order to deal with the effects of the climate change and prevent the depletion in the ozone layer, the environmentally friendly systems have to be improved and started to be used in the whole world. In recent years, the use of renewable energy sources rather than fossil sources in generation of electricity gains attention. However, the storage of the produced energy still requires improvements. Besides, the use of adsorption in energy recovery and storage systems is a promising technology.

According to the performed investigations for adsorption heat pumps, the following remarks can be concluded:

- The main drawback in the design of the adsorption heat pump is the low heat transfer properties within the adsorbent bed.
- The traditional adsorbent-adsorbate pairs are inefficient in enhancing the thermal conductivity within the bed, therefore new pairs with high thermal conductivity should be produced.
- Developing advanced cycle systems can be an alternative in order to reach the desired performance values of adsorption heat pump.

According to the information given above, the studies have been performed. The main goal is to design an adsorbent bed with high effective thermal conductivity in the scope of the thesis. The improvement of the effective thermal conductivity has been achieved by two ways:

1- Enhancing effective thermal conductivity of the adsorbent bed by continuous metal additives with different geometrical shapes (Unconsolidated adsorbent bed)

2- Enhancing effective thermal conductivity of the adsorbent (zeolite 13X) by adding high thermal conductive graphene (Consolidated adsorbent bed)

In designing an adsorption heat pump, the selection of the working pair is the main task. Due to the high affinity to water vapor and high heat of adsorption value, zeolite 13X-water pair has been chosen as working pair. Prior to theoretical analysis of the adsorbent bed, the characterization of zeolite 13X and determination of adsorption

equilibrium and kinetics properties of zeolite 13X-water pair has been performed experimentally. In order to analyse the effect of regeneration temperature of the adsorbent, the adsorption studies have been performed at regeneration temperature of 90°C and the isotherms have been obtained at adsorption temperature of 35, 45 and 60°C.

The remarks obtained from experimental studies can be summarized as the followings:

- When compared to other zeolite types, zeolite 13X has higher affinity to water vapor due to Si/Al ration which has been supported with thermal gravimetric analysis.

- The adsorption equilibrium of zeolite 13X-water pair is well defined by Sips Relationship rather than Langmuir and Toth's Relationships. Furthermore, the isosteric heat of adsorption is adsorbate loading dependent for zeolite 13X-water pair.

- Although the effective diffusivity is well defined by Crank's model, it is also logical to use LDF model to represent the mass transfer within the particle since it gives an approximate solution.

- The temperature increment at the beginning of the adsorption has been too low due to the weight ratio of adsorbent and bed. Therefore, the assumption of isothermal adsorption is reasonable for the zeolite 13X-water pair.

After determining the adsorption equilibrium and kinetic properties of zeolite 13X-water pair, the studies for designing adsorbent bed have been conducted. The thermal conductivity measurements for unconsolidated bed have been achieved with a homemade system. The results can be summarized as:

- Zeolite 13X bed has an effective thermal conductivity of 0.12 W/m.K.
- The thickness and shape of the continuous wire are effective on the effective thermal conductivity.
- The best configuration has been obtained when fin shape with 6 fins and 8 sides has been used. The effective thermal conductivity has increased 140% when fins have been located in the bed.

In theoretical analysis of the bed, heat, mass, and momentum transfer equations have been solved simultaneously. Three different beds have been evaluated during the theoretical analysis with different assumptions. The detail of the beds has been discussed in the Materials and Methods section. The effects of the effective thermal conductivity of

the bed and adsorbate loading and temperature dependence of effective diffusivity on performance of adsorption heat pump have been investigated for adsorbent bed-1 in one-dimensional analysis (Case I). As Case II, the two-dimensional analysis of the adsorbent bed-1 has been conducted.

The following remarks for Case I and Case II can be concluded from the theoretical studies:

- When the effective thermal conductivity of the adsorbent increases from 0.12 W/m.K to1 W/m.K, the effective thermal conductivity of the bed increases from 6.48×10^{-2} W/m.K and 2.51×10^{-1} W/m.K which directly effects specific cooling/heating power value of the adsorption heat pump. On the other hand, the indirect effect of thermal conductivity value on COP value is generally ignored in the studies. However, it has been seen that COP for cooling process increases from 0.01 to 0.10 and for heating process from 0.36 to 4.83 due to the change in heat amounts during cycle.

- Temperature and adsorbate loading dependence of effective diffusivity has not been significant in designing adsorption heat pump. Thus, it can be taken as constant during the analysis.

- The effect of flow of adsorptive in axial direction does not have significant effect, so making one-dimensional analysis will define the distributions within the bed sufficiently.

- The experimental data for Zeolite 13X-water pair is limited for validation of theoretical model. Due to the low accuracy of the devices used in the study of Mobedi, the validation should be performed with a new experimental set up.

In Case III, the design of the adsorbent bed was changed, and two-dimensional analysis were performed since two-dimensional heating of the bed was achieved. The following remarks for Case III can be concluded from the theoretical studies:

- Two-dimensional heating of the bed decreases cycle duration of the processes significantly. Furthermore, the average temperature of the bed decreased which indicated that the heat transfer within the bed was enhanced for this design.

For Case IV, heat transfer fluid was used for heating and cooling of the bed. The effects of velocity, cold temperature, and hot temperature of heat transfer fluid on performance of adsorption heat pump was analysed. The following remarks for Case IV can be concluded from the theoretical studies:

- The heat transfer fluid velocity in the range of 0.1-10 m/s have not significant effect on the performance of the adsorption heat pump which is also compatible with the literature.

- When the temperature of the heat transfer fluid is increased for the cooling processes, the time period of the processes increases which directly decreases the SCP value.

- On the other hand, when the temperature of the heat transfer fluid is increased for the heating processes, the duration of the processes decreases, so the SCP value increases.

In consolidated adsorbent bed studies, commercial graphene is used. Crystalline Zeolite 13X has been mixed with graphene by 1 wt% and then pelletized to enhance the effective thermal conductivity of the bed. The following remarks can be concluded:

- The graphene layers in the framework structure of zeolite which are observed in the SEM images show that the methodology is applicable to obtain a composite particle. On the other hand, low amount of graphene limits the characterization of the material.

- In thermal conductivity measurements which is performed with hot wire method, the thermal conductivity of zeolite 13X increased from 0.12 W/mK to 0.16 W/mK. According to the Maxwell equation, the thermal conductivity of graphene is in the range of 2.5-8 W/mK. Thus, at least 20 wt% of graphene should be used to obtain a material with 1 W/mK.

- In economical analysis, although the initial investment cost is high, considering the current electricity prices, it is seen that the cost of graphene is covered in a short period of 3 years.

Due to the high cost of commercial and difficulties in large scale productions of graphene, it has also been synthesized in the scope of the thesis. Since the manufacturing procedure has not been consistent in literature, first the manufacturing of graphite oxide and RGO is optimized. The following remarks can be concluded for the RGO manufacturing studies:

- In synthesizing graphite oxide, the reaction time, amount of H_2O_2 and amount of HCl and ethanol has significant effect on forming functional oxygen groups in the structure of GO.

- It can be said that the optimum reaction time is 12 hours to functionalize and obtain a stable GO. Furthermore, the stability of the GO reduces when the amount of H_2O_2 is reduced.

- In reduction of GO, hydrazine hydrate with NH_3 is efficient to remove functional groups. On the other hand, ascorbic acid can also be a good choice due to being environmentally friendly reducing agent.

Based on the obtained experimental and numerical results, further studies can be performed on the following issues:

- The studies on adsorption heat pump with zeolite 13X-water pair is limited. Therefore, studies should be focused on this pair due to high adsorption capacity and heat of adsorption value. Furthermore, the validation of the theoretical model with experimental data should be performed with a new experimental set up.

- The zeolite 13X/graphene pellet should be synthesized with higher concentration of the graphene and characterization of the pellet should be performed in detail. Furthermore, the adsorption equilibrium and kinetics behavior of the pellet should be determined.

- The thermal conductivity of synthesized reduced graphene oxide should be determined. Eco-friendly chemicals should be tried to synthesize reduced graphene oxide.

- In adsorption heat pump design, using both fins and zeolite 13X/graphene pellet at the same time can be beneficial to enhance the performance of the system.

REFERENCES

Afonso, M. R. A.; Silveira Jr, V. Characterization of Equilibrium Conditions of Adsorbed Silica Gel/Water Bed According to Dubinin Astakhov and Freundlich. *Revista de Engenharia Térmica*, 2005, *4*(1), 03-07.

Akahira, A.K.; Alam; C.A.; Hamamoto Y.; A. Akisawa; Kashiwagi T. Mass recovery adsorption refrigeration cycle—improving cooling capacity, International Journal of Refrigeration, 2004, **27**(3), 225-234.

Alam, S. N.; Sharma, N.; Kumar, L. Synthesis of graphene oxide (GO) by modified hummers method and its thermal reduction to obtain reduced graphene oxide (rGO). Graphene, 2014, *6*(1), 1-18.

Alelyani, S. M.; Bertrand, W. K.; Zhang, Z.; Phelan, P. E. Experimental study of an evacuated tube solar adsorption cooling module and its optimal adsorbent bed design. Solar Energy, 2020, *211*, 183-191.

Ammar, A.; Al-Enizi, A. M.; AlMaadeed, M. A.; Karim, A. Influence of graphene oxide on mechanical, morphological, barrier, and electrical properties of polymer membranes. *Arabian journal of chemistry*, 2016, *9*(2), 274-286.

Anyanwu, E. E.; Ogueke N. V. Thermodynamic design procedure for solid adsorption solar refrigerator. Renewable Energy, 2005,**30**(1): 81-96.

Aristov, Y. I.; Restuccia, G.; Cacciola, G.; Parmon, V. N. A family of new working materials for solid sorption air conditioning systems. Applied Thermal Engineering 2002, 22(2): 191-204.

Aristov, Y. I.; Dawoud, B.; Glaznev, I. S.; Elyas, A. A new methodology of studying the dynamics of water sorption/desorption under real operating conditions of adsorption heat pumps: Experiment. International Journal of Heat and Mass Transfer 2008, 51(19–20): 4966-4972.

Atakan, A.; Fueldner, G.; Munz, G.; Henninger, S.; Tatlier, M. Adsorption kinetics and isotherms of zeolite coatings directly crystallized on fibrous plates for heat pump applications. Applied Thermal Engineering, 2013, **58**(1–2): 273-280.

Balandin, A. A.; Ghosh, S.; Bao, W.; Calizo, I.; Teweldebrhan, D.; Miao, F.; Lau, C. N. Superior thermal conductivity of single-layer graphene. Nano letters, 2008, 8(3), 902-907.

Bart, H. J.; Germerdonk, R.; Ning, P. Two-dimensional non-isothermal model for toluene adsorption in a fixed-bed adsorber. Chemical Engineering and Processing: Process Intensification, 1996, 35(1), 57-64.

Bauer, J.; Herrmann, R.; Mittelbach, W.; Schwieger, W. Zeolite/aluminum composite adsorbents for application in adsorption refrigeration. International Journal of Energy Research, 2009, **33**(13): 1233-1249.

Ben Amar, N.; Sun, L. M.; Meunier, F. Numerical analysis of adsorptive temperature wave regenerative heat pump. Applied Thermal Engineering, 1996, **16**(5): 405-418.

Bird, R. B.; Stewart, W. E.; Lightfoot, E. N.;Meredith, R. E. Transport phenomena. *Journal of The Electrochemical Society*, 1961, 108(3), 78C.

Bish, D. L. *Thermal behavior of natural zeolites*. Los Alamos National Lab., 1993, (No. LA-UR--93-2881)

Bonaccorsi, L.; Calabrese, L.; Freni, A.; Proverbio, E.; Restuccia, G. Zeolites direct synthesis on heat exchangers for adsorption heat pumps. Applied Thermal Engineering, 2013, **50**(2): 1590-1595.

Botas, C.; Pérez-Mas, A. M.; Álvarez, P.; Santamaría, R.; Granda, M.; Blanco, C.; Menéndez, R. Optimization of the size and yield of graphene oxide sheets in the exfoliation step. *Carbon*, 2013, *63*, 576-578.

Boukhvalov, D. W.; Katsnelson, M. I.; Son, Y. W. Origin of anomalous water permeation through graphene oxide membrane. *Nano letters*, 2013, *13*(8), 3930-3935.

Brandani, F.; Ruthven, D. M. The effect of water on the adsorption of CO2 and C3H8 on type X zeolites. *Industrial & engineering chemistry research*, 2004, *43*(26), 8339-8344.

Breck, D. W. Zeolite Molecular Sieves, reprint, 1984.

Burhan, M.; Shahzad, M. W.; Ng, K. C. Energy distribution function based universal adsorption isotherm model for all types of isotherm. *International Journal of Low-Carbon Technologies*, 2018, *13*(3), 292-297.

Cacciola, G.; Restuccia, G. Reversible Adsorption Heat-Pump - a Thermodynamic Model. Int. J. Refrig., 18, no. 2, 1995, 100-106.

Cakicioglu-Ozkan, F.; Ulku, S. Adsorption Characteristics of Lead-, Barium- and Hydrogen-rich Clinoptilolite Mineral. Adsorption Science and Technology, 2003, Volume 21 (4), 309-317.

Cakicioglu-Ozkan, F.; Ulku, S. The Effect of HCl Treatment on Water Vapor Adsorption Characteristics of Clinoptilolite Rich Natural Zeolite. Microporous and Mesoporous Materials, 2005, 77, no. 1, 47-53.

Cakicioglu-Ozkan, F.; Ulku, S. Diffusion Mechanism of Water Vapour in a Zeolitic Tuff Rich in Clinoptilolite. Journal of Thermal Analysis and Calorimetry 94, no. 3, 2008, 699-702.

Cansever-Erdoğan, B.; Ülkü, S. Ammonium Sorption by Gördes Clinoptilolite Rich Mineral Specimen. Applied Clay Science, 2011, 54, 217-225.

Cao, N.; Zhang, Y. Study of reduced graphene oxide preparation by Hummers' method and related characterization. *Journal of Nanomaterials*, *2015*.

Chahbani, M. H.; Labidi, J.; Paris, J. Modeling of adsorption heat pumps with heat regeneration. Applied Thermal Engineering, 2004, **24**(2-3): 431-447.

Chan, K. C.; Chao, C. Y. H.; Sze-To, G. N.; Hui, K. S. Performance predictions for a new zeolite 13X/CaCl2 composite adsorbent for adsorption cooling systems. International Journal of Heat and Mass Transfer, 2012, **55**(11–12): 3214-3224.

Chekirou, W.; Boukheit, N.; Karaali, A. Performance improvement of adsorption solar cooling system. International Journal of Hydrogen Energy, 2016, **41**(17): 7169-7174.

Chen, W.; Yan, L.; Bangal, P. R. Preparation of graphene by the rapid and mild thermal reduction of graphene oxide induced by microwaves. *Carbon*, 2010, *48*(4), 1146-1152.

Cheng, Z. L.; Li, Y. X.; Liu, Z. Novel adsorption materials based on graphene oxide/Beta zeolite composite materials and their adsorption performance for rhodamine B. *Journal of Alloys and Compounds*, 2017, *708*, 255-263.

Chiu, N. F.; Huang, T. Y. Sensitivity and kinetic analysis of graphene oxide-based surface plasmon resonance biosensors. *Sensors and Actuators B: Chemical*, 2014, *197*, 35-42.

Cho, S. H.;Kim, J. N. Modeling of a silica gel/water adsorption-cooling system. *Energy*, 1992, *17*(9), 829-839.

Chua, H. T.; Ng, K. C.; Chakraborty, A.; Oo, N. M.; Othman, M. A. Adsorption Characteristics of Silica Gel Plus Water Systems. Journal of Chemical and Engineering Data, 2002, 47, no. 5, 1177-1181.

Chua, C. K.; Pumera, M. Selective removal of hydroxyl groups from graphene oxide. *Chemistry–A European Journal*, 2013, *19*(6), 2005-2011.

Clausse, M.; Meunier, F.; Coulie, J.; Herail, E. Comparison of adsorption systems using natural gas fired fuel cell as heat source, for residual air conditioning. Int. J. Refrig., 2009, 32, 712-719.

Close, D. J.; Dunkle, R. V. Use of Adsorbent Beds for Energy Storage in Drying of Heating Systems. Solar Energy, 1977, **19**: 233-238.

Critoph, R. E. Simulation of a continuous multiple-bed regenerative adsorption cycle." International Journal of Refrigeration, 2001, **24**(5): 428-437.

Dao, T. D.; Jeong, H. M. Graphene prepared by thermal reduction–exfoliation of graphite oxide: Effect of raw graphite particle size on the properties of graphite oxide and graphene. *Materials Research Bulletin*, 2015, *70*, 651-657.

Dawoud, B. Water vapor adsorption kinetics on small and full scale zeolite coated adsorbers; A comparison. Applied Thermal Engineering, 2013, **50**(2): 1645-1651.

Dawoud, B.; Vedder, U.; Amer, E. H.; Dunne, S. Non-isothermal adsorption kinetics of water vapour into a consolidated zeolite layer. International Journal of Heat and Mass Transfer, 2007, **50**(11–12): 2190-2199.

Delage, F.; Pre, P.; Le Cloirec, P. Mass transfer and warming during adsorption of high concentrations of VOCs on an activated carbon bed: experimental and theoretical analysis. *Environmental science & technology*, 2000, *34*(22), 4816-4821.

Demir, H. An Experimental and Theoretical Study on the Improvement of Adsorption Heat Pump Performance. PhD Dissertation, Izmir Institute of Technology, İzmir-Turkey, 2008.

Demir, H.; Mobedi, M.; Ülkü, S. A Numerıcal Study On Heat And Mass Transfer Through Adsorbent Bed Of An Adsorptıon Heat Pump.

Demir, H.; Mobedi, M.; Ülkü, S. Effects of porosity on heat and mass transfer in a granular adsorbent bed. *International Communications in Heat and Mass Transfer*, 2009, *36*(4), 372-377.

Demir, H.; Mobedi, M.; Ülkü, S. A review on adsorption heat pump: Problems and solutions. Renewable & Sustainable Energy Reviews, 2008, **12**(9): 2381-2403.

Demir, H.; Mobedi, M.; Ülkü, S. "Microcalorimetric Investigation of Water Vapor Adsorption on Silica Gel. " Journal of Thermal Analysis and Calorimetry, 2011, 105, no. 1, 375-382.

Demir, H.; Mobedi, M.; Ülkü, S. "The use of metal piece additives to enhance heat transfer rate through an unconsolidated adsorbent bed." International Journal of Refrigeration, 2010, **33**(4): 714-720.

Demir, H. Development of microwave assisted zeolite–water adsorption heat pump. International Journal of Refrigeration, 2013, **36**(8): 2289-2296.

Demir, H. The effect of microwave regenerated adsorbent bed on the performance of an adsorption heat pump. Applied Thermal Engineering, 2013, **50**(1): 134-142.

Deshmukh, H.; Maiya, M. P.; Srinivasa Murthy, S. Continuous vapour adsorption cooling system with three adsorber beds. Applied Thermal Engineering, 2015, **82**: 380-389.

Dieng, A. O.; Wang, R. Z. Literature review on solar adsorption technologies for ice-making and air-conditioning purposes and recent developments in solar technology. Renewable and Sustainable Energy Reviews, 2001, 5, 313-342.

Diker, H.; Durmaz, G. B.; Bozkurt, H.; Yeşil, F.; Varlikli, C. Controlling the distribution of oxygen functionalities on GO and utilization of PEDOT: PSS-GO composite as hole injection layer of a solution processed blue OLED. *Current Applied Physics*, 2017, *17*(4), 565-572.

Do, D. D. *Adsorption analysis: Equilibria and kinetics (with cd containing computer MATLAB programs)* (Vol. 2), World Scientific, 1998.

Do, D. D.; Jordi, R. G.; Ruthven, D. M. Sorption Kinetics in Zeolite Crystals with Finite Intracrystal Mass Exchange - Isothermal Systems. Journal of the Chemical Society-Faraday Transactions, 1992, 88, no. 1, 121-131.

Douss, N.; Meunier, F. Experimental study of cascading adsorption cycles. Chemical Engineering Science, 1989, **44**(2): 225-235.

Douss, N.; Meunier, F. E.; Sun, L. M. Predictive model and experimental results for a two-adsorber solid adsorption heat pump. Industrial & Engineering Chemistry Research, 1988, **27**(2): 310-316.

Dreyer, D. R.; Park, S.; Bielawski, C. W.; Ruoff, R. S. The chemistry of graphene oxide. *Chemical society reviews*, 2010, *39*(1), 228-240.

Duquesne, M.; Toutain, J.; Sempey, A.; Ginestet, S.; del Barrio, E. P. Modeling of a nonlinear thermochemical energy storage by adsorption on zeolites. *Applied thermal engineering*, 2014, *71*(1), 469-480.

Dzhigit, O. M.; Kiselev, A. V.; Mikos, K. N.; Muttik, G. G.; Rahmanova, T. A. Heats of adsorption of water vapour on X-zeolites containing Li+, Na+, K+, Rb+, and Cs+ cations. *Transactions of the Faraday Society*, 1971, *67*, 458-467.

Elsheniti, M. B.; Hassab, M. A.; Attia, A. E. Examination of effects of operating and geometric parameters on the performance of a two-bed adsorption chiller. *Applied Thermal Engineering*, 2019, *146*, 674-687.

Emiru, T. F.; Ayele, D. W. Controlled synthesis, characterization and reduction of graphene oxide: A convenient method for large scale production. *Egyptian Journal of Basic and Applied Sciences*, 2017, *4*(1), 74-79.

Eun, T.-H.; Song, H.-K.; Hun Han, J.; Lee, K.-H.; Kim, J.-N. Enhancement of heat and mass transfer in silica-expanded graphite composite blocks for adsorption heat pumps: Part I. Characterization of the composite blocks. International Journal of Refrigeration, 2000, **23**(1): 64-73.

Fan, M.; Panezai, H.; Sun, J.; Bai, S.; Wu, X. Thermal and kinetic performance of water desorption for N2 adsorption in Li-LSX zeolite. *The Journal of Physical Chemistry C*, 2014, *118*(41), 23761-23767.

Franco, A. An apparatus for the routine measurement of thermal conductivity of materials for building application based on a transient hot-wire method. *Applied Thermal Engineering*, 2007, *27*(14-15), 2495-2504.

Freni, A.; Frazzica, A.; Dawoud, B.; Chmielewski, S.; Calabrese L.; Bonaccorsi; L. Adsorbent coatings for heat pumping applications: Verification of hydrothermal and mechanical stabilities. Applied Thermal Engineering, 2013, 50(2): 1658-1663.

Freni, A.; Dawoud, B.; Bonaccorsi, L.; Chmielewski, S.; Frazzica, A.; Calabrese, L.; Restuccia, G. Adsorption Heat Exchangers. Characterization of Zeolite-Based Coatings for Adsorption Heat Pumps. Cham, Springer International Publishing, 2015, 35-53.

Fritz, W.; Schluender, E. U. Simultaneous adsorption equilibria of organic solutes in dilute aqueous solutions on activated carbon. *Chemical Engineering Science*, 1974, *29*(5), 1279-1282.

Gabruś, E.; Witkiewicz, K.; Nastaj, J. Modeling of regeneration stage of 3A and 4A zeolite molecular sieves in TSA process used for dewatering of aliphatic alcohols. *Chemical Engineering Journal*, 2018, *337*, 416-427.

Gao, X.; Jang, J.; Nagase, S. Hydrazine and thermal reduction of graphene oxide: reaction mechanisms, product structures, and reaction design. *The Journal of Physical Chemistry C*, 2010, *114*(2), 832-842.

Garcia-Cuello, V.; Moreno-Piraján, J. C.; Giraldo-Gutiérrez, L.; Sapag, K.; Zgrablich, G. A new microcalorimeter of adsorption for the determination of differential enthalpies. *Microporous and mesoporous materials*, 2009, *120*(3), 239-245.

Gediz İliş, G. An Experimental and Numerical Study on Heat and Mass Transfer in Adsorbent Bed of an Adsorption Heat Pump. " PhD Dissertation, Izmir Institute of Technology, Izmir-Turkey, 2012.

Gaeini, M.; Zondag, H. A.; Rindt, C. C. M. Effect of kinetics on the thermal performance of a sorption heat storage reactor. *Applied Thermal Engineering*, 2016, *102*, 520-531.

Gerente, C.; Lee, V. K. C.; Cloirec, P. L.; McKay, G. Application of chitosan for the removal of metals from wastewaters by adsorption—mechanisms and models review. *Critical reviews in environmental science and technology*, 2007, *37*(1), 41-127.

Glueckauf, E. Theory of chromatography. Part 10.—Formulæ for diffusion into spheres and their application to chromatography. *Transactions of the Faraday Society*, 1955, *51*, 1540-1551.

Golparvar, B.; Niazmand, H.; Sharafian, A.; Hosseini, A. A. Optimum fin spacing of finned tube adsorber bed heat exchangers in an exhaust gas-driven adsorption cooling system. *Applied Energy*, 2018, *232*, 504-516.

Goyal, P.; Baredar, P.; Mittal, A.; Siddiqui, A. R. Adsorption refrigeration technology – An overview of theory and its solar energy applications. Renewable and Sustainable Energy Reviews, 2016, 53: 1389-1410.

Graf, S.; Lanzerath, F.; Sapienza, A.; Frazzica, A.; Freni, A.; Bardow A. Prediction of SCP and COP for adsorption heat pumps and chillers by combining the large-temperature-jump method and dynamic modeling. Applied Thermal Engineering, 2016, 98: 900-909.

Gray, P. G.; Do, D. D. A graphical method for determining pore and surface diffusivities in adsorption systems. *Industrial & engineering chemistry research*, 1992, *31*(4), 1176-1182.

Gregg, S. J.; Sing, K. S. W. Adsorption, Surface Area and Porosity*, 2nd ed*.; Academic Press Inc., London, 1982.

Griesinger, A.; Spindler, K.; Hahne, E. Measurements and theoretical modelling of the effective thermal conductivity of zeolites. *International Journal of Heat and Mass Transfer*, 1999, *42*(23), 4363-4374.

Gui, Y. B.; Wang, R. Z.; Wu, J. Y.; Xu, Y. X.; Wang, W. Experimental Analysis on the Dynamic Characteristics of a Heat-Regenerative Adsorptive Air-Conditioning System. Adsorption, 2002, 8(2): 157-163.

Gupta, B.; Kumar, N.; Panda, K.; Kanan, V.; Joshi, S.; Visoly-Fisher, I. Role of oxygen functional groups in reduced graphene oxide for lubrication. *Scientific reports*, 2017, *7*(1), 1-14.

Hajji, A.; Worek, W. M. Simulation of a regenerative, closed-cycle adsorption cooling/heating system. *Energy*, 1991, *16*(3), 643-654.

Hall, K. R.; Eagleton, L. C.; Acrivos, A.; Vermeulen, T. Pore and Solid Diffusion Kinetics in Fixed Bed Adsorption under Constant Pattern Conditions. Ind. Eng. Chem. Fundamen., 1966, 5 (2), 212-223.

Hamamoto, Y.; Alam, K. C. A.; Saha, B. B.; Koyama, S.; Akisawa, A.; Kashiwagi, T. Study on adsorption refrigeration cycle utilizing activated carbon fibers. Part 2. Cycle performance evaluation. International Journal of Refrigeration-Revue Internationale Du Froid, 2006, 29(2): 315-327.

Han, Y.; Xu, Z.; Gao, C. Ultrathin graphene nanofiltration membrane for water purification. *Advanced Functional Materials*, 2013, *23*(29), 3693-3700.

Hassan, H. Z. Energy analysis and performance evaluation of the adsorption refrigeration system. *International Scholarly Research Notices*, *2013*.

Haubner, K.; Murawski, J.; Olk, P.; Eng, L. M.; Ziegler, C.; Adolphi, B.; Jaehne, E. The route to functional graphene oxide. *ChemPhysChem*, 2010, *11*(10), 2131-2139.

He, P.; Wang, W.; Du, L.; Dong, F.; Deng, Y.; Zhang, T. Zeolite A functionalized with copper nanoparticles and graphene oxide for simultaneous electrochemical determination of dopamine and ascorbic acid. *Analytica chimica acta*, 2012, *739*, 25-30.

Hill, T. L. Introduction to Statistical Thermodynamics. " Dover Publications, New York, 1960.

Huang, Y.; Ouyang, Q.; Guo, Q.; Guo, X.; Zhang, G.; Zhang, D. Graphite film/aluminum laminate composites with ultrahigh thermal conductivity for thermal management applications. *Materials & Design*, 2016, *90*, 508-515.

Huetter, E. S.; Koemle, N. I.; Kargl, G.; Kaufmann, E. Determination of the effective thermal conductivity of granular materials under varying pressure conditions. *Journal of Geophysical Research: Planets*, 2008, *113*(E12).

Ilis, G. G. Influence of new adsorbents with isotherm Type V on performance of an adsorption heat pump. *Energy*, 2017, *119*, 86-93.

Ilis, G. G.; Mobedi, M.; Ülkü, S. A dimensionless analysis of heat and mass transport in an adsorber with thin fins; uniform pressure approach." International Communications in Heat and Mass Transfer, 2011, 38(6): 790-797.

Ilis, G. G.; Mobedi, M.; Ülkü, S. A parametric study on isobaric adsorption process in a closed adsorbent bed. *International communications in heat and mass transfer*, 2010, *37*(5), 540-547.

Ilis, G. G.; Arslan, G.; Mobedi, M. Desıgn Of The Adsorbent Bed Of An Adsorptıon Refrıgeratıon System For Achıevıng The Hıghest Specıfıc Coolıng Power. *Heat Pipe Science And Technology, An International Journal*, 2016, *7*(1-2).

Ilis, G. G.; Demir, H.; Saha, B. B. Innovative approach in adsorption chiller: Combination of condenser-adsorber for improving performance. *Applied Thermal Engineering*, 2021, *192*, 116958.

Jaroniec, M. Fifty Years of the Theory of the Volume Filling of Micropores. Adsorption-Journal of the International Adsorption Society, 1997, 3, no. 3, 187-188.

Jiang, L.; Wang, L. W.; Wang, R. Z. Investigation on thermal conductive consolidated composite CaCl2 for adsorption refrigeration. International Journal of Thermal Sciences, 2014, 81: 68-75.

Jänchen, J.; Ackermann, D.; Stach, H.; Brösicke, W. Studies of the water adsorption on zeolites and modified mesoporous materials for seasonal storage of solar heat. *Solar energy*, 2004, *76*(1-3), 339-344.

Karger, J.; Ruthven, D. M. Diffusion in Zeolites and Other Microporous Solids, John Wiley & Sons, 1992.

Khan, M. Z. I.; Saha, B. B.; Alam, K. C. A.; Akisawa, A.; Kashiwagi, T. Study on solar/waste heat driven multi-bed adsorption chiller with mass recovery. Renewable Energy, 2007, 32(3): 365-381.

Khatamian, M.; Khodakarampoor, N.; Saket-Oskoui, M. Efficient removal of arsenic using graphene-zeolite based composites. *Journal of colloid and interface science*, 2017, *498*, 433-441.

Kim, J. H.; Lee, C. H.; Kim, W. S.; Lee, J. S.; Kim, J. T.; Suh, J. K.; Lee, J. M. Adsorption Equilibria of Water Vapor on Alumina, Zeolite 13x, and a Zeolite X/Activated Carbon Composite. Journal of Chemical and Engineering Data, 2003, 48, no. 1, 137-141.

Kim, K. M.; Oh, H. T.; Lim, S. J.; Ho, K.; Park, Y.; Lee, C. H. Adsorption Equilibria of Water Vapor on Zeolite 3A, Zeolite 13X and Dealuminated Y Zeolite. J. Chem. Eng. Data, 2016, 1547-1554.

Kim, C.; Cho, K.; Kim, S. K.; Lee, E. K.; Kim, J.-N.; Choi, M. Alumina-coated ordered mesoporous silica as an efficient and stable water adsorbent for adsorption heat pump. Microporous and Mesoporous Materials, 2017, 239: 310-315.

Knowlton, G. D.; White, T. R.; McKague, H. L. Thermal study of types of water associated with clinoptilolite. *Clays and Clay Minerals*, 1981, *29*(5), 403-411.

Kumar, K. V.; Sivanesan, S. Pseudo second order kinetics and pseudo isotherms for malachite green onto activated carbon: comparison of linear and non-linear regression methods. *Journal of Hazardous Materials*, 2006, *136*(3), 721-726.

Kumar, S.; Baruah, B.; Kumar, A. Tunable degree of oxidation through variation of H2O2 concentration and its effect on structural, optical and supercapacitive properties of graphene oxide powders synthesized using improved method. *Materials Today Communications*, 2017, *13*, 26-35.

Ladshaw, A.; Yiacoumi, S.; Tsouris, C.; DePaoli, D. Generalized gas–solid adsorption modeling: Single-component equilibria. *Fluid Phase Equilibria*, 2015, *388*, 169-181.

Largitte, L.; Pasquier, R. New models for kinetics and equilibrium homogeneous adsorption. *Chemical Engineering Research and Design*, 2016, *112*, 289-297.

Lavanchy, A.; Stockli, M.; Wirz C.; Stoeckli F. Binary Adsorption of Vapours in Active Carbons Described by the Dubinin Equation. Adsorption Science & Technology, 1996, 13, no. 6, 537-545.

Leong, K. C.; Liu, Y. Numerical study of a combined heat and mass recovery adsorption cooling cycle." International Journal of Heat and Mass Transfer, 2004, **47**(22): 4761-4770.

Leppäjärvi, T.; Malinen, I.; Kangas, J.; Tanskanen, J. Utilization of Pisat temperature-dependency in modelling adsorption on zeolites. *Chemical engineering science*, 2012, *69*(1), 503-513.

Li, S.; Wu, J. Y. Theoretical research of a silica gel–water adsorption chiller in a micro combined cooling, heating and power (CCHP) system. Applied Energy, 2009, **86**(6): 958-967.

Li, S. L.; Xia, Z. Z.; Wu, J. Y.; Li, J.; Wang, R. Z.; Wang, L. W. Experimental study of a novel CaCl2/expanded graphite-NH3 adsorption refrigerator. International Journal of Refrigeration, 2010, **33**(1): 61-69.

Lian, B.; De Luca, S.; You, Y.; Alwarappan, S.; Yoshimura, M.; Sahajwalla, V.; Joshi, R. K. Extraordinary water adsorption characteristics of graphene oxide. *Chemical science*, 2018, *9*(22), 5106-5111.

Llano-Restrepo, M.; Mosquera, M. A. Accurate correlation, thermochemistry, and structural interpretation of equilibrium adsorption isotherms of water vapor in zeolite 3A by means of a generalized statistical thermodynamic adsorption model. Fluid Phase Equilibria, 2009, 283, 73–88.

Liu, Y.; Leong, K. C. The effect of operating conditions on the performance of zeolite/water adsorption cooling systems. Applied Thermal Engineering, 2005, **25**(10): 1403-1418.

Liu, Y.; Leong, K. C. Numerical study of a novel cascading adsorption cycle. International Journal of Refrigeration-Revue Internationale Du Froid, 2006, **29**(2): 250-259.

Liu, R.; Gong, T.; Zhang, K.; Lee, C. Graphene oxide papers with high water adsorption capacity for air dehumidification. *Scientific reports*, 2017, *7*(1), 1-9.

Liu, H.; Yu, A.; Liu, H.; Chu, S.; Tan, S. Preparation of graphene/zeolite composites and the adsorption of pollutants in water. *Russian Journal of Applied Chemistry*, 2017, *90*(7), 1171-1180.

Lu, Z. S.; Wang, R. Z.; Li, T. X.; Wang, L. W.; Chen, C. J. Experimental investigation of a novel multifunction heat pipe solid sorption icemaker for fishing boats using CaCl2/activated carbon compound–ammonia. International Journal of Refrigeration, 2007, **30**(1): 76-85.

Meunier, F. Solid sorption: an alternative to CFCs. *Heat Recovery Systems and CHP*, 1993, *13*(4), 289-295.

Maggio, G.; Freni, A.; Restuccia, G. A dynamic model of heat and mass transfer in a double-bed adsorption machine with internal heat recovery. *International Journal of Refrigeration*, 2006, *29*(4), 589-600.

Malka-Edery, A.; Abdallah, K.; Grenier, P.; Meunier, F. Influence of traces of water on adsorption and diffusion of hydrocarbons in NaX zeolite. *Adsorption*, 2001, *7*(1), 17-25.

Marcano, D. C.; Kosynkin, D. V.; Berlin, J. M.; Sinitskii, A.; Sun, Z.; Slesarev, A.; Tour, J. M. Improved synthesis of graphene oxide. *ACS nano*, 2010, *4*(8), 4806-4814.

Marletta, L.; Maggio, G.; Freni, A.; Ingrasciotta, M.; Restuccia, G. A non-uniform temperature non-uniform pressure dynamic model of heat and mass transfer in compact adsorbent beds. *International Journal of Heat and Mass Transfer*, 2002, *45*(16), 3321-3330.

Meunier, F. Adsorptive cooling: a clean technology. Clean Products and Processes, 2001, **3**(1): 8-20.

Miles, D. J.; Shelton, S. V. Design and testing of a solid-sorption heat-pump system. Applied Thermal Engineering, 1996, **16**(5): 389-394.

Mobedi, M. Adsorpsiyonlu Isı Pompaları Üzerinde Teorik Ve Deneysel Bir Çalışma. MSc Dissertation, Dokuz Eylul University, Izmir-Turkey, 1987.

Mohammed, R. H.; Mesalhy, O.; Elsayed, M. L.; Chow, L. C. Performance evaluation of a new modular packed bed for adsorption cooling systems. *Applied Thermal Engineering*, 2018, *136*, 293-300.

Moıse, J. C.; Bellat, J. P.; Méthivier, A. Adsorption of water vapor on X and Y zeolites exchanged with barium. *Microporous and mesoporous materials*, 2001, *43*(1), 91-101.

Mu, X.; Wu, X.; Zhang, T.; Go, D. B.; Luo, T. Thermal transport in graphene oxide– from ballistic extreme to amorphous limit. *Scientific reports*, 2014, *4*(1), 1-9.

Nagarjuna, R.; Challagulla, S.; Alla, N.; Ganesan, R.; Roy, S. Synthesis and characterization of reduced-graphene oxide/TiO2/Zeolite-4A: a bifunctional nanocomposite for abatement of methylene blue. *Materials & Design*, 2015, *86*, 621-626.

Narayanan, S.; Yang, S.; Kim, H.; Wang, E. N. Optimization of adsorption processes for climate control and thermal energy storage. *International Journal of Heat and Mass Transfer*, 2014, *77*, 288-300.

Narin, G.; Balköse, D.; Ülkü, S. Characterization and dehydration behavior of a natural, ammonium hydroxide, and thermally treated zeolitic tuff. *Drying Technology*, 2011, *29*(5), 553-565.

Ng, K. C.; Burhan, M.; Shahzad, M. W.; Ismail, A. B. A universal isotherm model to capture adsorption uptake and energy distribution of porous heterogeneous surface. *Scientific Reports*, 2017, *7*(1), 1-11.

Niazmand, H.; Talebian, H.; Mahdavikhah, M. Bed geometrical specifications effects on the performance of silica/water adsorption chillers. *International journal of refrigeration*, 2012, *35*(8), 2261-2274.

Oliveira, R. G.; Wang, R. Z.; Wang, C. Evaluation of the cooling performance of a consolidated expanded graphite–calcium chloride reactive bed for chemisorption icemaker. International Journal of Refrigeration, 2007, **30**(1): 103-112.

Ostrovskii, V. E. Differential microcalorimeter for isothermal measurements of heat effects in two-phase systems and examples of its application. *Review of scientific instruments*, 2002, *73*(3), 1304-1312.

Palomba, V.; Vasta, S.; Giacoppo, G.; Calabrese, L.; Gulli, G.; La Rosa, D.; Freni, A. Design of an Innovative Graphite Exchanger for Adsorption Heat Pumps and Chillers. Energy Procedia, 2015, 81: 1030-1040.

Parfitt, R. L. Anion Adsorption by Soils and Soil Materials. In Advances in Agronomy, Brady N. C. ed., Academic Press Inc., New Zeland, 1978, Vol 30.

Park, S.; An, J.; Potts, J. R.; Velamakanni, A.; Murali, S.; Ruoff, R. S. Hydrazine-reduction of graphite-and graphene oxide. *Carbon*, 2011, *49*(9), 3019-3023.

Park, I.; Knaebel, K. S. Adsorption breakthrough behavior: unusual effects and possible causes. *AIChE journal*, 1992, *38*(5), 660-670.

Pei, S.; Cheng, H. M. The reduction of graphene oxide. *Carbon*, 2012, *50*(9), 3210-3228.

Perrozzi, F.; Prezioso, S.; Ottaviano, L. Graphene oxide: from fundamentals to applications. *Journal of Physics: Condensed Matter*, 2014, *27*(1), 013002.

Pinheiro, J. M.; Salústio, S.; Rocha, J.; Valente, A. A.; Silva, C. M. Analysis of equilibrium and kinetic parameters of water adsorption heating systems for different porous metal/metalloid oxide adsorbents. *Applied Thermal Engineering*, 2016, *100*, 215-226.

Poyelle, F.; Guilleminot, J.-J.; Meunier, F. Experimental Tests and Predictive Model of an Adsorptive Air Conditioning Unit. Industrial & Engineering Chemistry Research, 1999, 38(1): 298-309.

Purdue, M. J.; Qiao, Z. Molecular simulation study of wet flue gas adsorption on zeolite 13X. *Microporous and Mesoporous Materials*, 2018,*261*, 181-197.

Querol, X.; Moreno, N.; Umaña, J. T.; Alastuey, A.; Hernández, E.; Lopez-Soler, A.; Plana, F. Synthesis of zeolites from coal fly ash: an overview. *International Journal of coal geology*, 2002, *50*(1-4), 413-423.

Radke, C. J.; Prausnitz, J. M. Adsorption of organic solutes from dilute aqueous solution of activated carbon. *Industrial & Engineering Chemistry Fundamentals*, 1972, *11*(4), 445-451.

Radu, A. I.; Defraeye, T.; Ruch, P.; Carmeliet, J.; Derome, D. Insights from modeling dynamics of water sorption in spherical particles for adsorption heat pumps. International Journal of Heat and Mass Transfer, 2017, 105: 326-337.

Restuccia, G.; Freni, A.; Maggio, G. A zeolite-coated bed for air conditioning adsorption systems: parametric study of heat and mass transfer by dynamic simulation. Applied Thermal Engineering, 2002, 22(6): 619-630.

Rocky, K. A.; Pal, A.; Rupam, T. H.; Saha, B. B. Zeolite-graphene composite adsorbents for next generation adsorption heat pumps. *Microporous and Mesoporous Materials*, 2021, *313*, 110839.

Ruthven, D. M. Principles of Adsorption and Adsorption Processes. John Wiley & Sons, 1984.

Ruthven, D. M.; Rojo, J. C. A simple model for a non-isothermal adsorption column. *The Canadian Journal of Chemical Engineering*, 1990, *68*(5), 795-798.

Ruthven, D. M. Diffusion in type A zeolites: New insights from old data. *Microporous and Mesoporous Materials*, 2012, *162*, 69-79.

Saadi, R.; Saadi, Z.; Fazaeli, R.; Fard, N. E. Monolayer and multilayer adsorption isotherm models for sorption from aqueous media. *Korean Journal of Chemical Engineering*, 2015, *32*(5), 787-799.

Saha, B. B.; El-Sharkawy, I. I.; Chakraborty, A.; Koyama, S. Study on an activated carbon fiber–ethanol adsorption chiller: Part I–system description and modelling. *International Journal of Refrigeration*, 2007, *30*(1), 86-95.

San, J. Y. Analysis of the performance of a multi-bed adsorption heat pump using a solid-side resistance model. Applied Thermal Engineering, 2006, **26**(17-18): 2219-2227.

San, J. Y.; Lin, W. M. Comparison among Three Adsorption Pairs for Using as the Working Substances in a Multi-Bed Adsorption Heat Pump. Applied Thermal Engineering, 2008, 28, no. 8-9, 988-997.

Sayılgan, Ş. Ç. Determination of Characteristics of Adsorbent for Adsorption Heat Pumps. MSc Dissertation, Izmir Institute of Technology, Izmir-Turkey, 2013.

Sayılgan, Ş. Ç.; Mobedi, M.; Ülkü, S. Effect of Regeneration Temperature on Adsorption Equilibrium and Mass Diffusivity of Zeolite 13X-water Pair. " Microporous and Mesoporous Materials, 2016, Volume 224, 9-16.

Sayilgan, S. Ç.; Ülkü, S. Water Vapor Adsorption by Zeolites. In *Applied Chemistry and Chemical Engineering,* Apple Academic Press, 2017, 43-72.

Schnabel, L.; Tatlier, M.; Schmidt, F.; Erdem-Şenatalar; A. Adsorption kinetics of zeolite coatings directly crystallized on metal supports for heat pump applications (adsorption kinetics of zeolite coatings). Applied Thermal Engineering, 2010, **30**(11–12): 1409-1416.

Semprini, S.; Lehmann, C.; Beckert, S.; Kolditz, O.; Gläser, R.; Kerskes, H.; Nagel, T. Numerical modelling of water sorption isotherms of zeolite 13XBF based on sparse experimental data sets for heat storage applications. *Energy Conversion and Management*, 2017, *150*, 392-402.

Shahbeig, H.; Bagheri, N.; Ghorbanian, S. A.; Hallajisani, A.; Poorkarimi, S. A new adsorption isotherm model of aqueous solutions on granular activated carbon. *World Journal of Modelling and Simulation*, 2013, *9*(4), 243-254.

Singh, R. K.; Kumar, R.; Singh, D. P. Graphene oxide: strategies for synthesis, reduction and frontier applications. *Rsc Advances*, 2016, *6*(69), 64993-65011.

Sircar, S. Linear-driving-force model for non-isothermal gas adsorption kinetics. *Journal of the Chemical Society, Faraday Transactions 1: Physical Chemistry in Condensed Phases*, 1983, *79*(4), 785-796.

Sircar, S.; Kumar, R. Non-isothermal surface barrier model for gas sorption kinetics on porous adsorbents. *Journal of the Chemical Society, Faraday Transactions 1: Physical Chemistry in Condensed Phases*, 1984, *80*(9), 2489-2507.

Solmuş, İ.; Yamalı, C.; Yıldırım, C.; Bilen, K. Transient behavior of a cylindrical adsorbent bed during the adsorption process. *Applied Energy*, 2015, *142*, 115-124.

Subramanyam, B.; Ashutosh, D. Adsorption isotherm modeling of phenol onto natural soils–applicability of various isotherm models. *international Journal of environmental Research*, 2012, *6*(1), 265-276.

Sumathy, K.; Yeung, K. H.; Yong, L. Technology development in the solar adsorption refrigeration systems. Progress in Energy and Combustion Science, 2003, **29**: 301–327.

Sun, L.M.; Benamar, N.; Meunier, F. Numerical Study on Coupled Heat and Mass Transfers in an Adsorber with External Fluid Heating. Heat Recovery Systems & Chp. 15(1), 1995, 19-29.

Sun, L. M.; Feng, Y.; Pons, M. Numerical investigation of adsorptive heat pump systems with thermal wave heat regeneration under uniform-pressure conditions. *International Journal of Heat and Mass Transfer*, 1997, *40*(2), 281-293.

Sun, B.; Chakraborty, A. Thermodynamic formalism of water uptakes on solid porous adsorbents for adsorption cooling applications. *Applied physics letters*, 2014, *104*(20), 201901.

Suzuki, M. Adsorption Engineering, Elsevier Science, Vol. 25, 1990.

Szanyi, J.; Kwak, J. H.; Peden, C. H. The Effect of Water on the Adsorption of NO2 in Na− and Ba− Y, FAU Zeolites: A Combined FTIR and TPD Investigation. *The Journal of Physical Chemistry B*, 2004, *108*(12), 3746-3753.

TamainotTelto, Z.; Critoph, R. E. Adsorption Refrigerator Using Monolithic Carbon-Ammonia Pair. Int. J. Refrig. 20, 1997, no. 2, 146-155.

Tatlıer, M.; Erdem-Şenatalar, A. The effects of thermal gradients in a solar adsorption heat pump utilizing the zeolite–water pair. Applied Thermal Engineering, 1999, 19(11): 1157-1172.

Tatlier, M.; Munz, G.; Fueldner; G.; Henninger, S. K. Effect of zeolite A coating thickness on adsorption kinetics for heat pump applications. Microporous and Mesoporous Materials, 2014, 193: 115-121.

Teng, Y.; Wang, R. Z.; Wu, J. Y. Study of the Fundamentals of Adsorption Systems." Applied Thermal Engineering, 1996, 17, 327-338.

Teo, H. W. B.; Chakraborty, A.; Fan, W. Improved adsorption characteristics data for AQSOA types zeolites and water systems under static and dynamic conditions. *Microporous and Mesoporous Materials*, 2017, *242*, 109-117.

Todd, A. D.; Bielawski, C. W. Graphite oxide activated zeolite NaY: applications in alcohol dehydration. *Catalysis Science & Technology*, 2013, *3*(1), 135-139.

Tolazzi, N.; Steffani, E.; Barbosa-Coutinho, E.; Júnior, J. B. S.; Pinto, J. C.; Schwaab, M. Adsorption equilibrium models: computation of confidence regions of

parameter estimates. *Chemical Engineering Research and Design*, 2018, *138*, 144-157.

Tran, M. H.; Yang, C. S.; Yang, S.; Kim, I. J.; Jeong, H. K. Influence of graphite size on the synthesis and reduction of graphite oxides. *Current Applied Physics*, 2014, *14*, S74-S79.

Trisupakitti, S.; Jamradloedluk, J.; Wiriyaumpaiwong, S. Adsorption Cooling System Using Metal-Impregnated Zeolite-4A. Advances in Materials Science and Engineering 2016: 8.

Tsitsishvili, G. V.; Andronikashvili, T. G.; Kirov, G. N. *Natural zeolites*. Ellis Horwood Limited, 1992.

Tso, C. Y.; Chan, K. C.; Chao, C. Y. H.; Wu, C. L. Experimental performance analysis on an adsorption cooling system using zeolite 13X/CaCl2 adsorbent with various operation sequences. International Journal of Heat and Mass Transfer, 2015, 85: 343-355.

Umair, M.; Dwiputro, A. F.; Bagus Wirajati, I. G. A.; Ueda, Y.; Akisawa, A. Design and Investigation of Heat Transfer in a New Adsorbent Bed With CPC for Solar Adsorption Refrigeration Systems. Heat Transfer Engineering, 2016, **37**(7-8): 696-704.

Ülkü, S. Adsorption Heat Pumps. Heat Recovery Systems, 1986, **6**: 277-284.

Ülkü, S. Natural Zeolites in Energy Storage and Heat Pumps. Studies in Surface Science and Catalysis, 1986, **28**: 1047-1054.

Ülkü, S.; Gürses, A. Ç.; Toksoy, M. Enerji Tasarrufu ve Isı Pompaları. Enerji Tasarrufu Semineri Bildiriler Kitabı. İstanbul, 1987**,** 27-38.

Ülkü, S.; Mobedi, M. Adsorption in Energy Storage. Energy Storage Systems, 1989, 487-507.

Ülkü, S.; Balköse, D.; Alp, B. Dynamic Heat of Adsorption of Water Vapour on Zeolitic Tuff and Zeolite 4A by Flow Microcalorimetry. Oxidation Communications, 2006, 29, no. 1, 204-215.

Valsaraj, K. T.; Thibodeaux, L. J. On the Linear Driving Force Model for Sorption Kinetics of Organic Compounds on Suspended Sediment Particles. Environmental Toxicology and Chemistry, 1999, 18, no. 8, 1679-1685.

Van Reeuwijk, L. P. The thermal dehydration of natural zeolites. Wageningen University and Research, 1974.

Wang, R. Z. Performance improvement of adsorption cooling by heat and mass recovery operation. International Journal of Refrigeration, 2001, **24**(7): 602-611.

Wang, R. Z.; Li, M.; Xu, Y. X.; Wu, J. Y. An energy efficient hybrid system of solar powered water heater and adsorption ice maker. *Solar energy*, 2000, *68*(2), 189-195.

Wang, L. W.; Wang, R. Z.; Wu, J. Y.; Wang, K. Compound adsorbent for adsorption ice maker on fishing boats. International Journal of Refrigeration, 2004, **27**(4): 401-408.

Wang, L. W.; Wu, J. Y.; Wang, R. Z.; Xu, Y. X.; Wang, S. G.; Li, X. R. Study of the performance of activated carbon–methanol adsorption systems concerning heat and mass transfer. Applied Thermal Engineering, 2003, **23**(13): 1605-1617.

Wang, D. C.; Xia, Z. Z.; Wu, J. Y.; Wang, R. Z.; Zhai, H.; Dou, W. D. Study of a novel silica gel–water adsorption chiller. Part I. Design and performance prediction. International Journal of Refrigeration, 2005, **28**(7): 1073-1083.

Wang, X.; Chua, H. T.; Ng, K. C. Experimental investigation of silica gel–water adsorption chillers with and without a passive heat recovery scheme. International Journal of Refrigeration, 2005, **28**(5): 756-765.

Wang, D. C.; Xia, Z. Z.; Wu, J. Y. Design and performance prediction of a novel zeolite–water adsorption air conditioner. Energy Conversion and Management, 2006, **47**(5): 590-610.

Wang, D.; Wu, W. D.; Zhang, H.; Sun, D. W. Mathematical simulation and experimental study of a modified zeolite 13X–water adsorption refrigeration module. *Applied Thermal Engineering*, 2009, *29*(4), 645-651.

Wang, K.; Wu, J. Y.; Wang; R. Z.; Wang, L. W. Composite adsorbent of CaCl2 and expanded graphite for adsorption ice maker on fishing boats. International Journal of Refrigeration, 2006, **29**(2): 199-210.

Wang, L.; Zhu, D.; Tan, Y. Heat Transfer Enhancement of the Adsorber of an Adsorption Heat Pump. Adsorption, 1999, 5, 279-286.

Wang, Y.; LeVan, M. D. Adsorption Equilibrium of Carbon Dioxide and Water Vapor on Zeolite 5A and 13X and Silica Gel: Pure Components. J. Chem. Eng. Data, 2009, 54, 2839-2844.

Xu, C.; Yuan, R. S.; Wang, X. Selective reduction of graphene oxide. *New Carbon Materials*, 2014, *29*(1), 61-66.

Xue, B.; Meng, X.; Wei, X.; Nakaso, K.; Fukai, J. Dynamic study of steam generation from low-grade waste heat in a zeolite–water adsorption heat pump. *Applied Thermal Engineering*, 2015, *88*, 451-458.

Xiao, J.; Peng, Y.; Bénard, P.; Chahine, R. Thermal effects on breakthrough curves of pressure swing adsorption for hydrogen purification. *International Journal of Hydrogen Energy*, 2016, *41*(19), 8236-8245.

Yang, S.; Kim, H.; Narayanan, S.; McKay, I. S.; Wang, E. N. Dimensionality effects of carbon-based thermal additives for microporous adsorbents. *Materials & Design*, 2015, *85*, 520-526.

Yaïci, W.; Entchev, E. Coupled unsteady computational fluid dynamics with heat and mass transfer analysis of a solar/heat-powered adsorption cooling system for use in buildings. *International Journal of Heat and Mass Transfer*, 2019, *144*, 118648.

Yoo, B. M.; Shin, J. E.; Lee, H. D.; Park, H. B. Graphene and graphene oxide membranes for gas separation applications. *Current opinion in chemical engineering*, 2017, *16*, 39-47.

Yu, H.; Zhang, B.; Bulin, C.; Li, R.; Xing, R. High-efficient synthesis of graphene oxide based on improved hummers method. *Scientific reports*, 2016, *6*(1), 1-7.

Yu, Y.; Murthy, B. N.; Shapter, J. G.; Constantopoulos, K. T.; Voelcker, N. H.; Ellis, A. V. Benzene carboxylic acid derivatized graphene oxide nanosheets on natural zeolites as effective adsorbents for cationic dye removal. *Journal of hazardous materials*, 2013, *260*, 330-338.

Yucel, H.; Ruthven, D. M. Diffusion of CO2 in 4A and 5A Zeolite Crystals. Journal of Colloid and Interface Science, 1980, 74, no. 1, 186-195.

Yun, J. H.; Choi, D. K.; Moon, H. Benzene adsorption and hot purge regeneration in activated carbon beds. *Chemical engineering science*, 2000, *55*(23), 5857-5872.

Zhang, X. J.; R. Z. Wang Design and performance simulation of a new solar continuous solid adsorption refrigeration and heating hybrid system. Renewable Energy, 2002, **27**(3): 401-415.

Zhang, M.; Gao, B.; Pu, K.; Yao, Y.; Inyang, M. Graphene-mediated self-assembly of zeolite-based microcapsules. *Chemical engineering journal*, 2013, *223*, 556-562.

Zhao, G.; Li, J.; Ren, X.; Chen, C.; Wang, X. Few-layered graphene oxide nanosheets as superior sorbents for heavy metal ion pollution management. *Environmental science & technology*, 2011, *45*(24), 10454-10462.

Zhong, G. M.; Meunier, F.; Huberson, S.; Chalfen, J. B. Pressurization of a single-component gas in an adsorption column. *Chemical engineering science*, 1992, *47*(3), 543-550.

APPENDIX A

DERIVATION OF GOVERNING EQUATIONS

During the design of the adsorbent bed, the heat and mass transfer equations are solved simultaneously. In the following part, the derivation of the governing equations according to the assumptions are shown in detail. The derivation is obtained for the cylindrical bed in which the adsorptive flows through the annulus (Figure A.1).
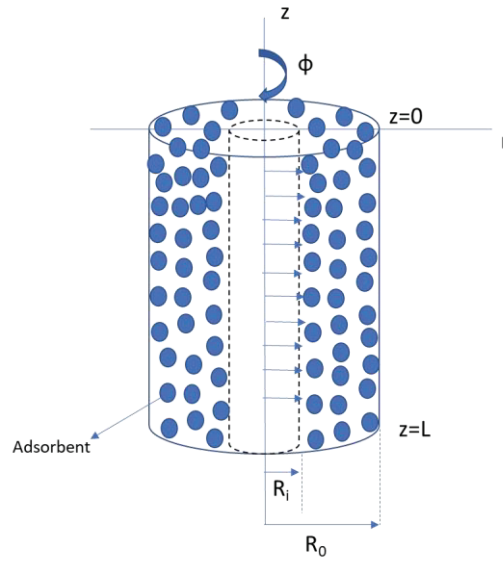

Figure A.1.The considered annular bed

A.1. Heat transfer equation

The overall energy balance for the control volume can be given as:

$$E_{in-}E_{out} + E_{generation} = E_{accumulation}$$

For two-dimensional case, the total energy inlet can be defined as:

$$E_{in} = q_{in,r} + q_{in,z}$$

where $q_{in} = q_{cond} + q_{conv}$

On the other hand, by using Taylor series expansion in which the higher order terms are neglected, the total energy outlet can be given as:

$$E_{out} = q_{out,r} + q_{out,z} = q_{in,r} + \frac{\partial q_{in,r}}{\partial r} dr + q_{in,z} + \frac{\partial q_{in,z}}{\partial z} dz$$

During the adsorption process, energy is generated due to the isosteric heat of adsorption. Then, the energy generation can be written as:

$$E_{gen} = q_{st} \rho_s \frac{\partial \overline{w}}{\partial t} (2\pi r dr dz)$$

Finally, the energy accumulation term can be given as:

$$E_{accumulation} = \left(\rho_z C_{p,z} + \rho_w C_{p,w} + \rho_z C_{p,w} \overline{w} \right) \frac{\partial T}{\partial t} (2\pi r dr dz)$$

When the equations given above are combined, the heat transfer equation can be written as:

$$\cancel{q_{in,r}} + \cancel{q_{in,z}} - \cancel{q_{in,r}} - \frac{\partial q_{in,r}}{\partial r} dr - \cancel{q_{in,z}} - \frac{\partial q_{in,z}}{\partial z} dz + E_{gen} = E_{accumulation}$$

$$-\frac{\partial}{\partial r} \left(-k_{eff} (2\pi r dz) \frac{\partial T}{\partial r} + \rho_w C_{p,w} (2\pi r dz) u_r T \right) dr$$

$$-\frac{\partial}{\partial z} \left(-k_{eff} (2\pi r dr) \frac{\partial T}{\partial r} + \rho_w C_{p,w} (2\pi r dr) u_z T \right) dz$$

$$+ q_{st} \rho_s \frac{\partial \overline{w}}{\partial t} (2\pi r dr dz) = \left(\rho_z C_{p,z} + \rho_w C_{p,w} + \rho_z C_{p,w} \overline{w} \right) \frac{\partial T}{\partial t} (2\pi r dr dz)$$

By dividing all the terms by $(2\pi r dr dz)$ and rearranging the equation, the final form of the heat transfer equation can be obtained as:

$$\frac{\partial}{\partial r} \left(k_{eff} \frac{1}{r} \frac{\partial T}{\partial r} \right) - \frac{\partial}{\partial r} (\rho_w C_{p,w} r u_r T) + \frac{\partial}{\partial z} \left(k_{eff} \frac{\partial T}{\partial z} \right) - \frac{\partial}{\partial z} (\rho_w C_{p,w} u_z T) + q_{st} \rho_s \frac{\partial \overline{w}}{\partial t}$$

$$= \left(\rho_z C_{p,z} + \rho_w C_{p,w} + \rho_z C_{p,w} \overline{w} \right) \frac{\partial T}{\partial t}$$

A.2. Continuity Equation

The overall mass balance for the control volume can be given as:

$$m_{in}-m_{out} - m_{consumed} = m_{accumulation}$$

$$m_{in,r} + m_{in,z} - m_{in,r} - \frac{\partial m_{in,r}}{\partial r} dr - m_{in,z} - \frac{\partial m_{in,z}}{\partial z} dz + m_{con} = m_{acc}$$

Since $m = \rho_v u A$ where A is the cross-sectional area, then the equation takes the form of:

$$-\frac{\partial}{\partial r}\left(\rho_v u_r(2\pi rdz)\right)dr - -\frac{\partial}{\partial z}\left(\rho_v u_z(2\pi rdr)\right)dz - \rho_s \frac{\partial \overline{w}}{\partial t}(2\pi rdrdz)$$

$$= \varepsilon \frac{\partial \rho_v}{\partial t}(2\pi rdrdz)$$

where $\rho_s \frac{\partial \overline{w}}{\partial t}(2\pi rdrdz)$ gives the amount of adsorptive consumed during the adsorption process and the $\varepsilon \frac{\partial \rho_v}{\partial r}(2\pi rdrdz)$ gives the accumulation of adsorptive within the bed. By dividing all the terms by $(2\pi rdrdz)$ and rearranging the equation, the final form of the heat transfer equation can be obtained as:

$$\varepsilon \frac{\partial \rho_v}{\partial t} + \frac{1}{r}\frac{\partial}{\partial r}(\rho_v r u_r) + \frac{\partial}{\partial z}(\rho_v u_z)dz + \rho_s \frac{\partial \overline{w}}{\partial t} = 0$$

VITA

EDUCATION

2023 Philosophy of Doctorate (PhD) Izmir Institute of Technology, Department of Chemical Engineering

2013 Master of Science (MSci.) Izmir Institute of Technology, Department of Energy Engineering

2010 Bachelor of Science (BS) Ege University, Department of Chemical Engineering

PUBLICATIONS

Sayılgan, Ş. Ç., Mobedi, M., Ülkü, S., Effect of Regeneration Temperature on Adsorption Equilibrium and Mass Diffusivity of Zeolite 13X-Water Pair, Microporous and Mesoporous Materials, Volume 224, p 9-16, 2016.

Sayılgan Ş.Ç., Ülkü S., Water Vapor Adsorption by Zeolites, Applied Chemistry and Chemical Engineering, Volume 5, Research Methodologies in Modern Chemistry and Science, 43-72,2018.

PRESENTATIONS

Sayılgan, Ş. Ç., Ülkü, S., Zeolitlerin Karakterizasyonu ve Rejenerasyon Sıcaklığının Adsorpsiyon Dengesi ve Kütle Transferi Üzerine Etkisi, 12. Ulusal Kimya Mühendisliği Kongresi, 23-26 Ağustos 2016, İzmir, Türkiye (poster presentation).

Sayılgan Ş.Ç., Ülkü S., Water Vapor Adsorption of Zeolite 13X and 4A, 3rd International Porous and Powder Materials Symposium and Exhibition, 12-15 Eylül 2017, İzmir, Türkiye (oral presentation).